Lead optimisation of dehydroemetine as an antimalarial option through drug repositioning and molecular modelling

Priyanka Panwar

School of Environment and Life Sciences

University of Salford, Manchester, UK

Submitted in Partial Fulfilment of the Requirements for the Degree of Doctor of Philosophy, 2019

Declaration

I certify that this thesis, submitted to the University of Salford in partial fulfilment of the requirements for a Degree of Doctor of Philosophy, is a presentation of my own research work and that this work has not been submitted for any other degree or processional qualification except as specified.

Although the author has carried out most experiments and analysis of this research, some parts of this thesis were carried out in collaboration with other colleagues. Wherever contributions of others are involved, every effort is made to indicate this clearly with due reference to the literature and acknowledgment of collaborative research and discussions.

Table of Contents

List of Figures

List of Tables

Acknowledgements:

I still remember my first day of starting this PhD and it has been a roller-coaster ride ever since. There are many fantastic people who have made this PhD a memorable journey for me. I would like to begin by expressing my appreciation and gratitude toward my supervisor, Prof. Niroshini Nirmalan, who has guided me, supported me, motivated me, and above all believed in me and my capabilities. Her work ethics are truly inspirational, and her wonderful parties are probably the best in Manchester!

I would also like to thank my colleagues in the malaria research group, Dr Muna Abubaker and Dr May Rajab, for their help and constant support. Together, we have been through so many ups and downs. May, I will always remember the Christmas roast you cooked for me, thank you! Muna, I am grateful to have you as a friend. You have given me advice and taken care of me in my times of need. Dr Basmah Allarakia and Rumana Rafiq, you have both been amazing to me. Dr Emyr Bakker, my friend and little brother, thanks for being in my life, and thanks for introducing me to Harlan. I will always remember all the fun video game nights at your apartment! Alice Guazzelli, Arvind Swami and Farnaz, you are the most amazing friends and thanks for putting up with all my quirkiness! Neha Tomar and Dr Chrow Khurshid, thanks for being the most wonderful flatmates. You are both like sisters to me. All of you have become my family away from home and I wish you every success in future.

I cannot express in words how lucky I am to have parents who have always believed in me and provided me with innumerable opportunities to become a responsible, independent person. To my brothers, Avinash and Abhilash, thank you for showering me with unconditional love. Last but not least, to the person who has recently walked in my life and has filled it with so much happiness. My husband, Viral Patel, I love you and feel blessed to share this life-long journey with you.

I would also like to thank our research collaborators Dr Richard Bryce, Dr Kepa K. Burusco, Dr David Greensmith and Natasha Hadcraft for their helpful guidance. Finally, I would like to acknowledge the grants I have received from the Salford Post-graduate Research Fund, Santander Universities and the British Society for Parasitology to attend various conferences which has helped me tremendously in my personal development as a researcher. I dedicate this study to all my family and friends.

List of Abbreviations

ACT	Artemisinin Combination Therapy
ADME	Absorption/distribution/metabolism/excretion
ART	Artemether
ATQ	Atovaquone
CI	Combination Index
CM	Complete Media
CQ	Chloroquine
DDT	2.2-bis-(p-chlorophenyl)-1,1,l-trichloroethane
DHE	(-)-R,*S-dehydroemetine*
DHFR	Dihydrofolate Reductase
DHPS	Dihydropteroate Synthase
ECG	Electrocardiogram
FACS	Flow Cytometry
FDA	Food and Drug Administration (USA)
FVM	Food Vacuole Membrane
LC50	Half Lethal Dose
LLINs	Long-Lasting Insecticide Treated Nets
LOPAC	Library of Pharmaceutical Active Compound
IC50	Half Maximal Inhibitory Concentration
iRBCs	Infected Red Blood Cells
IPT	Intermittent Preventive Treatment
IRS	Indoor Residual Spraying
ITN	Insecticide Treated Nets
MOE	Molecular Operating Environment, Chemical Computing Group
MDR	Multidrug Resistance
MMP	Mitochondrial Membrane Potential
MMV	Medicine for Malaria Venture
PDB	Protein databank structure file
PfCRT	*Plasmodium Falciparum* Resistance Transporter
PfHRPII	*Plasmodium Falciparum* Histidine- Rich Protein II
PfMRP1	Plasmodium Falciparum Multidrug Resistance-Associated Protein- 1
PG	Proguanil
PPM	Parasite Plasma Membrane
RBCM	Red Blood Cell Membrane
RBCs	Red Blood Cells
RDT	Rapid Diagnostic Test
ROS	Reactive Oxygen Species
SG-FCM	SYBR Green Flow Cytometry.
SI	Selectivity Index
SP	Sulfadoxine Pyrimethamine
TBV	Transmission Blocking Vaccine

TVM	Tubovesicular Membrane
WHO	World health organisation
WM	Washed Media

Abstract

Malaria is a life-threatening infectious disease caused by a parasitic protozoan belonging to the genus *Plasmodium*. Resistance has started to emerge for the currently recommended artemisinin combination therapies used to treat malaria. There is a great need for new anti-malarial drugs, but traditional drug discovery timelines take approximately 10-17 years. Drug repositioning offers a very effective alternative to *de novo* drug design and could minimise the long timescales involved in the process of bringing a drug to the market. Work at the University of Salford identified the previously widely-used anti-amoebic drug emetine dihydrochloride as a potent inhibitor of *Plasmodium falciparum* K1 strain parasites (IC_{50}: 47 $\pm$ 2.17 nM). Emetine is not currently in use due to its emetic and cardiotoxic effects.

The cryo-EM structure (3J7A) depicting the emetine binding site on the 40S subunit of the 80S *P. falciparum* ribosome has recently been published as a potential target binding site for emetine, enabling rational design of safer synthetic analogues. This study focuses on using molecular modelling tools to predict activities of the two isomers of dehydroemetine, a synthetic analogue of emetine developed in the 1960s by Roche. Studies conducted in the mid-20th century found dehydroemetine to be less toxic than emetine; however, its use as an anti-amoebic was replaced due to the introduction of the safer drug metronidazole, although dehydroemetine still remains as a WHO recommended drug for use in amoebiasis in metronidazole treatment failure. Using MOE and Autodock vina docking software, the activities of two isomers of dehydroemetine; (-)-*R,S*-dehydroemetine and (-)-*S,S*-dehydroisoemetine were predicted. Docking studies predicted a better binding conformation for (-)-*R,S*-dehydroemetine compared to (-)-*S,S*-dehydroisoemetine. The two diastereomers of dehydroemetine were synthesised and tested against the multi-drug resistant K1 strain of *Plasmodium falciparum*. It was found that of the two diastereomers, (-)-*R,S*-dehydroemetine (IC_{50}: 69.58 $\pm$ 2.62 nM) shared almost similar potency with emetine (47 $\pm$ 2.17 nM), whereas (-)-*S,S*-dehydroisoemetine (IC_{50}: 1.85 $\pm$ 0.2 µM) was much less active as predicted through modelling studies. Stage specificity studies of both compounds showed more activity against the trophozoite erythrocytic stages of the parasite. The IC_{50} speed assays carried out to verify onset of antimalarial activity in emetine and the dehydroemetine diastereomers, found that although the compounds started activity within 24 hours, the IC_{50} values were achieved only at 48 hours. Cell cytotoxicity assays showed both compounds to be potent against HepG2

hepatic cancer cell lines seeded at 5000 cells/well with low selectivity indices (SI = ~3 and ~1 for (-)-*R,S*-dehydroemetine and (-)-*S,S*-dehydroisoemetine). To achieve further dose reduction to minimise toxicity, CalcuSyn-based drug interactivity assays were optimised and validated on known synergistic antimalarial drug combinations (atovaquone/proguanil). Drug interaction analysis performed using the validated CalcuSyn method found the antimalarial drug atovaquone to be synergistic with (-)-*R,S*-dehydroemetine at IC_{50}, IC_{75} and IC_{90} values (Combination indices (CI): 0.88-0.89). Proguanil displayed moderate synergy (CI: 0.67), additivity (CI: 1.04) and antagonism (CI: 1.6) with (-)-*R,S*-dehydroemetine at IC_{50}, IC_{75} and IC_{90} combinatory doses, respectively. Combination studies with artemether (CI: 1.6) and doxycycline (CI: 1.5) were found to be antagonistic. Emetine and (-)-*R,S*-dehydroemetine were found to display gametocidal activity against both male and female gametes with no cross-resistance observed on 3D7A, Dd2 and W2 strains.

Further experiments were conducted to investigate the possibility of a multimodal mechanism of action for emetine and its analogues. ATP proliferation experiments on parasite-infected erythrocytes showed emetine and (-)-*R,S*-dehydroemetine caused a reduction in cellular ATP concentrations. Emetine and (-)-*R,S*-dehydroemetine also resulted in the disruption of the parasite mitochondrial membrane potential in infected erythrocytes in a manner similar to the slow-acting antimalarial atovaquone. The results support multimodal mechanisms of action in addition to inhibition of protein translation.

Experiments were also conducted to determine the cellular basis of cardiotoxicity previously reported in emetine and dehydroemetine therapy for amoebiasis. hERG K^+ channel blocking assays showed that emetine and (-)-*R,S*-dehydroemetine did not result in inhibition (Selectivity indices > 285), indicating a differential mechanism of action for cardiotoxicity. To explore this further, experiments were done to evaluate the effect of emetine and (-)-*R,S*-dehydroemetine on calcium regulatory mechanisms on sheep ventricular myocytes. Both emetine and (-)-*R,S*-dehydroemetine displayed potentiation of ryanodine receptors, lowering the threshold for generation of calcium waves with consequent increased susceptibility for arrhythmias. (-)-*R,S*-dehydroemetine however, also displayed negative inotropic effects in comparison to emetine, thus making the compound potentially less arrhythmogenic and supporting early clinical observations reported in the 1960s during anti-amoebic therapy.

Chapter 1 Introduction

Malaria is a life-threatening infectious disease characterised by a febrile illness and caused by a parasitic protozoan belonging to the genus *Plasmodium*. It is transmitted through the bites of infected female *Anopheles* mosquitoes. Malaria is a preventable and curable disease. As per the WHO fact sheet, the mortality rate from malaria has fallen by 47% globally and 54% in WHO African region since 2000, but the disease still plays a major role in global health issues. Every minute a child dies from malaria in Africa. As per WHO report 2015, the global incidence of malaria was 198 million cases in 2013 with an estimated 584,000 deaths mostly among the African children (Rodriguez-Morales et al., 2015) and in 2017, the number of malaria cases increased to 219 million with an estimated 435,000 deaths (WHO, 2018). Malaria is mostly prevalent in tropical and sub-tropical regions and presents a huge burden on economic development of malaria endemic countries by having an impact on population growth, absenteeism, workforce productivity, medical costs and mortality (Sachs and Malaney, 2002).

1.1 History of malaria and discovery of the parasite:

Historically, malaria has been around for a long time and was described in China about 5000 years ago (Cui et al., 2015). Ancient Greeks were familiar with the disease since 500 BC. Hippocrates is known to have described the disease and its symptoms as early as 46 BC and Columella (AD 116) characterised it as a disease caused by germs breeding around swamps (Jamieson and Toovey, 2006). The English word for malaria was ‘Ague’ and has been mentioned in eight of William Shakespeare’s plays (Reiter, 2000). Malaria was known to be indiscriminate in choosing its casualties. Famous victims include Hadrian, Vespasian, Titus, St. Augustine and Alexander the Great (Jamieson and Toovey, 2006). The term malaria comes from the Italian ‘mala aria’ which means ‘bad air’, a reference to the presence of a peculiar sulphurous odour produced by anaerobic bacterial flora in brackish mud along river estuaries where the disease was more prevalent, reflecting the ecology and distribution of the mosquito vectors (Reiter, 2000).

Since the first to the nineteenth century, the ‘miasmic theory’ dominated Europe as the cause of malaria. It was not until 1880, that a French Army doctor, Charles Louis Alphonse

Laveran observed the presence of parasites in the red blood cells of malaria-infected people while working in the military hospital in Constantine, Algeria. Laveran found pigmented bodies in peripheral blood films and observed exflagellation of the parasite. He proposed that malaria was caused by an organism, a protozoan he named *Haemamoeba malariae* (Ferri, 2009). His discovery was initially met with scepticism but was gradually accepted as further confirmatory researches were published by other scientists. He was awarded the Breant Prize by the Academy of Sciences in 1889 for his discovery and later a Nobel Prize in 1907 for his work on protozoans causing diseases (Alphonse, 2009). In 1877, Patrick Manson, considered by many as the father of tropical medicine, discovered the role of mosquitoes in transmission of filarial parasites and drawing inference from this, Albert Freeman Africanus King, in 1883 suggested the possibility of malaria also being transmitted by mosquitoes (Cook and Webb, 2000). In 1881, Carlos Jan Finlay provided evidence of the role of mosquitoes in transmission of diseases in humans (Tan and Sung, 2008). Manson himself believed that malaria was transmitted by mosquitoes and formulated a hypothesis which he later called 'Mosquito-Malaria theory' (Capanna, 2006).

In 1892, a British physician Sir Ronald Ross commenced a study on malaria (Chernin, 1988). Ross met Manson in London in 1894, which proved to be a turning point in solving the life cycle of the malaria parasite, as Manson demonstrated the presence of parasitic bodies described by Laveran in the blood films of malaria infected patients and provided Ross with the knowledge he desperately sought (Ferri, 2009). While working in India, Ross conducted experiments to prove the hypothesis of the role of mosquitoes in transmission of malaria. He initially used the *Culex* mosquitoes and his research bore no results. Disheartened by the lack of results, Ross lost interest in it only to be encouraged by Manson to not give up. Ross later conducted research on other species of mosquitoes found in highly malarious areas and discovered single large cells in the stomach walls of the mosquitoes fed on malaria-infected patients. These cells increased in diameters with each passing day thus demonstrating growth. Ross was able to show that the parasite reproduced sexually in the stomach of the mosquito. He continued his research on transmission of malaria in birds and noted the passage of parasites from stomach to salivary glands of the infected mosquito, from where it then passed into the bloodstream of the healthy bird when bitten by such mosquitoes. In 1902, Ross earned the Nobel Prize in medicine for demonstrating the life cycle of the malaria parasite

and establishing the mosquito species *Anopheles* as the vector carrier of malaria (Chernin, 1988).

1.2 Geography and Incidence:

Malaria was widely prevalent in Medieval Europe until the breeding habits of the mosquito vectors were disrupted by land reclamation, building of well-lit and ventilated houses, and improved drainage (Jamieson and Toovey, 2006). Today, malaria is mainly a disease of tropical and sub-tropical regions. Implementation of Malaria Control Programmes and increased financing has seen a huge reduction in the malaria incidence and mortality since 2010 (Mita and Jombart, 2015). The figures 1.2.1 and 1.2.2 respectively show the trend in the estimated cases and deaths due to malaria since 2000. The past few years have seen little progress in the fight against malaria (WHO, 2018).

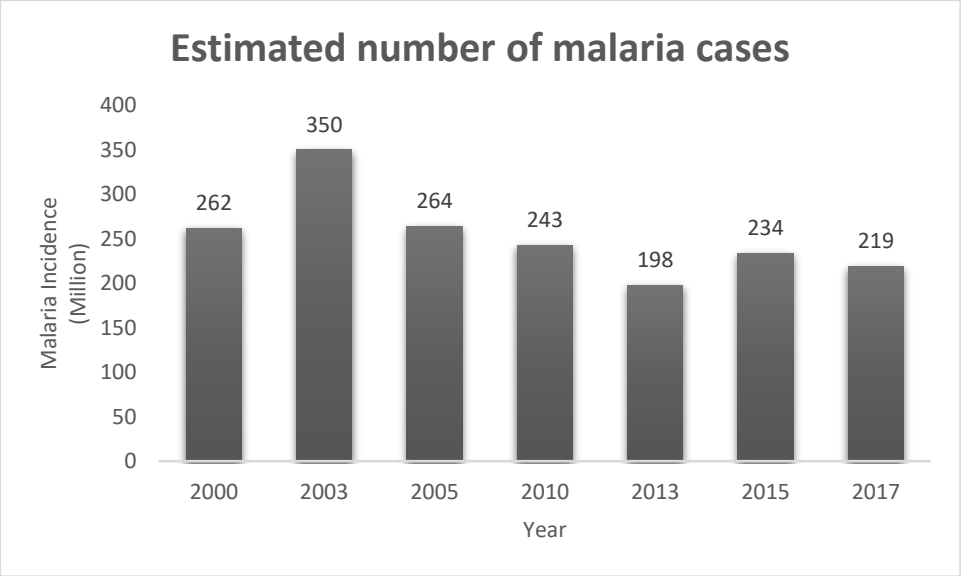

Figure 1.2.1 Estimated number of malaria cases (WHO, 2018)

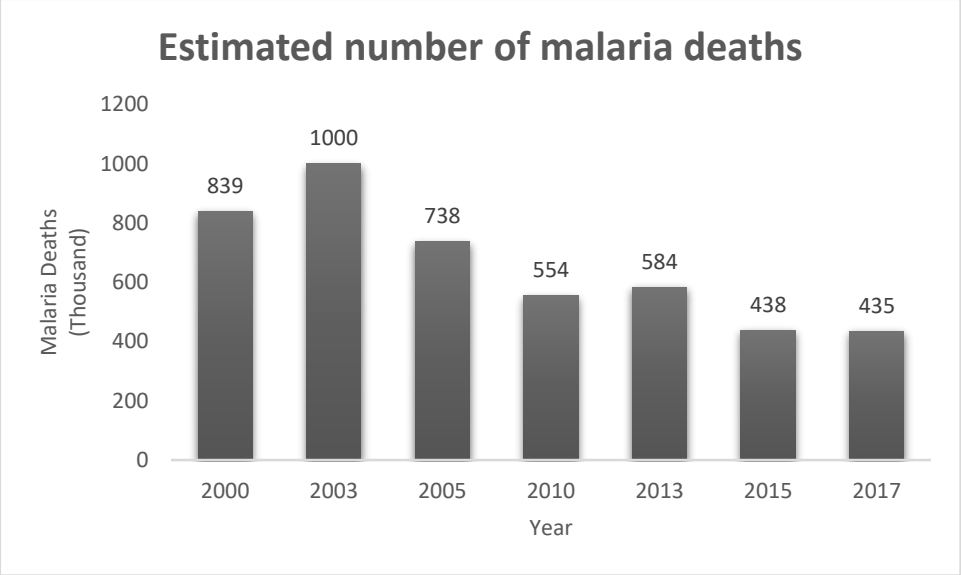

Figure 1.2.2 Estimated number of malaria deaths (Source: WHO 2018)

Climate plays an important role in the life cycle of malaria parasites as rainfall, humidity and ambient temperatures determine the survival of the mosquito vector. Warm tropical and sub-tropical temperatures are ideal for the parasite to complete the growth cycle. At temperatures 15 °C or 59 °F for *Plasmodium vivax*, 20 °C or 68 °F for *Plasmodium falciparum* the growth cycle is not completed and thus the transmission of malaria is difficult (Ecology of malaria, 2015). The ecological conditions required for the more efficient mosquito vectors of malaria to thrive, determine the intensity of the disease and its distribution (Gallup and Sachs, 2001). There is a compelling correlation between malaria and poverty. Human societies have prospered least in areas where malaria has prospered most (Rodriguez-Morales et al., 2015). Cases and deaths from malaria started to increase globally since 1990 and reached a peak in 2003 with more than 350 million cases and more than 1 million deaths (WHO, 2005). A decrease in child mortality rates has been observed in the sub-Saharan region since 2004, while the malaria mortality rate has been on a steady decline since 1990 in regions outside of Africa (Murray et al., 2014). Artemisinin-based combination therapies (ACT) have played a major role in decreasing the global burden of malaria but the emergence and potential spread of strains of malaria parasites resistant to artemisinin in Southeast Asia and variations in sensitivities to artemisinin partner drugs is a major cause for concern (Cui et al., 2015). Figure 1.2.3 shows the global distribution of malaria in 2000 and 2016.

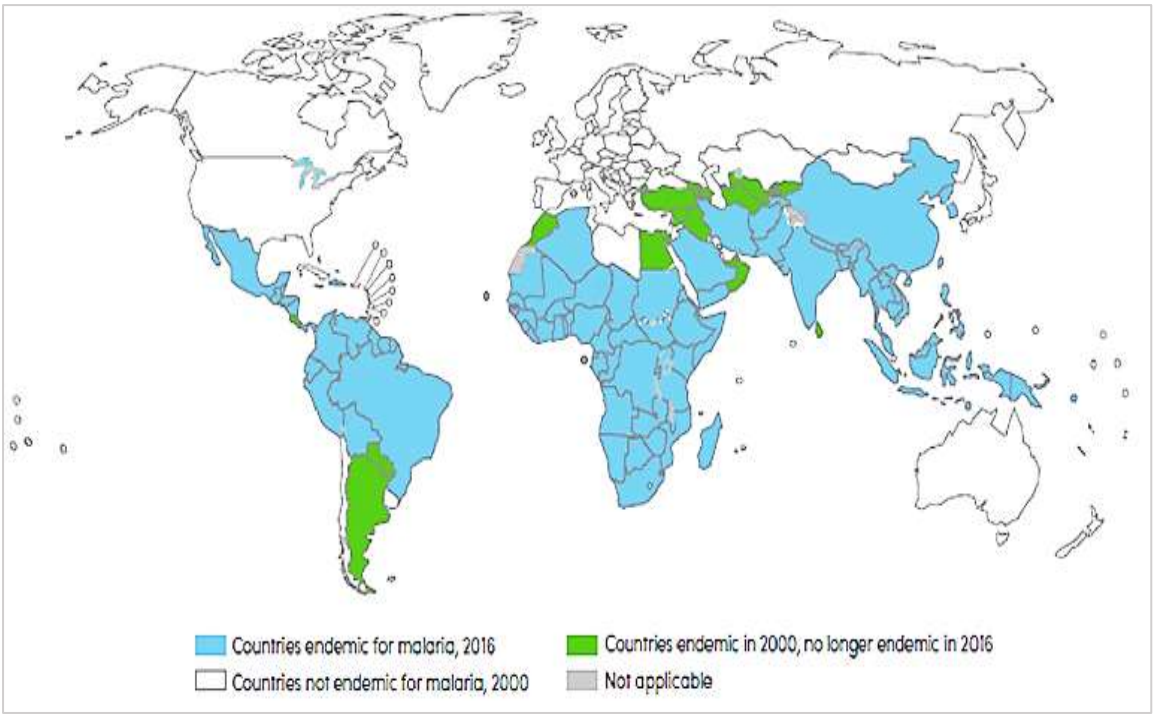

Figure 1.2.3 Map of countries endemic for malaria from 2000 to 2016 (WHO, 2016)

1.3 Malaria parasite, mosquito vector and Life-cycle:

Malaria in humans is caused by a protozoan parasite belonging to one of the following four *Plasmodium* species: *Plasmodium falciparum, Plasmodium vivax, Plasmodium ovale and Plasmodium malariae* (Franco-Paredes and Santos-Preciado, 2006). *Plasmodium knowlesi* is a zoonotic parasite and is known to cause infections in humans.

The malaria parasite is transmitted to humans through bites of female *Anopheles* mosquitoes. The ability to transfer malaria parasite differs among the various species of *Anopheles*. Some female *Anopheles* species have an inclination towards human blood for their meals (anthropophilic) whereas some others prefer animals (zoophilic). Some have indoor biting habits (endophagic) whereas the others have outdoor (exophagic). All the other factors being equal, the better vectors for malaria transmission are the species with anthropophilic, endophagic habits as they tend to have more frequent contacts with humans. A field study observed that *Plasmodium falciparum* alters the behavioural patterns of the mosquito vector host *Anopheles gambiae* and increases the frequency of multiple feeding, thereby facilitating a more rapid spread and increase in the transmission in humans (Koella et al. (1998). There

are many countries which have eliminated malaria but the *Anopheles* mosquito is still present in these countries, and presents a potential for reintroduction of malaria through cases in returning travellers or immigrants (imported malaria), if such cases are not treated promptly (Odolini et al., 2012).

The malaria parasite requires two hosts to complete the life cycle; humans and the female *Anopheles* mosquito. In the human host the parasite presents different antigens throughout the several life stages which are useful targets for vaccine development (Florens et al., 2002). The mosquito transmits the disease from one human to another but itself does not suffer from the presence of parasites.

1.3.1 **Life cycle of Plasmodium parasites:**

- *Plasmodium* parasites in the form of sporozoites are introduced into the bloodstream of human hosts by bites of infected female *Anopheles* mosquitoes. These sporozoites reach the liver and over the period of 7 to 10 days the sporozoites multiply asexually producing no symptoms (pre-erythrocytic stage).
- The parasites, in the form of merozoites are released in the bloodstream where they infect the red blood cells (erythrocytes) and multiply further. The erythrocytes burst releasing the merozoites which invade more erythrocytes thus repeating the cycle and causing fever each time there is the release of merozoites from the erythrocytes (erythrocytic stage).
- Some of these merozoites leave the asexual cycle and develop into the sexual forms called gametocytes.
- These gametocytes enter the mosquito during a blood meal when it bites an infected human and develops into mature sex cells called gametes.
- Ookinetes are formed on fertilization of the female gamete. The ookinetes actively move through the midgut wall of the mosquito and develop into an oocyst inside which several thousands of sporozoites are formed. These sporozoites are released into the body cavity when the oocyst burst.
- The sporozoites then travel to the mosquito's salivary gland and the cycle is completed when the infected mosquito bites a human (Soulard et al., 2015).

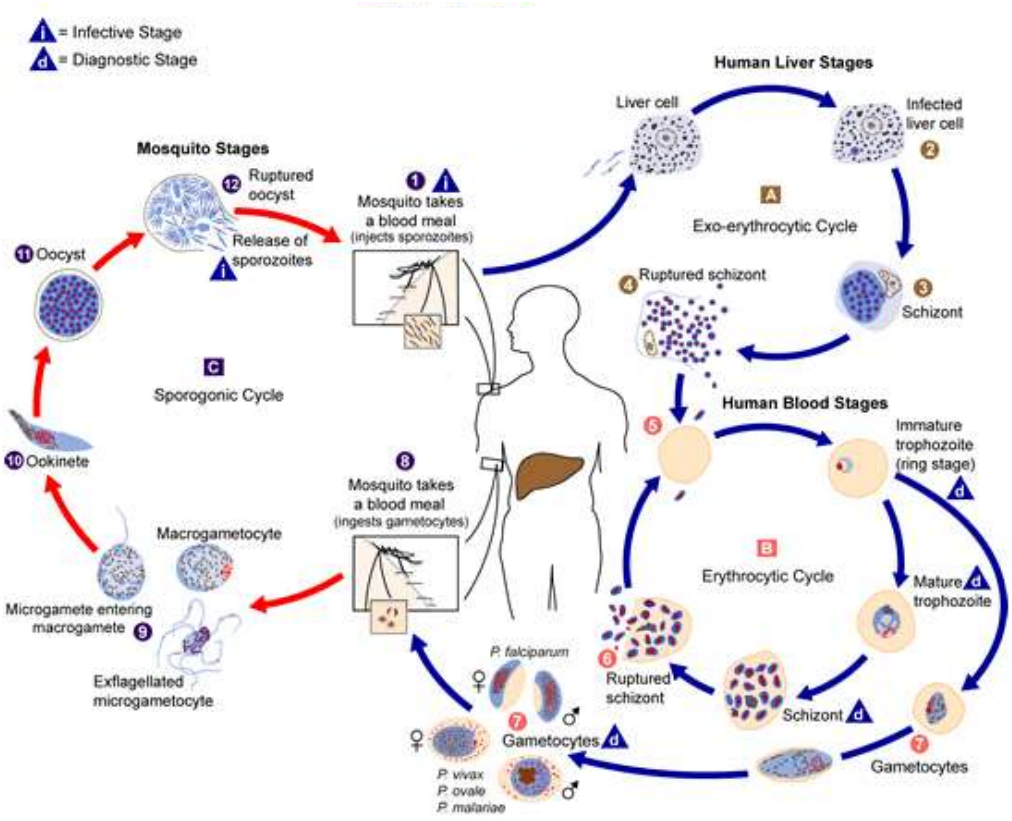

Figure 1.3.1 Life-cycle of malaria parasite.

Sexual and asexual stages of malaria parasite life cycle. Adapted from Centres of Disease Control and Prevention, 2016.

P. vivax and P. ovale have stages in their asexual life cycle in humans (hypnozoites) wherein they remain in a dormant state in liver and can reactivate later. They can invade the blood stream causing relapses. Vertical transmission through the mother (congenital malaria), shared needles, organ transplantation or transfusion are rare modes of malaria transmission from person to person without the involvement of the mosquito vector (Zoller et al., 2009). Figure 1.3.1.1 shows the life cycle of the *Plasmodium* parasite.

1.3.2 **Signs and symptoms of malaria:**

Incubation period of Malaria is between 9 to 30 days depending on the *Plasmodium* species and the patient usually presents with non-specific flu-like syndrome with fever, malaise, headache, myalgias, nausea, vomiting, sometimes diarrhoea or jaundice. Diagnosis or exclusion of malaria should be confirmed by microscopic examination of blood films

(Bartoloni and Zammarchi, 2012). There are three stages in the classical malaria paroxysm lasting for 6 to 10 hours and usually beginning in afternoon or evening:

Cold stage- The patient feels cold and may shiver. The phase usually lasts up to 10 – 30 minutes and the temperature begins to gradually rise usually to 39°C to 41°C
Hot stage- The shivering stops, and the temperature may rise further to hyperpyrexial levels. The skin is hot and dry, the face appears flushed, and patient may suffer from vomiting, diarrhoea, retro-orbital headache, altered consciousness. Convulsions might occur in children. The phase lasts for 2 to 6 hours (Bartoloni and Zammarchi, 2012).
Sweating stage- The phase is characterised by profuse sweating and rapid fall in temperature. The patient feels better but is usually tired and the stage lasts for 2 to 3 hours.
Fever is usually synchronised with schizogony and occurs every alternate day (Tertian) in *P. vivax, P. ovale or P. falciparum* malaria and every third day (Quartan) in *P. malariae* malaria (Ferri, 2009).

P. falciparum is the only species causing severe malaria leading to death by causing acidosis, respiratory distress, severe anaemia, acute renal failure, haemoglobinuria, severe anaemia or shock (Algid malaria), encephalopathy and coma due to cerebral malaria (Bartoloni and Zammarchi, 2012) (Krungkrai et al., 2010). This occurs due to the ability of the *P. falciparum* parasites to sequester in brain and various other organs (Greenwood et al., 2008).

1.4 Malaria prevention, control and treatment:

1.4.1 Malaria vaccines:

Vaccines have been instrumental in reducing the burden of infectious diseases. Vaccines could be attenuated microbes, killed microbes or protein subunits. Repeated exposure to malaria infection gives strain-specific protective acquired immunity people which helps to reduce inflammatory response to the parasite (Artavanis-Tsakonas et al., 2003) (Heppner, 2013). This immunity is ineffective against a different strain (Wang et al., 2009) (Artzy-Randrup et al., 2010). Efforts to develop an effective vaccine against malaria started over six decades ago; however, there is still no licensed vaccine against malaria. Nonetheless, the development of a vaccine against malaria has provided a leading edge for assessing many

new vaccine technologies such as novel adjuvants, vectored prime-boost regimes and the concept community vaccination to prevent transmission of malaria. It has been over 60 years but chemotherapy and insecticides still remain the main tools in the fight against malaria (White, 2004) (Na-Bangchang and Karbwang, 2009). It has proven difficult to develop and administer attenuated whole parasite vaccine. Comparable efficacy has not been observed in subunit vaccines. Malaria vaccines can be classified into three distinct categories:

i. Pre-erythrocytic vaccines:

Sporozoites and hepatic stages of the parasite are the targets for pre-erythrocytic vaccines. They aim to destroy infected liver cells and prevent the emergence of merozoites into the bloodstream (Duffy et al., 2012). The main challenge is the short time frame of two hours within which sporozoites have to reach the liver once injected by the mosquito bite (Mac-Daniel et al., 2014). The pre-erythrocytic stage vaccine candidate RTS/S/AS01 is the most promising to date and has entered the Phase III trial (Tinto et al., 2015) (von Seidlein and Bejon, 2013). The large Phase III trial of RTS,S/ AS01 involving more than 15,000 children over 11 sites in sub-Saharan Africa has had only some successes (Barry and Arnott, 2014). It is still considered effective in averting a substantial number of malaria cases with the European Medicines Agency recommending the use of vaccine in young children in Africa in July 2015 (Takashima et al., 2016).

This vaccine is based on a region of the circumsporozoite protein, fused to the surface antigen of the hepatitis B virus and combined with $AS01_B$ (liposome-based adjuvant) to target the sporozoite stage. RTS,S was found to be moderately efficacious in sub-Saharan Africa with efficacy being 36.3% in children and 25.9% in infants following fourth booster at 20 months, well below the efficacy target set at 75% by WHO (Kurtovic et al., 2019) (Tinto et al, 2015). The vaccine will undergo pilot implementation in Kenya, Malawi and Ghana to evaluate safety and reduction in childhood mortality amid reports of rapidly declining protection after vaccination (Ghana, 2017).

ii. Erythrocytic vaccines or blood-stage vaccines

Asexual reproduction of the parasite in RBCs is the target for erythrocytic vaccines which aim to significantly reduce the number of merozoites and reduce the parasite density. This also reduces the density of gametocytes besides preventing the clinical symptoms (Barry and

Arnott, 2014). The *P. falciparum* erythrocyte membrane protein (PfEMP1) which mediates adhesion of parasite cells to host cells is another target. Most blood-stage vaccines are still undergoing Phase I or II trials (Takashima et al., 2016).

iii. Transmission blocking vaccine (TBV)

Transmission blocking subunit vaccines which target blood-stage merozoites, or gametocytes have also been studied (von Seidlein and Bejon, 2013). Antigens expressed during parasite stages in the mosquito host are the target for transmission blocking vaccines (Barry and Arnott, 2014) (Birkett et al., 2013). Vaccine induced antibodies along with *Plasmodium* gametes are taken up by the mosquito during the blood meal resulting in interference with parasite's development thereby preventing parasite transmission from mosquito to the human host. The Pfs25 protein expressed on the surface of zygotes and ookinetes is one of the targets and Phase I human trial have been conducted with little success using a recombinant Pfs25H/Montanide ISA51 formulation (Jones et al., 2015, Shimp et al., 2013). Detoxified form of *Pseudomonas aeruginosa* exo-protein A (EPA) has been developed as an adjuvant for Pfs25 but its safety and immunogenicity in humans remains to be evaluated (Shimp et al., 2013).

Vaccines targeting early pre-erythrocytic stages have shown most success. The currently available vaccines usually target a single stage of parasite's life cycle. Viral vector vaccines target the intracellular liver-stage of the parasite through cellular immunity and a protein adjuvant vaccine targets the sporozoites through antibodies. But these have only been partially effective in humans. A multi-component vaccine targeting more than one stage of the parasite is required to be more effective against malaria (Hill, 2011). Vaccine candidates with attenuated whole-parasite are highly protective but there are difficulties with manufacturing and administration of these vaccines.

In the absence of any known correlates for immunity, expensive clinical trials in humans remain the only way to evaluate a vaccine's efficacy. Poor immunogenicity in the blood-stage candidates and unlikelihood of any candidate vaccine which targets only a single antigen to provide complete protection has left development of a multistage, multicomponent vaccine to be the only feasible option to achieve success, the possibility of which seems unlikely in near future (Guerin et al., 2002) (Heppner, 2013) (von Seidlein and Bejon, 2013) (Hill, 2011).

1.4.2 **Mosquito control methods:**

Draining of swampland, standing water resources, layering of potholes and puddles were done in mid-20th century to eliminate the *Anopheles* vector by targeting its breeding sites. Insecticide treated bed nets (ITNs) and indoor residual spraying (IRS) are currently the two major strategies for vector control (N'Guessan et al., 2007). Distribution of pyrethroid insecticide treated bed nets has been part of many vector control programmes since 1980s as most *Anopheles* mosquito bites usually occur at night and thus bed nets help to reduce the disease. Pyrethroid insecticides most in use were the ones which killed rather than deflected the mosquitoes and remained active for six months. Long lasting insecticide treated bed nets (LLIN) which remain effective for almost five years have been developed recently.

Mosquitoes which rest up on the walls are the targets for indoor residual spraying (IRS) and a much broader range of insecticide can be used for this purpose. A significant effect has been observed on the disease prevalence due to sustained IRS but the spread of insecticide resistance has emerged as a major challenge for vector control (Nkya et al., 2014). Evolved resistance to one pyrethroid usually gives protection against the whole family.

Some mosquitoes are poor vectors for transmitting malaria as they either lack the essential factor for *Plasmodium* or they attack the parasite. Another method is to genetically engineer mosquitoes in such a way as to reduce or hamper their capacity to transmit malaria. It was in 2000, that the *Anopheles* mosquitoes were successfully genetically transformed for the first time (Grossman et al., 2001).

1.4.3 **DDT and the Malaria Eradication Programme:**

The first samples of DDT (2,2-bis-(p-chlorophenyl)-1,1,l-trichloroethane) were synthesised by Othmar Zeidler in 1874 in the University of Strassburg in the laboratory of Professor Adolf von Baeyer but were left on the shelves for nearly 65 years. DDT was synthesised in 1939 by Paul Müller, in the laboratory of a Swiss dyestuff manufacturer, as an insecticide and this discovery won him the Nobel Prize in 1948 (Metcalf, 1973). DDTs insecticidal properties appeared to be a blessing in disguise in the post-World War II era as it was a cheap synthetic chemical which was apparently safe for humans and persisted long enough on

houses sprayed with DDT to kill mosquitoes even months after application. DDT was first used against malaria by the US Army during World War II as it required only semestrial or annual applications (Najera et al., 2011).

Discovery of DDT in 1939 played an important in the fight against malaria (Sadasivaiah et al., 2007). In 1955, the Global Health Assembly announced eradication of malaria, as the parasite does not have an animal reservoir and effective measures to interfere with the transmission or achieve radical cure existed. Haemoglobin provides amino acids to the parasites and haeme is its toxic by-product. Haeme is biocrystallised to haemozoin (malaria pigment) to detoxify it. Chloroquine acts by accumulating in parasite's food vacuole and interfering with sequestration of haeme (Djimdé et al., 2001) (Hyde, 2007). Malaria eradication programme employed a two-pronged attack against the mosquito and the parasite by using DDT and chloroquine (Dondorp et al., 2010) (Jensen and Mehlhorn, 2009). It involved DDT indoor residual house spraying and mass drug administration programmes with chloroquine and pyrimethamine (Talisuna et al., 2004). This resulted in Europe being free from malaria in 1975 and disease localising in sub-tropical and tropical regions.

37 countries with a population of 728 million were pronounced malaria free by 1972. Another 90 countries were either under complete or partial control as per WHO in 1972 (Metcalf, 1973). But the resistance to DDT soon emerged in house flies and by 1960s, the mosquitoes resistant to DDT effectively interfered with the worldwide eradication of malaria (Ramirez et al., 2009). It was soon evident that DDT was an environmental micro-pollutant and accumulated in the food chain due to its low vapour pressure (1.5×10^{-7} mm at 20^{o}), its high fat solubility, low water solubility and its stability to photo-oxidation (Metcalf, 1973). Use of DDT as an insecticide was eventually banned (Butler et al., 2010).

Due to mosquito vector resistance to DDT, objection of locals to the entry of spray men in their household, increase in exophilic mosquitoes which do not stay indoors long enough to pick up the lethal dose and lack of stable and organisational infrastructure of the vector control programmes, it was realised that in a large number of countries eradication of malaria was an unrealistic goals (Talisuna et al., 2004).

The success of the eradication programme was hence short-lived as environmental concerns were raised due to bioaccumulation of DDT in humans and wildlife, the development of insecticide resistance and development of chloroquine resistance. Resistance to chloroquine is due to multiple mutations on pfcrt gene which encodes the digestive vacuole membrane transporter protein (PfCRT) which progressively diminishes the level of chloroquine inside the food vacuole (White, 2004). Resistance to chloroquine first emerged in Thailand-Cambodia border (1957), South America (1959), and in Africa (1974) leading to the abandonment of the malaria eradication programme in 1972 (Greenwood et al., 2008). This lead to resurgence of the disease and efforts were then directed towards treatment and control of malaria (Carter and Mendis, 2002).

Realising the limitations of the eradication programme, WHO announced the 'Roll Back Malaria' programme in 1998 with an intention to approach malaria by strengthening health services to make effective prevention and treatment services accessible to all who need it. The programme aimed build on past experiences and halve the mortality rate by 2010 and again by 2015 by using existing tools against malaria more effectively (Nabarro, 1999).

1.5 Malaria chemotherapy:

Humankind has suffered since early ages without any specific treatment for malaria until the seventeenth century when a Peruvian tree bark was brought back by the Spanish colonisers from which quinine was later extracted. Medication for malaria (antimalarial drugs) are given either to treat a suspected or confirmed infection, or as prophylaxis to individuals with no immunity travelling to areas endemic to malaria, or as intermittent preventive treatment to certain groups in malaria endemic regions (Franco-Paredes and Santos-Preciado, 2006).

Certain antimalarials such as hydroxychloroquine and chloroquine have been repositioned for use in other diseases such as lupus-associated arthritis and rheumatoid arthritis (Shippey et al., 2018). Benefits for giving combination treatment for malaria are not just increased compliance and decreased side-effects but it also reduces the risk of development of drug resistance (Blasco et al., 2017). It is recommended that confirmation of presence of malaria parasites is done prior to the starting of antimalarial therapy by detection of parasites through

microscopy or through rapid diagnostic tests (RPT) (Moody, 2002). The antimalarials differ in their mechanism of action based on their chemical structure.

1.5.1 **Quinine:**

A fascinating story exists on the discovery of quinine. It was believed that the Spanish realised about the curative power of Peruvian tree when the wife of Spanish viceroy of Peru, Countess of Chinchón, fell ill with an intermittent fever around 1630 and the prefect of Loxa, a city in Ecuador, brought a bark of a locally found tree as a cure which restored the Countess back to health. It was therefore called 'Countess's powder' by local people and was brought to Europe by the Countess and her husband as a treatment for malaria. Unfortunately, the legend is not true as the Countess died in 1625 before her husband moved to Peru. The Count remarried but his second wife had robust good health and died of an epidemic illness in 1641 on her way to Madrid. Nonetheless, for the new binomial system when the bark was sent to Carl Linnaeus in Sweden in the next century for naming, he had heard of the story of the Countess and named the genus of the tree 'Cinchona' after her (Butler et al., 2010). It is still known as the cinchona bark.

The Peru tree bark was actually introduced in Europe by Spanish priests when they brought it to Rome in 1632. It became known as the 'Jesuits bark' and the interest of Cardinal Juan de Lugo facilitated its widespread use in Europe. Due to its connection with the Roman Catholic Church, Protestant England was a bit wary of the use of the bark but when it cured King Charles II tertian fever, it began to be more widely accepted and was included in the London Pharmacopoeia in 1677 as *Cortex peruanus*. The British and the Dutch introduced it in India and in 1765 James Lind in Calcutta proved that full doses of the drug are required to achieve best results. The crude bark was used for 200 years for preparing powders and infusions. It was only in 1820, the two basic alkaloids 'quinine and cinchonine' were isolated by the French chemists Pierre Pelletier and Joseph Caventou (Kyle and Shampe, 1974). Following the isolation of two other alkaloids 'quinidine and cinchonidine', factories were set up in many parts of the world for the production of cinchona bark alkaloids.

The production was insufficient to meet the demand and attempts were made to cultivate cinchona plantations in other parts of the world. In 1864, the Dutch started cinchona

cultivation in Java with the help of botanist Justus Hasskarl and the British established cultivations in Ceylon and Nilgiri hills in India, but these seedlings had low yield in quinine. It was the British collector Charles Ledger who sold the high quality seeds, which he obtained with huge difficulty from Bolivia, to the Dutch and within 50 years the Dutch plantations in Java were producing 97% of the world's quinine (Kitchen et al., 2006).

Quinine and its derivatives are still often used in acute cases of malaria and in areas where high levels of resistance is observed against other antimalarials (Achan et al., 2011). It is also used as post-exposure treatment in individuals who have travelled to malaria endemic regions (Tan et al., 2011). It is an alkaloid which acts on the blood schizont stages and has weak gametocidal properties. It accumulates in the food vacuoles and causes aggregation of haeme which is cytotoxic in nature. It does this by preventing the crystallisation of haeme into haemozoin, a process known as haemozoin-biocrystallisation (Hempelmann, 2007) (Fong and Wright, 2013).

Quinine could be given orally, intramuscularly or intravenously and WHO recommends in cases sensitive to quinine, it could be given 20 mg/kg initially followed by 8 mg/kg three times a day for 5 to 7 days in combination with doxycycline, clindamycin or tetracycline (Lalloo et al., 2016). Quinine stimulates insulin secretion and can result in hypoglycaemia. Hence, it is imperative to observe blood glucose levels every 4 to 6 hours in patients receiving quinine (Gribble et al., 2000). 'Cinchonism' is a syndrome characterised by tinnitus, nausea, vomiting, rashes, vertigo and abdominal pain. It can occur during quinine therapy. Neurological effects such as delirium, confusion or coma could also be seen as quinine also affects the excitability of motor neuron end plates. Respiratory and renal failure could also result during quinine therapy (Kuhlmann and Fleckenstein, 2017).

Commonly related compounds are also used as antimalarials. Warburg's tincture, with quinine as its main ingredient was developed for use as an antimalarial in 1834 by Carl Warburg (Maclean, 1875). Quinidine, a diastereoisomer with similar properties to quinine, and 'quinimax', a slightly more effective combination of quinine, quinidine, cinchonine and cinchonidine are also presently used (Sharma et al., 2015). Figure 1.5.1 shows the chemical structures quinine and its analogues.

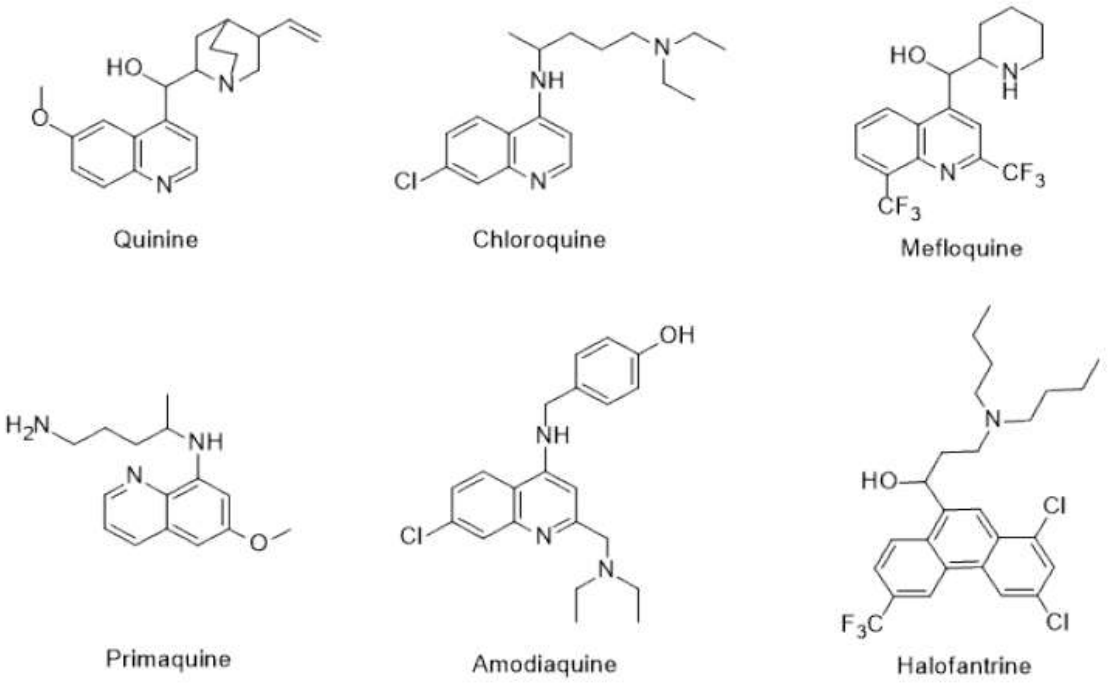

Figure 1.5.1 Chemical structure of quinine and its analogues (Na-Bangchang and Karbwang, 2009) (Butler et al., 2010)

1.5.2 **Alternatives to quinine: mepacrine and chloroquine:**

The Germans developed a synthetic alternative ‘mepacrine’ as they were unable to obtain quinine for the German soldiers during the world wars (Bruce-Chwatt, 1964). Mepacrine is a version of quinine with an acridine ring system rather than quinoline. Mepacrine was also manufactured in the USA, which was given to American soldiers during the Second World War as prophylaxis. When Japan entered the world war, the supply of quinine from Java was cut off and the Japanese realised the potential of malaria as a killer. They spread the propaganda against mepacrine using Japanese–American broadcaster known as ‘Tokyo Rose’ (a name given by Americans to a number of English speaking Japanese broadcasters) that intake of the drug causes skin to become yellowish, which was true, and also causes sterility, which was incorrect. Thus the American soldiers stopped using mepacrine and fell victim to malaria.

America responded by developing a chemical variant of sontoquine, another anti-malarial drug developed by Germans and obtained by Americans in North Africa from prisoners of

war. This chemical variant was more effective than mepacrine and sontoquine against malaria parasite, with apparently no adverse side effects and was easy to manufacture. Chloroquine was thus born and it played an important role in the world war against Japan (Butler et al., 2010).

Chloroquine, a quinolone-containing drug was highly successful against malaria and its mode of action was accumulation in the acidic food vacuoles of intra-erythrocytic trophozoites by a weak base mechanism. It prevents the degradation of haeme to haemozoin occurring in the food vacuoles by increasing the internal pH. Haeme which is toxic to the malaria parasite results in its killing (Slater, 1993). It is also believed that production of nucleic acids are affected in parasites due to formation of chloroquine-haeme or chloroquine-DNA complexes (Surolia and Padmanaban, 1991). Chloroquine has schizonticidal and gametocidal properties against *P. vivax*, *P. malariae*, and *P. ovale* (Williams et al., 2003). WHO recommends an initial dose of 10 mg/kg followed by 5 mg/kg after 6 to 8 hours and then 5 mg/kg for the next 2 days. Chloroquine can also be given in a single dose of 5 mg/kg/week as a prophylactic treatment for individuals travelling to areas affected by *P. vivax* and chloroquine sensitive *P. falciparum* strains (Organization, 1995).

The effectiveness of chloroquine has decreased due to the emergence of resistance but it is still used in sub-Saharan regions, mainly in combination with other antimalarials (Winstanley et al., 2004). It is one of the safest drugs available compared to other antimalarials although it can cause itching and could be a provocation factor for psoriasis (Olsen, 1981). It does not have teratogenic or abortifacient properties and can be safely administered during pregnancy (Wolfe and Cordero, 1985).

1.5.3 **Amodiaquine:**

It is a 4-aminoquinolone, similar to chloroquine (Figure 1.5.1) in mechanism of action and structure, causes less side-effects and is recommended by WHO as a combination therapy with artesunate in areas with chloroquine resistance. It is usually given 25 mg/kg for 3 days (WHO, 2015).

1.5.4 **Mefloquine:**

Mefloquine and halofantrine, the two aryl amino alcohols discovered in Walter Reed Army Institute of Research (WRA) were granted FDA approval by 1989 and 1992, respectively (Croft, 2007). Reports of neuropsychiatric disturbances and cardiotoxicity, emergence of resistance due to its similarity to quinolones and high costs limited their use especially in Africa (Na-Bangchang and Karbwang, 2009) (Ridley, 2002). Mefloquine is structurally similar to chloroquine and has schizonticidal activity (Thompson et al., 2007). It damages the food vacuoles by formation of haeme complexes which are toxic to the parasite. Recommended dose is 15 – 25 mg/kg and can be given for the treatment of acute infection or for prophylaxis. It is used in resistant *P. falciparum* strains. Side-effects include vomiting, diarrhoea and oesophagitis. It can also cause sleep disturbances, anxiety disorders, delirium, bradycardia and sinus arrhythmia. Mefloquine can be safely administered in all trimesters in pregnancy (Schlagenhauf et al., 2012).

1.5.5 **Primaquine:**

Another potent class of antimalarials was discovered during the 30 years between the World Wars I and II. In 1925, pamaquine or plasmochin, an 8-aminoquinoline was found to be effective against the gametocytes of the malaria parasites when it was used along with quinine and could prevent the relapse of *Plasmodium vivax* infection. But it was not effective as a blood schizontocide and its high toxicity led to pamaquine being abandoned for its therapeutic use. In 1946, a safer synthetic 8 aminoquinoline SN-13,272 was developed in United States by Elderfield and co-workers, which was named Primaquine. Due to its high efficacy and low toxicity as a gametocytocide, primaquine was employed primarily as a transmission blocking antimalarial and also as a tissue schizontocide (Vale et al., 2009). Primaquine can cause haemolysis in humans with glucose-6 phosphate dehydrogenase (G6PD) deficiency, a genetic condition more commonly found in African men.

Primaquine, an 8-aminoquinolone, acts by blocking the oxidative metabolism in malaria parasite. It can cure both acute infections and relapsing ones as well (Baird and Hoffman, 2004). It is effective on the erythrocytic stages in asexual cycle, gametocytes and also on hypnozoites of *P. vivax* and *P. ovale*. Recommended dose is 0.15 mg/kg for 14 days in cases

of relapse in *P. vivax* and *P. ovale* and 0.75 mg/kg single dose for gametocidal effect. It can cause nausea, vomiting, anaemia, abdominal pain and granulocytopenia (Martins et al., 2015).

1.5.6 **Anti-folate antimalarials:**

Anti-folates, originally developed as the treatment for cancer due to their action on rapidly dividing cells, helped stall the resurgence of malaria. In 1945 during the Second World War, proguanil was found to be effective against malaria (Nzila, 2006). This lead to the development of drugs such as pyrimethamine and cycloguanil which target dihydrofolate reductase (DHFR) enzyme, and sulpha drugs (supladoxine, sulfalene, dulfone and dapsone) which target dihydropteroate synthetase (DHPS) enzyme in the folate synthesis pathway. The combination of DHFR inhibitors and DHPS inhibitors was found to be synergistic and more effective than its respective monotherapy (Gregson and Plowe, 2005). These drugs results in reduced folate co-factors which impairs DNA synthesis in rapidly multiplying parasites during the erythrocytic cycle (Hyde, 2005) (Hyde, 2007). The combination therapy replaced chloroquine therapy as the first line of treatment in late 1980s until the resistance began to emerge (Miller and Su, 2011) (Koram et al., 2005) (Ratcliff et al., 2007).

1.5.7 **Pyrimethamine:**

Pyrimethamine (Figure 1.5.2) is a dihydrofolate reductase inhibitor which affects the DNA replication, cell division and reproduction by preventing the formation of purines and pyrimidines (Sienkiewicz et al., 2008). It is used in combination with a sulphonamide in chloroquine-resistant strains (Chin et al., 1966). DHFR inhibitor drugs are used in other diseases as well, such as methotrexate in cancer and trimethoprim in bacterial infections.

1.5.8 **Proguanil:**

Proguanil, a synthetic derivative of pyrimidine, developed in 1945 is a biguanide which upon administration is converted to the active metabolite cycloguanil by the dihydrofolate reductase enzyme in *P. falciparum*, *P. vivax* and *P. ovale* (Gelband et al., 2004). It is active in the primary tissue stages and has a weak schizonticidal activity. Recommended dose is 3

mg/kg per day. It can also be given with atovaquone and chloroquine as prophylaxis (Overbosch et al., 2001). Figure 1.5.2 shows the chemical structures of proguanil, cycloguanil and pyrimethamine.

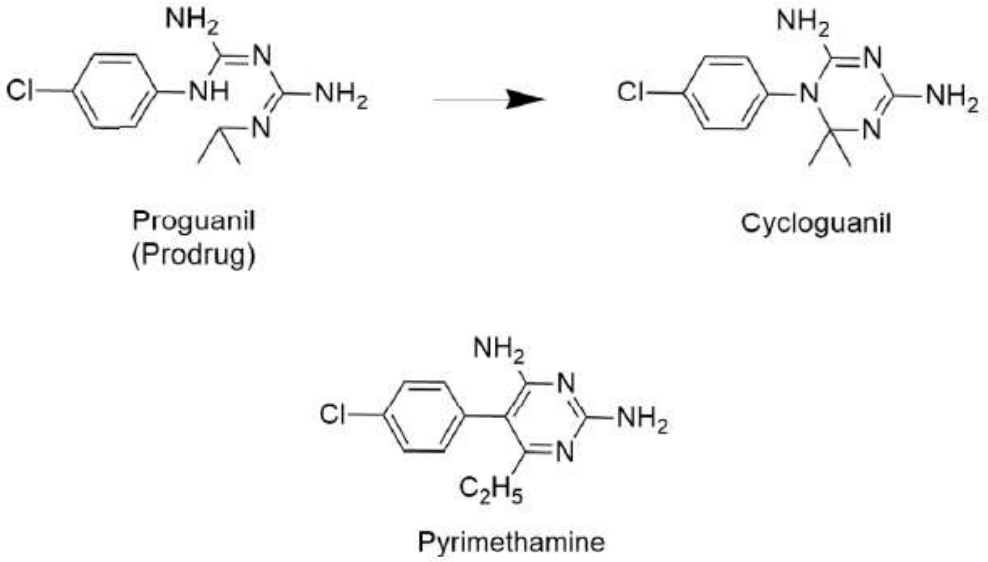

Figure 1.5.2 Chemical structures of pyrimethamine, the prodrug proguanil and its active metabolite cycloguanil (Sienkiewicz et al., 2008) (Gelband et al., 2004).

Combination of sulphadoxine and pyrimethamine (SP) came to be used as an alternative antimalarial due to widespread chloroquine resistance. The parasite soon developed resistance to this combination resulting in lowering the drug binding affinity to the parasite enzymes involved in the obligatory parasite-folate biosynthesis pathway. Mutations in the gene for parasite enzyme dihydrofolate reductase are responsible for pyrimethamine resistance and mutations in the gene for parasite enzyme dihydropteroate synthetase are attributed to sulphadoxine resistance (Mbugi et al., 2006). Triple mutation on dhfr gene and double mutation on dhps gene results in treatment failure (Gregson and Plowe, 2005) (White, 2004). Pattern of emergence and spread of resistance to anti-folate drugs was similar to chloroquine resistance with emergence in South America and South-East Asia, independently, and then the spread to Africa (Plowe, 2009).

1.5.9 **Sulfonamides:**

Sulfamethoxypyridazine and sulfadoxin are structural analogue of p-aminobenzoic acid (PABA) and acts on the folate synthesis pathway by inhibiting dihydropteroate synthetase enzyme. It competes with PABA and prevents the production of dihydrofolic acid (de Beer et al., 2006). Fansidar is available as a synergistic combination of sulfadoxin and pyrimethamine (Bojang et al., 1998).

1.5.10 **Atovaquone:**

Malarone is the synergistic combination of atovaquone with proguanil and is used against *P. falciparum* for treatment as well as for prophylaxis (Looareesuwan et al., 1999). Mepron is a liquid oral suspension of atovaquone (Baggish and Hill, 2002).

1.5.11 **Artemisinin:**

During the Vietnam War, a cultural revolution took place in China as they supported the North Vietnamese in the war against the United States. Malaria was a big problem in the war zone with a rise in chloroquine resistant *Plasmodium falciparum* cases. On-going research work on both sides led to the discovery of mefloquine in the US, and in China a secret nationwide program called the Project 523 was started in 1967 which recruited over 500 scientists in ~60 different laboratories and institutes. The project's short term goal was to come up with an antimalarial for immediate use in the battlefield, with a long term goal of discovering new antimalarial drugs by screening synthetic chemicals and investigating the ancient recipes and practices of traditional Chinese medicine (Miller and Su, 2011). The turning point came when one of the research groups, headed by Professor Youyou Tu, discovered that extracts from *Artemisia annua* or the sweet wormwood, were very effective against inhibiting the parasite growth which led to further investigations. On 4th October 1971, the group isolated a non-toxic, neutral extract from the plant which was 100% effective again *Plasmodium berghei* in mice and *Plasmodium cynomolgi* in monkeys. Following this success, trials were carried out in patients infected with *Plasmodium vivax* and *Plasmodium falciparum* to determine clinical efficacy which showed reduced blood parasite levels and disappearance of symptoms as compared to patients on chloroquine. In 1972, a colourless,

crystalline substance with a molecular formula $C_{15}H_{22}O_5$, molecular weight of 282 Da and a melting point of 156-157°C was isolated as the active ingredient of the extract. It was named 'quinhaosu' in Chinese, known in the rest of the world as 'artemisinin' (Tu, 2011). But it was only in 1980s that the world noticed the efficacy of artemisinin against malaria. Professor Youyou Tu was awarded the 2015 Nobel Prize in Physiology or Medicine for her work in discovery of artemisinin (Su and Miller, 2015).

Artemisinin is a sesquiterpene lactone with a peroxide-bridge linkage and is derived from the plant *Artemisia annua*. It has been used in Chinese herbal medicine as a treatment for fever for over 1000 years (Brown, 2010) predating the western world's use of quinine. Ge Hong documented the use of artemisinin in his book Zhou Hou Bei Ji Fang (A handbook of prescriptions for emergencies) in 340 AD. Artemisinin was extracted by Ge Hong using a simple macerate (Yarnell, 2014). It was suggested by the first studies on mechanism of action of artemisinin that 1,2,4 trioxanes generate toxic reactive oxygen species (ROS) in presence of iron. There are two other models which have been suggested to explain the mechanism of action since the initial theory and these differ based on their dependency on iron and involvement of carbon centred radicals (Cui and Su, 2009).

Currently there are four compounds in use; artemisinin, the parent compound and its more active derivatives, the water-soluble hemisuccinate: artesunate, oil-soluble ethers: arteether and artemether. All these compounds are readily metabolised to dihydroartemisinin, which is the biologically active metabolite. Figure 1.5.3 shows the chemical structures artemisinin and its analogues.

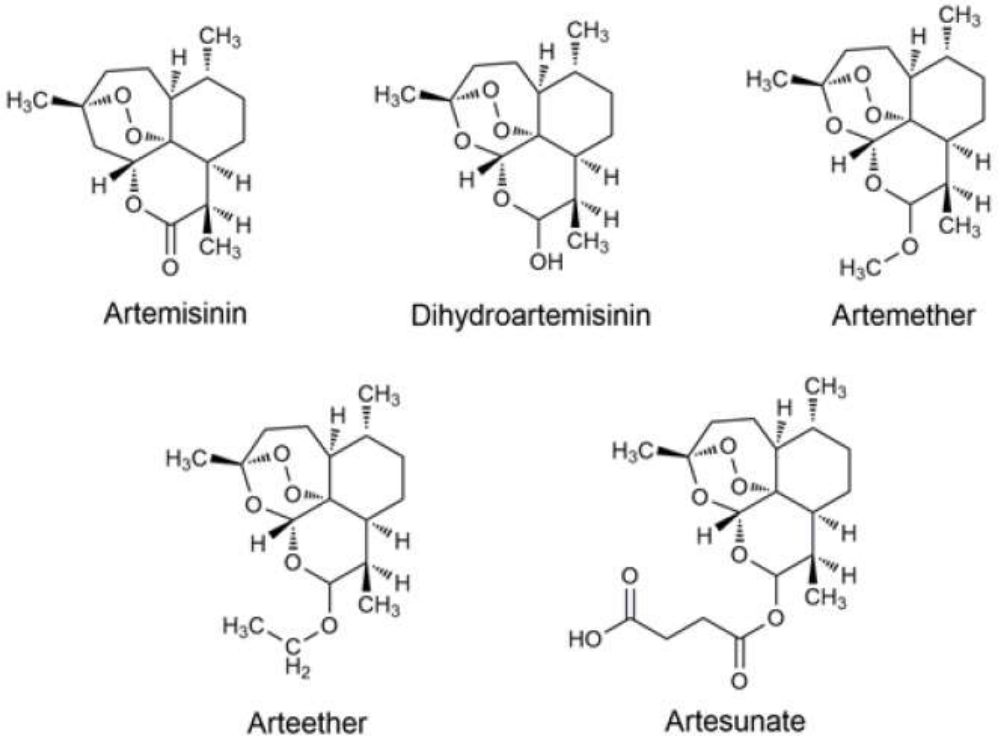

Figure 1.5.3 Chemical structures of artemisinin and analogues (Tu, 2011) (Brown, 2010).

i. *Artemsinin:*

It is used to treat acute infections and rapidly clears the parasites from the blood. Recommended dose is 20 mg/kg on the first day followed by 10 mg/kg for the next 5 days. Side effects usually observed are headaches, nausea, vomiting, dark coloured urine and occasional non-specific ST changes.

ii. *Artemether (methyl ether):*

It is a semi-synthetic derivative of artemisinin which is converted in the body to active metabolite dihydroartemisinin. It is used in combination therapy to treat resistant cases of *P. falciparum*. Recommended dose is 4 mg/kg for 3 days and 1.6 mg/kg for the next 4 days.

iii. *Artesunate:*

It is a hemisuccinate derivative of dihydroartemisinin and is used in combination therapy in a 5 or 7 day course usually with mefloquine. Recommended dose is 4 mg/kg for the first 3 days and 2 mg/kg afterwards. No adverse side-effects have been observed.

iv. Arteether (ethyl ether):

It is a semi-synthetic derivative of artemisinin and converts to the active metabolite dihydroartemisinin in the body. It is administered intramuscularly and recommended dose is 150 mg/kg/day for 3 days.

v. Dihydroartemisinin:

It is the active metabolite, and has gametocidal and schizonticidal activity. Recommended dose is 4 mg/kg on first day and then 2 mg/kg for the next 6 days. No adverse side-effects have been observed.

1.5.12 **Halofantrine:**

Halofantrine is structurally related to quinine (Figure 1.5.1) and was developed in 1960s by Walter Reed Army Institute of Research (Croft, 2007). It belongs to the class of phenanthrene compounds and acts by damaging the parasite membranes by forming cytotoxic complexes with ferritoporphyrin XI. Its use is limited due to the high costs and the potential of cardiotoxicity due to prolongation of QT interval. Recommended dose is 8 mg/kg. Lumefantrine, which is related to halofantrine is used in combination therapy with other antimalarials (Byakika-Kibwika et al., 2011).

1.5.13 **Doxycycline:**

Doxycycline is an oxytetracycline derivative and is one of the most widely used drugs in malaria (Tan et al., 2011). It inhibits protein synthesis by binding to the 30S ribosomal unit. It can be used in combination with quinine to treat acute cases of *P. falciparum* resistant strains and for chemoprophylaxis in chloroquine resistant cases. Recommended dose is 100 mg per day for 7 days in combination with a fast acting antimalarial for acute infections (Tan et al., 2011). Tetracycline in doses of 250 mg can be used in combination with other antimalarials for treatment of infection. These drugs can cause enamel hypoplasia and depression of bone growth. Hence it is not used in pregnant or lactating women and children under 8 years of age. It is also not used in patients suffering from liver dysfunction.

1.5.14 **Clindamycin:**

Clindamycin is a lincomycin derivative and has a slow action. It can be used in combination with quinine at 300 mg four times a day for 5 days (Obonyo and Juma, 2012). It can cause nausea, vomiting and abdominal pain.

1.6 Combination therapies:

Drugs can be used in combinations and have been found to be effective in inflammation, cancer and type 2 diabetes (Feala et al., 2010) (Yin et al., 2014). Simultaneous use of two drugs could produce synergistic or antagonistic effects (Yeh et al., 2009). An enhanced effect could sometimes be elicited from the combination of two or more drugs with similar activity. Synergy is when this enhanced effect produced by drugs in combination is greater that their individual potencies. It allows for dose reduction and possibly reduction in adverse reactions as well (Tallarida, 2011).

Synergy between codeine and paracetamol leads to an increased analgesic effect (Mattia and Coluzzi, 2015). Anti-bacterial resistance could be overcome by synergistic effect of clauvulanic acid with amoxicillin (Matsuura et al., 1980). Administration of combination therapy is a successful way for combating antimalarial resistance. Two or more schizonticidal drugs having different biochemical targets with a mechanism of action independent of each other are given in a combination therapy (Agarwal et al., 2017). High throughput screening for synergistic drugs have a low hit rate (<10%) (Borisy et al., 2003) (Roy, 2018). The expense of combination therapy is however, 10 times more than using the drugs in mono-therapy. The combinations could be artemisinin-based or non-artemisinin based. They could be given as two separate drugs or could be administered as a single tablet which has both drugs in a fixed-ratio co-formulated into one tablet. Chloroquine is the drug of choice for *P. vivax* except in the regions with high prevalence of chloroquine resistance. ACTs are the recommended treatment for uncomplicated *P. falciparum* cases. In pregnant women, ACTs such as artesunate plus clindamycin for 7 days or quinine with clindamycin for 7 days is recommended by WHO guidelines. Dapsone, primaquine and tetracyclines should be avoided in lactating women and young children (Phillips-Howard and Wood, 1996). A minimum of 24 hours of parenteral treatment with intramuscular or intravenous artesunate or quinine as a

possible alternative should be administered in severe cases of *P. falciparum* malaria. It should be followed by ACT such a clindamycin or doxycycline with artesunate. Quinine could be used as an alternative in the absence of artesunate.

New anti-malarial drug policies (ADMPs) were adopted by many countries in view of the widespread resistance of malaria parasite to commonly available drugs. The most preferred is the artemsinin-based combination therapies (ACTs) due to their enhanced efficacy and their potential to reduce the rate of emergence and spread of resistance. WHO Expert Consultative Group in 2001 recommended four ACTs: artemether-lumefantrine (Coartem), artesunate-mefloquine, artesunate-amodiaquine and artesunate-sulfadoxine/pyrimethamine. Progression to severe disease and malaria mortality rate can be controlled by treating early cases of uncomplicated malaria by ACTs due to their rapid parasite clearance time (Mutabingwa, 2005).

1.6.1 **Non-artemisinin-based combination therapies:**

Fansidar (Sulphadoxine-pyrimethamine): It is a fixed dose combination with both drugs acting on the folate pathway (Salako et al., 1990). It is not recommended to use fansidar alone for treatment of malaria caused by *P. falciparum*.

Fansidar plus chloroquine: It is used only in few areas due to high levels of resistance.

Fansidar plus amodiaquine: Clinical recovery is fast but ACTs are preferred.

Fansidar plus mefloquine (Fansimef): Widespread resistance implies the drug is used only in few areas (Ellis-Pegler et al., 1988).

Quinine plus doxycycline/tetracycline: In addition to side-effects such as ‘cinchonism’ and contraindication of tetracyclines in children and lactating women, the complicated 7 day regime of quinine 10 mg/kg every 8 hours and tetracyclines 4 mg/kg every 6 hours has made this combination a less popular option (Newton et al., 2005).

1.6.2 **Artemisinin-based combination therapy (ACTs):**

Due to the multi-modal mechanism of action, transmission blocking properties and rapid clearance of parasites from blood, artemisinin is a useful drug and is recommended only in combination therapy to prevent emergence of resistance against it. Emergence of resistance to artemisinin has been reported but the data available is limited (Lim et al., 2009).

Artesunate with amodiaquine (Coarsucam or ASAQ): It can cause neutropenia in certain cases but is recommended as one of the treatments for uncomplicated *P. falciparum* malaria.

Artesunate and mefloquine (Artequin or ASMQ): Mefloquine has a long half-life and could result in a high-selection pressure on parasites thus facilitating resistance. WHO recommends this combination as one of the treatments for uncomplicated cases of *P. falciparum* malaria.

Artemether and Lumefantrine (Coartem, Riamet, Amatem, Faverid, Lonart or AL): Side-effects are very few and its availability in fixed-dose formulation gives it a good compliance rate. It is widely used to manage uncomplicated *P. falciparum* malaria cases.

Artesunate with sulphadoxin/pyrimethamine (Airplus or Amalar plus): It is one of the WHO recommended treatment for uncomplicated *P. falciparum* malaria, but the resistance to sulphadoxin/pyrimethamine limits its use (Adam et al., 2006).

Dihydroartemisinin-piperaquine (Duo-Cotecxin or Artekin): It has shown high efficacy in the treatment of uncomplicated *P. falciparum* malaria.

Pyronaridine and artesunate (Pyramax): The only ACT approved by the European Medicines Agency (EMA) for its quality, safety and efficacy in the treatment of both *P. falciparum* and *P. vivax*, it was developed by Medicines for Malaria Venture (MMV) and Shin Poong Pharmaceutical (Roth et al., 2018).

Artesunate with chlorproguanil-dapsone (CDA): It is efficacious but can cause haemolysis in patients suffering from glucose-6-phosphate dehydrogenase (G6PD) deficiency (Premji et al., 2009).

Fast elimination of malaria through source eradication (FEMSE) is a protocol found to drastically reduce the number cases of malaria (Feng et al., 2016). Three doses of artequick (fixed-dosed combination of artemisinin (80 mg), piperaquine (400 mg) and primaquine (4 mg)) are given with a month between each dose and primaquine is administered with the first dose as per the protocol.

1.7 Development of resistance:

Due to the absence of a currently available or under development therapy to provide total protection against malaria, the emergence and spread of antimalarial resistance is a serious threat to public health. The rate of development of new drugs or therapies for malaria lags far behind the rate of emergence of resistance (Ashley et al., 2014). Careful usage of the available drugs is a necessity to control the development of resistance as the development of new drugs or therapies is expensive and the population in need of these drugs live in some of the poorest regions of the world (Vestergaard and Ringwald, 2007). Sound primary care structure with necessary supplies and adequately trained staff are imperative for effective prevention and control (Alonso et al., 2011). This is a major concern as most malaria endemic countries have inadequate fundamental health care structure (Ricci, 2012). Resistance to antimalarials is not uncommon. Besides drug resistance, treatment failure could be due to a number of issues such as non-compliance, interaction with other co-administered drugs, improper diagnosis, poor quality of the drugs, incorrect dosage and improper absorption. These factors could also lead to the emergence of drug resistance (Klein, 2013).

Initial reports of chloroquine resistance started emerging almost 6 decades ago and by late 1980s resistance to sulphadoxine-pyrimethamine and mefloquine were also reported in Thai-Cambodia and Thai-Myanmar. Resistance to chloroquine emerged in 1957 in Thailand (Hanboonkunupakarn and White, 2016) and was attributed to development of an efflux mechanism by the parasite to remove chloroquine, leading to inefficient levels of drug to cause an effective inhibition of haeme polymerisation. The resistance could be reduced by addition of compounds which stop the efflux (Henry et al., 2006). A similar mechanism is responsible for the development of resistance to amodiaquine, mefloquine, halofantrine and quinine (Cui et al., 2015). Resistance to anti-folates, sulphadoxin and pyrimethamine is attributed to two gene mutations in the folate synthesis pathway (Heinberg and Kirkman,

2015). Resistance to atovaquone is believed to be due to a cytochrome-b single-point gene mutation (Peters et al., 2002). Resistance in the parasite could develop due to spontaneous single-point or multiple mutations reducing the drug sensitivity and providing an evolutionary benefit to the parasite. Some parasites with resistant alleles survive even if the mutation proves fatal for most of the parasites in a population. Selection of these resistant parasites over a long period of time establishes the resistance firmly (Plowe, 2009). Table 1.7.1 shows the year on introduction of the antimalarial and the year that the resistance was first reported.

Table 1.7.1 The year of introduction of the anti-malarial drug and the year resistance was first reported (Wongsrichanalai et al., 2002)

Antimalarial drug	Introduced	Resistance first reported	Difference in years
Quinine	1632	1910	278
Chloroquine	1945	1957	12
Proguanil	1948	1949	1
Sulfadoxin-Pyrimethamine	1967	1967	0
Mefloquine	1977	1982	5
Atovaquone	1996	1996	0

1.8 Spread of resistance:

Various factors from economics to parasite and vector biology, and human behaviour to pharmacokinetics of drugs could lead to the spread of resistance (Olasehinde et al., 2015). Resistance could emerge due to a number of reasons which lead to the survival of the parasite in the presence of an antimalarial. This could happen when the host's immune system is compromised or in cases of non-compliance with treatment. Drugs with longer half-live can cause periods where the drug concentration is low leading to development of resistance. Cross-resistance could emerge for antimalarials with similar chemical structures such as amodiaquine and chloroquine (Croft et al., 2012).

Countless lives have been saved by the use of artemisinins but resistance has started to emerge in Thailand-Cambodia border which is the historical epicentre for the emergence of multidrug resistance. Resistance has also been observed at the Myanmar-Thailand, China–Myanmar borders and a province of Vietnam (Dondorp et al., 2010) (Ioset and Kaur, 2009).

It is believed the resistant population of parasites were able to emerge here and establish due to poor compliance with treatment, use of sub-lethal doses and low malaria transmission leading to ideal conditions for high drug pressure in this area which resulted in emergence of resistance to chloroquine (1957), sulfadoxine/pyrimethamine (1982) and mefloquine (1990s) (Alker et al., 2007) (Dondorp et al., 2010) (Krungkrai et al., 2010) (Plowe, 2009). Development of resistance to artemisinin was perceived to be difficult due to the rapid parasite clearance times and short half-life but recently slower parasite clearance in the presence of adequate drug concentrations and re-emergence of parasites after 28 days of treatment have been observed (Krungkrai et al., 2010) (Noedl et al., 2008). Artemisinin-resistant parasites could be identified by using specific region of the kelch gene (K13) as a genetic marker. Artemisinin resistant *P. falciparum* parasites have been identified using the K13 marker in Myanmar, just 25 km from the Indian border (Tun et al., 2015). It is vital to prevent the spread of resistance to high transmission areas such as the Indian border which has historically served as the gateway to the global spread of antimalarial drug resistance (Bhattarao et al., 2007) (Miller and Su, 2011) (Obonyo and Juma, 2012).

The need for anti-malarial therapy could be decreased and spread of resistance could be countered by preventing the transmission of parasites with resistant alleles and by preventing the transmission of malaria infections. Chemoprophylaxis to travellers, mosquito repellents, insecticide treated bed-nets, indoor residual spraying, swamp draining and other environmental methods are effective in preventing the transmission of parasites (Dondorp et al., 2017). Development of a malaria vaccine could result in enormous public health benefits as it could not only limit the transmission of gametocytes but also the onset of malaria infection. Antimalarial chemotherapy could be given in addition to the vaccine to limit the emergence of vaccine resistance (Lorenz et al., 2014). Currently there are no drugs in the pipeline to replace artemisinins hence strategies such as identification of all cases of artemisinin resistance, use of artemisinin-based combination therapy, impregnated bed nets and mosquito control methods, education of local communities on risk of using counterfeit drugs and reduction of drug pressure in affected areas have been employed to contain the spread of artemisinin resistance (Ioset and Kaur, 2009) (WHO, 2010). Figure 1.8.1 shows the geographical distribution of drug resistant *P. falciparum*.

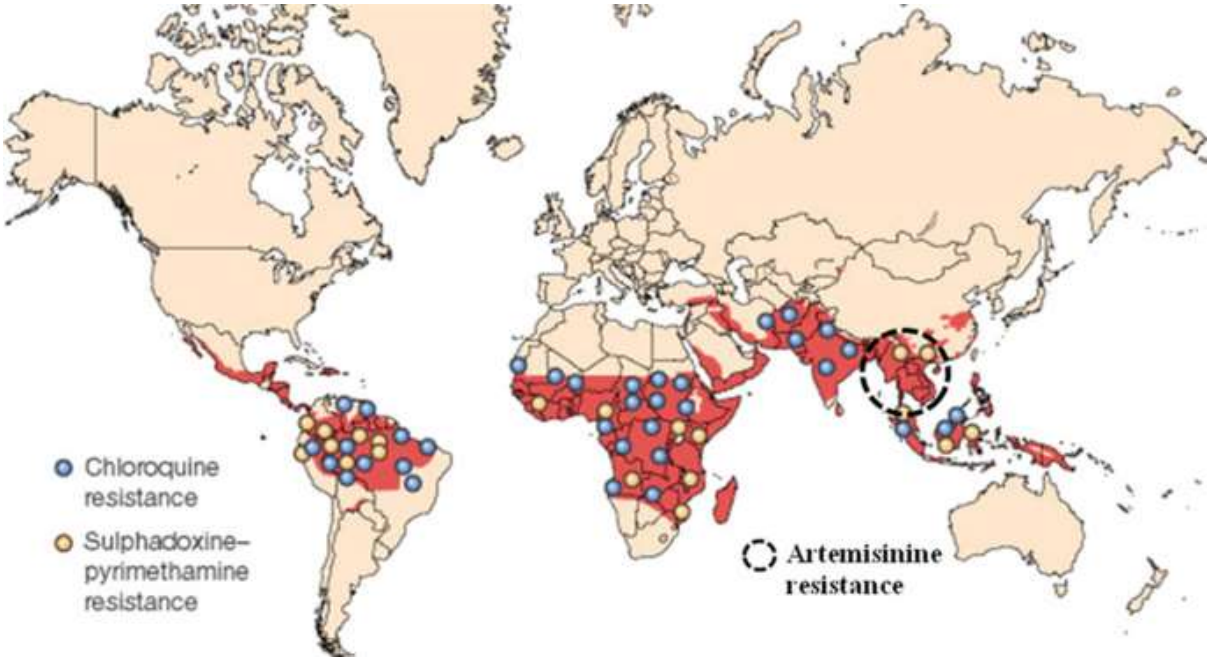

Figure 1.8.1 Geographic distribution of antimalarial drug resistant *P. falciparum*.
Blue and yellow circles represent the resistance to chloroquine and sulphadoxine-pyrimethamine respectively. The black circular dash area represents artemisinin resistance, spreading over Southeast Asia, from Vietnam to Myanmar in 2014. Source: (Krungkrai and Krungkrai, 2016)

1.9 Malaria today:

Pyrethroids remains an important component of control programmes for indoor residual spraying (IRS). Insecticide treated bed nets (ITN) and long-lasting insecticide treated bed nets (LLITN), with a 3-year lifespan, have been instrumental in malaria prevention in recent years. Careful monitoring and insecticide rotation for IRS are vital as there is already resistance to pyrethroids in the field (WHO, 2013).

Avoidance of pharmacokinetic mismatch of current combinations is imperative (Kremsner and Krishna, 2004) (Nandakumar et al., 2006) (Ramharter et al., 2003). Combination of a fast-acting compound with a slow-acting compound was though to provide dissimilar killing profile of each drug in the combination and reduce the chances of recrudescent infections. However, in such a combination the longer plasma half-life partner is left exposed towards the end of the treatment regime and its sub-lethal concentrations may lead to the selection of drug resistant mutants (Na-Bangchang and Karbwang, 2009) (Dondorp et al., 2010) (Koram et al., 2005) (Walsh et al., 2007). Antimalarial drug discovery has been a challenging

endeavour as longevity of second-generation compounds is a formidable concern due to resistance against the parent molecules.

1.10 Drug discovery:

Although there is no genetic inheritance or mutation in the process of drug discovery, it still draws many parallels with the selection processes of evolution. With a high rate of attrition, through a meticulous selection process only a handful of medicines, from countless potential candidate molecules become successful (Warren, 2011). Many new drugs are developed by modifying the earlier designs and are referred to as first, second or third generation products.

A number of natural products have potent anti-inflammatory, anti-infective, anti-oxidative and anti-carcinogenic properties and have served as a source for effective synthetic and semisynthetic lead compounds (Ramana et al., 2014). Since historical times, medicinal plants or minerals were the main source of therapeutic drugs (Takenaka, 2001). Serendipity of the medicinal chemist in the nineteenth century marked the first notable period in drug discovery (Pina et al., 2010). Active principles of the natural products were isolated using purification methods developed in the nineteenth century and many of these agents were used in the treatment of diseases (Li, 2013). Serendipitous discovery of natural product remedies include the treatment of congestive heart failure with digitalis (foxglove), treatment of dysentery with *Ipecacuanha* (*cephaelis* plant bark or root), treatment of fever with willow tree bark and the treatment of malaria with quinine (cinchona bark) (Permin et al., 2016). Essential foundations of chemical theory were laid by late-19th century. Theory on structure of aromatic organic compounds was formulated by August Kekule in 1865 which led to the development of dye chemistry. Paul Ehrlich, while working on dyes with selective affinity to biological tissues (1872 and 1874) postulated the existence of chemoreceptors which eventually resulted in the birth of chemotherapy in the 20th century (Drews, 2000).

19th century saw drug discovery move from usage of dried and ground preparations to the isolation and purification of active components. ‘Mauve’ created by William Henry Perkin in an attempt to synthesise quinine lead to the creation of first synthetic textile dye (Schlitzer, 2007). Paul Ehrlich (1890) stained the malaria parasite with methylene blue which has had a huge impact on drug discovery. The ability of chemical dyes to selectively stain certain

biological tissues lead to the development of the drug receptor concept. This connection between drug structure and biological activity lead to the birth of medicinal chemistry (Drews, 2000).

Major classes of molecular drugs used for treating almost 87% human diseases belong to natural products isolated from natural sources such as vertebrates, invertebrates, plants or micro-organisms (Pina et al., 2010). Morphine was isolated from opium extracts by F. W. Serturner in 1815, papaverin was discovered in 1848 but it was only in 1917 its antispasmodic properties came to light, and coal-tar, an industrial by-product with many aromatic or aliphatic compounds became an important tool for medicinal chemistry. Discovery of penicillin from the mould *Penicillium* by Alexander Fleming in 1929 revolutionised the treatment of bacterial infections and led to the development of many other antibiotics (Drews, 2000) (Rubin, 2007). Natural products lead to discovery of several immunosuppressive agents (cyclosporins and rapamycin), anti-cancer agents (paclitaxel and camptothecin) and cholesterol-lowering agents (lovastatin and mevastatin) (Pina et al., 2010).

1928 to 1962 was considered the golden era of drug discovery. Fritz Mietzsch and Josef Klarer synthesised prontosil, a sulfonamide derivative (1935). Prontosil was also found to demonstrate 100 % cure rates against *P. falciparum* (Gregson and Plowe, 2005). 1950/1960s saw interest in sulpha compounds emerge as potential antimalarials. Treatments for malaria, tuberculosis, hypotension, diabetes and many other diseases became available. Biological activity was first tested *in-vivo* in animal models and then compounds were subsequently purified and synthesised followed by lead optimisation through structural modification (Pina et al., 2009). *P. relictum* in canaries (1926-1935), *P. gallinaceum* in either chicks, ducklings or turkeys (1935-1948) and the rodent *P. berghei* model, first isolated from the thicket rat (central Africa, 1948), were the animal models used in malaria (Cellier-Holzem et al., 2010) (Frevert et al., 2008). The rodent *P. berghei* model is still in use today. *In vitro* culture methods eventually replaced the need to conduct the preliminary investigations through *in vivo* methods. This transition for malaria was made possible by Trager and Jensen in 1976, by isolating *P. falciparum* parasites from *Aotus trivirgatus* monkey and successfully culturing them in human blood (Trager and Jensen, 1976). In 1980s, in-depth understanding of disease aetiology, cellular processes and molecular biology made a rational approach to drug design norm which was supplemented by the advent of genomic revolution (Chatterjee and Yeung,

2012) (Jana and Paliwal, 2007) (Wells, 2010). For malaria, the sequencing of the *P. falciparum* genome (Gardner et al., 2002) renewed hope in finding a new effective antimalarial as no orthologues were discovered for 60 % of the parasite proteins (Guiguemde et al., 2012).

New drug structures found in the early twentieth century led to an era of antibiotics discovery. The field of drug discovery saw rapid advances towards the end of last century with the development of techniques such as computer-based drug design, combinatorial chemistry, automated high-throughput screening and recombinant DNA technology which made it possible to develop new drug target candidates and marked the onset of 'Omics' revolution (Pina et al., 2010). In the last two decades, drug discovery has gradually shifted from a physiology-based to target-based approach. Physiology based approach relies on physiological effects of drugs in disease-relevant models. The weakness of this method lies in the lack of complete understanding of relationship between the mechanism of action of the drug, its biological effect and low-throughput screening (Sams-Dodd, 2005). Phenotypic screens and target-based screens have sequentially ruled over the drug development stages (Kotz, 2012). The ratio of success rate of a new drug to pass the approval stage to the investment required for research and development is very low (Figure 1.10.1).

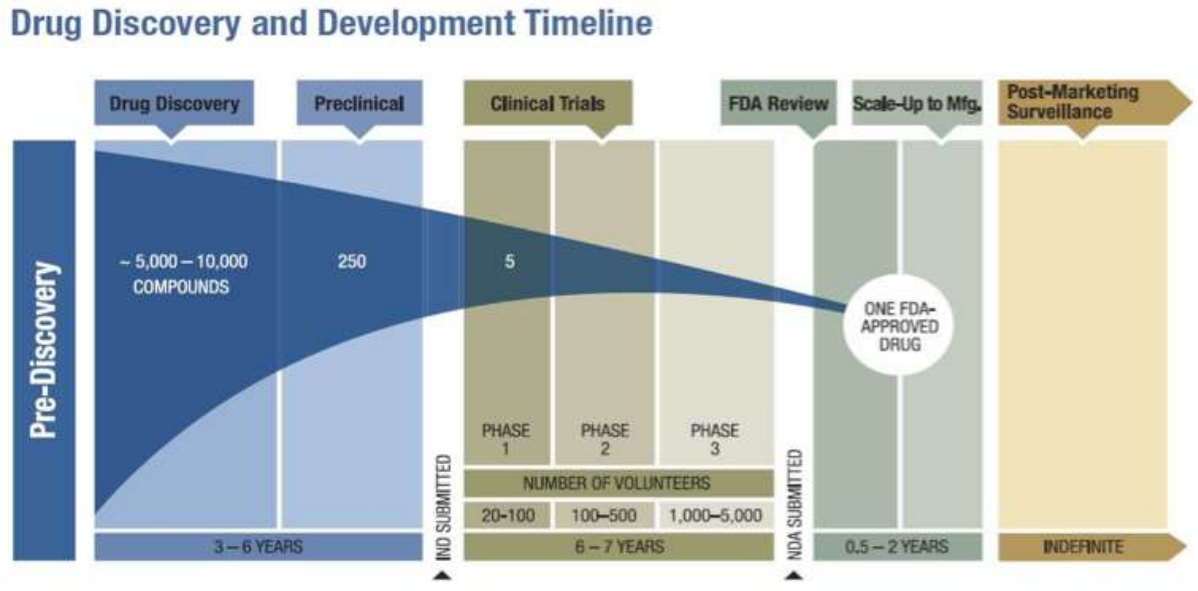

Figure 1.10.1 The drug development to market timelines for de novo drug discovery.

De novo drug discovery can take 10-17 years with very low probability of success. ADMET, absorption, distribution, metabolism, excretion and toxicity information may already be available for the repositioned drug candidate (Somerville, 2015).

1.10.1 **Target-based drug discovery**

The target, ideally specific to the disease causing organism is usually identified to avoid the chances of adverse effects (Chatterjee and Yeung, 2012). After the identification of the target and genetic validation through knock-out studies, high-throughput screening is conducted *via in vitro* chemical assays using 'druggable' small molecules, which obey the rule of 5 (more than 5 H-bond donors, 10 H-bond acceptors, the molecular weight greater than 500, and the calculated Log P (CLog P) greater than 5 are more likely to result in poor absorption or permeation) (Frearson et al., 2007) (Blaazer et al., 2015) (Benet et al., 2016). Structural optimisation is done to increase pharmacokinetic properties of the hit compounds. X ray crystallography and computational 3D modelling can also be used to aid in the process (Gilbert, 2013). After determining the selectivity of hit compounds in cellular assays and evaluating the toxicity profile, the hit compound is only validated when it shows efficacy in the clinical settings (Gilbert, 2013). This approach has led to development of many successful drug therapies such as imatinib and gefitinib against cancer (Swinney, 2013). Cysteine proteases, protein farnesyl transferases, dihydrofolate reductase and phospholipid biosynthesis are few of the many putative targets which have emerged for the development of new antimalarials (Fidock et al., 2008) (Gelb, 2007) (Jana and Paliwal, 2007) (Nwaka et al., 2004) (Winstanley, 2000). Problems with this approach is that target based drugs have limited impact on disease treatment (Sams-Dodd, 2005). Unfortunately, *in vitro/ in vivo* disconnect is observed more frequently than desired and leads to disappointing results during clinical validation for many novel targets, mostly due to lack of cellular context which is used for identification of hit compounds. This ultimately causes problems with cellular penetration, sequestration in lipid compartments, non-specific binding, undesirable kinetic properties or alterations in molecule in the active site of the enzyme (Chatterjee and Yeung, 2012) (Gilbert, 2013). Lactate dehydrogenase (LDH), thioredoxin reductase (TrxR) and the fatty acid biosynthesis enzyme (FabI) were used as targets for enzyme inhibition in malaria but failed when tested for whole-parasite activity. FabI was eventually found to be dispensable in the intraerythrocytic cycle whereas LDH and TrxR were found not druggable despite intensive lead optimisation (Guiguemde et al., 2012).

1.10.2 **Validated antimalarial drug targets**

Our existing knowledge of parasite biology has led to the realisation that novel modes of metabolism, cell division, signalling and communication pathways are commonly used by the parasite causing unexpected adverse effects leading to poor attrition rates (Reaume, 2011) (Jana and Paliwal, 2007). The three validated targets namely the haemozoin pathway (chloroquine), the folate pathway (anti-folates; dihydrofolate reductase and dihydropteroate synthase inhibitors) and mitochondria's cytochrome bcl complex (atovaquone) developed based on action of pre-existing antimalarials and not through modern fully rational, target-based drug discovery framework, have dominated the antimalarial development pipeline (Chatterjee and Yeung, 2012) (Gilbert, 2013) (Na-Bangchang and Karbwang, 2009). Figure 1.10.2 shows the various targets for antimalarials in *P. falciparum*. Most new antimalarial compounds are generally the less toxic and efficacious second or third generation compounds (Gelb, 2007). The longevity of such second generation compounds is questionable due to the parasite's pre-existing resistance capabilities (Canfield et al., 1995) (Wells, 2010).

The reduction in development of novel first class drugs has questioned the over-reliance of drug discovery on the target-based strategy and genetic approach to drug discovery (Kotz, 2012). Conserved homology dictates the rarity of selective compounds in reality (Chatterjee and Yeung, 2012). The other important issue affecting the malaria drug market is the half a billion people needing treatment in a year that cannot afford to pay for it leading to a negligible profit margin, making it unattractive for large pharmaceutical companies to invest in antimalarial drug development (Craft, 2008) (Muthyala, 2011) (Winstanley, 2000).

The Medicine for Malaria venture (1999) and the Bill and Melinda Gates foundation, the non-profit public, private and philanthropic partnerships have fortunately revitalised efforts to develop new antimalarials (Fidock et al., 2004). This has led to formation of academic and industrial partnership programs focussing on novel antimalarials to sustain the drug discovery pipeline for antimalarials (Gelb, 2007) (Gilbert, 2013). High failure rate of candidates with only 7% becoming a drug further hampers the long *de novo* drug development process. Faster development processes are thus imperative to avoid an imminent void in the malaria drug market currently under threat of spread of artemisinin resistance (Craft, 2008) (Gelb, 2007).

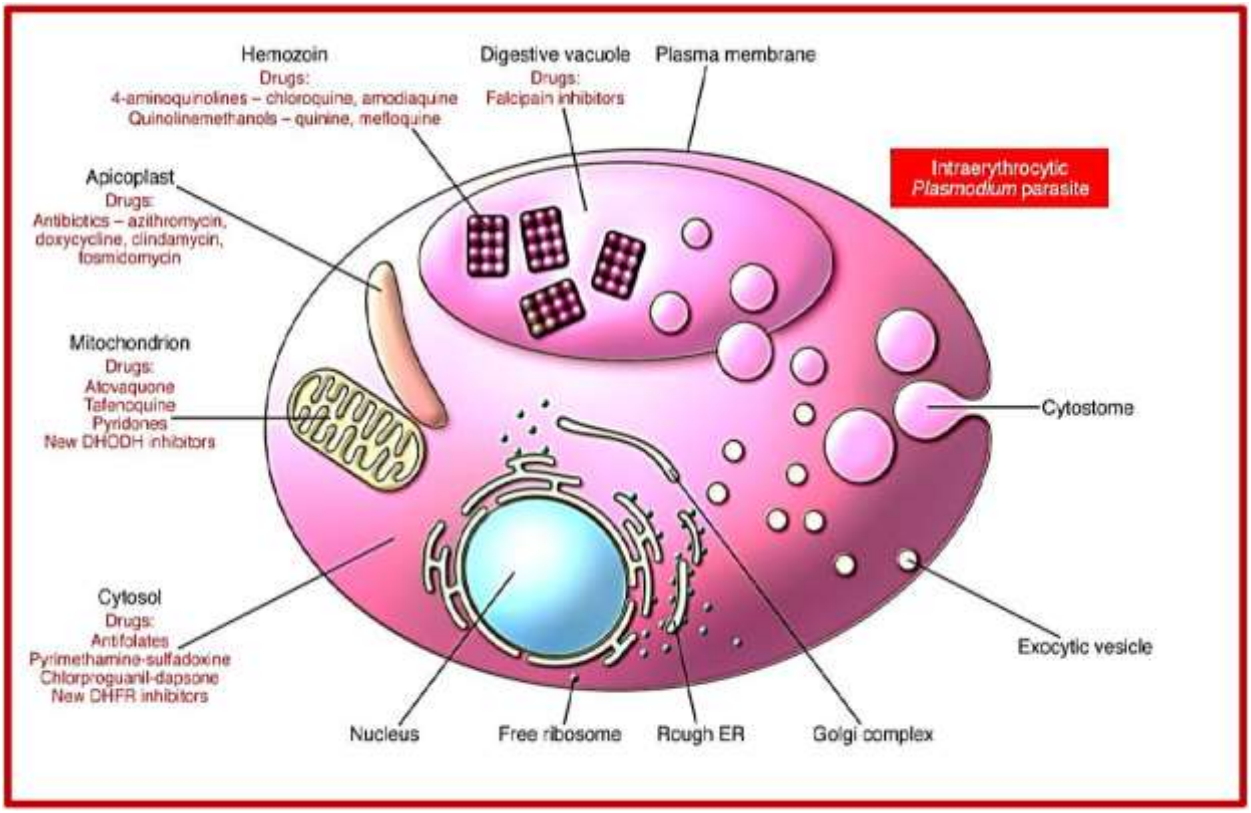

Figure 1.10.2 Various antimalarials with their targets in *P. falciparum*. Source: (Greenwood et al., 2008)

1.10.3 **Phenotypic drug screening/ high-throughput Screening (HTS)**

Phenotypic screening exploits diverse chemical libraries developed over nearly 100 years of medicinal chemistry and involves high throughput *in vitro* whole-cell screening followed by compound purification according to potency. It is a top-down development process with retrospective identification of drug targets and mechanisms of action (Gilbert, 2013).

The main purpose of high-throughput screening (HTS) is to screen a large number of biological modulators and effectors against selected and specific targets and has become a standard in the pharmaceutical industry (Szymanski et al., 2012). In one HTS, nearly 1.7 million compounds were screened, with ~6,000 small molecules identified as having potent antimalarial activity (<1.25 μM) (Plouffe et al., 2008). Another screen of nearly two million compounds in GlaxoSmithKline's chemical library identified 13,533 hits with activity against *P. falciparum* at 2 μM concentration (Gamo et al., 2010). 275 primary hits with sub-micromolar activity against *P. falciparum* were identified from a screen of ~ 12,000 pure natural products (Rottmann et al., 2010).

1.10.4 **Phenotypic screening for malaria**

Whole-parasite high-throughput screening techniques such as hypoxanthine incorporation assay, ELISA and SYBR green-based methods to evaluate compounds against the erythrocyte stages have made phenotypic screening for malaria a possibility. This addresses the aforementioned issues of permeability and cellular efflux by screening the compounds against whole parasites. Mammalian cell lines are used to determine selectivity and toxicity (Wells, 2011). Improvements in compound activity through structural alterations are limited due to lack of prior knowledge of the target (Gilbert, 2013). Nonetheless, regulatory approval of drugs does not require prior knowledge of targets and historically it has been observed the most successful antimalarials have multiple targets, with difficult to elucidate pathways (Chatterjee and Yeung, 2012) (Medina-Franco et al., 2013).

1.11 Compounds from natural sources in malaria:

Tetracycline discovered in 1940's is a natural product-derived compound with antimalarial activity. Several classes of compounds such as alkaloids, terpenes, flavonoids, quinones, xanthones, coumarins, peptides, phenols and lignans have been identified as having antimalarial properties (Wells, 2011).

By 1950s, 8-aminoquinoline, 4-aminoquinoline and folic acid synthesis inhibitors replaced quinine in the treatment of malaria and it was widely believed malaria would soon be eradicated from the world (Mojab, 2012). Emergence of drug resistance and insecticide resistance quashed any hopes of eradicating the disease (Churcher et al., 2017). Drug resistance to artemisinin has reached Thai-Cambodia border and the world is in dire need of a new effective anti-malarial (Phyo et al., 2012). Natural products have played an important role in shaping the treatment for malaria (Wells, 2011). Quinine which is derived from *Cinchona* (White, 1985) and artemisinin which is derived from Chinese herb *Artemisia annua* (Warhurst, 1985) have proven to be the two strongest antimalarials till date. *Dichroea febrifuga*, another species used in Chinese herbal medicine has been found to be effective against malaria (Phillipson et al., 1987). *Simaroubaceae* is another species traditionally used in Asia, Africa and America against malaria (Bertani et al., 2006).

Another species with activity against the malaria parasite is *Bignoniaceae*, whose active ingredient lapachol and its derivative lapinone led to the development of atovaquone (Carvalho et al., 1988) (Fawaz and Fieser, 1950). Cryptolepine from *Cryptolepis sanguinolenta* is marketed in Ghana as PHYTO-LARIA (Lisgarten et al., 2002) (Wright et al., 1996). Gedunin from *Azadirachta indica*, has been used in India (Willcox et al., 2004) and is available as capsules (IRACARP) in Nigeria (Anyaehie, 2009).

Natural source based antimalarials such as quinine (effective despite being in use for nearly 400 years) and artemisinin are in stark contrast when compared with development of resistance in targeted anti-folate class of drugs which emerged within 5 years of use (Achan et al., 2011) (Craft, 2008). Artemisinin is believed to act through multiple targets with reports suggesting involvement of reduction of the endoperoxide bridge through generation of free radicals (Meshnick, 2002), activation on the mitochondrial electron transport chain leading to generation of reactive oxygen species (Mercer et al., 2011), interference with haemoglobin and haeme pathway (Klonis et al., 2011) (Zhang and Gerhard, 2009), and the interaction with the calcium pump PfATP6 (ortholog of endoplasmic reticulum pump SERCA) (Valderramos et al., 2010).

1.12 Molecular Modelling:

Drugs are either provided through discovery or through design in medicinal chemistry. Mapping of the human genome has led to molecular biological revolution and exponential growth in potential therapeutic targets. Intelligent molecular mimicry and structural analyses of binding domains of the biological targets with the agonist or antagonist co-crystallised with it provides a significant understanding of the receptor-ligand interactions (Krogsgaard-Larsen et al., 2010). Growth in protein databank (RCSB), better docking algorithms, large scale quantum calculations, computational models to predict pharmacophore and prediction absorption/distribution/metabolism/excretion (ADME) - toxicity coupled with advancement in computer power has led to the incorporation of molecular modelling in the process of drug discovery. It involves a large bio-molecular target which binds with a small molecule leading to the activation or inhibition of the target. It is helpful for lead generation and lead optimisation. Deleting (knocking-out) a reaction in the metabolic network *in silico* and comparison of reconstructed metabolic network models can help determine essential enzymes

(Fatumo et al., 2009). Structure-based designs require a three dimensional target structure and graphic tools to observe the ligand interactions in the binding site with insight into the molecular energetics of the binding process. Ligand-based designs are based on the analysis of structure/activity data of compounds observed on assays measuring the target's biological function (Wilson and Lill, 2011). Ability to accurately predict a ligand's potency to bind with the intended target is invaluable in the drug-discovery process. Molecular docking is used to dock ligands to the active site of the target and scoring functions are used to analyse the resulting receptor-ligand interactions to provide a quantitative measure of fit quality (Rajamani and Good, 2007). Computer-aided drug design could be ligand-based or structure-based (Osakwe and Rizvi, 2016) (Mortier et al., 2018) (Vyas et al., 2012).

Benefits of predicting inter-molecular interactions are immense. In the process of rational drug design or elucidation of biochemical processes, the knowledge of the binding conformation of the target with a small molecule ligand is important for structure-based drug design (Kitchen et al., 2004). The analogy of 'lock and key' is often used for the ligand fitting in the binding pocket of the target, similar to a key which fits in a lock (Du et al., 2016) (Tripathi and Bankaitis, 2017) (Kuntz et al., 1994). Due to the flexible nature of the proteins and the ligand, a 'hand in glove' analogy is a better fit (Jorgensen, 1991). The conformational adjustment of protein and the ligand leading to overall binding is known as 'induced-fit' (Bucher et al., 2011) (Wei et al., 2004). The purpose of simulation is to identify a conformational pose between the ligand and the target protein such that the system has the minimum 'free energy' (Meng et al., 2011) (Gray, 2006). In docking two main approaches are popular: 'Shape complementarity' and 'Simulation'.

1.13 Mechanics of docking:

Energetically acceptable poses of the ligand are usually identified by evaluation of force-field energy (Liu and Wang, 2015). Systematic, stochastic, molecular dynamics simulation and genetic algorithms are various strategies used to develop the search algorithm (Dastmalchi, 2016). Most ligand poses generated during docking result in clashes with the protein and are rejected immediately (Osada, 2009) (Friesner et al., 2006). A force-field based scoring function, which assesses the energy of the pose in relation to the binding site, is then used to evaluate remaining poses and rank them based on how favourable a binding interaction they

represent (Murcko, 1995). A stable system has a negative or low energy. Knowledge-based approach is an alternative which utilizes the ligand-protein complexes data from large databases to predict the best fit of the pose for a given potential (Yang et al., 2006) (Roche et al., 2001). Examples of computer-aided drug design are dorzolamide, a carbonic anhydrase inhibitor approved in 1995 (Greer et al., 1994) (Gubernator and Böhm, 1998) and imatinib which inhibits tyrosine kinase as a treatment for Philadelphia-chromosome positive leukaemias (Capdeville et al., 2002).

Molecular docking has the potential to efficiently predict non-covalent binding of macromolecules (protein-protein docking) or a macromolecule and a small molecule (receptor-ligand docking) using a computational procedure. The knowledge of bound conformation and the binding affinity is used to virtually screen libraries of drug-like molecules for lead generation and lead optimisation for further drug development. In this study, the molecular docking software, MOE (Molecular Operating Environment) and AutoDock Vina were used for molecular docking and virtual screening.

1.14 Virtual Screening

Until recently, drug discovery by empirical screening has dominated the search of new ligands for biological target structures. Virtual screening has now established its place in drug discovery (Shoichet, 2004). Despite recent advances in combinatorial chemistry, it is not possible for the chemists to synthesis all the possible compounds in the drug library. Virtual screening offers a solution by reducing the library to a manageable size which could be synthesised (Walters et al., 1998). Hit identification and lead optimisation frequently employs virtual screening to dock possible ligands into macromolecular structures and score their potential complementarity to the binding pocket (Kitchen et al., 2004). There are still many issues in the application of screening approaches, but HIV protease inhibitors are a good example where screening and structure-based design played an important role in the development of new drugs (Yadav et al., 2012).

In silico assessment of large libraries of chemical structures either alone or in combination with high-throughput screening is being used regularly. Availability of computational screening approaches has increased with the increase in molecular databases of compounds

and target structures. Virtual screening acts as a fast-tract method. Large compound libraries containing bioactive molecules have already been screened for malaria and other diseases but very few have progressed beyond the hit identification stage (Baniecki et al., 2007) (Chong et al., 2006) (Jones et al., 2010) (Lucumi et al., 2010) (Major and Smith, 2011).

1.15 Drug Repositioning:

De novo drug discovery through target-based strategy has less than 10% success rate and can take 10-17 years. Novel drug discoveries to increase productivity of biopharmaceutical companies have not achieved the desired results. As such, repositioning the existing drugs towards new indications can help increase the productivity needed by the industry. 'Drug repositioning' or 'repurposing' is a strategy where abandoned or existing pharmacotherapies are used on novel indications identified through phenotypic screening (Boguski et al., 2009) (Medina-Franco et al., 2013). Drug repositioning offers a solution to the dilemma of reducing the research and development timelines without increasing the associated risks as the *in vitro* and *in vivo* screening, chemical optimization, toxicology, formulation development, side-effects profiling, bulk manufacturing and clinical development have already been completed and so can potentially be bypassed thus eliminating the costs of substantial risks and several years from the development to market pathway (Ashburn and Thor, 2004).

Many drugs have been successfully repositioned for use in various diseases, such as sildenafil (Viagra) originally developed to treat cardiovascular diseases is now used for erectile dysfunction (Fink et al., 2002), thalidomide which was developed to treat morning sickness was found to be effective against Erythema nodosum leprosum and for the treatment of multiple myeloma (Walker et al., 2007). Buproprion (Wellbutrin) and Duloxetine (Cymbalta) developed for treating depression were found to be effective as a smoking cessation aid and for stress urinary incontinence, respectively (Boguski et al., 2009).

Clinically/FDA approved drugs could serve as sources for drug repositioning (Andrews et al., 2014) (Lotharius et al., 2014). Doxycycline, an antibiotic has been repositioned for use in malaria. Medicines for Malaria Venture (MMV) supported the high-throughput screening of approximately 4 million compounds by Novartis, GlaxoSmithKline (GSK) and St. Jude Children's Research Hospital in the late 2000s leading to identification of over 20,000

compounds with antimalarial activity which were deposited in the public domain (Guiguemde et al., 2012) (Fong et al., 2015). Drug repositioning could potentially have reduced risks of drug failure in addition to reduced cost and time due to the availability of pre-clinical toxicology data, pharmacokinetics and dose range in some instances (Baek et al., 2015). Although legal issues could arise with regards to intellectual property of the drug.

Derived from *Psychotria ipecacuanha*, emetine, a hydrochloride of an alkaloid in ipecac root, has been used to treat amoebiasis, cough, and as the name suggests, to induce emesis or vomiting (Lee, 2008). Methylation of cephaeline could also be used to prepare emetine (Jain et al., 2012). Emetine has been found to be active against leukemia (Möller et al., 2007) and dengue virus infection (Yin Low et al., 2009) amongst other diseases. Dehydroemetine, the synthetic derivative of emetine has been tested for activity in amoebiasis (Hilmy Salem and Abd-Rabbo, 1964), leishmaniasis and herpes zoster (Hernandez-Perez, 1980).

1.16 Previous drug repositioning work conducted at the University of Salford:

Drug repositioning studies were conducted in the University of Salford in a bid to identify compounds with activity against *Plasmodium falciparum*. Optimisation of reliable *in vitro* drug susceptibility assays was done and two FDA-approved libraries, LOPAC and ENZO (~700 compounds) were screened. Around 60 compounds were identified as potential hits, and emetine dihydrochloride hydrate, an anti-amoebic compound was found to be approximately 1000-fold more potent an inhibitor (IC50 = 47 $\pm$ 2.17 nM) of the multidrug resistant *Plasmodium falciparum*, strain K1 compared to *Entamoeba histolytica* (26.8 $\pm$ 1.27 µM) (Bansal et al., 2004). Parasite reduction ratios (PRR), parasite clearance time (PCT) and drug interaction analysis with existing antimalarials were conducted in the second-phase characterisation of the compound. Emetine and atovaquone were found to have ideal pharmacokinetic matching and synergy (Matthews *et al*, 2013).

1.17 Emetine and dehydroemetine:

A natural alkaloid native to Brazil extracted from plant source *Psychotria ipecacuanha* (plant family *Rubiaceae*) also known as *Cephaelis ipecacuanha* has been used in the past for the treatment of amoebiasis. Mitochondrial and ribosomal protein synthesis is inhibited by

emetine and it has antiviral, anti-parasitic, contraceptive and anti-cancer properties. 40S ribosomal subunit of the eukaryotic 80S ribosome is the site of action of emetine (Jimenez et al., 1977). Poliovirus infected HeLa cells treated with emetine have been reported to show inhibition of viral RNA synthesis (Akinboye and Bakare, 2011). Human cytomegalovirus, Zika virus and Ebola virus are also inhibited by emetine at nanomolar concentrations (Mukhopadhyay et al., 2016) (Yang et al., 2018).

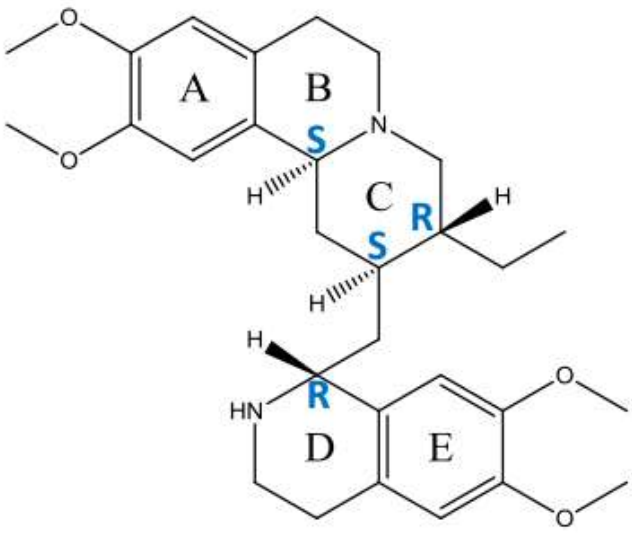

Figure 1.17.1 Emetine structure from pubchem showing R configuration at C-1'

The (R) configuration at C-1´ and the presence of secondary nitrogen at 2´ position are important for emetine's biological activity (Figure 1.17.1), as (S) configuration at C-1´ (isoemetine) or substitution of secondary amine results in the loss of activity. Symmetry at carbons 2 and 3 is lost with unsaturation at 2-3 position (dehydroemetine) but the biological activity is retained (Grollman, 1966). The cross-resistance of emetine-resistant mutants of Chinese hamster ovary cells to related compounds such as (-)-cryptopleurine (phenanthroquinolizidine-type alkaloids), (-)-tylocrebrine (phenanthroindolizidine type), and (-)-emetine, (-)-tubulosine, (-)-cephaeline, and (-)-dehydroemetine (benzoiosoquinoline alkaloids) was observed (Gupta and Siminovitch, 1977). The study concluded that the planar structure of the molecule with two aromatic rings made slightly electronegative by hydroxyl or methoxyl groups, the distance between two aromatic rings and the angle between nucleophilic element such as nitrogen and the rings are essential to maintain biological activity.

The important side-effects of emetine are vomiting and cardio-toxicity. Emetine's cardio-toxicity was immediately recognised since it was first advocated in 1912 by Sir Leonard Rogers. Boyd and Scherf in 1941, found widening of QRS complexes, PR interval prolongation, T wave changes and extra-systoles in the electrocardiograms of animals. In 1944, Hardgrove and Smith found cardiographic changes especially in T waves of 53% of the study subjects (Turner, 1963).

Reports of emergence of resistance to the artemisinins is a call to discover novel anti-malarial drugs and drug repositioning *via* screening existing FDA-approved drug libraries can offer a short term solution.

Cytoplasmic ribosome, mitochondrial ribosome and non-photosynthetic plastid, the apicoplasts are responsible for protein synthesis in the *Plasmodium* parasite (Jackson et al., 2011) (McFadden et al., 1996). Delayed death effect is observed in second generation drug exposure in parasites treated with macrolide antibiotics such as azithromycin which target the apicoplast ribosome (Dahl and Rosenthal, 2007). Cytosolic protein translation inhibition displays quick results due to its dominance in blood stages of the parasite (Waters et al., 1989).

The *Pf*80S ribosome is comprised of large (*Pf*60S) and small subunit (*Pf*40S) with a total of 74 proteins as well as the 5S, 5.8S, 18S, and 28S rRNAs and a tRNA bound (Figure 1.10.4.1) at the E-site (Wong et al., 2014). 18S rRNA helices 23, 24, 45, and the C-terminus of uS11 form the emetine binding pocket (Figure1.17.2). No changes are induced in the pocket due to binding of emetine.

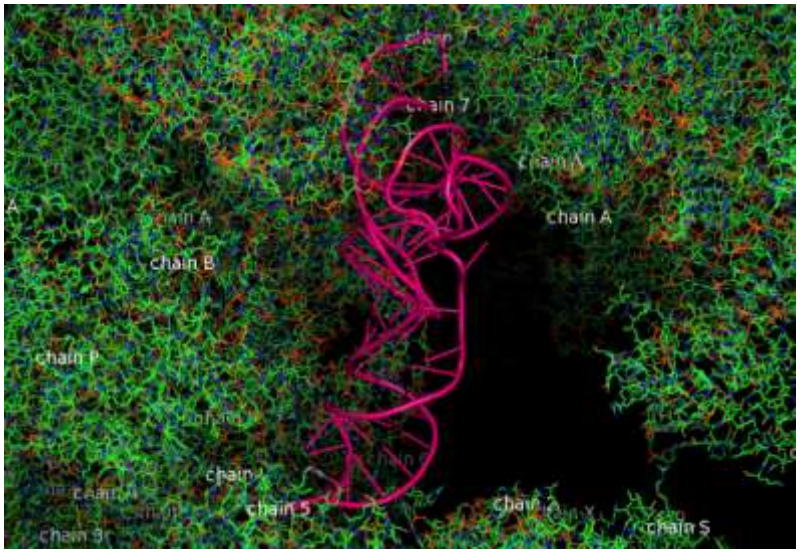

Figure 1.17.2 tRNA (in pink) bound to the E-site of *Pf*80S ribosome reproduced through a molecular graphics software, PyMol.

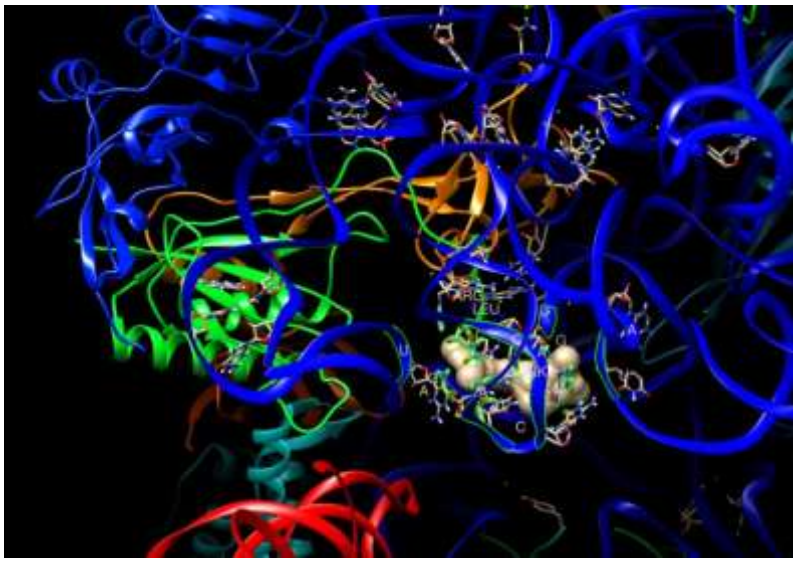

Figure 1.17.3 Emetine binding site with emetine (in white) in the binding pocket reproduced through a molecular graphics software, Discovery Studio (3J7A by Wong et al, 2014).

Base-stacking interaction is formed between G973 of h23 and the benzo[a]quinolizine ring of emetine whereas a hydrophobic interaction is formed by its ethyl group with C1075 and C1076 of h24. The isoquinoline ring stacks against the C-terminal Leu151 of protein uS11 and a hydrogen bond formed between the NH group of emetine's isoquinoline ring and an oxygen atom on the backbone of U2061 of h45 stabilizes this interaction. Emetine possibly binds to the cytoplasmic host ribosomes in a way similar to that of *Plasmodium* as each of the

core binding elements in the emetine binding site in *Pf*80S appear to be conserved (Figure 1.17.3) when compared with the equivalent region in the 4.8 Å human structure (Anger et al., 2013) (Wong et al., 2014). This could be the reason behind observed cytotoxicity in humans.

Mutations of Arg149 and Arg150 of protein uS11 in Chinese hamster ovary (CHO) cells lead to development of resistance to emetine (Madjar et al., 1982). The molecular basis of resistance could be explained by mutations of the C-terminal arginine residues of uS11 which disrupts the emetine binding pocket by destabilizing h23 and h45. In *Plasmodium*, a long coil with seven basic residues (residues 141–151; RKKSGRRGRRL) is formed by the C-terminus of uS11, leading to electrostatic interactions with the phosphate backbones of h45, h23 and h24, which is necessary for the stabilisation of the conformation of this coil with the 18S rRNA (Wong et al., 2014). Pactamycin, which binds to the bacterial 30S and acts by blocking mRNA/tRNA entry into the E-site during the translocation step of protein synthesis share the same binding pocket as emetine (Dinos et al., 2004) (Brodersen et al., 2000). Emetine thus possibly acts *via* the same mechanism as pactamycin. Figure 1.17.4 shows the comparison of emetine binding residues between human (S14) and *Plasmodium* (uS11) proteins.

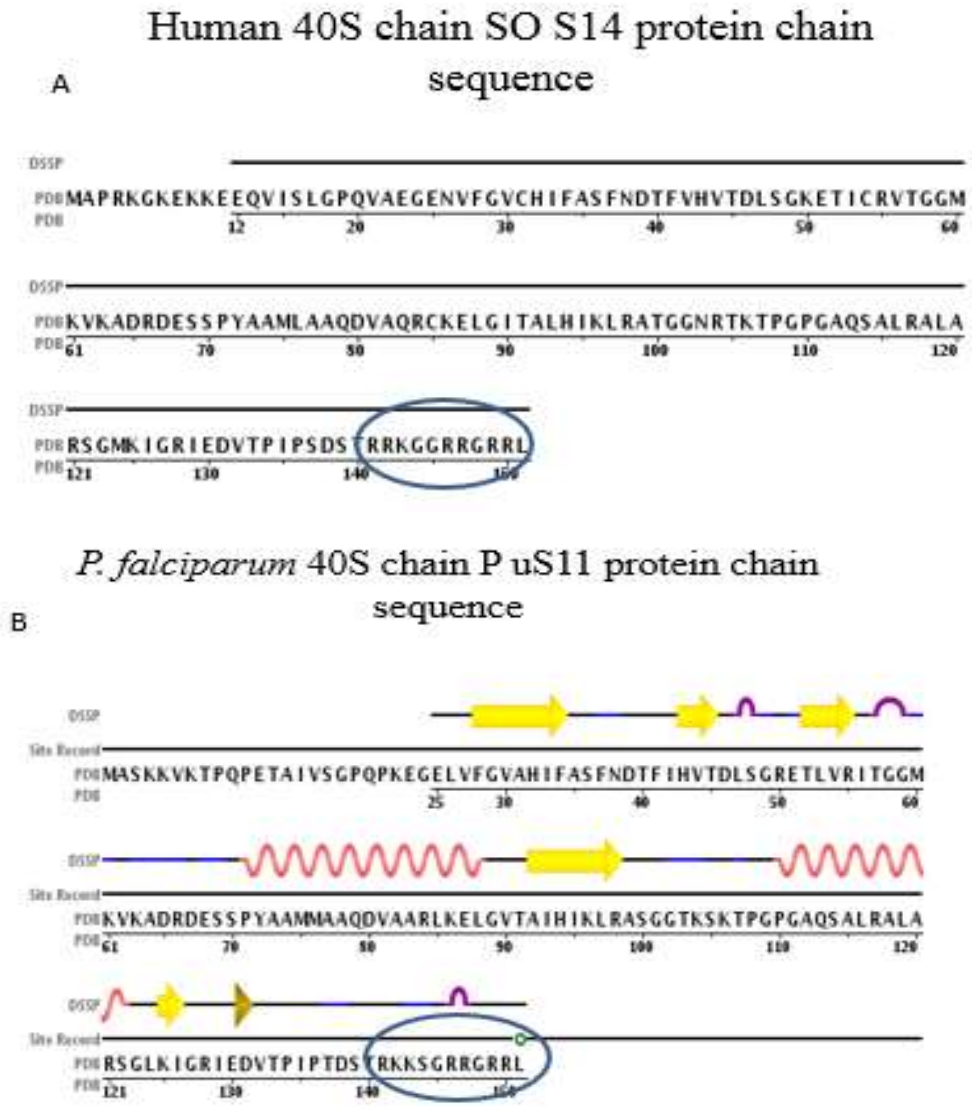

Figure 1.17.4 Comparison of human and *Plasmodium* ribosomal emetine binding sequence.

(A) human 80S ribosome small subunit 40S ribosome protein S14 (4UG0) and (B) *P. falciparum* 3J7A ribosomal 40S small subunit protein uS11 with residues (141–151; RKKSGRRGRRL) forming emetine binding site. Sequence adapted from Protein Data Bank.

Pactamycin and its analogues with reduced cytotoxicity have been shown to be potent against *P. falciparum* (Otoguro et al., 2010) (Lu et al., 2011). Similarly, dehydroemetine, a synthetic derivative of emetine which differs from its parent compound by a double bond next to the ethyl group of benzo[a]quinolizine ring, has been found to maintain anti-parasitic properties but produces less toxic effects (Dempsey and Salem, 1966) (Chintana et al., 1986). Structural modification of emetine is unlikely to avoid binding to mammalian ribosome due to conserved nature of the binding site in humans. Reduced cytotoxicity observed in

dehydroemetine could possibly be due to its faster excretion from the body (Schwartz and Herrero, 1965).

Dehydroemetine, a synthetic analogue of emetine hydrochloride has been claimed to have less cardio-toxic effect than emetine in a study to assess the effect of combination of chloroquine with emetine hydrochloride and dehydroemetine in the treatment of amoebic liver abscess (Scragg and Powell, 1968). It can thus serve as an interesting lead to test the compound for antimalarial activity. In this study, we have tested the two diastereomers of dehydroemetine, (-),-*R,S*-dehydroemetine and (-),-*S,S*-dehydroisoemetine for the activity against the multi-drug resistant strain K1 of *P. falciparum*.

1.18 Future directions

Identification of new antimalarials to circumvent the spread of resistance is of utmost importance. The faster pace of drug repositioning in treatment of diseases which often relies on serendipity, offers a valuable option especially in diseases like malaria. It could bridge the gap arising from treatment failure due to spread and emergence of resistance, and time and cost of future drug developments by identifying suitable candidates not only for novel therapy but also for combinatory regimes with existing antimalarials. This should run in parallel with existing target-based studies. Expedition of the drug discovery timeline is crucial and drug repositioning could be used as one of the methods for developing new antimalarials (Grimberg and Mehlotra, 2011, Lotharius et al., 2014).

With these statements in mind, the main aims and objectives of this research are to:

1. To use computational tools to locate the binding site and predict the activity of the two isomers of dehydroemetine.
2. To investigate the antimalarial efficacy of the two isomers of dehydroemetine against the multidrug resistant *P. falciparum* K1 strain through IC_{50} level of inhibition and killing profile in order to develop an understanding of the mode of action.
3. Evaluate the toxicity of the tested compounds on human cell lines.

4. To further characterise the action of the selected isomer of dehydroemetine by investigating its interaction with currently used antimalarial drugs to look for a synergistic partner, and to determine suitability and potential for combination therapy.
5. To define the cellular basis for cardiotoxicity observed during emetine and dehydroemetine anti-amoebic therapy and propose possible remedies.

Chapter 2 General materials and methods

All materials for the *Plasmodium falciparum* culture and experiments were prepared in a sterile fume hood after generous spraying with 70 % ethanol (ESCO class II Biological safety cabinet) and using pre-sterilised equipment in the pathogen laboratory (University of Salford). All biological waste was disinfected with 2% Virkon (Antec International, UK) which was prepared by adding 2 scoops of Virkon (Antec International, UK) to 1 litre of water, prior to autoclaving. All routine culture methods were consistent with those employed by (Read and Hyde, 1993)). Health and Safety risk assessment has been carried out according to COSHH protocols.

Ethics Statement:

For routine malaria culture, anonymised whole blood packs deemed unfit/outdated for clinical use were purchased from the NHS Blood Bank at Plymouth Grove, Manchester, UK. For experiments carried out in GlaxoSmithKline, Diseases of the Developing World Medicines Development Campus, Tres Cantos, Spain, the human biological samples were sourced ethically and their research use was in accord with the terms of the informed consents under an IRB/EC approved protocol. All procedures carried out at the University of Manchester accord with the Animals (Scientific Procedures) Act, UK, 1986 and Directive 2010/63/EU of the European Parliament (Home Office, 1986).

2.1 Preparation of complete media:

500 ml RPMI 1640 media containing 1x (+) L-Glutamine (+) 25 mM Hepes (Gibco, Life Technologies, UK) was used for the culture and experiments. Complete media was prepared by adding 2.5 g Albumin bovine serum fraction V (Sigma, UK), 2.5 ml 1 mg/ml hypoxanthine (Sigma, UK) in phosphate buffered saline (PBS) (Fisher Chemical, UK), 2.5 ml 40% glucose (Dextrose Anhydrous, Fisher Scientific, UK) in sterile water and 0.5 ml 50 mg/ml gentamycin (Sigma, UK) in PBS to 20 ml of RPMI 1640 in a falcon tube which was subsequently added directly into the 500 ml bottle of RPMI 1640 medium using a 20 ml syringe after passing through a 0.22 µm filter. The complete media was stored at 2-8^{o}C.

2.2 Preparation of washing media:

For washing media a 500 ml bottle of pre-sterilised RPMI 1640 1x (+) L-Glutamine (+) 25mM Hepes (Gibco, Life Technologies, UK) devoid of additives was used and stored at 2-8^{o}C for up to 2 weeks.

2.3 Preparation of human blood:

O+ whole blood (obtained from the human blood bank) was washed immediately before use to remove the leucocytes. Blood was centrifuged in a falcon tube for 5 minutes at 3000 rpm and the supernatant two layers containing the plasma and buffy coat were removed. Equal volume of washing media (sterile RPMI) was added to the remaining layer composed of red blood cells. After mixing it well, RPMI with blood was centrifuged at 3000 rpm for 5 mins and the supernatant was removed. Washing step was repeated two more times to ensure the white blood cell layer does not exist.

A final wash was done using 5 to 10 ml of the complete media and the top layer was discarded leaving a layer of RBCs with 100% haematocrit. RBCs were re-suspended in equal volume of complete media to obtain 50% haematocrit which was then stored at 2-8 °C. RPMI and blood used in the process were maintained at similar temperature to prevent lyses of RBCs.

2.4 Cryopreservation of *Plasmodium falciparum*:

The strain used in the experiments was K1 multi-drug resistant *P. falciparum* strain which is resistant to chloroquine, pyrimethamine and sulphadoxin. Culture selected for cryo-preservation was over 10% parasitaemia with more than 50% ring stage as larger parasites gets lysed in due course. The parasitized blood was centrifuged and brought to 50% haematocrit by re-suspending in complete media. 0.5 ml of this blood was taken in a sterile cryotube and 0.5 ml of 20 % dimethyl sulphoxide (sterile filtered DMSO, Sigma, UK) in Ringers solution (9 g NaCl, 0.42 g KCl and 0.25 g $CaCl_2$/ Litre) was added. The cryotube was immediately placed in the liquid nitrogen to snap-freeze at -80^{o}C.

2.5 Retrieval from liquid nitrogen:

Parasitized blood was removed from the cryovial and placed in a microcentrifuge tube which was centrifuged in a minispin centrifuge (eppendorf, UK) at 13000 rpm for 90 seconds. DMSO supernatant was removed and 1 ml of 10% sorbitol (Fisher Scientific, UK), prepared in sterile phosphate buffer solution was added. After mixing gently, it was centrifuged again as mentioned above. Supernatant was discarded and the process was repeated with 1 ml of 5% sorbitol in sterile phosphate buffer solution. Three washes were done by 1 ml of complete media and after removing the supernatant, it was re-suspended in complete media, bringing the haematocrit to 50%. This parasitized blood was then added to the culture flask containing 10 ml of complete media and 0.5 ml of washed blood, maintaining the haematocrit for the culture at 5%.

2.6 Routine *Plasmodium falciparum* culture and determination of parasitaemia:

Existing *P. falciparum* culture was taken in the sterile hood without dislodging the parasites. Approximately 9 ml of medium was removed by using a serological pipette by tilting the flask. The waste medium was disposed in Virkon. Remaining parasite blood was mixed thoroughly. A drop was placed and smeared on a microscope slide to check the parasitaemia. After parasitaemia was estimated as mentioned (below), parasitized blood was diluted with fresh blood to give approximately 0.5 to 1% parasitaemia at 50% haematocrit. Culture was maintained in 10 ml or 30 ml culture flasks.

1 ml of 50% haematocrit parasite blood was transferred to 10 ml culture flask and 9 ml of complete media was added to bring the haematocrit to 5%. For a 30 ml culture flask 3 ml of parasite blood was added to 27 ml of complete media bringing 5% haematocrit. The flask was gassed with a 5% CO_2, 5% O_2 and 90% N_2 gas mixture (BOC Limited, UK) while creating small ripples on the surface of culture medium for about 15 seconds and then placed in the incubator at 37°C.

2.7 Estimating parasitemia through blood film:

A drop of parasitized blood from the culture was taken on a microscope slide and a thin smear was prepared. After air drying the slide, it was fixed with 100% methanol. The slide was again left to air dry and then stained with Giemsa prepared by diluting Gurr's Giemsa solution (BDH/VWR international limited, UK) in the ratio 1:10 in Sorensen buffer (BDH laboratory supplies, England). The slide was left in Giemsa stain for 20-30 minutes and then rinsed gently under tap water. It was left to air dry. The slide was viewed in Leica DM 500 compound microscope at 100x magnification under oil immersion to determine the degree and stage of parasitaemia.

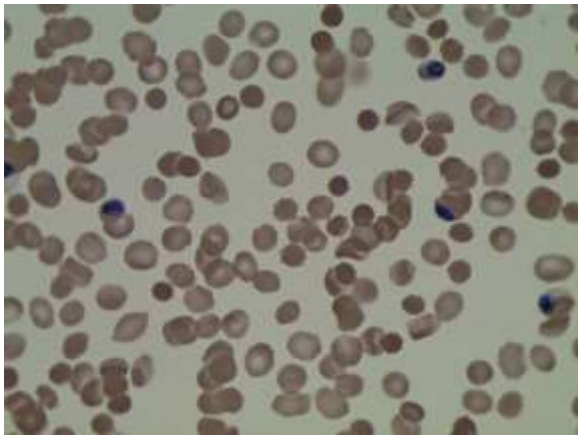

Figure 2.7.1: Microscopic view of RBCs infected with *Plasmodium falciparum* in trophozoite stage. Parasites were stained with Giemsa.

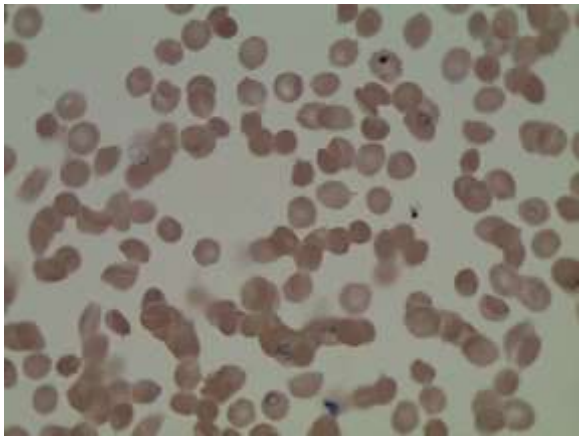

Figure 2.7.2: Microscopic view of RBCs infected with *Plasmodium falciparum* in ring stage. Parasites were stained with Giemsa.

Parasitaemia was calculated by counting the total number of RBCs in a field and total number of infected RBCs in that particular field. The step was repeated for 5 different fields selected randomly and average was taken.

Parasitaemia was estimated using the following formula:

$$\text{Parasitaemia} = \frac{\text{Average infected RBC} \times 100}{\text{Average total RBCs}}$$

2.8 Synchronization of *P. falciparum* culture:

Different stages are observed in the asexual life cycle of malaria parasite: merozoites, ring-stages, trophozoites and schizont stages. In natural hosts the parasite maintains synchronous development, but synchrony is lost quite rapidly in *in-vitro* cultures. Larger parasites in trophozoites and schizont stages are destroyed by sorbitol and so treatment with sorbitol is used to maintain tight synchrony. 1 ml of parasitized blood pellet was treated with 9 ml of 5% sorbitol (prepared in distilled water and filtered using 0.22 mm porosity millipore filter). After mixing gently, it was allowed to remain at room temperature for 5 minutes and centrifuged at 3000 rpm for 5 minutes. Supernatant was discarded, and complete media was used to wash the pellet 3 times after which an equal volume of complete media was added to the pellet to bring haematocrit at 50%. The freshly prepared RBCs were used to set up new culture.

2.9 Drug treatment of *P. falciparum* K1 Strain:

Drug stock solutions were prepared in DMSO unless otherwise stated for a particular compound. A serial dilution of the working solution was made using complete media. Parasite culture used for the experiment was diluted to approximately 0.5% to 1% for 72 hours or 48 hours experiment, respectively. Haematocrit was maintained at 5%. 100 µl of drug solution in serial dilution was added in the black bottom 96 well plate (Nunc, Denmark). 100 µl of the parasite blood was then added to these wells bringing the haematocrit to 2.5%. Control wells contained 100 µl of complete media and 100 µl of parasite blood. The plate

was kept in an airtight jar sterilised with 70% ethanol. It was gassed with 5% CO_2, 5% O_2 and 90% N_2 gas mixture for 2½ minutes. The jar was closed and incubated for 48 or 72 hours at 37°C.

2.10 Staining sample with SYBR green for microtitre plate assay:

SYBR green 1 (nucleic acid gel stain 10,000 x, Sigma, UK) staining solution (5 x SG in wash media or PBS) working solution was prepared by using following formula:

$$\frac{3.3 \times (\text{total volume of solution need for experiment in ml})}{10000}$$

(150 µl of SYBR green 1 working solution was needed per well, so the total volume required is calculated by multiplying 150 µl by number of wells used in the experiment)

Following the incubation period for the experiment, 150 µl of complete media was removed from each well and 150 µl SYBR green l working solution was added to these wells. Each well sample was mixed gently by pipetting up and down, the plate was covered with aluminium foil and left to incubate for 40 minutes. The experiment was read using a GENius plate reader (Tecan) with excitation and emission measured at 485 nm and 535 nm, respectively.

2.11 Using the GENius Tecan plate reader:

The computer and the plate reader were switched on. Plate reader software was selected. The correct plate (Nunc 96) was selected and the reading parameters were set to fluorescence with excitation and emission set as 485 nm and 535 nm, respectively. Plate was read from the top.

2.12 Staining sample with SYBR green 1 for flow-cytometry:

After the incubation period was over, 50 µl from the control and drug treated wells on a 96 well plate used in drug efficacy experiments were transferred to a microcentrifuge tube. Both

infected and non-infected blood samples were washed once with PBS. After removing the supernatant, 1 ml of 5 x SYBR green 1 solution (in PBS) was added to each sample (prepared by adding 5 µl of 10,000 x SG to 10 ml PBS). Incubation was done in the dark at room temperature for 20 minutes.

2.13 Fixing the sample for flow-cytometry:

After staining, the samples were centrifuged for 1 minute at 14,000 rpm and the supernatant was discarded. Samples were re-suspended in 250 µl of 0.37% formaldehyde fixation solution which was prepared by diluting 36.5% formaldehyde (Sigma, UK) with PBS to a final concentration of 0.37%. The samples were placed in the fridge and incubated at 4°C for 15 minutes. Samples were centrifuged as above and supernatant was discarded. 1 ml of PBS was used to wash the samples 3 times and analysis was done using the GENius plate reader (Tecan) or the FITC channel of the BD FACsVerse flow cytometer system.

2.14 Using the BD FACs Verse flow-cytometer

2.14.1 Setup and Performance QC

BD FACs Verse flow-cytometer was turned on and left for 20 minutes for warming up. Green light indicated the machine was ready to use, amber- it was warming up, while red- signified problem. After assuring there was good connection between the computer and the machine (indicated by a green light on the software programme at the bottom left of the computer screen), cytometer setup and tracking (CST) with the CST Beads was performed by clicking 'Setup & QC'. To run performance QC, 2 drops of CST bead was added to 0.5 ml sheath fluid. Performance QC was selected from the drop down menu next to 'task' and the number entered was matched to that on the CST bead stock vial used. Tube containing diluted CST beads was put on the machine when prompted and instructions were followed.

2.14.2 Running samples on the FACs machine

New experiment was created, and each tube was read. The axis on the default graph was changed by right clicking and selecting a different axis label. 'PMTV' was used to alter axis

voltage. Gates were added by selecting the required shape from the toolbar (Figure 2.14.1). The number of events acquired was altered by right clicking on the tube, selecting properties and then acquisition. For this study, the required number of events required to read the samples was selected as 50,000. Once the samples were read, FACs daily clean was performed using 3 ml of de-ionised water and 2 ml of FACs clean in separate tubes.

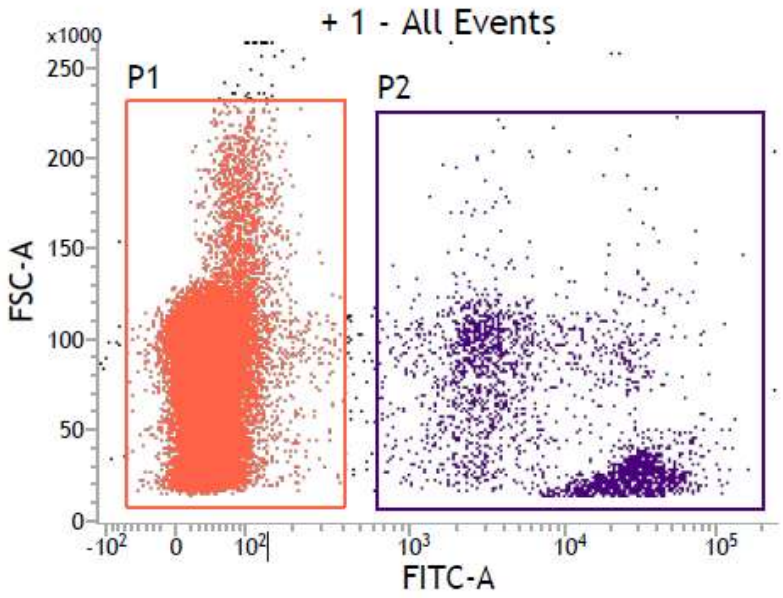

Figure 2.14.1 Flow-cytometer graph showing two populations of RBCs measured on the FITC-A channel. P1 is the population of non-infected RBCs and P2 is the population of *Plasmodium falciparum* infected RBCs.

2.15 Optimisation for medium used to read the experiments:

Optimisation was performed to determine the best medium for washing and diluting the samples for reading the experiments through plate-reader. Phosphate Buffer Solution (PBS) or RPMI 1640 containing HEPES and L-glutamine were evaluated. Complete medium RPMI 1640 contains albumax which could interfere with the detection of signal due to its inherent fluorescence and hence was not considered for the optimisation experiment.

Two sets (Set A and Set B) of three samples each of *P. falciparum* blood cultures were prepared by 2 fold serial dilution such that if parasitaemia was considered to be 100% in sample 1, parasitaemia would be 50% in sample 2 and 25% in sample 3, as shown in Table 2.15.1.

2.15.1 **Estimation of parasitaemia through microscopy:**

Slides were prepared from each sample and viewed under the light microscope as per the methods mentioned in Chapter 2, section 2.7. Parasitaemia in sample 1 was found to be 1.72%, sample 2 was 0.81% and sample 3 was 0.39%. If percentage of parasitaemia was considered 100% in sample 1, based on calculating the parasitaemia through microscopy, parasitaemia in sample 2 was 47% and in sample 3 was 23%.

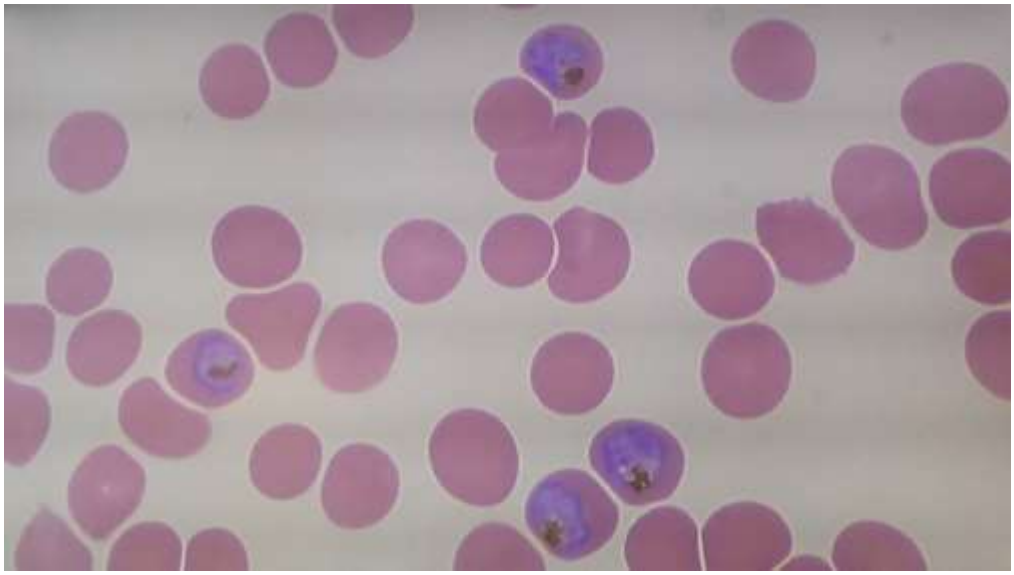

Figure 2.15.1 Light microscopy view of red blood cells infected with *P. falciparum* trophozoites stained with Giemsa.

2.15.2 **Estimation of parasitaemia through plate-reader:**

All three samples in Set A were washed and diluted with PBS, whereas all three samples in Set B were washed and diluted with RPMI 1640. The samples were incubated for 40 minutes after staining with SYBR green. Post-incubation, the samples were read through plate-reader as per the methodology mentioned in Chapter 2. The experiments were read at Gain 60, Gain 70 and Gain 80 to determine the best setting for reading the experiment. Percentage of parasitaemia was determined. It was observed in Set A (PBS as wash medium), if parasitaemia was considered to be 100% in sample 1, parasitaemia in samples 2 and 3 were found to be 50% and 29% respectively in Gain 60, 49% and 28% respectively in Gain 70 and

50% and 29% respectively in Gain 80. In Set B (RPMI 1640 as the wash medium), if parasitaemia was considered to be 100% in sample 1, parasitaemia in samples 2 and 3 were found to be 54% and 0% respectively in Gain 60, 57% and 0% respectively in Gain 70 and 54% and 0% respectively in Gain 80. Results are shown below in Table 2.15.1

Table 2.15.1 Determination of percentage of parasitaemia

P. falciparum culture	Percentage of parasitaemia through microscopy	% Parasitemia in Set A			% Parasitemia in Set B		
		Gain 60	Gain 70	Gain 80	Gain 60	Gain 70	Gain 80
Sample 1 (1.72%)	100	100	100	100	100	100	100
Sample 2 (0.81%)	47	50	49	50	54	57	54
Sample 3 (0.39%)	23	29	28	29	0	0	0

The serial dilution of infected blood starting at 1.72 % to 0.39% parasitaemia was analysed using the SYBR Green MicroPlate assay at Gain 60, 70 and 80. Comparisons were made between parasite infected blood samples diluted in either PBS (Set A) or RPMI 1640 (Set B).

No difference was observed Gain 60, Gain 70 and Gain 80 measuring the parasitaemia in both sets. It was observed, whilst there was not much difference between PBS and RPMI 1640 in measuring parasitaemia at higher percentages, but the plate-reader was unable to detect signals in samples washed with RPMI 1640 at parasitaemia lower than 0.25%.

PBS was found to be a good medium to wash and dilute the culture samples for the purpose of reading the experiments through plate-reader.

2.16 Calculation of IC_{50} values:

Values obtained from all dose response data sets were transferred into Microsoft excel from respective software programmes. The infected blood controls were set at 100% and percentage parasitaemia was calculated for drug treated samples relative to the infected control. For IC_{50}, Graphpad prism 5.0 was used to further process the data. The largest value in the data set was set to correspond to 100% and the smallest value to 0% by normalising the data. IC_{50} values were calculated using nonlinear regression (Graphpad prism 5.0) by using log-transformed drug concentrations plotted against the dose response. The log(inhibitor) vs. normalised response-variable slope option was used for IC_{50} calculation.

2.17 Synthesis of dehydroemetine:

The synthesis process was outsourced to Chiroblock GMBH, Germany. Isomers of dehydroemetine were synthesised by differential substitution on the four aryl oxygen as per the established literature (Scheme 1, Brossi 1967, Patent No. 3,311633 [16]). Derivatives were validated using NMR, HPLC and FTIR. In the 1950's and 1960's, the chemistry of 2-dehydroemetine **13** was published, mostly in German, in a number of patents and applications by chemists at Hoffmann-La Roche. However, in most cases no conventional analytics, like ^{1}H-NMR spectra or MS, were presented. Therefore, it was decided to reproduce the synthesis with slight modifications to get the authentic specimen of 2-dehydroemetine **13** claimed in the patents (Figure 2.17.1).

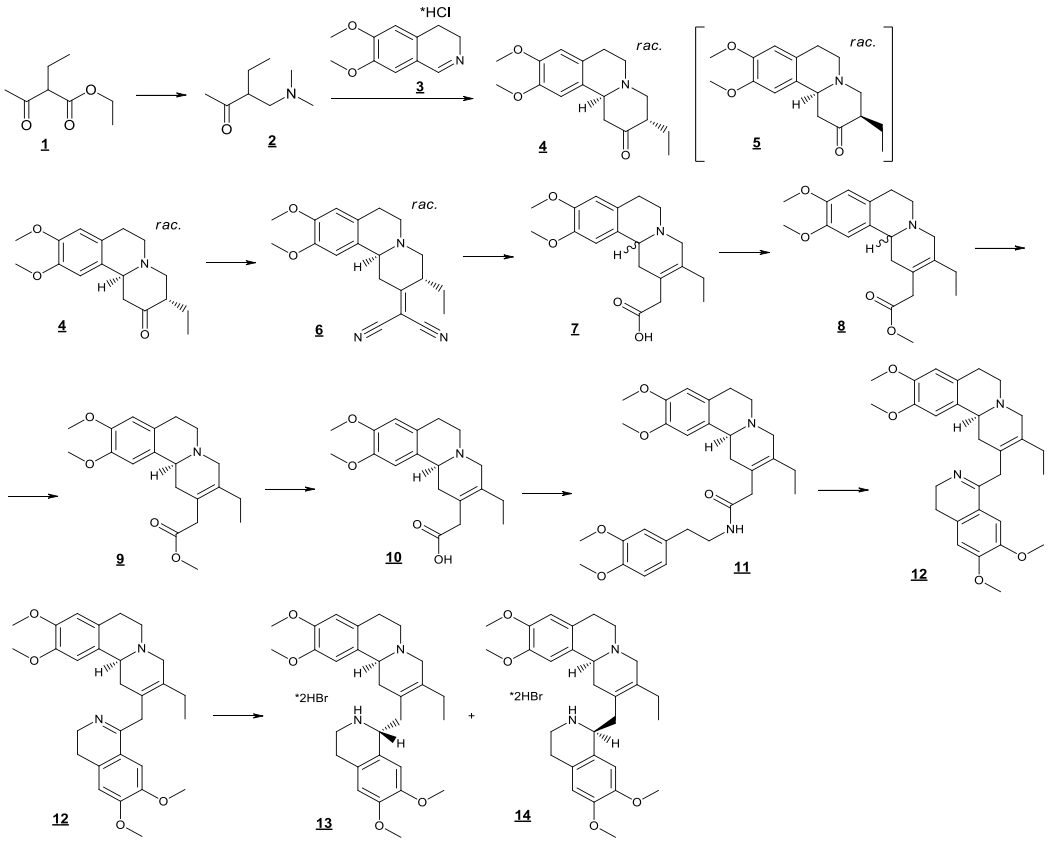

Figure 2.17.1 Schematic representation of the steps involved in the synthesis of 2-dehydroemetine (13) and its diastereomer (14).

The two compounds synthesised were (-)-*R,S*-dehydroemetine and (-)-*S,S*-dehydroisoemetine. The methodology for synthesis of is mentioned in Appendix I.

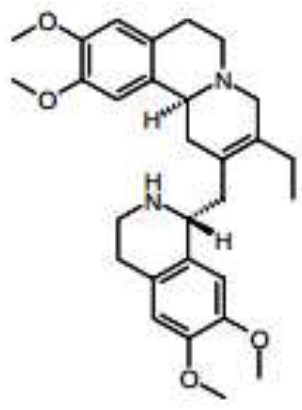

(S)-2-((R)-6,7-Dimethoxy-1,2,3,4-tetrahydro-isoquinolin-1-ylmethyl)-3-ethyl-9,10-dimethoxy-1,6,7,11b-tetrahydro-4H-pyrido[2,1-a]isoquinoline * dihydrobromide

Figure 2.17.2: Chemical structure of (-)-*R,S*-dehydroemetine

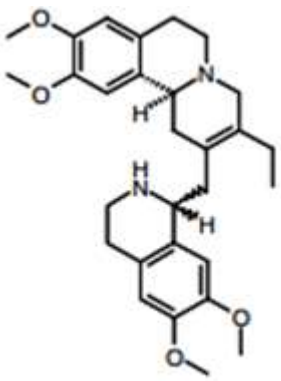

(S)-2-((S)-6,7-Dimethoxy-1,2,3,4-tetrahydro-isoquinolin-1-ylmethyl)-3-ethyl-9,10-dimethoxy-1,6,7,11b-tetrahydro-4H-pyrido[2,1-a]isoquinoline * dihydrobromide

Figure 2.17.3: Chemical structure of (-)-*S,S*-dehydroisoemetine

2.18 Drug interaction analysis for *(-)-R,S*-dehydroemetine:

Preparation of the primary stock solutions was done as mentioned above. For experimental set up a dose range of 0.125–8 x the IC_{50} was made by a two-fold serial dilution for each compound tested. The compounds were co-administered at each level and the parasites were treated at ring stage in a 96 well plate. They were incubated for 72 hours at 37ºC. For drug susceptibility, the plates were read using SYBR green plate reader method. CalcuSyn software (Biosoft) was used for analysing the data. The methodology for the experiment is explained in detail in Chapter 4.

Chapter 3 Molecular modelling of emetine and dehydroemetine

3.1 Introduction:

Drug discovery depends on testing compounds on cultured cells or animals in a trial and error method to determine if a compound could be a potential treatment (Ginsburg and McCarthy, 2001) (Boran and Iyengar, 2010). In contrast to this, knowledge of a biological target could also be used to identify or invent new drugs. This process is called rational drug design (Stocks, 2013) (Takenaka, 2001). This requires a biological target molecule whose modulation or mutation is associated with the disease process and has the capacity to interact with a small molecule (druggability) which would result in the modulation of the target biomolecule (Yuan et al., 2013). It is more appropriate to call it a process for 'ligand design' as once a compound is identified to have a good binding affinity to a target, its half-life in the body, absorption and excretion profile, and side-effects determine if the ligand could be optimised as a drug to be safely and efficaciously used for treatment (White et al., 2004) (Tollenaere, 1996). *In-vitro* experiments to determine the ADMET profiles together with computational modelling techniques are frequently used to determine the physiochemical properties of a ligand in drug design in a bid to minimize high attrition rates in the drug delivery pipelines (Merz Jr et al., 2010) (Waring et al., 2015) (Yu and Adedoyin, 2003).

Computer-aided drug design could be ligand-based or structure-based (Merz Jr et al., 2010). Knowledge of molecules which bind to a particular target could help design a pharmacophore model which specifies certain characteristics a small molecule must have structurally, in order to bind to the target molecule in ligand-based drug design (Güner, 2000). On the other hand, structure-based drug design relies on NMR spectroscopy, X-ray crystallographic or a homology model three dimensional structure of a biological target molecule and screens a database of small molecules to selectively identify the ones which bind with high affinity and form a stable complex (Li et al., 1996) (Hillisch et al., 2004). Few examples of drugs discovered *via* computer-aided drug design are dorzolamide, a carbonic anhydrase inhibitor approved in 1995 (Greer et al., 1994) (Talele et al., 2010) (Song et al., 2009), imatinib which inhibits tyrosine kinase as a treatment for Philadelphia-chromosome positive leukemias (Capdeville et al., 2002) and raltegravir, which is an HIV integrase inhibitor (Mouscadet and Tchertanov, 2009).

Drug design could be aided by use of docking for rapid identification of a potential hit by scanning through large databases of compounds (Ekins et al., 2007). The potential lead could be optimised to design analogues which are more potent and selective (Rees et al., 2004). The orientation in which two molecules bind or interact with each other to make a stable complex could be predicted by docking (Lengauer and Rarey, 1996). Scoring functions could be used to analyse the orientation of the molecules with respect to each other and help in the prediction of binding affinity or the strength of association (Warren et al., 2006). Benefits of predicting inter-molecular interactions are immense. In the process of rational drug design, elucidation of biochemical processes and knowledge of the binding conformation of the target with a small molecule ligand in the binding site is important for structure-based drug design (Anderson, 2003).

The analogy of a 'hand in glove' is a better fit than the century old 'lock and key' analogy by Fisher and Ehrlich (Dunker et al., 1998). In docking, the main approaches are 'shape complementarity' or 'simulation'. The fast and robust shape complementarity methods could scan thousands of ligands in a very short span of time but are unable to accurately model the dynamic changes in the conformations of proteins or ligand (Grünberg et al., 2004) (Mukesh and Rakesh, 2011) (Forli et al., 2016). The method considers that a dockable or complementary set of features, such as molecular surfaces, are present between the protein and ligands and utilizes these features to predict if a ligand would bind to the active site of a protein (Goldman and Wipke, 2000) (Grant et al., 1996). 'Simulation' is a computationally expensive method to calculate the interaction energies between the ligand and the protein separated by some distance (Feig et al., 2004). Ligand flexibility is incorporated in this method and the ligand undergoes a number of moves to bind into the active site of the protein (Joseph-McCarthy et al., 2003). Every move follows calculation of the total energy of the system as every move result in an energetic cost to the system (Tripathi and Misra, 2017) (Alonso et al., 2006)..

For docking, a protein structure is used and ligand database could be used to retrieve ligands for docking (Irwin and Shoichet, 2005) (Nealon et al., 2017) (Wolber and Langer, 2005). A docking program relies on the search algorithm and scoring function (Perola et al., 2004) (Ferreira et al., 2015). It is not possible for search algorithms to exhaustively explore all the possible conformations of the protein relative to the ligand and so most docking programs

consider the ligand as flexible and the protein as a rigid structure (Sousa et al., 2006) (Claussen et al., 2001). Proteins being highly flexible large molecules, makes it challenging to model its conformation (Ciemny et al., 2018). Ignoring the flexibility of the receptor does lead to poor docking results in some instances (Cerqueira et al., 2009). A scoring function, which assesses the energy of the pose in relation to the binding site, is used to evaluate ligand poses and rank them based on how favourable a binding interaction they represent. A stable system has the minimum energy (Halperin et al., 2002).

In this study, various docking approaches were used to replicate the predicted binding pose of emetine (Wong, *et al*, 2014) and model synthetic dehydroemetine diastereomers in the binding pocket. *Alangiaceae, Icacinaceae,* and *Rubiaceae* are the three plant families in which emetine and its analogues occur. Native to Brazil, *Psychotria ipecacuanha* also known as *Cephaelis ipecacuanha*, belonging to the family *Rubiaceae* is the major source. Emetine, the main active ingredient in ipecac syrup, has been widely used as an anti-parasitic drug and in phytomedicine in the past. Emetine exhibits antiviral, anti-parasitic, anticancer and contraceptive activities due to its ability to inhibit both ribosomal and mitochondrial protein synthesis. It is also known to cause the up-regulation and down-regulation of certain genes and to interfere with the synthesis and activities of DNA and RNA (Akinboye and Bakare, 2011). Emetine and its derivatives have been tested in laboratories and have shown potent activity on prostate cancer, ovarian cancer, pancreatic cancer and a few other cancer cell lines (Akinboye et al., 2016) (Sun et al., 2015) (Han et al., 2014) (Uzor, 2016). Various small clinical trials were conducted to evaluate the potency and side-effects of emetine.

Dehydroemetine, was first synthesised in Switzerland by Roche as an effective but less toxic derivative of emetine (1967). It is a synthetic emetine analogue and is a WHO recommended drug for use in metronidazole therapy failure in amoebiasis and giardiasis (Appendix II). It is irritant if taken orally but is less toxic than its parent compound emetine. It is assumed that like emetine, dehydroemetine also exerts its effects by inhibiting protein translation (Hellgren et al., 2014). It has been investigated for use in cutaneous amoebiasis (Magańa-García and Arista-Viveros, 1993), amoebic dysentery (Knight, 1980) (Rubidge et al., 1970), amoebic liver abscess (Nigam et al., 1985) (Peters et al., 1979), herpes zoster (Hernandez-Perez, 1980) (Glaser, 1983) and leishmania infection (Al-Khateeb et al., 1977) (Fouarge et al., 1989).

Emetine has been identified as a potent antimalarial and this chapter focuses on modelling the two diastereomers of dehydroemetine on the emetine binding site on the published cryo-EM structure (3J7A).

3.2 Methods:

3.2.1 Generation of emetine, *(-)-R,S*-dehydroemetine and *(-)-S,S*-dehydroisoemetine structures:

The cryo-EM structure of *P. falciparum* 80S ribosome bound to emetine dihydrochloride was obtained from the Protein Data Bank (PDB code 3J7A) (Wong et al., 2014) to predict the bound position of emetine and its synthetic analogues. Emetine structure was extracted from 3J7A and analysed. The emetine conformer was also generated from the software package Molecular Operating Environment (MOE). Subsequently, MOE was used to construct the emetine derivatives *(-)-R,S*-dehydroemetine and *(-)-S,S*-dehydroisoemetine (MOE, 2016). Crystallographic water molecules were removed, and hydrogens were assigned. PyRx, Autodock vina and MOE-Dock were used to perform docking of ligands to the *Pf*40S subunit. The cryo-EM ligand location was used to define the binding site region. Internal flexibility was allowed for ligands but not the ribosome and poses were scored automatically by the software's scoring system.

3.2.2 Autodock vina for docking:

Autodock tools is a software used to prepare the receptor (ribosome) and ligands for docking. Significant improvement in the accuracy of the binding mode predictions of autodock vina and about two orders of magnitude speed-up has been observed in comparison with the molecular docking software AutoDock 4. Autodock vina calculates the grid maps automatically and the results are clustered in a way that is transparent to the user (Trott and Olson, 2010). Autodock vina tutorials were followed to perform docking (Trott and Olson, 2010). Ribosome receptor was protonated with polar hydrogens and saved as .pdbqt file. Similarly, the ligand was also prepared and saved as .pdbqt file by adding polar hydrogens, selecting the number of rotatable bonds and assigning torsion value. For the search space, grid was centred on the ligand. Configuration text file was prepared with the grid parameters.

The receptor, ligand and configuration files were saved in the autodock vina path and the programme was run using command prompt. The vina output results were viewed using PyMol and Discovery Studio.

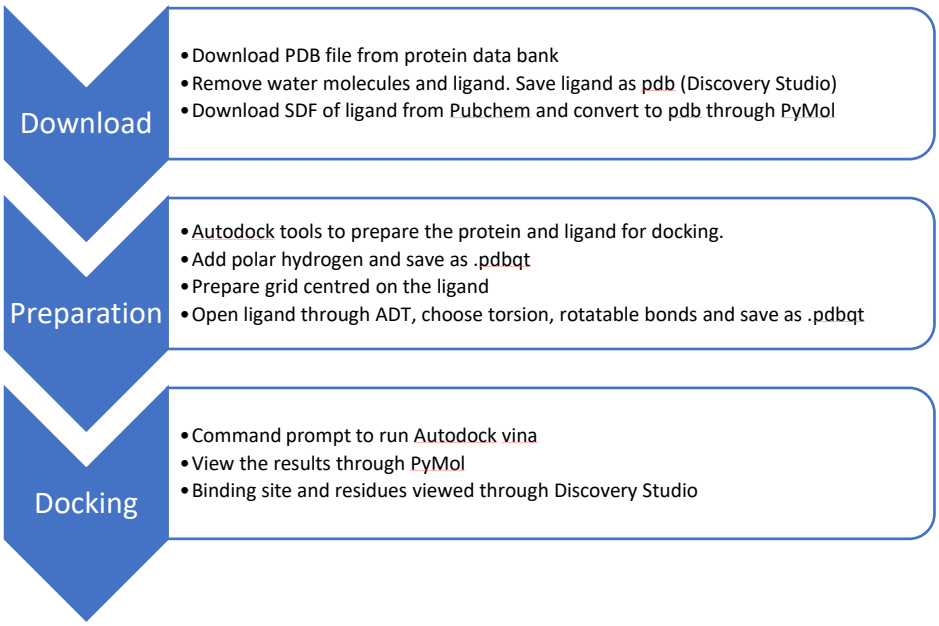

Figure 3.2.1: Methodology for performing receptor-ligand docking through Autodock vina.

3.3 Results:

3.3.1 Structure analysis of 3J7A cryo-EM structure of emetine bound to 40S subunit of 80S ribosome:

The availability of a high resolution cryo-EM structure of *Plasmodium falciparum* 80S ribosome bound to emetine (Wong et al., 2014) has given rise to the possibility of structure based changes to further modify the drug. This study aims to use molecular modelling as a tool for lead optimisation of synthetic analogues of emetine dihydrochloride to identify molecules with similar potency as emetine but potentially reduced side effects. The study began by analysing the bound position of emetine in 3J7A cryo-EM structure.

The Cryo-EM structure of *P. falciparum* 80S ribosome 3J7A has a resolution of 3.2A. The pdb structure file does not mention the overall anisotropic B-factor value. B-factor of less

than 60 is usually indicative of good temperature stability but the b-factor map of the ribosome structure in MOE displayed poor resolution as shown in Figure 3.3.1 – Figure 3.3.3.

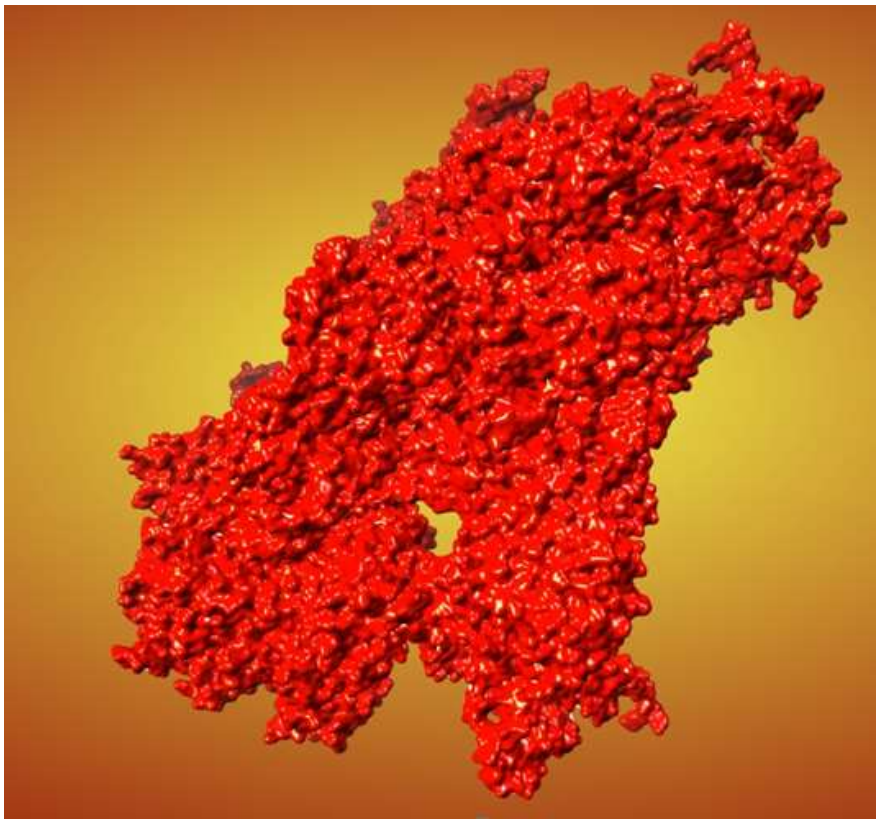

Figure 3.3.1 B-factor map of 40S subunit of 80S ribosome in 3J7A cryo-EM structure. B-factor value > 60 (red map) is indicative of poor temperature stability.

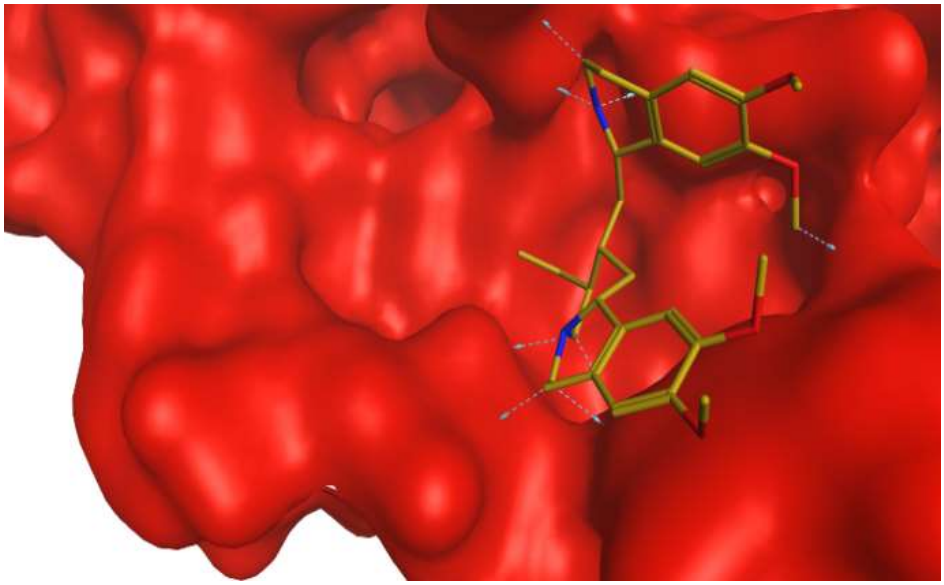

Figure 3.3.2 B-factor map of the binding pocket on 40S subunit of 80S ribosome in 3J7A cryo-EM structure. Emetine is seen in the pocket in a U-shaped conformation. B-factor value > 60 (red map) is indicative of poor temperature stability.

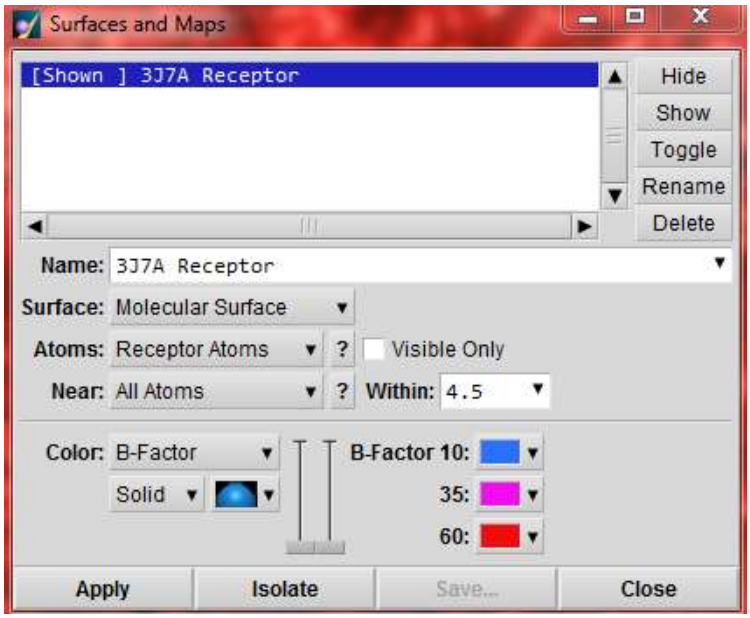

Figure 3.3.3: Settings in MOE depicting the colour code for B-factor map.
B-factor value > 60 (red map) is indicative of poor temperature stability.

3.3.2 **Structure of emetine in 3J7A cryo-EM model of emetime bound *P. falciparum* 80S ribosome:**

Chemical degradation experiments were conducted in the past to elucidate the chemical structure and stereochemistry of emetine. Structure activity relationship studies showed (Grollman, 1966) that C-1´ must have the R configuration and the 2´ position must be a secondary amine for emetine to be biologically active. The S configuration at C-1´ as seen in 'isoemetine' makes the compound inactive.

Emetine was extracted from the cryo-EM structure through Discovery Studio and the structure was analysed for its stereochemistry using Molecular Operating Environment (MOE). It was found that the emetine in the cryo-EM structure in 3J7A (Wong et al., 2014) has incorrect chirality (Figure 3.3.2.3). For comparison, emetine structure was downloaded from pubchem (Figure 3.3.2.2) and referenced with the published emetine structure (Figure 3.3.2.1) (S Akinboye and Bakare, 2011). It was found that in 3J7A (Wong et al., 2014), not only the important chiral centre at C-1´ had S configuration instead of R configuration but the other 2 chiral centres in the cryo-EM emetine structure are also incorrect as shown Figure 3.3.4 – Figure 3.3.10.

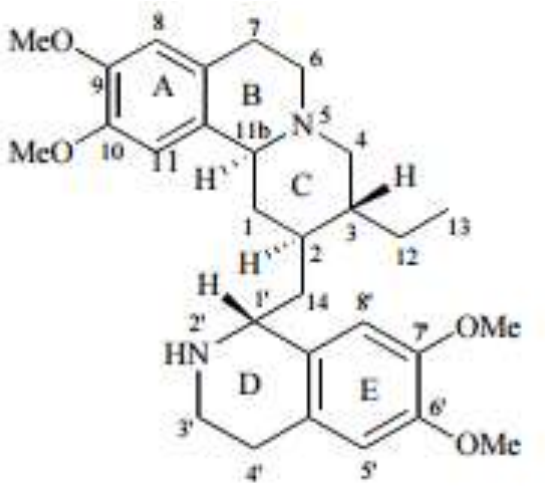

Figure 3.3.4: Emetine structure adapted from (Akinboye and Bakare, 2011) showing R configuration at C-1'

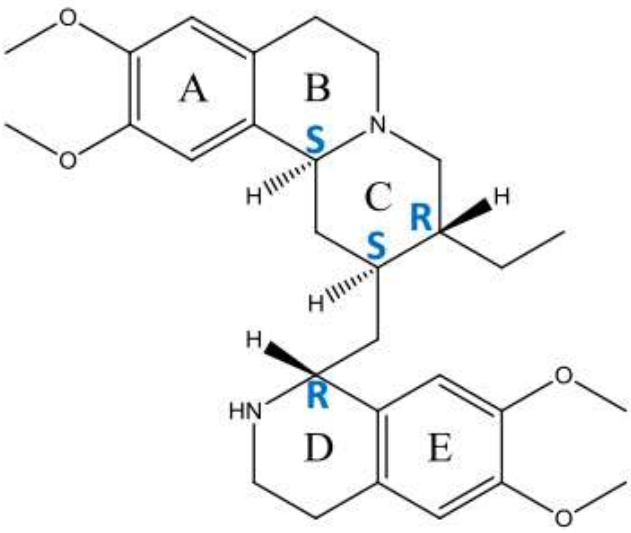

Figure 3.3.5: Pubchem (database of chemical molecules) emetine structure showing R configuration at C-1'

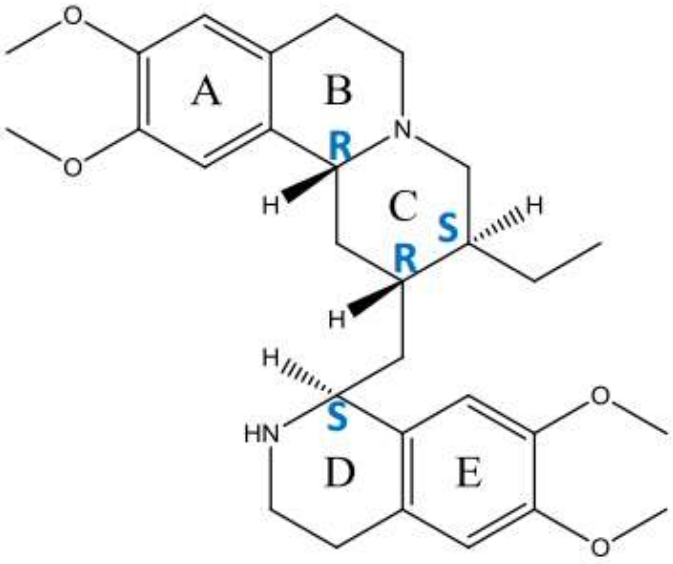

Figure 3.3.6: Emetine structure in 3J7A pdb structure file published by Wong et al, 2014 showing S configuration at C-1'

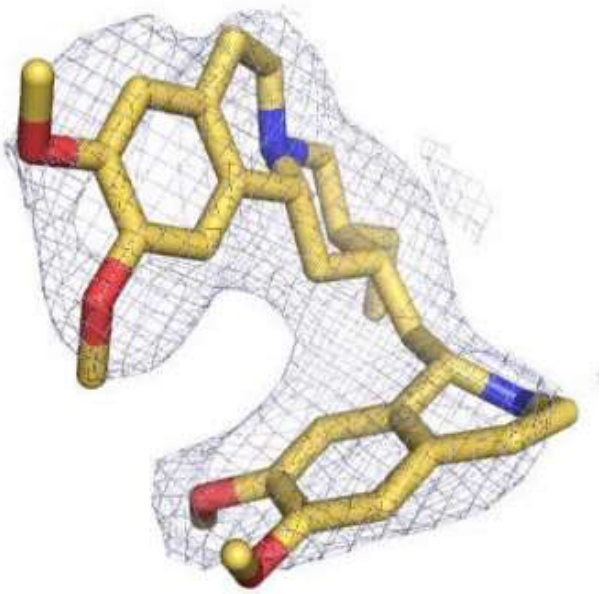

Figure 3.3.7: Emetine structure in 3J7A pdb structure file in the electron density map published by Wong et al, 2014 showing R configuration at C-1'

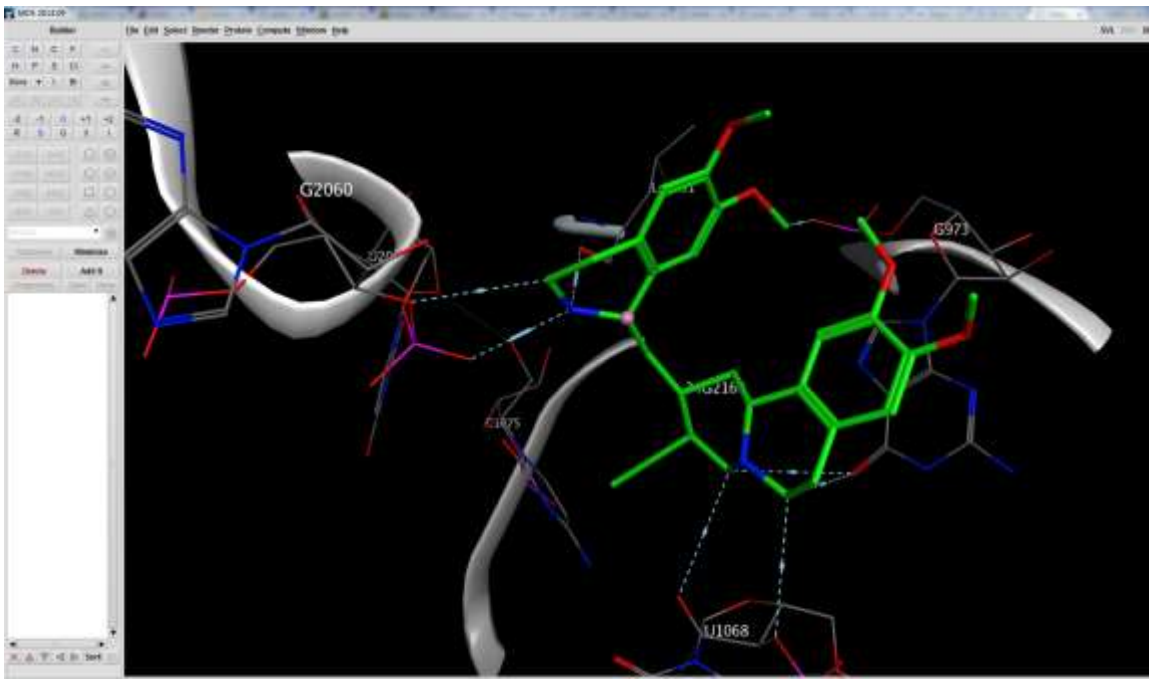

Figure 3.3.8 S-configuration at the C1 chiral centre of emetine in 3J7A cryo-EM model (highlighted on the toolbox on the left). Natural emetine has a R-configuration.

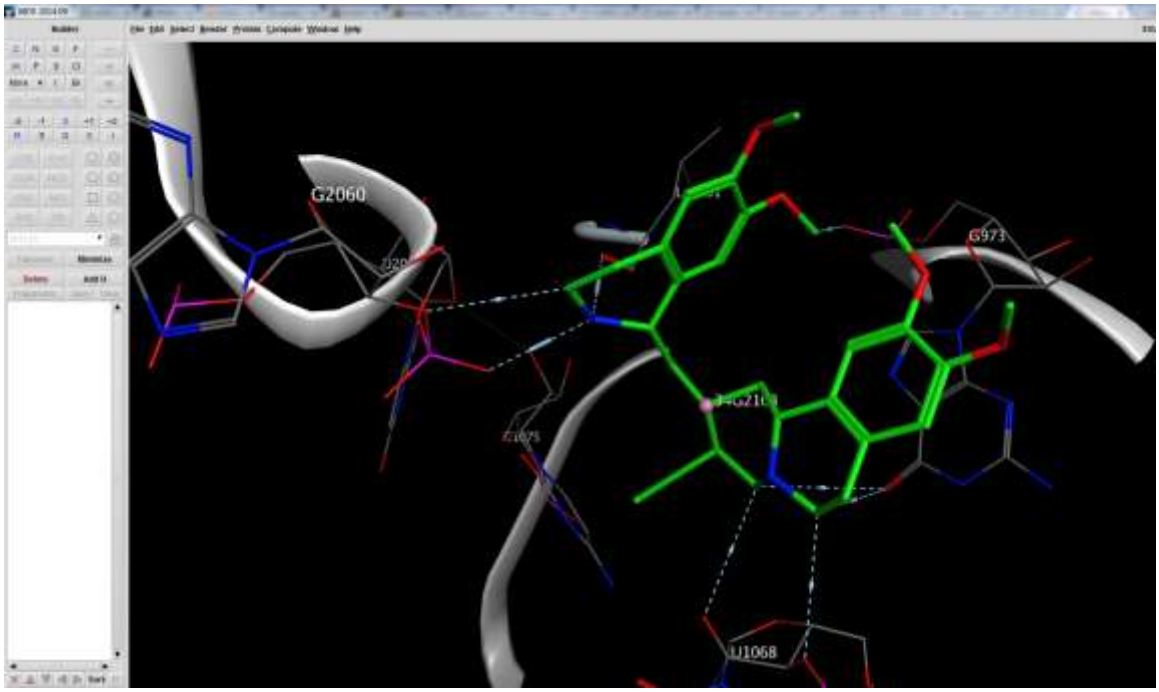

Figure 3.3.9 R-configuration at the second chiral centre of emetine in 3J7A cryo-EM model (highlighted on the toolbox on the left). Natural emetine has a S-configuration.

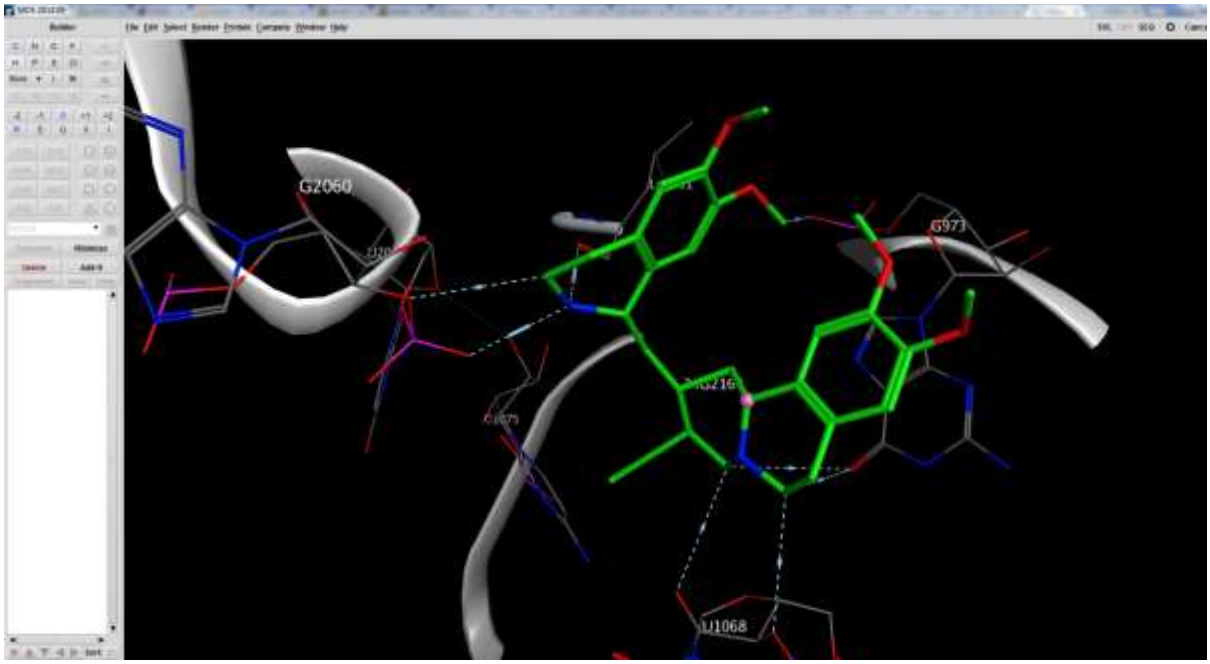

Figure 3.3.10 R-configuration at the third chiral centre of emetine in 3J7A cryo-EM model (highlighted on the toolbox on the left). Natural emetine has a S-configuration.

3.3.3 **Docking of emetine and dehydroemetine**

Dehydroemetine, a synthetic analogue of emetine hydrochloride has been claimed to have less cardio-toxic effects than emetine. Dehydroemetine can exist in R and S isomeric forms, which are diastereomers of each other. Being an analogue of emetine, it is likely that dehydroemetine also binds to the emetine binding site on 40S subunit of the 80S ribosome. To test the hypothesis, docking was performed on the 80S ribosome (3J7A) with emetine, *(-)-R,S*-dehydroemetine and *(-)-S,S*-dehydroisoemetine.

The PDB file of *P. falciparum* 80S ribosome bound to emetine dihydrochloride (3J7A) was downloaded from protein databank and the program Discovery Studio was used to remove any solvents in the structure. The structure was saved in the .pdb format. The ribosome was then separated from the bound ligand emetine. Both the receptor and the ligand were saved separately as .pdb files. The 3D drug structure of emetine was also downloaded from the Pubchem database due to the incorrect chirality of emetine molecule in 3J7A. Structures of *(-)-R,S*-dehydroemetine and *(-)-S,S*-dehydroisoemetine were drawn using MOE software (Figure 3.3.11). The receptor was treated as rigid and the ligands as flexible molecules.

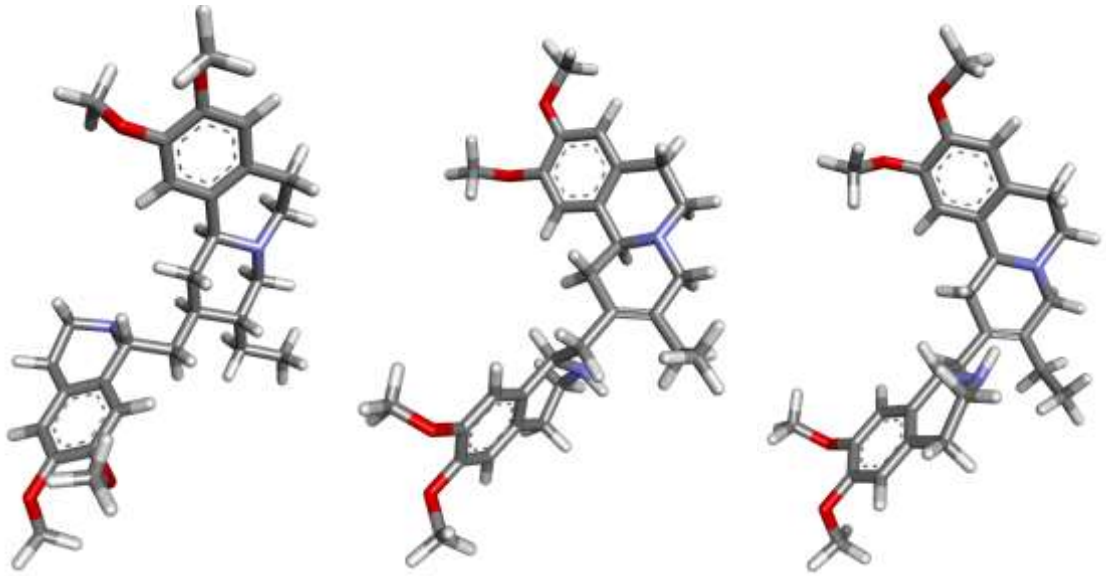

Figure 3.3.11: From left to right, 3D structures of emetine dihydrochloride, (-)-*R,S*-dehydroemetine and (-)-*S,S*-dehydroisoemetine drawn using MOE software.

Various docking programs were used to perform the docking of emetine, *(-)-R,S*-dehydroemetine and *(-)-S,S*-dehydroisoemetine.

3.3.4 **PyRx for molecular modelling:**

A virtual screening software for computational drug discovery known as PyRx was used to perform receptor-ligand (Dallakyan and Olson, 2015). PyRx has a plugin for autodock vina which enables it to perform the docking. It provides support to the users and guides them through every step of this process - from data preparation to job submission and analysis of the results. In this study the free version of PyRx was used.

The pdb structures of the ribosome receptor and emetine molecule were uploaded on PyRx and the search grid was selected around the emetine binding site (Figure 3.3.12. and Figure 3.3.13). Docking was performed through the autodock vina plugin to check if the emetine binding site could be replicated through PyRx. Many docking runs were performed but PyRx was unable to replicate the binding conformation of emetine as predicted in 3J7A.

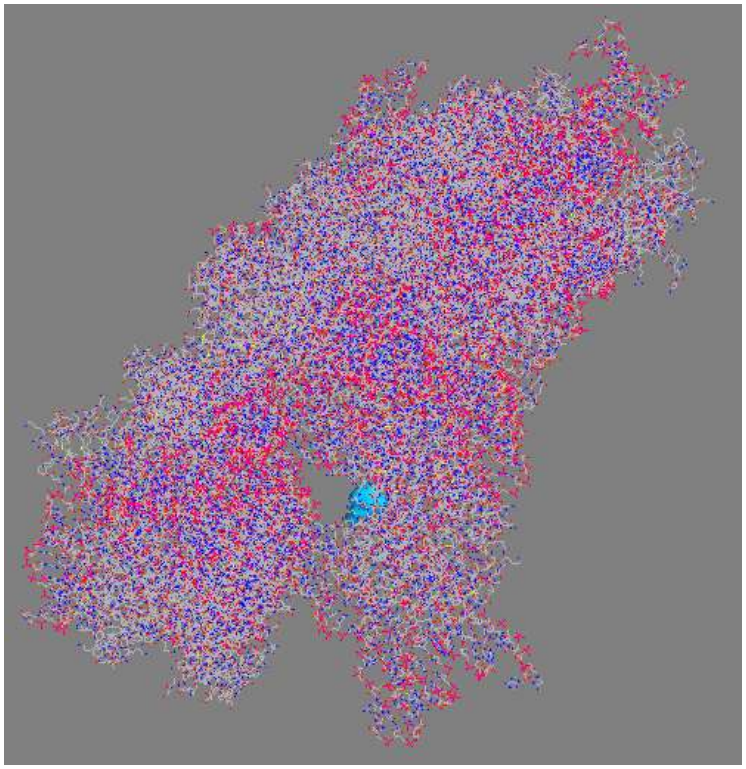

Figure 3.3.12: Emetine bound 3J7A pdb structure of 80S ribosome as observed in PyRx. Emetine is depicted in sky blue colour in the binding pocket.

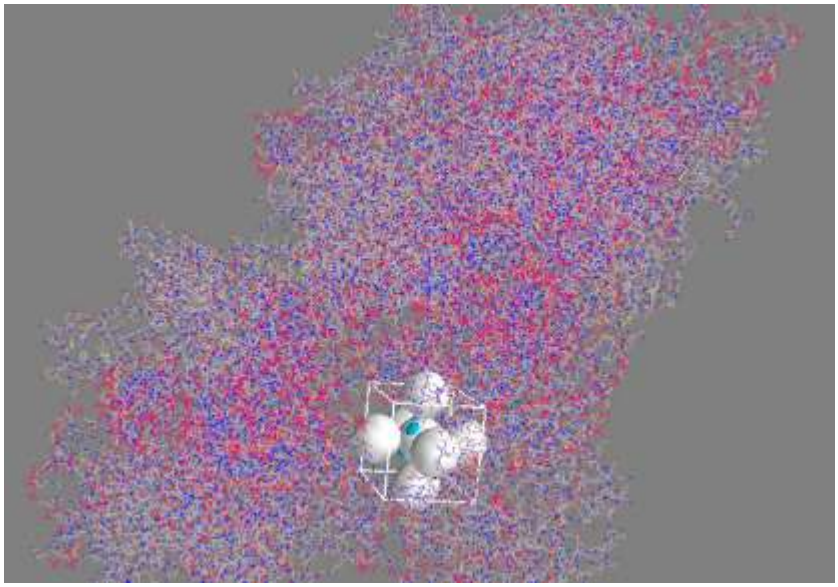

Figure 3.3.13: Grid map with grid parameters around the emetine binding site.

The binding site predicted by PyRx did not overlap with the 3J7A published binding site Figure 3.3.14. So, it was decided to not go ahead with PyRx for the docking of dehydroemetine.

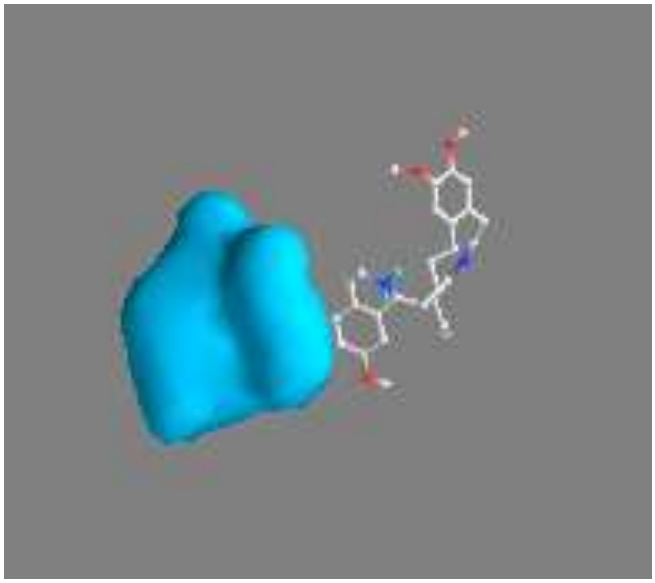

A

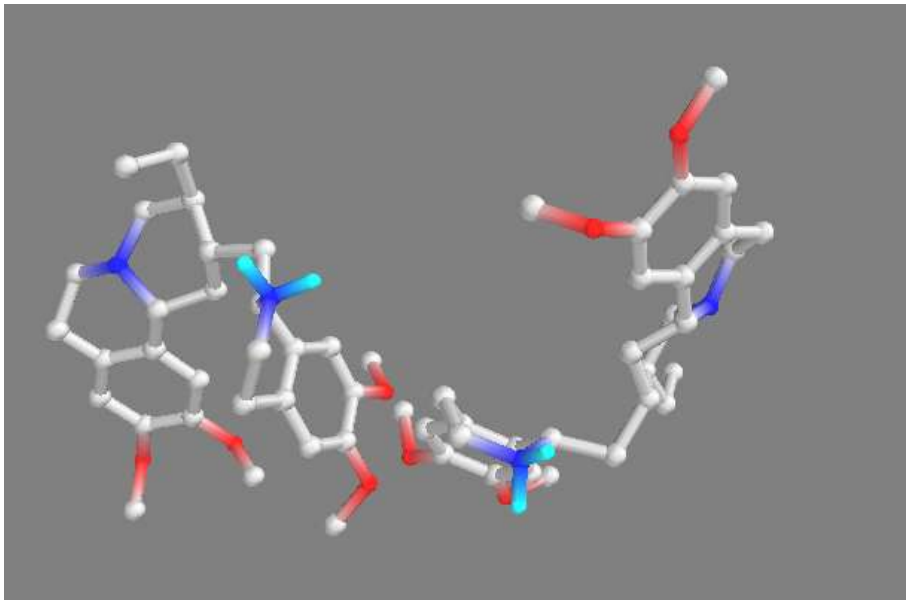

B

Figure 3.3.14: Difference in the binding site predicted by PyRx and published literature.

(A). The molecule in blue is the binding site predicted by Wong *et al*, 2014. As seen in the above images, PyRx was unable to accurately locate the emetine binding site. No superimposition of the binding poses from PyRx with the published pose in 3J7A (B).

3.3.5 **Receptor-ligand docking:**

The PDB file (3J7A) of 40S subunit of 80S Ribosome of *P. falciparum* bound to emetine was downloaded from the Protein databank. The file was opened in Discovery studio and the solvent water molecules were removed. The structure was saved in .pdb format. The

ribosome was then separated from the bound ligand (emetine) and both the ribosome and emetine molecule were saved in .pdb format (Figure 3.3.15 – Figure 3.3.17)

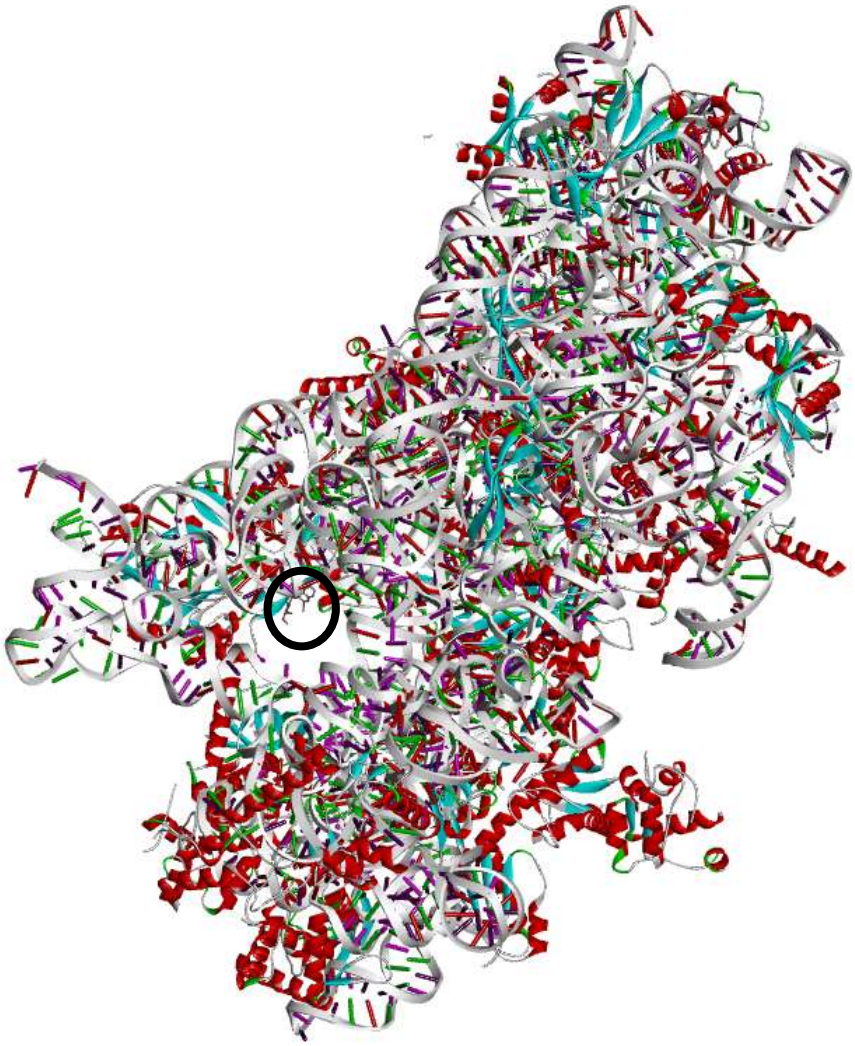

Figure 3.3.15: Emetine bound 40S subunit of 80S ribosome. The black outlined circle focuses on the binding pocket. Emetine is visualised in the binding site.

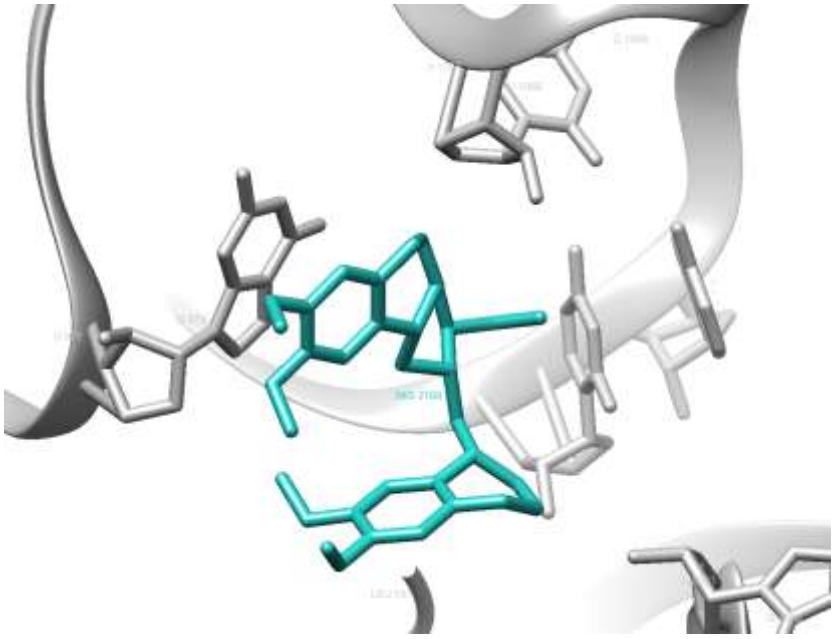

Figure 3.3.16: Focused view of emetine binding site on 40S subunit of 80S ribosome published in the cryo-EM structure 3J7A.

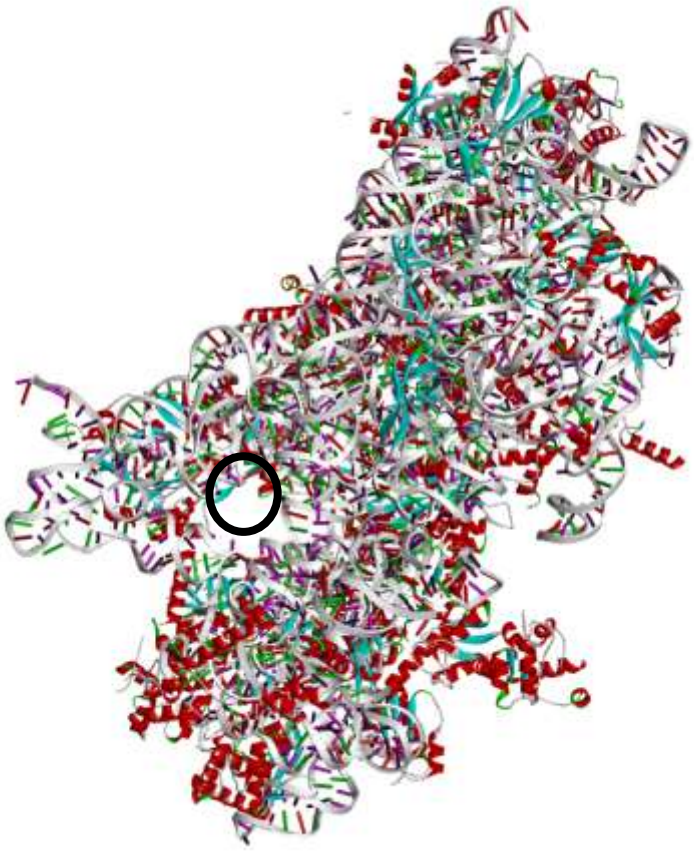

Figure 3.3.17 View of 3J7A 40S subunit of 80S ribosome after the removal of the bound ligand, emetine. Black outlined circle focuses on the binding pocket. Emetine is absent from the binding site.

3D structures of emetine dihydrochloride hydrate was downloaded from pubchem. Structure of (-)-*R,S*-dehydroemetine and (-)-*S,S*-dehydroisoemetine were drawn using MOE. Autodock tools was used to prepare the receptor and ligand molecules, and docking was performed for all ligand molecules following the steps outlined in methodology.

Polar hydrogens were added to the ribosome and parameters were specified to prepare the grid and configuration file, respectively. Multiple unbound magnesium atoms were observed, and the software was directed to go ahead and add the hydrogens. In a bid to replicate the binding conformation in 3J7A, emetine from cryo-EM structure, emetine from pubchem, and (-)-*R,S*-dehydroemetine and (-)-*S,S*-dehydroisoemetine were docked on the 40S subunit of the 80S ribosome using the same grid parameters keeping the x, y and z dimension of the grid box at 30 units. Figure 3.3.18 – Figure 3.3.20, depict the process in step by step manner.

Autodock vina was unable to reproduce the binding pose published by Wong et al, 2014. The docking results for the two emetine structures (cryo-EM and pubchem) were similar. Autodock vina output result for emetine and the binding site residues are also shown in Figure 3.3.21 and Figure 3.3.22.

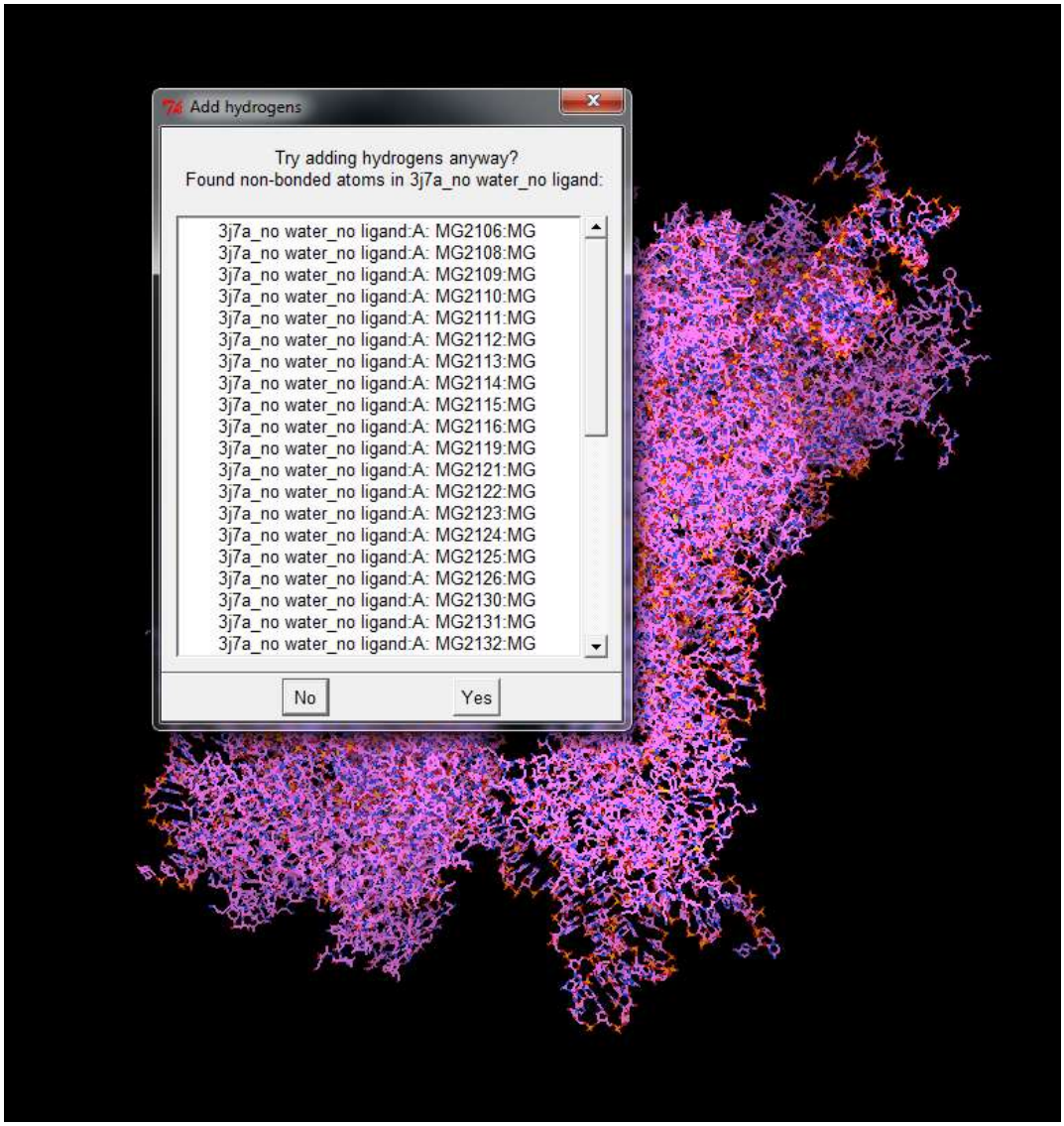

Figure 3.3.18 Autodock vina prompt to indicate presence of unbound magnesium ions prior to receptor preparation for docking. 40S subunit of 80S ribosome is visualised in the background in the working space window of Autodock Tools software.

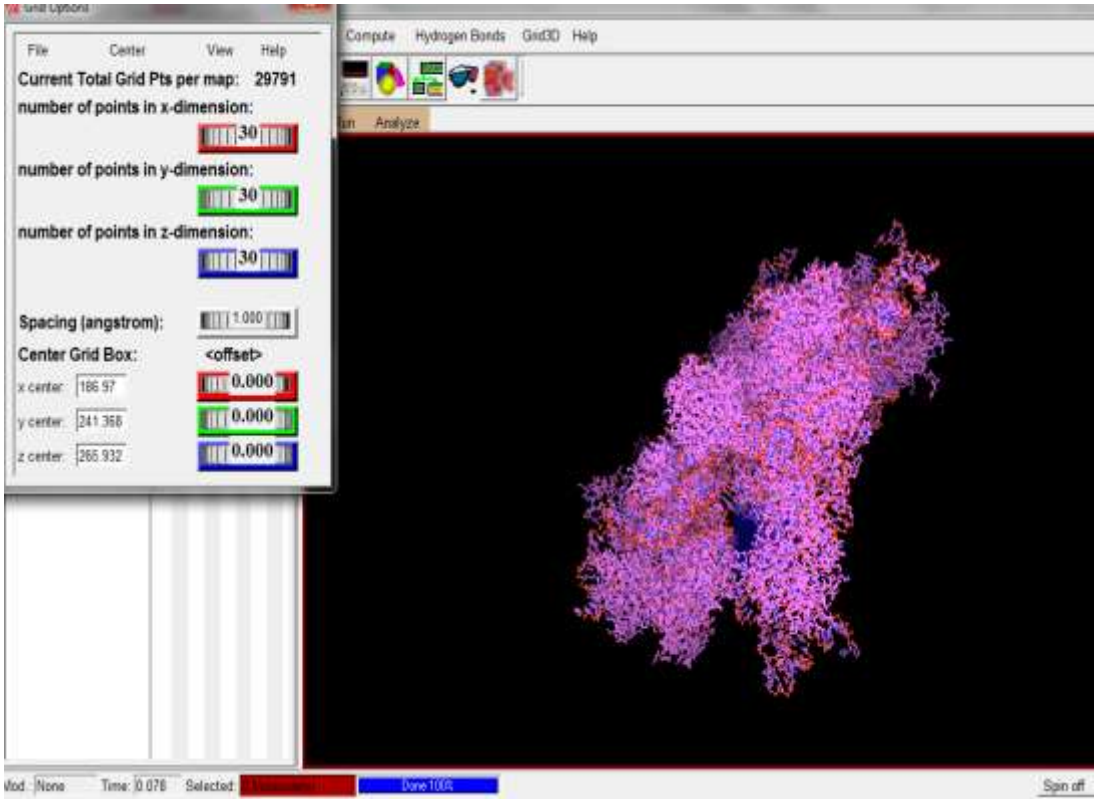

Figure 3.3.19: Specifications of the grid map selected on 3J7A through Autodock tools. The x, y and z dimensions were set at 30ºA. 40S subunit of 80S ribosome is visualised in the working space window of Autodock Tools software.

```
receptor = Ribosome40S.pdbqt
ligand = Emetine.pdbqt

out = out.pdbqt

center_x = 186.97
center_y = 241.368
center_z = 265.932

size_x = 30
size_y = 30
size_z = 30
```

Figure 3.3.20: Specifications of the configuration text file for performing docking through Autodock vina. It specifies the grid dimensions and identifies the receptor and ligand input files for docking

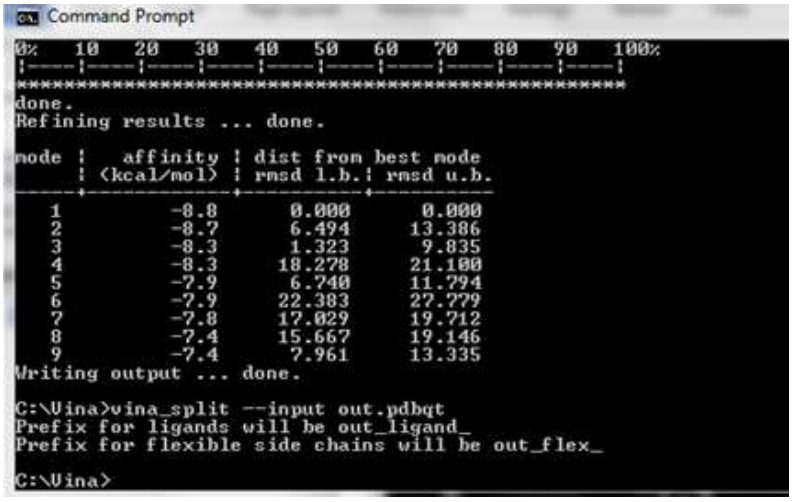

Figure 3.3.21 Autodock vina results showing the top 9 binding poses for emetine obtained from pubchem on 40S subunit of 80S ribosome structure obtained from protein data bank (3J7A).

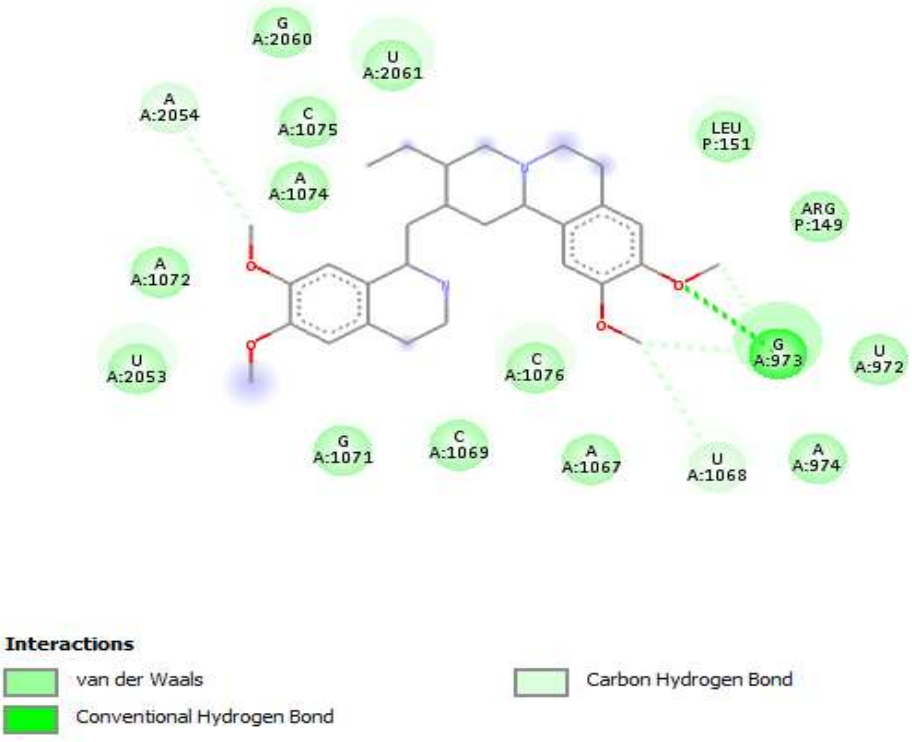

Figure 3.3.22: Binding site residues for emetine obtained from pubchem on 40S subunit of 80S ribosome structure obtained from protein data bank (3J7A).

Docking was first performed with grid space of 30ºA. Since autodock vina was unable to reproduce the published binding pose, the grid space was reduced to 20ºA and then further again to 15ºA to limit the number of conformations away from the binding pocket residues. Reducing the grid dimensions to 15ºA, autodock vina was able to produce a bent U-shaped conformation for emetine and dehydroemetine but it was not completely superimposable on the conformation predicted in 3J7A (Wong et al, 2014). Figures 3.3.23 – 3.3.30 show the various conformations observed by limiting the grid space for emetine from 3J7A cryo-EM model, emetine structure from pubchem, (-)-*R,S*-dehydroemetine and (-)-*S,S*-dehydroisoemetine.

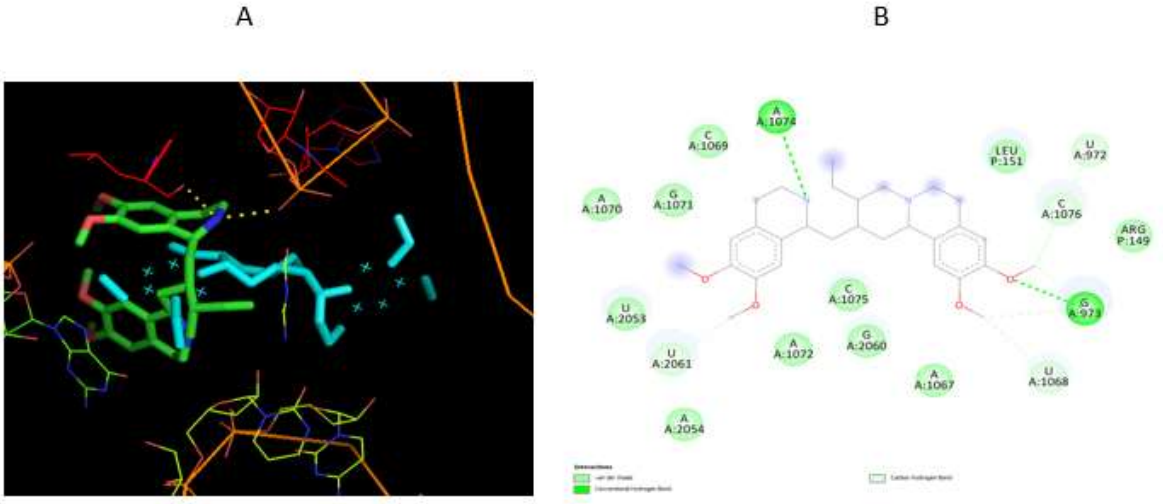

Figure 3.3.23 Superimposition of autodock vina top pose for emetine (cyan) from cryo-EM model 3J7A with x, y and z grid dimensions set at 30ºA with the published U-shaped pose of emetine (green) (A). Discovery studio was used to view the binding site residues (B).

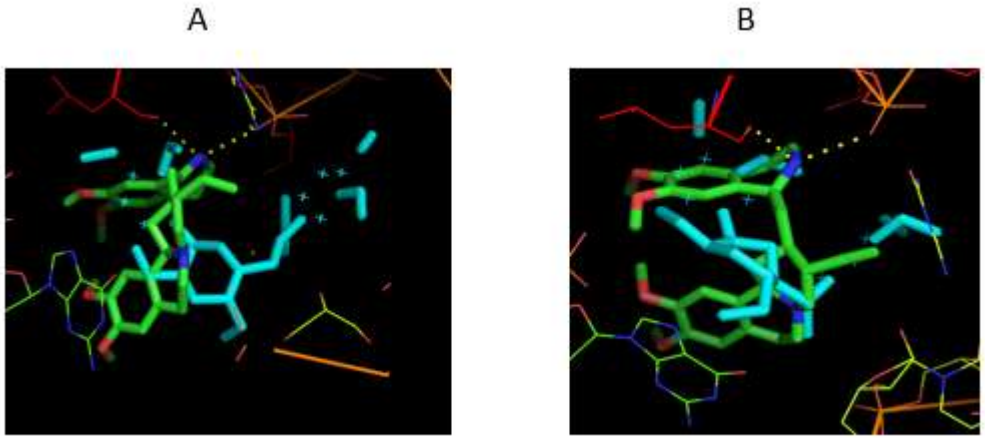

Figure 3.3.24 (A) Superimposition of autodock vina top pose for emetine from cryo-EM model 3J7A (cyan) with x, y and z grid dimensions set at 20ºA with the published U-shaped pose of emetine (green). (B) Autodock vina top pose for emetine from cryo-EM model 3J7A with x, y and z grid dimensions set at 15ºA.

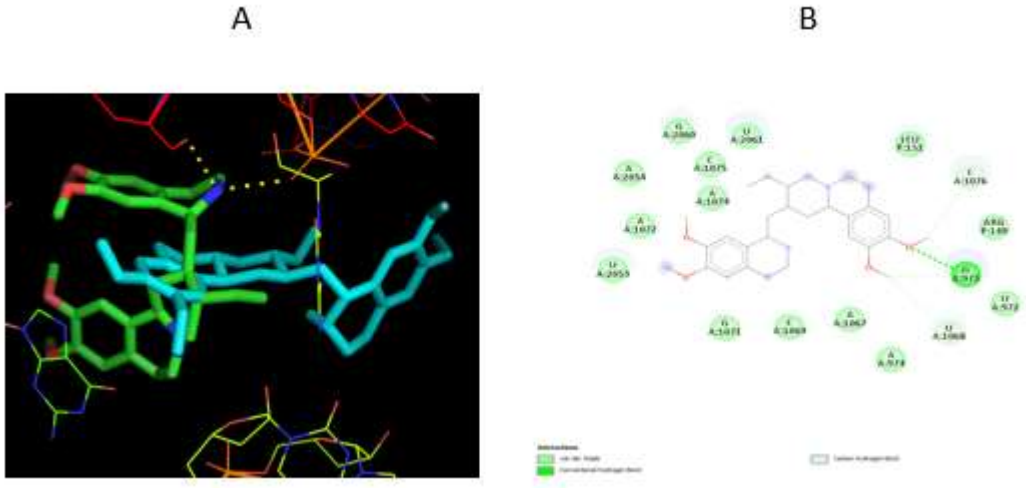

Figure 3.3.25 Superimposition of autodock vina top pose for emetine obtained from pubchem (cyan) with x, y and z grid dimensions set at 30ºA with the published U-shaped pose of emetine (green). (A) Discovery studio was used to view the binding site residues (B).

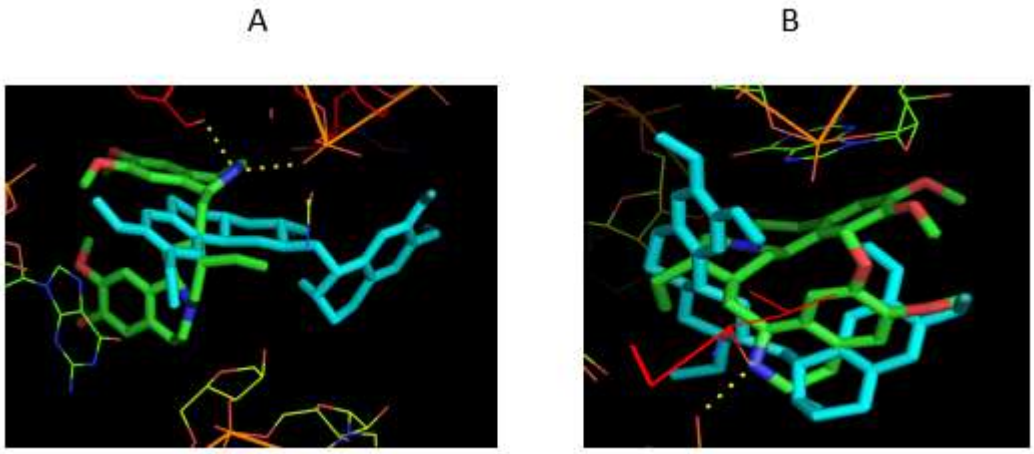

Figure 3.3.26 (A) Superimposition of autodock vina top pose for emetine obtained from pubchem (cyan) with x, y and z grid dimensions set at 20ºA with the published U-shaped pose of emetine (green). (B) Autodock vina top pose for emetine obtained from pubchem with x, y and z grid dimensions set at 15ºA.

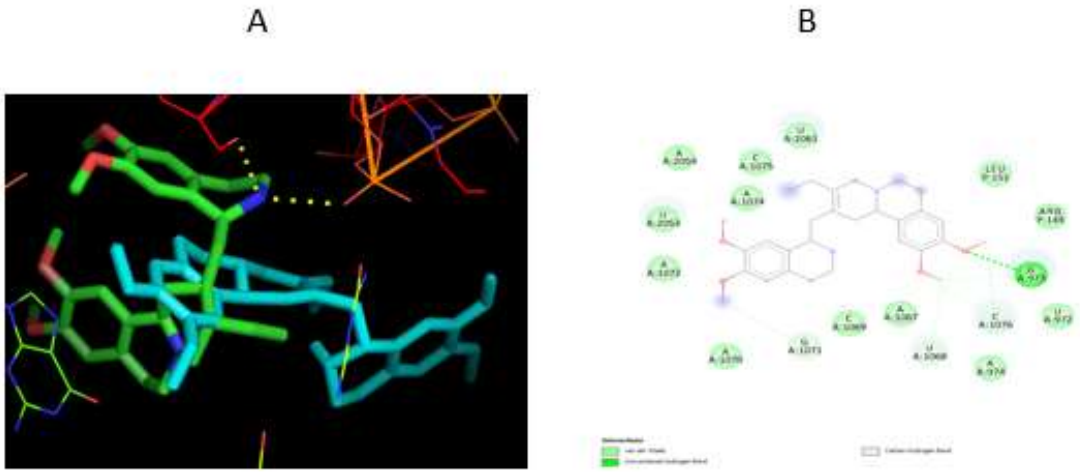

Figure 3.3.27 Superimposition of autodock vina top pose for (-)-R,S-dehydroemetine (cyan) with x, y and z grid dimensions set at 30ºA with the published U-shaped pose of emetine (green) (A). Discovery studio was used to view the binding site residues (B).

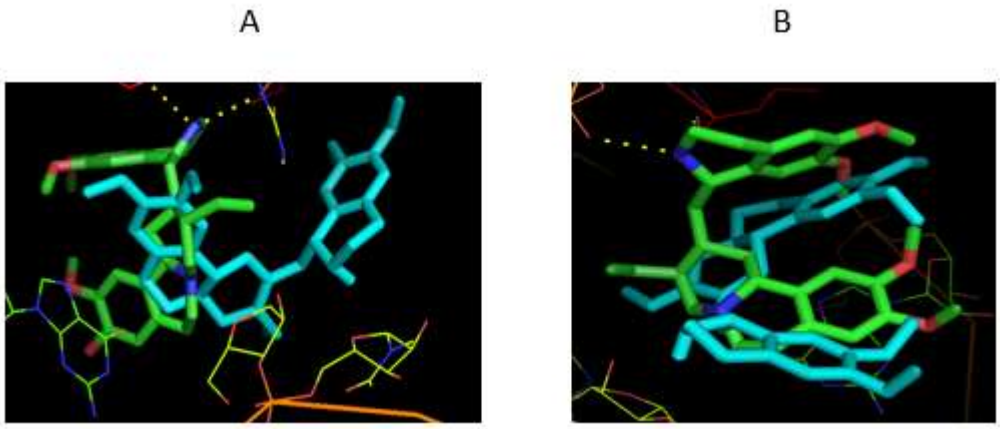

Figure 3.3.28 (A) Superimposition of autodock vina top pose for (-)-*R,S*-dehydroemetine (cyan) with x, y and z grid dimensions set at 20ºA with the published U-shaped pose of emetine (green). (B) Autodock vina top pose for *(-)-R,S*-dehydroemetine with x, y and z grid dimensions set at 15ºA.

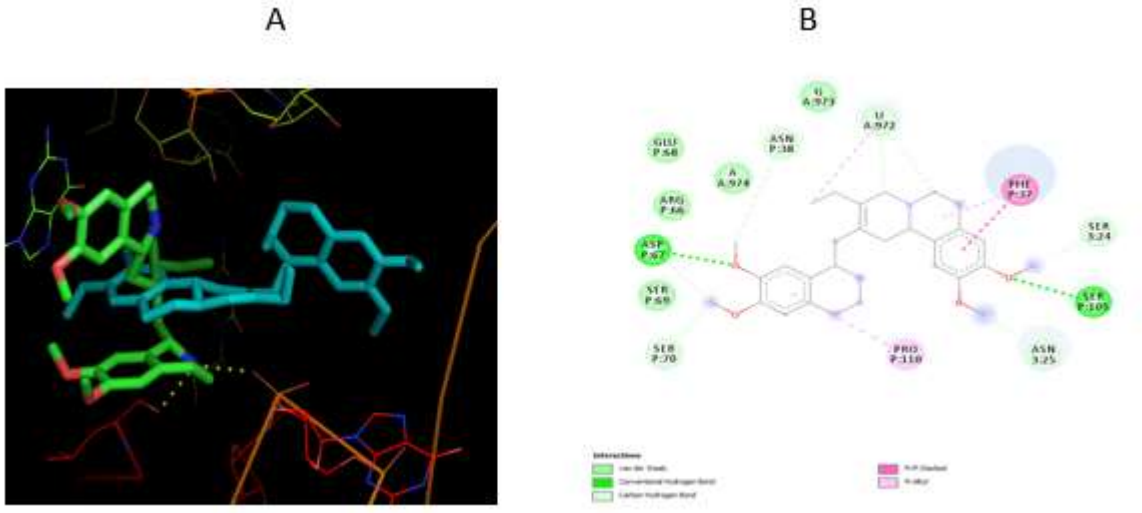

Figure 3.3.29 Superimposition of autodock vina top pose for (-)-S,S-dehydroisoemetine (cyan) with x, y and z grid dimensions set at 30ºA with the published U-shaped pose of emetine (green) (A). Discovery studio was used to view the binding site residues (B).

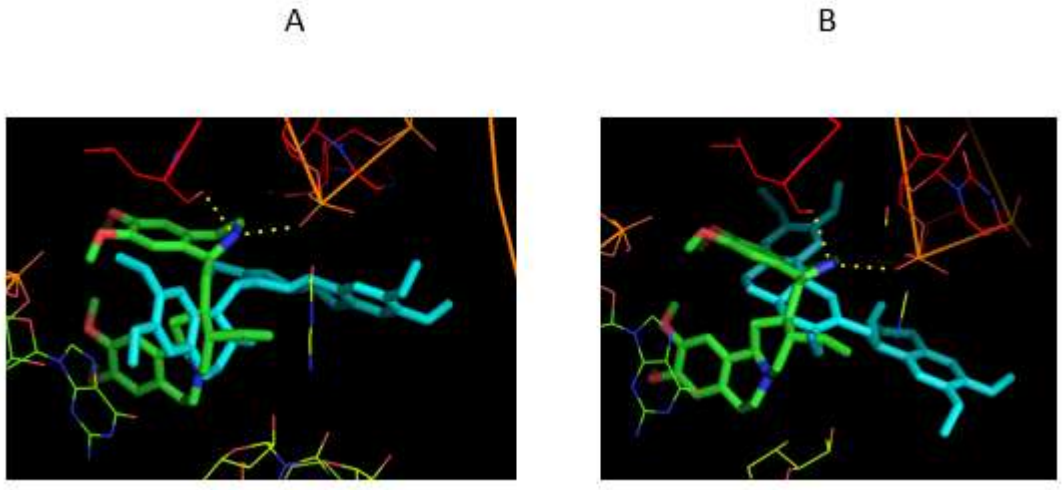

Figure 3.3.30 (A) Superimposition of autodock vina top pose for (-)-S,S-dehydroisoemetine (cyan) with x, y and z grid dimensions set at 20ºA with the published U-shaped pose of emetine (green). (B) Autodock vina top pose for S dehydremetine with x, y and z grid dimensions set at 15ºA.

The top poses obtained of emetine from 3J7A and emetine from pubchem, with the grid dimension 30ºA were superimposed on each other (Figure 3.3.31). They were found to completely superimpose indicating the two structures were treated similarly even though they differed in chirality but neither pose was similar to the published pose in 3J7A.

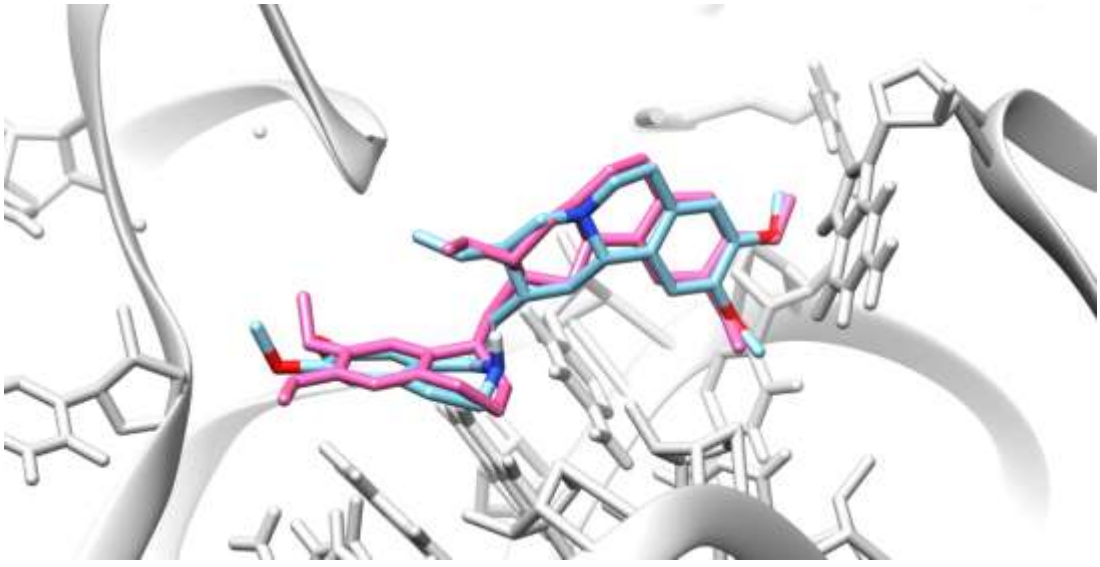

Figure 3.3.31 Superimposition of top poses obtained for emetine from 3J7A (pink) and emetine from pubchem (blue), with the grid dimension 30ºA. The two molecules differ in chirality.

3.3.6 **Docking through MOE:**

Due to incorrect chirality, non-natural enantiomer of emetine, (1*S*,2*R*,3*S*,11b*R*)-emetine was not used to perform docking through MOE. Emetine, i.e. the (1*R*,2*S*,3*R*,11b*S*) structure, was docked into the identified *Pf*40S binding site using MOE-Dock (Chemical Computing Group, 2016.). Docking was repeated with MOE and none of the resulting poses of the two emetine structures matched that of the published literature (Figure 3.3.33 and Figure 3.3.34).

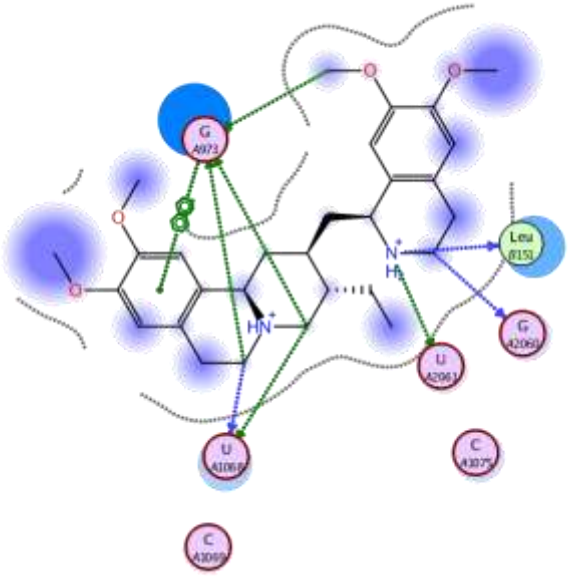

Figure 3.3.32 View of emetine binding site amino acid residues, in 3J7A cryo-EM structure of 40S subunit of 80S ribosome, as observed through MOE software.

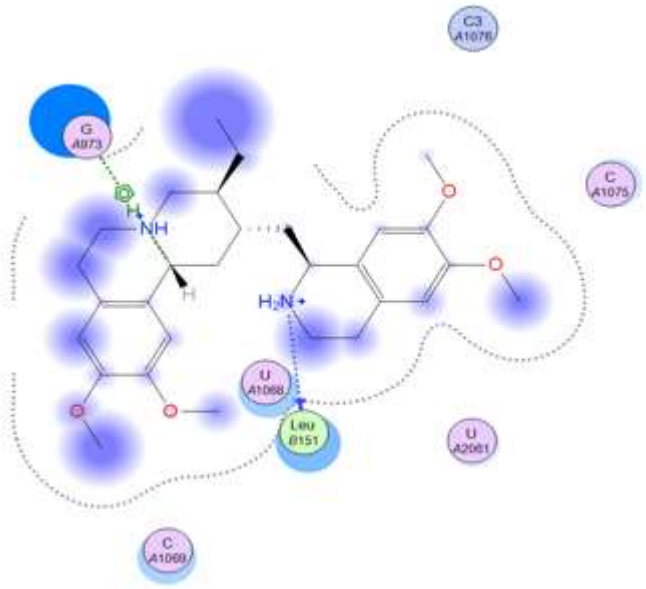

Figure 3.3.33 View of docked emetine and the binding site amino acid residues after performing docking through MOE software.

On closer inspection, it was observed that a magnesium ion close to the binding pocket was affecting the docking results, probably by pulling the ligand towards it. The magnesium ion was thus deleted from the ribosome receptor structure and docking was performed again with both Autodock vina and MOE. Figure 3.3.35 and Figure 3.3.36 depict the position of magnesium ion close to the binding pocket.

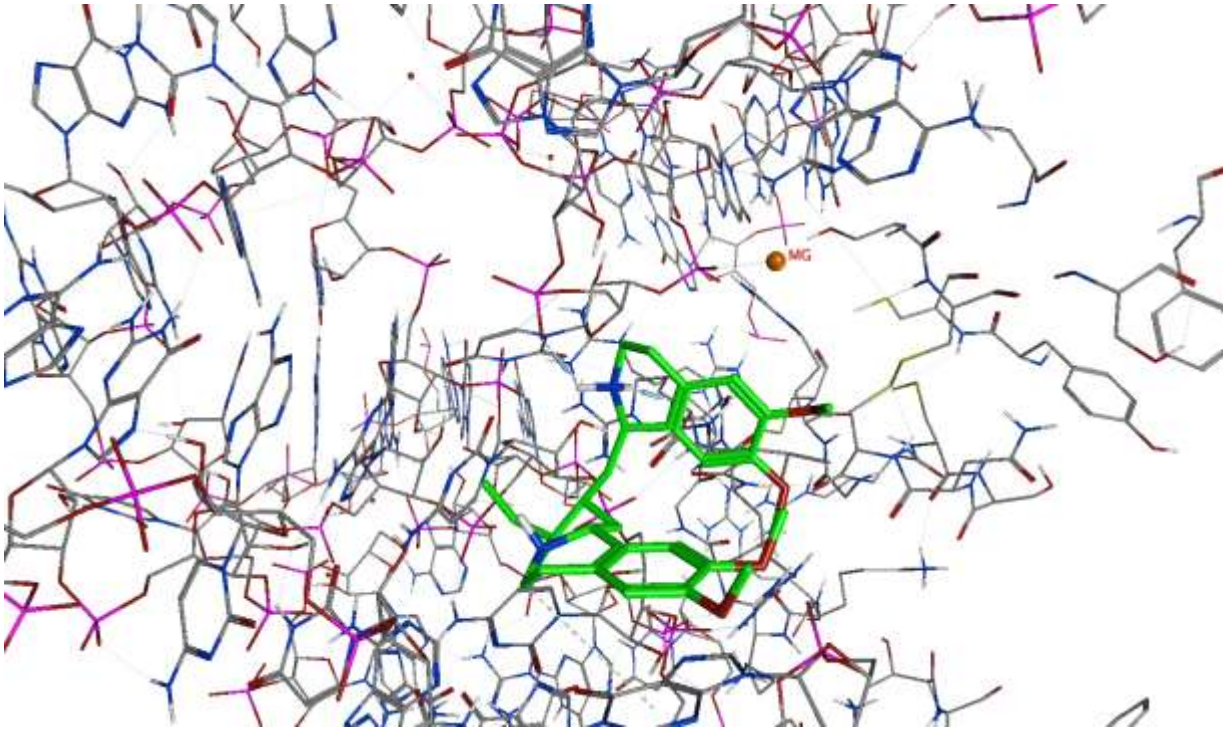

Figure 3.3.34: View of magnesium ion within 13.5ºA of the binding pocket. Emetine is shown in green. Structure visualised through MOE software.

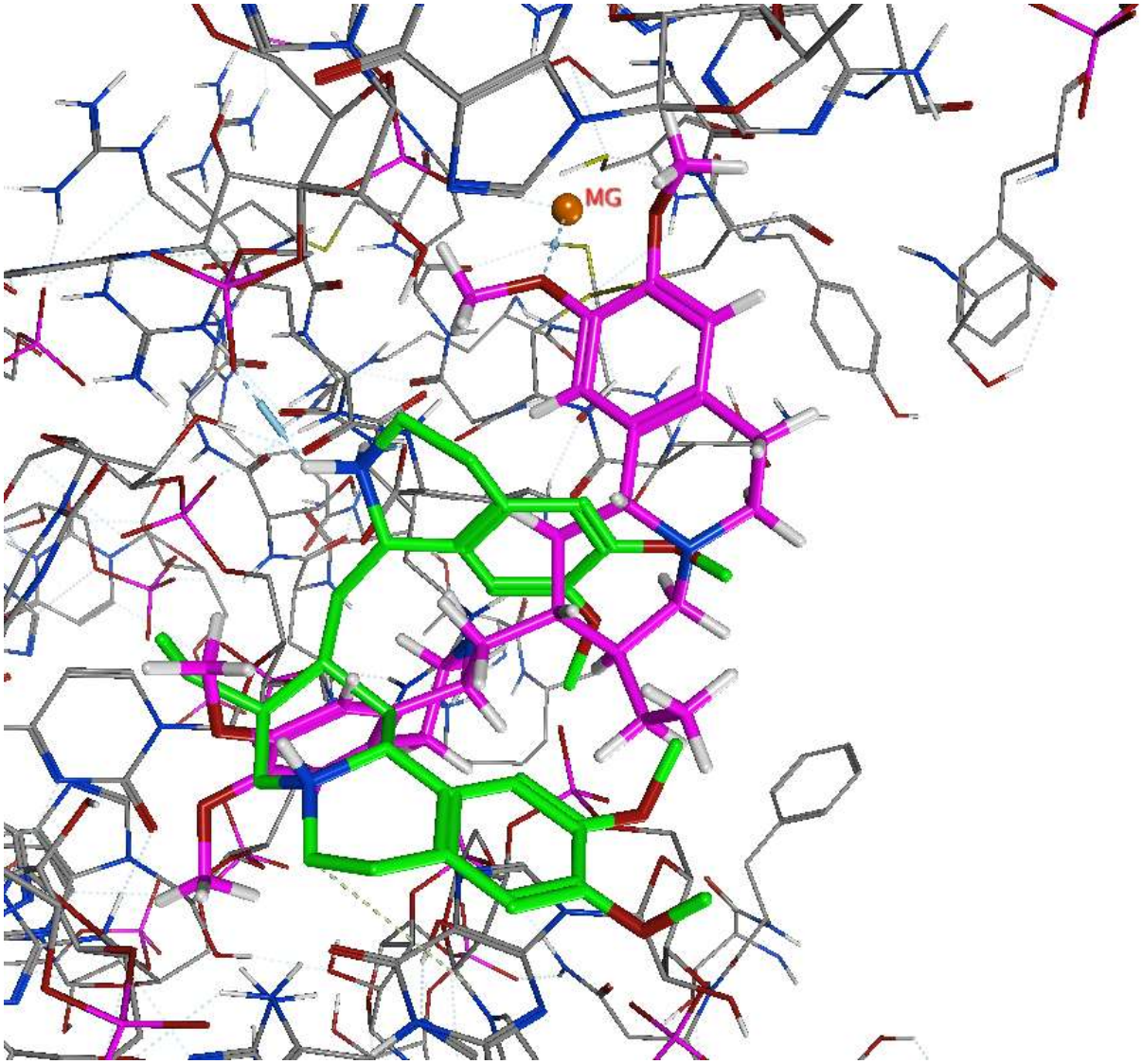

Figure 3.3.35: View of magnesium ion in the binding pocket.

Magnesium ion exerting a pull towards the ligand. Molecule in green is emetine from cryo-EM structure and the molecule in pink is emetine obtained from Pubchem. Structure visualised through MOE software.

After the removal of magnesium ion docking was performed once again with autodock vina and MOE. Autodock vina was still unable to reproduce the binding pose for Emetine. MOE, on the other hand, was able to reproduce the binding pose with good superimposition to that predicted by published literature. The docked emetine geometry mapped well into the electron density envelope (shown at a contour level 0.1542e/A^3 (3.50rmsd) in Figure 3.3.37 A; the bound pose broadly follows the twisted U-shape conformation of the observed electron density, resembling some aspects of the previously modelled non-natural emetine enantiomer geometry (Figure 3.3.37 B).

A

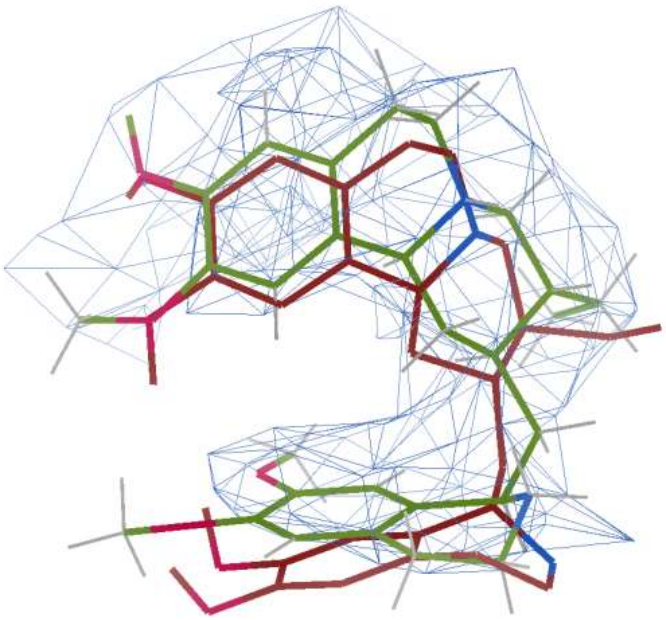

B

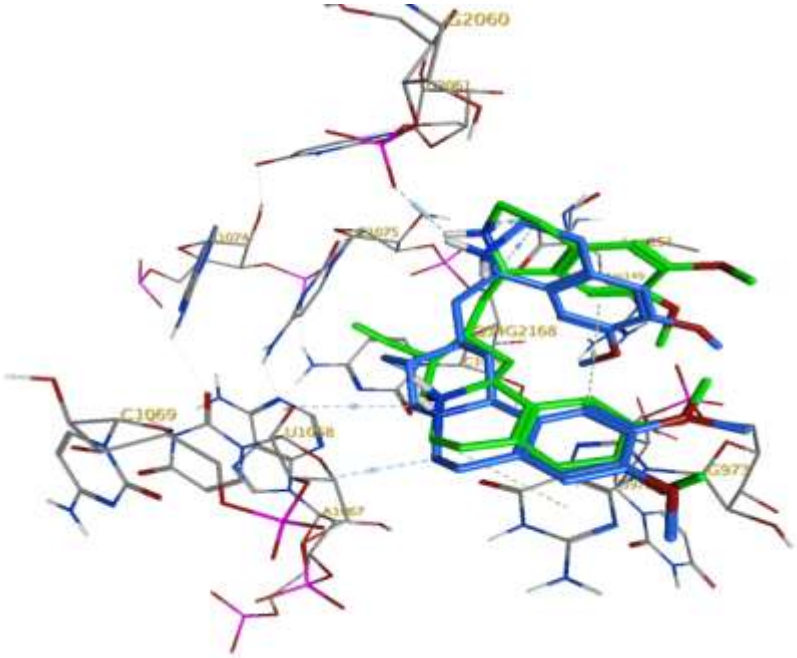

Figure 3.3.36 (A) Overlay of docked pose of emetine (green) with its enantiomer present in the cryo-EM structure (maroon); observed electron density envelope is also shown (wireframe surface with contour level 0.1542e/A^3 (3.50rmsd)); (B) Interactions of docked emetine (green) with Pf40S residues and comparison with previously modelled interactions of its enantiomer (maroon) (Wong *et al*., 2014)

In this U-shape, an intermolecular T-shaped π-stacking interaction was observed between the two cyclic systems of emetine, ie. benzo[a]quinolizine rings A/B/C and isoquinoline rings D/E. The docked emetine also forges a number of comparable interactions with the *Pf*40S subunit as its modelled enantiomer, with a key π-stacking interaction between the A/B/C rings of emetine with the purine ring of Gua973 of h23 (Wong et al., 2014). The location of the emetine secondary and tertiary amines are broadly similar (within 1 - 2 Å), allowing hydrogen bonding interactions with a backbone oxygen atom of Ura2061 (h45) and the 2'-hydroxyl group of Ura1068 (h24) respectively (Figure 3.3.38 B). The tertiary amine also forms a salt bridge interaction with the carboxylate side chain of C-terminal residue Leu151 of uS11 (Figure 3.3.38 B). This interaction was not highlighted in the cryo-EM study and is a consequence of modelling into the E-site the natural emetine geometry.

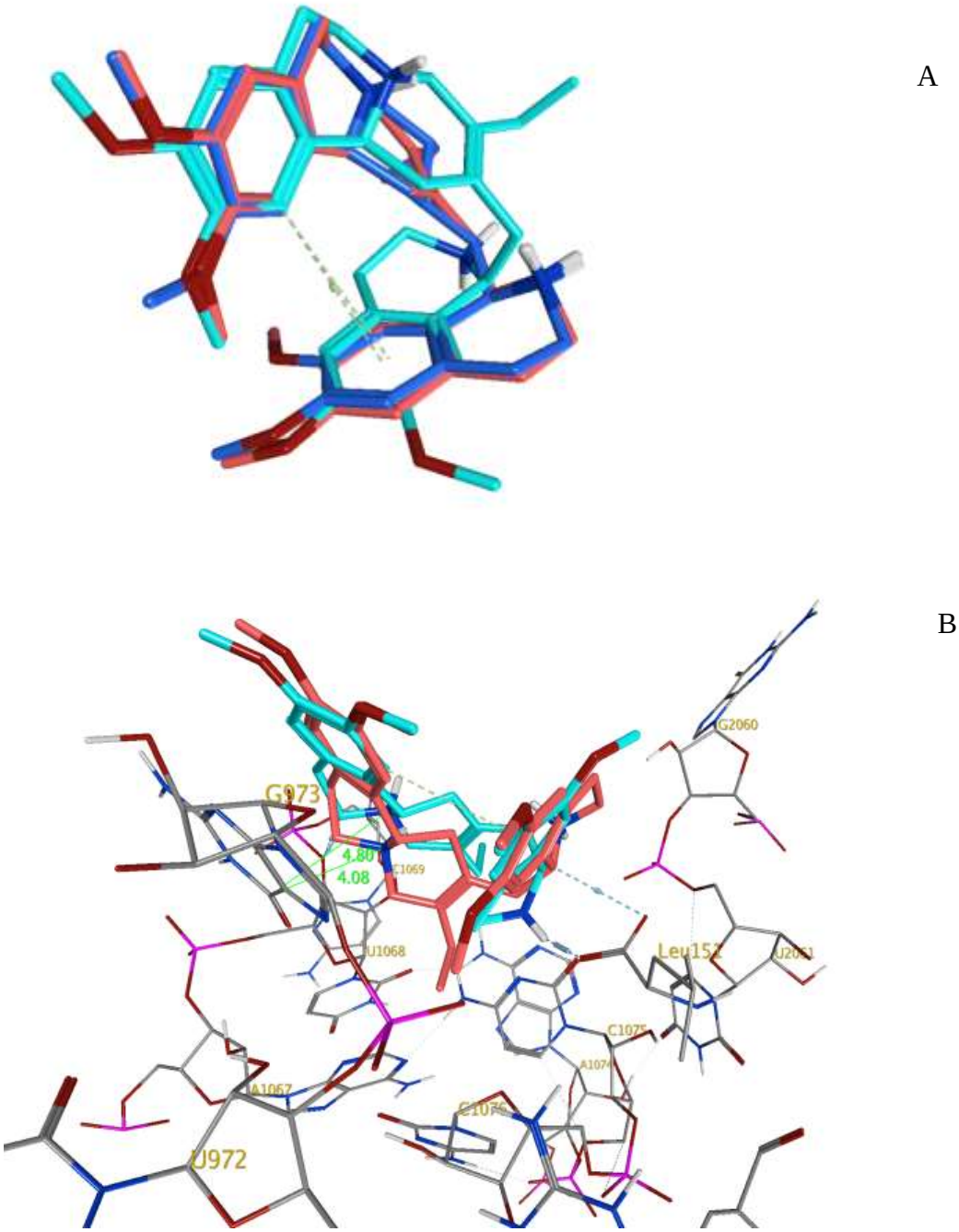

Figure 3.3.37 Overlay of docked poses.

(A) Overlay of docked poses of (-)-*R*,*S*-dehydroemetine (red) and (-)-*S*,*S*-dehydroisoemetine (cyan) with emetine (blue). (B) Interactions of (-)-*R*,*S*-dehydroemetine (red) and (-)-*S*,*S*-dehydroisoemetine (cyan) with the *Pf*40S binding site. Distances (dotted lines) in Å.

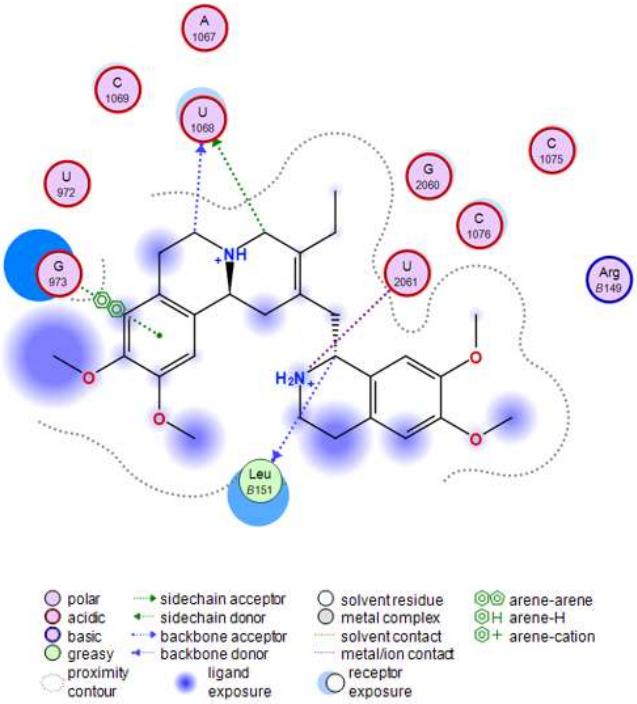

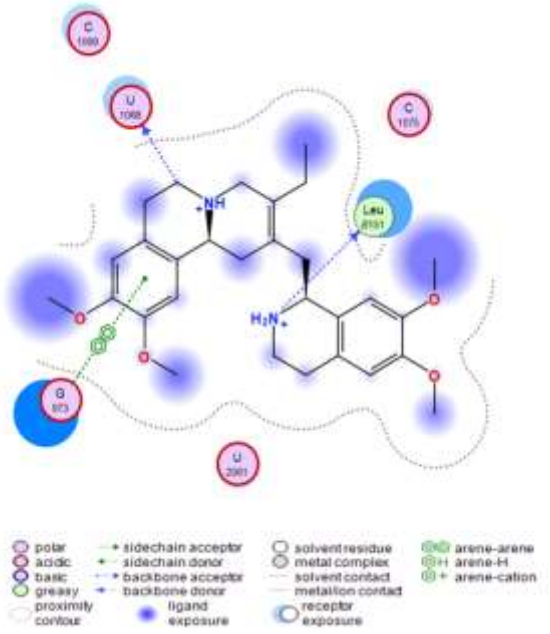

Figure 3.3.38 Binding site residues for (-)-*R,S*-dehydroemetine and (-)-*S,S*-dehydroisoemetine.

(A) Docking through MOE showing the amino acid binding site residues for (-)-*R,S*-dehydroemetine molecule. (B) Docking through MOE showing the amino acid binding site residues for (-)-*S,S*-dehydroisoemetine molecule.

Subsequently, the two diastereomers of emetine, *(-)-R,S*-dehydroemetine and *(-)-S,S*-dehydroisoemetine, were docked in turn into the emetine-binding region of the *Pf*40S subunit. It was found that the preferred docked pose of the *(-)-R,S*-dehydroemetine adopts the familiar U-shaped conformation, superimposing rather closely onto the bound pose of emetine (Figure 3.3.38 A). The docking scores were correspondingly similar for emetine, with a London dG value of -7.2 kcal/mol, and *(-)-R,S*-dehydroemetine, which has a dG score of -7.3 kcal/mol. As observed for emetine, the *(-)-R,S*-dehydroemetine forms the π–π stacking interaction with the Gua973 pyrimidine ring and polar interactions with Ura2061, Ura1068 and Leu151 (Figure 3.3.38 B).

However, *(-)-S,S*-dehydroisoemetine docks into the binding site with a lower dG score of -6.5 kcal/mol and does not overlay in conformation so readily with emetine or the *(-)-R,S*-dehydroemetine. The particular stereochemical configuration of *(-)-S,S*-dehydroisoemetine appears to result in its secondary amine being more distant from the E-site residues of *Pf*40S. Consequently, this amine N···O Ura2061 distance extends by 0.8 Å in proceeding from R to S isomer. The tertiary amine interaction with Ura1068 is maintained, however, as is the interaction with the terminal carboxylate of Leu151 (Figure 3.3.38 B). The π stacking interaction with Gua973 is also present, but at a slightly larger distance between planes, increased by ~0.7 Å. Figure 3.3.39 (A) and (B) shows the predicted binding site residues for *(-)-R,S*-dehydroemetine and *(-)-S,S*-dehydroisoemetine.

3.4 Conclusion

The study performed to replicate the binding conformation of emetine on 40S subunit of 80S ribosome shows the chirality of emetine molecule in the 3J7A cryo-EM model is incorrect and requires revision. Most docking software were unable to replicate the bound conformation of emetine. Poor resolution of ribosome and presence of magnesium ion in the vicinity of the binding pocket is another factor which complicates the docking. MOE was able to replicate the U-shaped binding conformation and predicted a better fit for (-)-*R,S*-dehydroemetine in comparison with (-)-S,S-dehydroisoemetine. The prediction of binding site interactions suggests potentially better activity for (-)-*R,S*-dehydroemetine amongst the two diastereomers.

Chapter 4 Lead optimisation and drug interaction analysis of dehydroemetine

4.1 Introduction:

In the course of drug discovery, through a meticulous selection process, only a handful of drugs, from countless potential candidate molecules become successful (Baek et al., 2015). Drug repositioning offers a solution to the dilemma by reducing the research and development timelines. The emergence and spread of drug resistance in *Plasmodium falciparum* has prompted a renewed call to develop new antimalarials. The Malaria research group at the University of Salford has identified the anti-amoebic drug emetine dihydrochloride as a potent antimalarial option with IC_{50} of 47 $\pm$ 2.17 nM against the K1 strain (Matthews *et al.*, 2013). Emetine is not currently used as an antiprotozoal drug due to its emetic and cardiotoxic side effects.

Until the mid-20th century, emetine was widely used as a treatment for amoebic dysentery. First brought to Europe by Piso, emetine was introduced in large doses in 1858 in Mauritius by E. S. Docker and helped reduce the death rate from dysentery from 10-18% to 2% (Thompson, 1913). Emetine with oral chloroquine, niridazole and metronidazole were given to three groups of 20 patients each in a controlled clinical trial. It was observed that while metronidazole was unable to effectively treat seven patients and niridazole showed toxic side-effects, emetine with oral chloroquine was able to effectively treat all but one patient (Datta et al., 1974). Emetine and its derivatives have been tested in laboratories and have shown potent activity on prostate cancer, bladder cancer, ovarian cancer, pancreatic cancer and a few other cancer cell lines (S Akinboye and Bakare, 2011) (Foreman et al., 2013) (Sun et al., 2015) (Han et al., 2014).

A synthetic analogue of emetine, dehydroemetine could be given intramuscularly or orally as resinate for slow release. It was synthesised by Roche and Glaxo (Mebadin) (1967). In the second edition of WHO model prescribing information: Drugs used in parasitic diseases, WHO recommends the use of a 1 ml ampoule of 60 mg of dehydroemetine to be given intramuscularly as one of the most effective treatment for amoebic dysentery or amoebic abscesses (Appendix II). It is an irritant if taken orally but is less toxic than its parent

compound emetine. It could be used as an alternative to metronidazole or other 5-nitroimidazoles if there is an inadequate response to the treatment. The drug is usually administered not more than 60 mg/day (1mg/kg/day) for 4 to 6 days in a hospital setting and could be repeated after 6 weeks in severe cases or relapses. A supplementary treatment with chloroquine or diloxanide is also usually recommended. It should be avoided in patients with renal, cardiac or neuromuscular diseases due to side-effects. It is contra-indicated in pregnancy but could be given to the mother in life-threatening cases of amoebic dysentery (Goessling and Chung, 2002). Weakness, muscular pain, hypotension, purpuric rashes, tachycardia, inversion of T-wave, prolongation of QT interval and dysrhythmias could manifest as side-effects (Folb and Trounce, 1970).

Oral dehydroemetine was used in a study of 24 patients with intestinal amoebiasis, given post-prandial for 10 days in a dose of 1 mg/kg/day. Dehydroemetine resulted in a cure rate of 71% and symptomatic relief by 85% without any severe side-effects. Most patients tolerated it well and it was proposed to be a safe and potent drug for intestinal amoebiasis (Salem, 1967). In another study of 144 patients, the effect of injectable dehydroemetine, slow release oral dehydroemetine and niridazole were observed in mild, moderate and severe cases of dysentery. Oral dehydroemetine was found to be a well-tolerated, safe and an effective treatment in all cases of dysentery in a dose of 1 to 1.5 mg/kg /day for 10 days (Wolfensberger, 1968).

The preference of combinatorial regimes over monotherapy for the treatment of malaria has affected the drug discovery pipeline in a crucial way (Bell, 2005). More often than not, instead of developing two new drugs for combination therapy, newer drug candidates are tested for synergistic activities with existing anti-malarial treatments (Kremsner and Krishna, 2004). Combination therapy not only helps in dose reduction and better therapeutic efficacy, it is also useful in delaying the emergence of resistance and widens the shelf-life of the existing cohort of drugs (Harasym et al., 2010). The drugs used in combinatorial regimes should ideally be free of major side-effects and have matching pharmacokinetics besides showing synergistic activity against drug resistant strains (Kremsner and Krishna, 2004).

Similar to emetine, dehydroemetine also has emetic and cardiotoxic side-effects and combinatorial partner drugs showing synergistic activity could potentially decrease the dose-dependent toxicity profile of this potent compound (Chou, 2006).

Bliss independence and Loewe additivity methods form the basis of most methods (Matthews et al., 2017). Bliss independence (fractional product method) is based on the assumption that each drug acts independently whereas Loewe additivity assumes that a drug cannot interact with itself (Yeh et al., 2009). Additivity is thus defined if the inhibition is constant along a line of equal effective dose and uses an isobole (a line of constant inhibition). Antagonism is defined by deviations above the line (convex) and synergism by deviations below the line (concave). Fractional Inhibitory Concentration (FIC) is based on the isobologram and sum of the FIC (∑FIC) value where 1 is additivity, <1 is synergism and >1 is antagonism.

Drugs could exhibit synergy by interacting physically or with a target at the molecular level (Zimmermann et al., 2007). Lack of clear definition has resulted in many unsubstantiated claims of potential synergistic drug candidates. Chou and Talalay developed a method based on the argument that the issue of synergy is more physiochemical rather than statistical in nature and employed the mass-action law principle to derive a median-effect equation where additivity could be defined using the resulting combination index (CI = 1) with antagonism and synergism defined as >1 and <1 respectively. CalcuSyn and Compusyn are two software programmes based on the complex algorithms for median-effect analysis to allow automation and eliminate subjectivity during data analysis (Chou, 2010). The Chou-Talalay method incorporates a unified theory which takes into consideration four existing physiochemical equations namely; Michaelis-Menten (enzyme kinetics), Henderson-Hasselbalch (pH ionization), Hill (higher order ligand binding saturation), and Scatchard (receptor binding).

The median-effect principle of Chou and Talalay were used to determine the drug interactions with the help of the isobologram and combination index method (CalcuSyn software, Biosoft: Chou, 2010). The median effect principle formula $f_a/f_u = [D/D_m]^m$ used in CalcuSyn assesses drug-drug interactions where fa is the fraction of affected cells, $f_u = 1-f_a$, the unaffected fraction of cells, D equals the drug concentration, D_m the drug dose needed for 50% inhibition, and m the slope of the median effect curve. A straight line joining the F_a points against the fixed ratio combinations of Drug 1 and Drug 2 on the x and y axes,

represents the isobologram graphically depicting the pharmacological interaction (Matthews et al., 2017).

The pharmacological interactivity is quantitatively represented by the combination index (CI) which accounts for both the shape of the dose response curve and the potency (Dm, ED_{50}). The following formula is used to derive the CI for the classic isobologram (CI = 1); CI = $(D)_1/(D_x)_1 + (D)_2(D_x)_2 + (D)_1(D)_2/(Dx)_1(D_x)_2$ where $(D_X)_1$ and $(D_X)_2$ are the concentrations for Drug 1 and Drug 2 resulting in X% inhibition when acting singly and $(D)_1$ and $(D)_2$ the concentrations of the respective drugs when acting in combination to achieve the same (iso-effective) percentage inhibition (Reynolds and Maurer, 2005). The CalcuSyn software generates the CI over a range of f_a levels at different growth inhibition percentages. The interpretation of CI was done in accordance with Table 4.4.1.

Use of CalcuSyn has been demonstrated as a reliable method to define interactivity in drug combination (Matthews et al., 2017). Atovaquone and proguanil were first evaluated to test the efficacy of the method as the two drugs are known to exhibit synergism (Radloff et al., 1996). The methodology was then applied to evaluate combinatorial partner drugs for dehydroemetine. This chapter reports on a series of experiments carried out to define antimalarial potency and drug interactivity of the lead. The current antimalarial drugs, artemether, atovaquone, proguanil and doxycycline were investigated for their interaction with dehydroemetine using the optimised 72 hour treatment regimen. Predetermined IC_{50} values for each compound were used to select the constant-ratio for each combination. Atovaquone was selected as it is already known to be synergistic with emetine dihydrochloride hydrate (Matthews *et al*., 2013). Artemether, doxycycline and proguanil were selected as they are currently used in the treatment and prophylaxis of malaria.

4.2 Methods:

4.2.1 Culture of *Plasmodium falciparum*

Erythrocytic stage, strain K1, *P. falciparum* parasites (gifted by Prof J. E. Hyde) were cultured in RPMI 1640 1x (+) L-Glutamine (+) 25 mM Hepes (Gibco, Life Technologies, UK) in accordance with Read and Hyde, 1993 as mentioned in General materials and

methods (Chapter 2). The parasites were routinely maintained in O+ human blood (NHS Blood Bank, Manchester, UK). Multi-drug resistant strain K1 of *P. falciparum* is resistant to chloroquine, pyrimethamine and sulphadoxin.

4.2.2 **Experimental determination of IC_{50}:**

Experiments to test drug efficacy were performed following the protocol mentioned in Chapter 2. Briefly, 2-fold serial dilutions of (-)-*R,S*-dehydroemetine and (-)-*S,S*-dehydroisoemetine from 200 nM to 12.5 nM and 20 µM to 1.25 µM, respectively were tested against multi-drug resistant K1 strain of *P. falciparum*.

4.2.3 **Time-course analysis through IC_{50} speed assay for determination of speed of action of (-)-*R,S*-dehydroemetine and (-)-*S,S*-dehydroisoemetine:**

In 2012, Tres Cantos developed a labour intensive low-throughput assay taking up to 28 days to determine *in vitro* parasite reduction ratio (PRR) and presence of lag phase in response to the drug (Sanz et al., 2012). Besides rapid relief of symptoms, a fast-acting drug also helps to curtail the mutations which lead to the development of new mechanisms of drug resistance. The method used in this study to differentiate between fast and slow acting compounds gives initial results in 4 to 7 days (Le Manach et al., 2013).

Unsynchronised *Plasmodium falciparum* culture were used, and parasites were grown in presence of (-)-*R,S*-dehydroemetine and (-)-*S,S*-dehydroisoemetine for three incubation periods of 24 hours, 48 hours and 72 hours. The assays were analysed by determining SYBR green fluorescence as described in Chapter 2. Error bars on the graphs represent the standard error on the experiments performed twice with each concentration of (-)-*R,S*-dehydroemetine and (-)-*S,S*-dehydroisoemetine tested in triplicates.

4.2.4 **Stage-specific profiling of (-)-*R,S*-dehydroemetine and (-)-*S,S*-dehydroisoemetine:**

Parasite cultures with ≥ 80% trophozoites and ≥ 80% rings were obtained by synchronisation with 5% Sorbitol (Le Manach et al., 2013). The cultures were synchronised twice, at 0 hours

and 31 hours to obtain young rings which were up to 3 hours old. To obtain early schizont stages, the culture was synchronised twice with the second synchronisation being 6 to 8 hours after the first. Each synchronous stage was incubated for 24 hours at 37°C on a 96-well microtitre plate with two fold serial dilution of the drugs ranging from 1.6 to 100 times the IC_{50} of each drug. The plates were washed 4 times after the incubation in order to dilute the drug concentration by > 1000 fold. The plates were incubated for another 24 hours at 37°C following which SYBR green staining was used to read the plates as described in general materials and methods in Chapter 2. Error bars on the graphs represent the standard error on the experiments performed twice with each concentration of (-)-*R,S*-dehydroemetine and (-)-*S,S*-dehydroisoemetine tested in triplicates

4.2.5 **MTT cell viability assay for determination of cell cytotoxicity:**

Human hepatoma (HepG2) cells were grown in Dulbecco's modified eagle medium (DMEM) containing (+) 4.5 g/L D-glucose, L-glutamine and supplemented with 10% fetal calf serum (FCS), 1% non-essential amino acids, and 1% penicillin/streptomycin, in a 5% CO_2 atmosphere at 37^0C. Media was changed where cells reached approximately 80% confluency.

The MTT (3-(4,5-dimethyltrazol-2-yl)-2,5-diphenyl tetrazolium bromide) assay was performed using the protocol described by Mosmann (1983). The assay was carried out in a 96 well plate. Media from the cell culture flask was removed and discarded. 3-5 ml of PBS was used to wash the cells and 0.75 ml of trypsin-EDTA reagent was added to the cells. Flask was incubated at 37^0 C with 100% humidity and 5% CO_2 for approximately 3 minutes. To detach the cells, the flask was tapped gently until the cells detached. Cells were re-suspended in 4-5 ml of media and centrifuged at 1500 rpm for 5 minutes and the supernatant was discarded. The cell pellet was re-suspended in 5 ml of media and 10 µl of this cell solution was used to count the cells on a haemocytometer. Cells were calculated to make a new 'cell-media' solution to a concentration of 5000 cells/100 µl as mentioned below in cell count protocol. 100 µl of this new cell solution was added into each well of the 96 well plate and 100 µl of the drug prepared in media was also added to each well. This was repeated in triplicate and the 96 wells plate was incubated for 3 days. After the 3 days incubation, 50 µl of MTT solution was added to each well and incubated for 3 hours. The liquid in each well was aspirated carefully making sure the purple formazan crystals formed at the bottom of the

well were not removed. 200 µl of DMSO was added to each well and the results were read on the Ascent plate reader. The optical density was determined spectrophotometrically with a 570 nm filter and a back-ground at 630 nm. Absorbance from the appropriate background was subtracted and cell viability was expressed as a percentage of the control absorbance in the untreated sample. Graphpad Prism **(**GraphPad Prism 5.0) was used to construct dose-response curves to obtain the IC_{50} values using. A 25-0.39 µM two-fold dilution dose series of cisplatin (Sigma-Aldrich) was included on each plate as a control drug. Selectivity index was calculated by dividing IC_{50} values by LD_{50} values.

Table 4.2.1 Layout of a typical MTT plate assay

<table>
<tr><td rowspan="8">Blank</td><td colspan="3">Control – Media Only</td><td rowspan="8">Blank</td><td rowspan="8">Blank</td></tr>
<tr><td>1.56 µM Cisplatin</td><td>Drug 1</td><td>Drug 2</td></tr>
<tr><td>3.12 µM Cisplatin</td><td>Drug 1</td><td>Drug 2</td></tr>
<tr><td>6.25 µM Cisplatin</td><td>Drug 1</td><td>Drug 2</td></tr>
<tr><td>12.5 µM Cisplatin</td><td>Drug 1</td><td>Drug 2</td></tr>
<tr><td>25 µM Cisplatin</td><td>Drug 1</td><td>Drug 2</td></tr>
<tr><td>50 µM Cisplatin</td><td>Drug 1</td><td>Drug 2</td></tr>
<tr><td>100 µM Cisplatin</td><td>Drug 1</td><td>Drug 2</td></tr>
</table>

Cisplatin was used as the positive control drug. The stock solution of cisplatin used was 3.33mM dissolved in 0.9% saline. Serial dilutions of the control and test drugs were prepared in working solutions for the experiment.

Figure 4.2.1 Examplar MTT assay plate.

MTT assay performed on HepG2 cancer cell lines. Cells seeded at 5000 per well. Sample read after 72 hours incubation.

4.2.6 **Determination of cross-resistance in multidrug resistant *Plasmodium falciparum* strains:**

The experiment was carried out by GSK Tres Canto Laboratory in Madrid, Spain. The three strains used for the assay were 3D7A, Dd2 and W2 based on their resistance profiles. 3D7A is chloroquine–sensitive, Dd2 is resistant to chloroquine, mefloquin and pyrimethamine (Sun et al., 2014) and W2 is resistant to chloroquine, quinine, pyrimethamine, cycloguanil, and sulfadoxine (Rathod et al., 1997) (gifted from the Malaria Research and Reference Reagent Resource Centre MR4). A culture of infected red blood cells (RBC) of the corresponding strain, (0.5% parasitaemia, 2% haematocrit) in RPMI-1640, 5% albumax and 5 µM hypoxanthine was exposed to 9 dilutions (3-fold serial dilutions) of the compound starting at 5 µM. 100 µl of culture volume was plated in 96-well flat bottom microtitre plates with 0.5 µl drug (stock x200 in DMSO). Plates were incubated for 24 h at 37 ºC, 5% CO_2, 5% O_2, 90% N_2. Next, 3H-hypoxanthine was added, and plates were incubated for another 24 hours period. Following this, the parasites were harvested on a glass fiber filter using a TOMTEC Cell harvester 96. Filters were dried, and melt-on scintillator sheets were used to determine the incorporation of 3Hhypoxanthine. Radioactivity was measured using a microbeta counter.

Data was normalized using the incorporation of the positive control, (parasitized red blood cells without drug). IC_{50} values were determined using Grafit 7 program (Sanz et al., 2012).

4.2.7 **Determination of transmission blocking potential through *in vitro* inhibition of gamete activation**

The experiment was carried out by GSK Tres Canto Laboratory in Madrid, Spain. Asexual cultures of *P. falciparum* NF54 strain parasites were used to seed gametocyte cultures at 0.5% parasitemia, 4% hematocrit in 50 ml total volume under 3% O_2/5% CO_2/92% N_2 gas. Culture medium (RPMI 25 mM HEPES, 50 mg/l hypoxanthine, 2 g/l $NaHCO_3$ without *L*-glutamine + 5% human serum and 5% Albumax) was replaced daily for 14 days. At day 14, the concentration of non-purified cultures was adjusted to plate 700,000 total cells per well in each 384-well plate. The test drugs were then added in two-fold serial dilutions starting at 10 µM (10 µM – 0.00976 µM) and incubated 48 h at 37 ºC (3% 0_2, 5% CO_2, 92% N_2). DMSO was used as the negative control and Thiostrepton as the positive control. Activation was performed with ookinete medium (same RPMI base used for culture but supplemented with xanthurenic acid 50 µM) supplemented with the antibody anti-Pfs25-Cy3 at a final concentration of 1/2000 (from 1 mg/ml stock). Plates were analysed to detect exflagellation centres. "Triggered" cultures were then incubated (protected from light) at 26 °C for 24 h (in a thermoregulated incubator). Following this the plates were analyzed to detect female activated gametes. Activation of male gametes was detected based on light changes provoked by flagella movements which caused movement of surrounding cells. A 10-frame video was taken and then analyzed to determine these changes in cell position based on pixels change. The exflagellation centres were located by the script, based on size and intensity of light changes. Activation of female gametes was based on detection of fluorescent Cy3-Anti Pfs25 antibody (as the primary parameter) followed by a selection of events according to their size, roundness and the intensity of the fluorescence. Both measurements were performed using automated inverted microscope Ti-E Nikon using JOBS software. Analysis of images and videos was performed with the ICY program. The IC_{50} value was determined using Microsoft Excel and Graphpad.

4.2.8 **Preparation of drugs for drug interaction analysis**

Primary stock solutions were prepared as mentioned in Chapter 2 Materials and methods. In brief, atovaquone (MW = 366.84) was dissolved at 5 mg/ml (13.63 nM) in DMSO. Proguanil was dissolved at 1 mg/ml in acetonitrile: water (60/40). All primary stock solutions were passed through a 0.22 µm porosity filter, aliquoted and stored at -20°C until further use. For experimental set up the primary stock solutions were further diluted with complete medium to give final test concentrations.

A dose range of 0.125–8 x the IC_{50} was made by a two-fold serial dilution for artemether, atovaquone, proguanil, doxycycline and (-)-*R,S*-dehydroemetine. For artemether, the doses ranged from 1.875 to 120 nM. For atovaquone, the doses ranged from 0.25 nM to 16 nM for combination with proguanil, and 0.5 nM to 32 nM for combination with (-)-*R,S*-dehydroemetine. For proguanil the doses ranged was from 1.75 µM to 112 µM. For (-)-*R,S*-dehydroemetine the doses ranged was from 25 nM to 1600 nM for combination with doxycycline, and 12.5 nM to 800 nM for combination with atovaquone and proguanil. For doxycycline the doses ranged from 2.5 µM to 160 µM. For artemether the dose ranged from 1.875 nM to 120 nM. At each level, the compounds were co-administered for example IC_{50} of atovaquone was combined with the IC_{50} of (-)-*R,S*-dehydroemetine and 2 x IC_{50} atovaquone was combined with 2 x IC_{50} (-)-*R,S*-dehydroemetine and so forth. Parasites were treated at ring stage and incubated for 72 hours in a 96 well plate format. The SYBR green plate reader method was used to determine drug susceptibility as described in general materials and methods in Chapter 2. The data was analysed for the median-effect using CalcuSyn software (Biosoft) by converting triplicate data to an averaged percentage. The Dm, m and r values are also reported for all sets of data. Dm depicts the median effect dose at the ED_{50} level of inhibition. The m value refers to the kinetic order and shape of the curve m = 1, > 1, and < 1 indicates hyperbolic, sigmoidal, and negative sigmoidal shape, respectively. The r value represents the linear correlation coefficient for the median effect plot and indicates conformity to the mass action law.

4.2.9 **Virtual screening of FDA approved drug library to identify compounds for drug-interaction analysis with (-)-*R*,*S*-dehydroemetine:**

The orientation in which two molecules bind or interact with each other to make a stable complex could be predicted by docking (Shoichet et al., 1992) (Lengauer and Rarey, 1996). Scoring functions could be used to analyse the orientation of the molecules with respect to each other and help in the prediction of binding affinity or the strength of association (Berry et al., 2015). Drug designing could be aided by use of docking as it could quickly identify a potential hit by scanning through large databases of compounds. The potential lead could be optimised to design analogs which are more potent and selective (Jorgensen, 2009).

Autodock vina was used in this study for performing the virtual screening of drugs on various *P. falciparum* target receptors. Cygwin was used to run Autodock vina virtual screening commands. Following script was used to perform virtual screening (Trott and Olson, 2010).

```
#! /bin/bash
for f in ligand_*.pdbqt; do
   b=`basename $f .pdbqt`
   echo Processing ligand $b
   mkdir -p $b
   vina --configure conf.txt --ligand $f --out $10/out.pdbqt --log $/log.txt
done
```

4.3 Results:

4.3.1 Experimental determination of IC_{50} values for (-)-*R,S*-dehydroemetine and (-)-*S,S*-dehydroisoemetine:

Synthesis of the analogues of emetine dihydrochloride, ((-)-*R,S*-dehydroemetine and (-)-*S,S*-dehydroisoemetine) was outsourced to Chiroblock GMBH, Germany. Receptor-ligand docking predicted the activities of the two diastereomers with the possibility of (-)-*R,S*-dehydroemetine being more active than (-)-*S,S*-dehydroisoemetine.

(-)-*R,S*-dehydroemetine was tested in serial dilutions of 200nM, 100nM, 50nM, 25nM and 12.5nM. Dose response experiment was set up to be read at 72 hours. Based on the drug efficacy experiments, IC_{50} of (-)-*R,S*-dehydroemetine was found to be 69.58 $\pm$ 2.62 nM. Results are shown in the Figure 4.3.1.

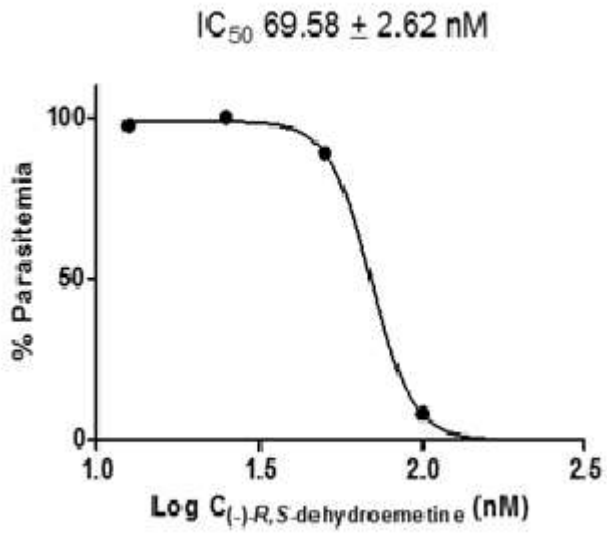

Figure 4.3.1: Dose response experiment for (-)-*R,S*-dehydroemetine.

The effective dose of (-)-*R,S*-dehydroemetine (dose range tested in serial dilutions from 12.5 nM to 200 nM) on *P. falciparum* (K1) infection after an incubation period of 72 hours using SYBR Green-based plate-reader assay. Data were analysed using GraphPad prism. Each value is a mean ± SD of triplicate data values.

(-)-*S,S*-Dehydroisoemetine was tested in serial dilutions of 20 µM, 10 µM, 5 µM, 2.5 µM and 1.25 µM. 50% reduction was observed at 1.85 + 0.2 µM concentration. Results are shown in the Figure 4.3.2.

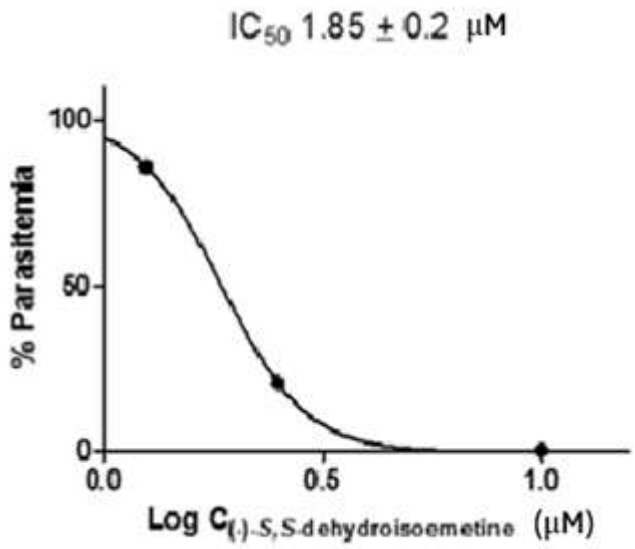

Figure 4.3.2: Dose response experiment for (-)-*S,S*-dehydroisoemetine.

The effective dose of (-)-*S,S*-dehydroisoemetine (dose range tested in serial dilutions from 2.5 µM to 20 µM) on *P. falciparum* (K1) infection after an incubation period of 72 hours using SYBR Green-based plate-reader assay. Data were analysed using GraphPad prism. Each value is a mean ± SD of triplicate data values.

4.3.2 **Time-course analysis through IC_{50} speed assay for determination of speed of action of (-)-*R,S*-dehydroemetine and (-)-*S,S*-dehydroisoemetine:**

The IC_{50} speed assay was performed for (-)-*R,S*-dehydroemetine and (-)-*S,S*-dehydroisoemetine (with concentrations of 25 nM, 125 nM, 625 nM, 3125 nM and 15625 nM and 0.5 µM, 2.5 µM, 12.5 µM, 62.5 µM and 312.5 µM, respectively) using unsynchronised cultures of *P. falciparum* (n = 3). The ratio of 24 hours IC_{50} values to 72 hours IC_{50} values for (-)-*R,S*-dehydroemetine and (-)-*S,S*-dehydroisoemetine could not be determined as IC_{50} could not be reached within 24 hours. Both compounds exhibited onset of activity within 24 hours but achieved 50% inhibition at the previously defined IC_{50} values only after 48 hours of exposure, indicating that the isomers have delayed action against the multi-drug resistant K1 strain of *P. falciparum*. Figures 4.3.3 and 4.3.4 show the results for IC_{50} speed assay for (-)-*R,S*-dehydroemetine and (-)-*S,S*-dehydroisoemetine respectively (error bars represent the

standard error on the experiments performed twice with each concentration of (-)-*R,S*-dehydroemetine and (-)-*S,S*-dehydroisoemetine tested in triplicates).

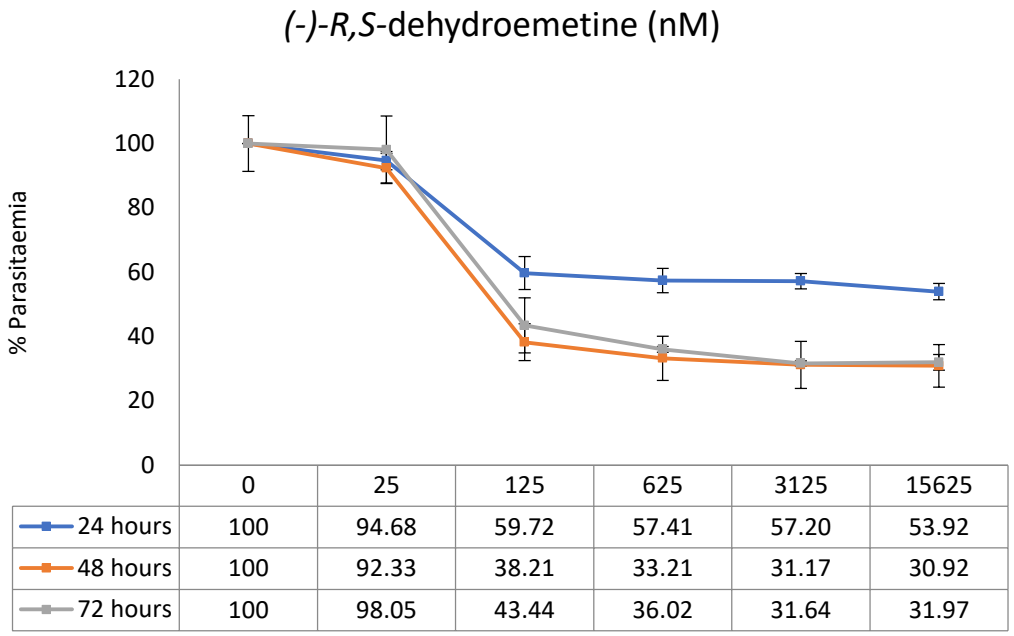

	0	25	125	625	3125	15625
24 hours	100	94.68	59.72	57.41	57.20	53.92
48 hours	100	92.33	38.21	33.21	31.17	30.92
72 hours	100	98.05	43.44	36.02	31.64	31.97

Figure 4.3.3: Time course analysis of (-)-*R,S*-dehydroemetine against *Plasmodium falciparum* K1.
Effect of (-)-*R,S*-dehydroemetine on unsynchronised cultures of *P. falciparum* at 24h, 48h and 72h. Dose range: 25 nM, 125 nM, 625 nM, 3125 nM and 15625 nM. IC_{50} could not be reached within 24 hours. (-)-*R,S*-Dehydroemetine reached the IC_{50} by 48 hours. Error bars represent the standard error on the experiments performed twice with each concentration of (-)-*R,S*-dehydroemetine tested in triplicates.

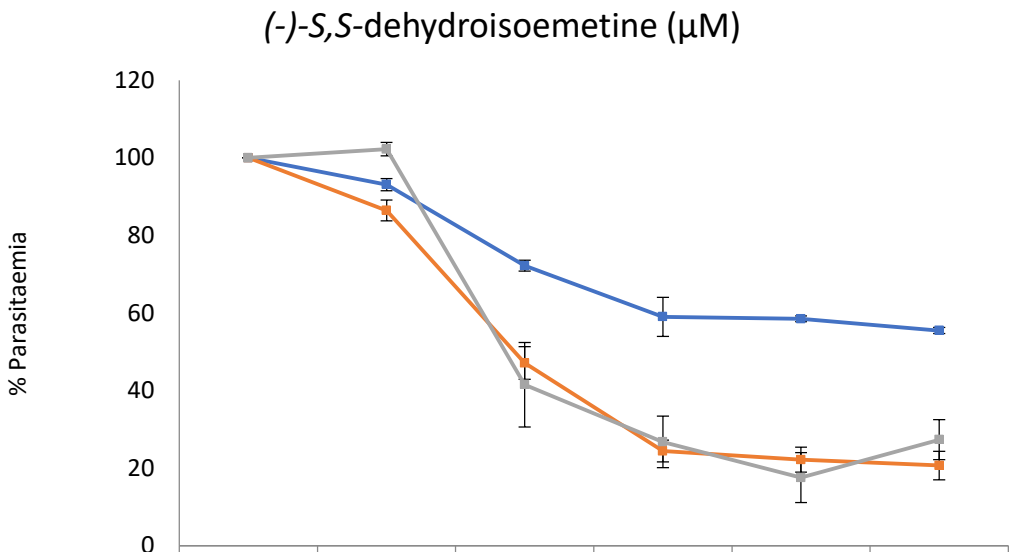

	0	0.5	2.5	12.5	62.5	312.5
24 hours	100	93.10	72.19	59.01	58.49	55.50
48 hours	100.00	86.45	47.12	24.42	22.19	20.68
72 hours	100	102.25	41.54	26.76	17.54	27.34

Figure 4.3.4: Time course analysis of (-)-*S,S*-dehydroisoemetine against *Plasmodium falciparum* K1.
Effect of (-)-*S,S*-dehydroisoemetine on unsynchronised cultures of *P. falciparum* at 24h, 48h and 72h. Dose range 0.5 µM, 2.5 µM, 12.5 µM, 62.5 µM and 312.5 µM. IC_{50} could not be reached within 24 hours. *(-)-S,S*-Dehydroisoemetine reached the IC_{50} by 48 hours. Error bars represent the standard error on the experiments performed twice with each concentration of (-)-*S,S*-dehydroisoemetine tested in triplicates.

4.3.3 **Stage-specific profiling of (-)-*R,S*-dehydroemetine and (-)-*S,S*-dehydroisoemetine:**

The two isomers of dehydroemetine were tested on synchronous cultures (*(-)-R,S*-dehydroemetine was tested in two fold serial dilutions from 132.81 nM to 8500 nM and *(-)-S,S*-dehydroisoemetine was tested in two fold serial dilutions from 3.13 µM to 200 µM) to determine the stage-specificity of the compounds by measuring the concentration dependent growth of trophozoites/schizonts and rings following incubation with the two compounds.

It was observed that (-)-*R,S*-dehydroemetine and (-)-*S,S*-dehydroisoemetine affect both the ring and schizont stages of the parasite (Figures 4.3.5 and 4.3.6, error bars represent the standard error on the experiments performed twice with each concentration of (-)-*R,S*-dehydroemetine and (-)-*S,S*-dehydroisoemetine tested in triplicates). The decrease in growth

of schizonts was observed to be more marked in comparison to rings. Both the isomers were thus found to be more active against the late trophozoite/schizont stages.

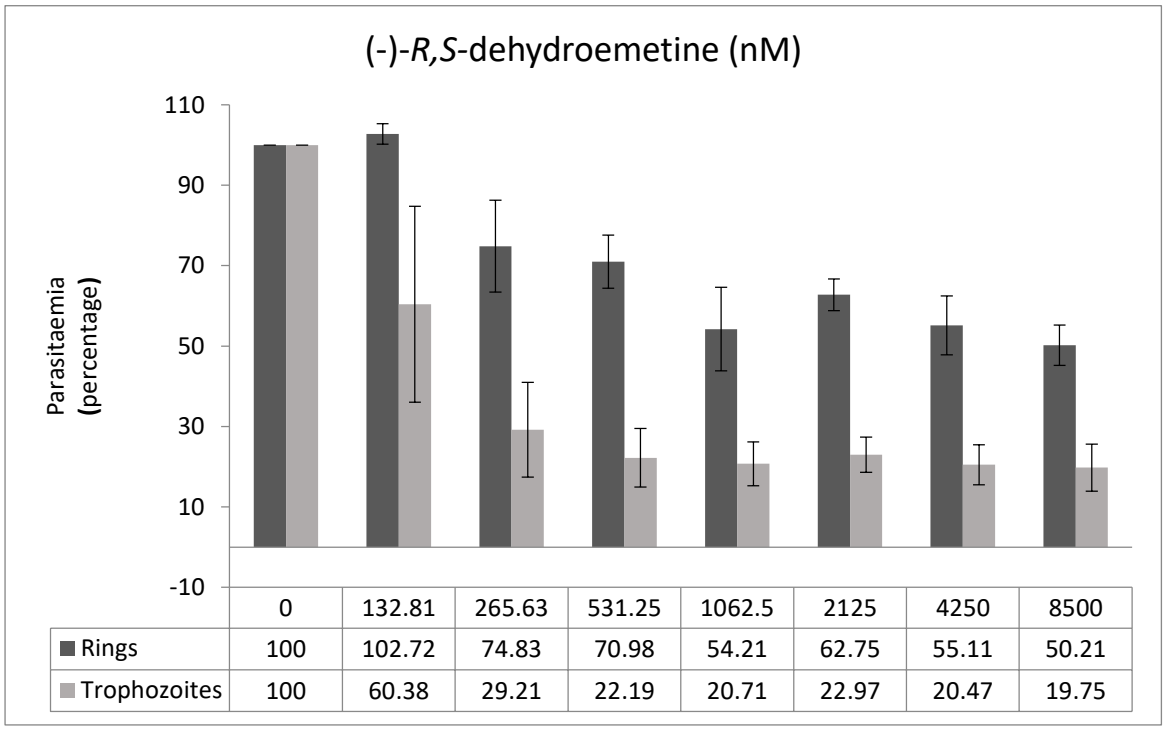

Figure 4.3.5: Stage-specific effects of (-)-*R,S*-dehydroemetine on synchronous ring and trophozoite cultures of *P. falciparum* K1 strain.

The decrease in growth of trophozoites/schizonts was observed to be more marked in comparison to rings. Cultures were exposed to a serial dilution of (-)-*R,S*-dehydroemetine (from 132.81 nM to 8500 nM) for 24 hours. The drug effects are expressed as a percentage of growth of the rings relative to trophozoites/schizonts 24h after post-exposure wash. Error bars represent the standard error on the experiments performed twice with each concentration of (-)-*S,S*-dehydroisoemetine tested in triplicates.

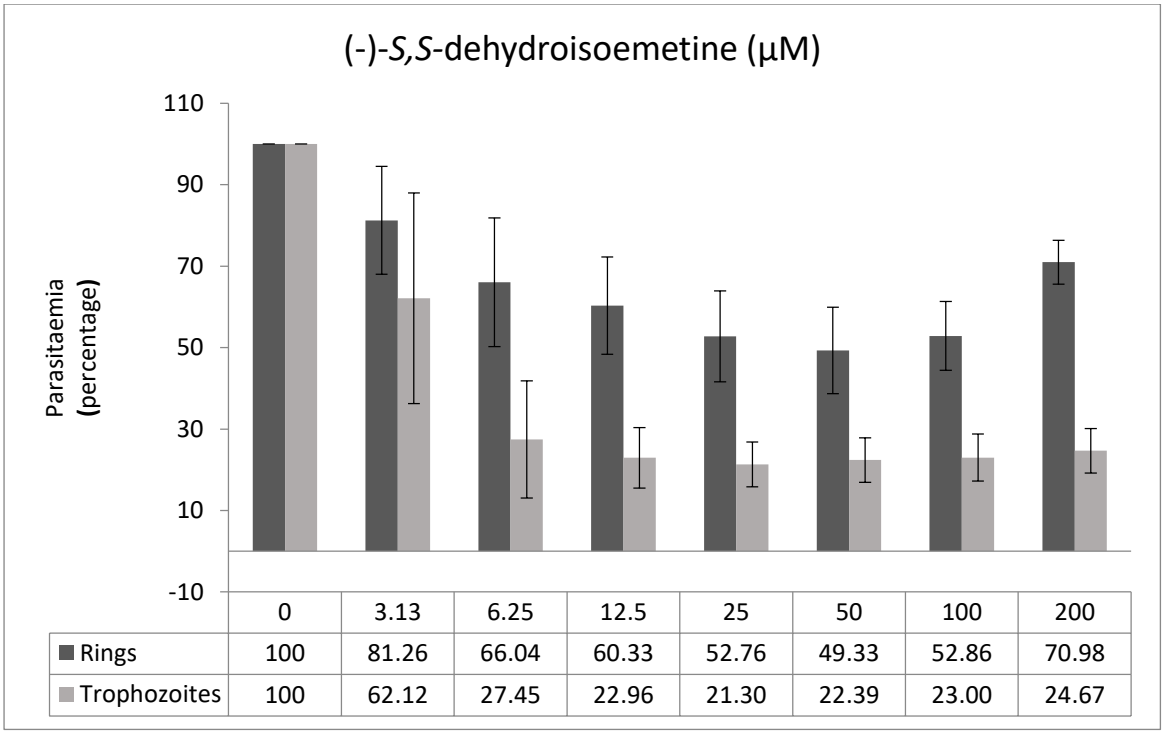

	0	3.13	6.25	12.5	25	50	100	200
Rings	100	81.26	66.04	60.33	52.76	49.33	52.86	70.98
Trophozoites	100	62.12	27.45	22.96	21.30	22.39	23.00	24.67

Figure 4.3.6: Stage-specific effects of (-)-*S,S*-dehydroisoemetine on synchronous ring and trophozoite cultures of *P. falciparum* K1 strain.

The decrease in growth of trophozoites/schizonts was observed to be more marked in comparison to rings. Cultures were exposed to a serial dilution of (-)-*S,S*-dehydroisoemetine (from 3.13 µM to 200 µM) for 24 hours. The drug effects are expressed as a percentage of growth of the rings relative to trophozoites/schizonts 24h after post-exposure wash. Error bars represent the standard error on the experiments performed twice with each concentration of (-)-*S,S*-dehydroisoemetine tested in triplicates.

4.3.4 **MTT cell viability assay for determination of cell cytotoxicity:**

MTT assay for cell cytotoxicity was performed to determine the safety profile as mentioned in the methodology section for (-)-*R,S*-dehydroemetine and (-)-*S,S*-dehydroisoemetine (n = 3). Emetine and Cisplatin were used as control drugs. The plate was read at 48 hours. Emetine was tested in two-fold serial dilutions from 31.25 nM to 2000 nM with IC_{50} observed to be 225.1 $\pm$ 17.2 nM (Figure 4.3.7). *(-)-R,S*-Dehydroemetine was tested in two-fold serial dilution from 11.72 nM to 750 nM with IC_{50} observed to be 196.4 $\pm$ 11 nM (Figure 4.3.8). *(-)-S,S*-Dehydroisoemetine was tested in two fold serial dilutions from 0.312 µM to 10 µM with IC_{50} observed to be 1.429 $\pm$ 0.18 µM (Figure 4.3.9). Cisplatin was tested in two fold serial dilutions from 0.78 µM to 25 µM and with IC_{50} observed to be 10.16 $\pm$ 2.6 µM (Figure

4.3.10). Selectivity indices (ratio of LD50 by IC50) for emetine, (-)-*R,S*-dehydroemetine and (-)-*S,S*-dehydroisoemetine were calculated to be ~4.5, ~3 and ~1 respectively.

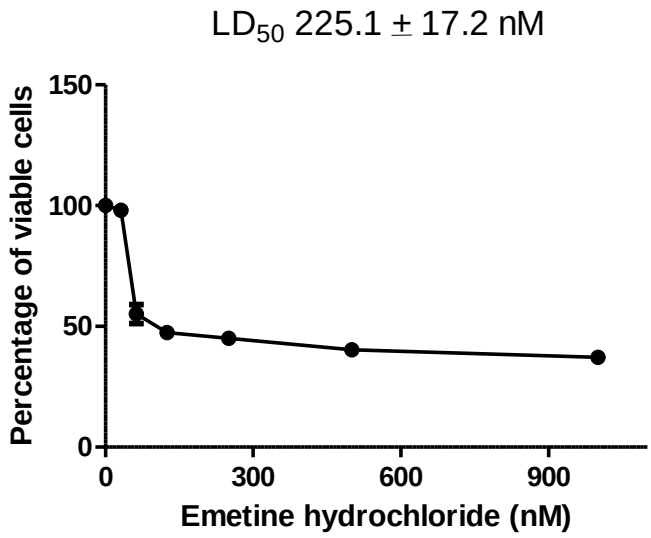

Figure 4.3.7: 48 hour MTT cytotoxicity assay for emetine in HepG2 Cell lines.

Cells were seeded at 5000 cells per well. Cell viability was determined using standard MTT assay. Emetine hydrochloride was tested in two fold serial dilutions from 31.25 nM to 2000 nM. Data was analysed using GraphPad prism. Error bars represent triplicate data values (mean ± SD).

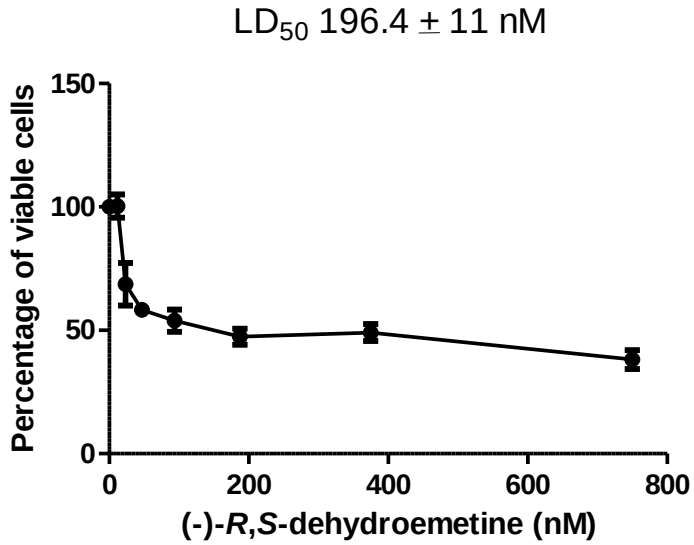

Figure 4.3.8: 48 hour MTT cytotoxicity assay for (-)-*R,S*-dehydroemetine in HepG2 Cell lines.

Cells were seeded at 5000 cells per well. Cell viability was determined using standard MTT assay. (-)-*R,S*-Dehydroemetine was tested in two fold serial dilutions from 11.72 nM to 750 nM. Data was analysed using GraphPad prism. Error bars represent triplicate data values (mean ± SD).

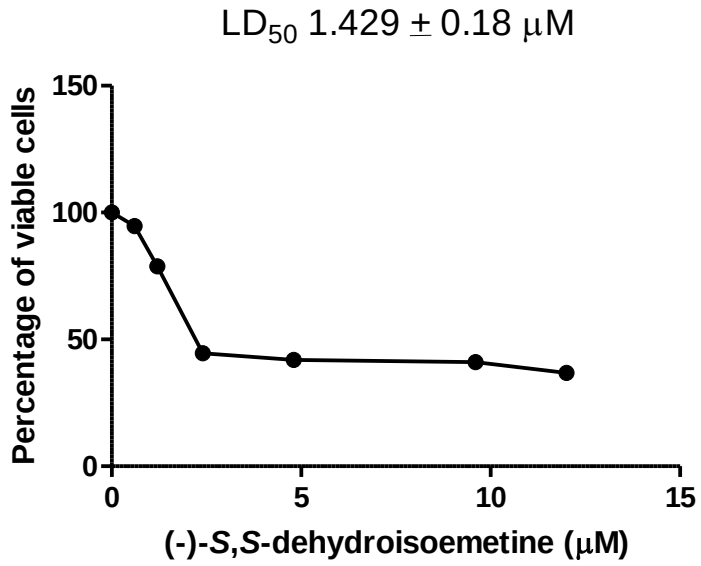

Figure 4.3.9: 48 hour MTT cytotoxicity assay for (-)-*S,S*-dehydroisoemetine in HepG2 Cell lines.

Cells were seeded at 5000 cells per well. Cell viability was determined using standard MTT assay. (-)-S,S-Dehydroisoemetine was tested in two fold serial dilutions from 0.312 μM to 10 μM. Data was analysed using GraphPad prism. Error bars represent triplicate data values (mean ± SD).

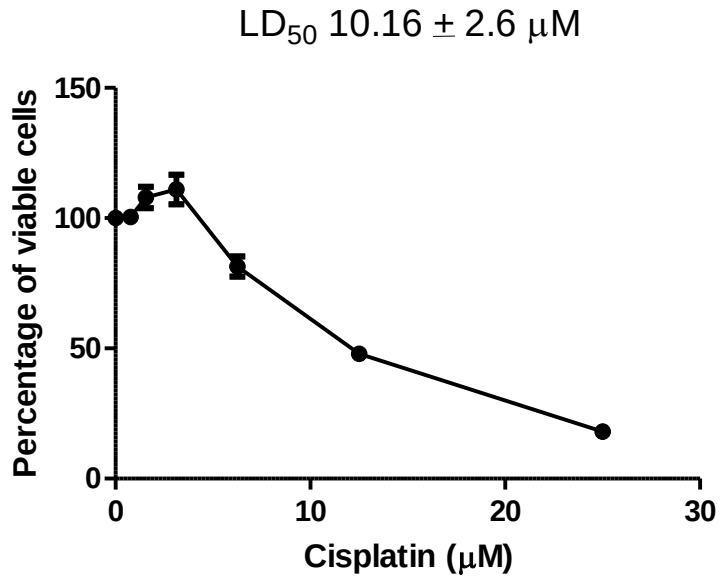

Figure 4.3.10: 48 hour MTT cytotoxicity assay for cisplatin in HepG2 Cell lines.

Cells were seeded at 5000 cells per well. Cell viability was determined using standard MTT assay. Cisplatin was tested in two fold serial dilutions from 0.78 μM to 25 μM. Data was analysed using GraphPad prism. Error bars represent triplicate data values (mean ± SD).

4.3.5 **Determination of cross-resistance by hypoxanthine incorporation assay**

This assay was carried out at GSK Tres Cantos, Madrid (Spain) and relies on the parasite incorporation of labelled hypoxanthine that is proportional to *P. falciparum* growth. *In vitro* cross-resistance of the compounds was measured as an IC_{50} ratio between the IC_{50} value for the corresponding *P. falciparum* strain versus the IC_{50} value for 3D7A. Every replicate from an MDR strain involved a simultaneous determination using a 3D7A replicate to avoid any artefact linked to experimental conditions. Table 4.3.1 shows the IC_{50} values of emetine dihydrochloride, *(-)-R,S*-dehydroemetine and *(-)-S,S*-dehydroisoemetine in *P. falciparum* sensitive strain (3D7A) and two *Pf* resistant strains (Dd2 and W2). The ratios of *in vitro* cross-resistance of emetine dihydrochloride in both resistant strains (Dd2 and W2) using 3D7A strain as reference was found 1.15 and 0.77, respectively. The ratios of in vitro cross-resistance of *(-)-R,S*-dehydroemetine in both resistant strains (Dd2 and W2) using 3D7A strain as reference was found 1.21 and 1.15 respectively. The results showed that the inhibitory potency observed for emetine dihydrochloride and *(-)-R,S*-dehydroemetine in both multidrug resistant strains (Dd2 and W2) is similar to the sensitive strain 3D7A. These results suggest that there is no cross-resistance of emetine dihydrochloride and *(-)-R,S*-dehydroemetine with any of the MDR strains tested. (-)-*S,S*-Dehydroisoemetine did not achieve 50% inhibitory values for Dd2 and W2, hence displayed cross-resistance against the strains tested.

Table 4.3.1 Analysis of results to determine cross-resistance through hypoxanthine incorporation assay.

Compounds	3D7A		Dd2		W2			
	Pf IC50 (µM)	st dev	Pf IC50 (µM)	st dev	Pf IC50 (µM)	st dev	ratio Dd2/3D7A	ratio W2/3D7A
Emetine dihydrochloride	0.234	0.022	0.269	0.025	0.181	0	1.15	0.77
(-)-*R,S*-dehydroemetine	0.146	0.003	0.177	0.014	0.168	0.005	1.21	1.15
(-)-*S,S*-dehydroisoemetine	1.031	0.041	NA		NA			

In-vitro IC_{50} values of emetine dihydrochloride, *(-)-R,S*-dehydroemetine and *(-)-S,S*-dehydroisoemetine in *P. falciparum* sensitive strain (3D7A) and *Pf* resistant strains (Dd2 and W2). It also shows the ratios of *in vitro* cross-resistance of emetine dihydrochloride and *(-)-R,S*-dehydroemetine in both resistant strains (Dd2 and W2) using 3D7A strain as reference. NA represents IC_{50} not achieved. Bioassay carried out at GSK Tres Cantos, Madrid (Spain).

4.3.6 **In vitro IC_{50} against *P. falciparum* male and female activated gametes:**

This bioassay was carried out at GSK Tres Cantos, Madrid (Spain) to assesses the malaria transmission blocking potential of compounds by estimating their ability to prevent male mature gametocytes to progress to male microgametes or/and to inhibit female gamete activation, as indicators of gametocyte functionality. The activation of male gametocytes into mature microgametes is evaluated by the process of exflagellation (extrusion of rapidly waving flagellum-like microgametes from the infected erythrocyte). The activation of female gametocytes is evaluated based on the specific expression of the Pfs25 protein at the surface of the female activated gametes (Miguel-Blanco et al., 2015). Male *P. falciparum* gametocytes exflagellate when activated, causing the movement of the surrounding RBCs in the media. Detecting these changes in cells position, it was possible to detect activated male gametes. Female *P. falciparum* gametocytes round up when activated and the *Pf*s25 protein distributes widely in the membrane of the gamete. Using a monoclonal antibody against this protein it was possible to specifically detect activated female gametes. Dual gamete formation assay was performed and the results are shown in Table 4.3.2 *(-)-R,S*-dehydroemetine was found to display gametocidal activity against both male and female gametes whereas *(-)-S,S*-dehydroisoemetine was found to be not gametocidal.

Table 4.3.2 Activity against male and female activated gametes.

	P. falciparum Dual Gamete Formation Assay			
	Male		Female	
Compounds	Average	Stdev	Average	stdev
(-)-R,S-dehydroemetine (µM)	0.43	0.02	1.04	0.02
(-)-S,S-dehydroisoemetine (µM)	>10		>10	

In-vitro IC_{50} values of *(-)-R,S*-dehydroemetine and *(-)-S,S*-dehydroisoemetine against male and female gametocytes in *P. falciparum* NF54 strain. Bioassay carried out at GSK Tres Cantos, Madrid (Spain).

4.4 Results for *in-vitro* CalcuSyn-based drug interaction analysis of (-)-*R,S*-dehydroemetine:

Experimental results of (-)-*R,S*-dehydroemetine and (-)-*S,S*-dehydroisoemetine showed (-)-*R,S*-dehydroemetine to be highly potent against the K1 strain of P. *falciparum* whereas (-)-*S,S*-dehydroisoemetine was found to be less potent. IC_{50} of (-)-*R,S*-dehydroemetine was found to be 69.58 + 2.62 nM and that of (-)-*S,S*-dehydroisoemetine was found to be 1.85 $\pm$ 0.2 µM. As such only the more potent isomer of dehydroemetine, (-)-*R,S*-dehydroemetine was taken forward for drug interaction analysis. The Dm, m and r values are also reported for all sets of data. Dm depicts the median effect dose at the ED_{50} level of inhibition. The m value refers to the kinetic order and shape of the curve m = 1, > 1, and < 1 indicates hyperbolic, sigmoidal, and negative sigmoidal shape, respectively. The r value represents the linear correlation coefficient for the median effect plot and indicates conformity to the mass action law.

4.4.1 Validation of the CalcuSyn assay for malaria

CalcuSyn method has been previously validated in our laboratory as a useful tool for antimalarial drug interaction analysis (Matthews et al., 2017). To establish the robustness of the method, the known synergistic drug combination, atovaquone and proguanil, was used. The doses selected for the experiment were based on the respective IC_{50} values for atovaquone (0.25nM-16nM) and proguanil (1.75 µM to 112 µM). Triplicate samples were analysed by SG-plate-reader after 72 hours. Calclusyn predicted strong synergism between the two drugs which is in accordance with the published literature (Table 4.4.1).

Table 4.4.1 Combinatory Index values.

Range of CI	Symbol	Description
<0.1	+++++	Very strong synergism
0.1-0..3	++++	Strong synergism
0.3-0.7	+++	Synergism
0.7-0.85	++	Moderate synergism
0.85-0.90	+	Slight synergism
0.90-1.10	±	Nearly additive
1.10-1.20	-	Slight antagonism
1.20-1.45	--	Moderate antagonism
1.45-3.3	---	Antagonism
3.3-10	----	Strong antagonism
>10	-----	Very strong antagonism

Classification of synergism or antagonism using CI (Combination Index) values generated by Chaou-Talalay method (Chou, 2010).

4.4.2 **CalcuSyn-based dranalysis of the atovaquone - proguanil combination**

The CalcuSyn based analysis of the drug interactivity between atovaquone and proguanil using a constant-ratio combination of 1:7000 dose was performed. The output includes a dose-effect curve and a median-effect plot in addition to the Combination Index (CI) and an isobologram plot, to figuratively depict the compound's potency and conformity to the mass action law (Figure 4.4.1). Specifically, CI = 0.20, 0.34 and 0.57 at the IC_{50}, IC_{75} and IC_{90} levels, respectively were obtained inferring strong synergism at IC_{50} and $IC_{75,}$ and synergism at IC_{90}. Good correlation coefficients of the median-effect plot were reported for atovaquone (r = 0.99), proguanil (r = 0.89), and the combination (r = 0.93), inferring good conformity to the mass-action law (Table 4.4.2).

Table 4.4.2 CalcuSyn based drug interaction analysis of atovaquone and proguanil.

Drug	CI Values at			nM		
	IC_{50}	IC_{75}	IC_{90}	Dm	m	r
Atovaquone	N/A	N/A	N/A	6.53	0.88	0.99
Proguanil	N/A	N/A	N/A	27771	1.06	0.89
Combination (1:7000)	0.21	0.34	0.57	0.56	0.68	0.93

Dm depicts the median effect dose at the ED_{50} level of inhibition. The m value refers to the kinetic order and shape of the curve m = 1, > 1, and < 1 indicates hyperbolic, sigmoidal, and negative sigmoidal shape, respectively. The r value represents the linear correlation coefficient for the median effect plot and indicates conformity to the mass action law.

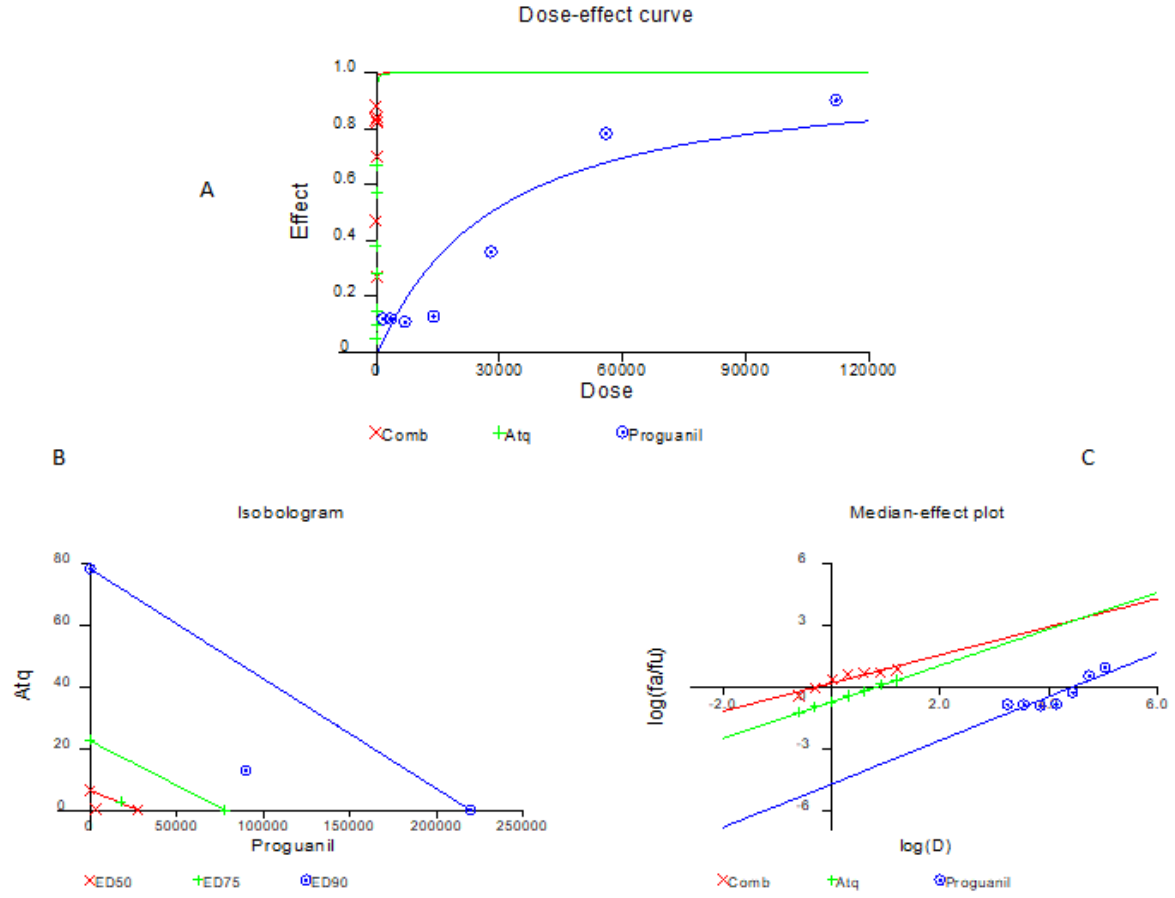

Figure 4.4.1: CalcuSyn drug interactivity analysis for atovaquone and proguanil.

CalcuSyn based dose-effect curve (A), CalcuSyn based isobologram and CalcuSyn based median effect plot (C) for drug interactivity between atovaquone and proguanil. Atovaquone and proguanil (1:7000) combination was found to be strongly synergistic at IC_{50} (CI = 0.21), and synergistic at IC_{75} (CI = 0.34) and IC_{90} (CI = 0.57).

4.4.3 **CalcuSyn analysis of (-)-*R,S*-dehydroemetine:**

Following validation of the CalcuSyn software employing Chou-Talalay method for drug interaction analysis using the atovaquone-proguanil combination, the interaction between (-)-*R,S*-dehydroemetine – artemether, (-)-*R,S*-dehydroemetine - atovaquone, (-)-*R,S*-dehydroemetine - proguanil and (-)-*R,S*-dehydroemetine – doxycycline were studied. The doses used for each compound were based on the known IC_{50} values which served as the midpoint for a two-fold, constant-ratio dose series as shown in Table 4.4.3.

Table 4.4.3 The dose series used for the combination of existing antimalarials with (-)-*R,S*-dehydroemetine

Dose	Dose (nM or µM)					
Level	(-)-*R,S*-dehydroemetine (nM) (for doxycycline)	(-)-*R,S*-dehydroemetine (nM) for (artemether, atovaquone and proguanil)	Artemether (nM)	Atovaquone (nM)	Proguanil (µM)	Doxycycline (µM)
A	25	12.5	1.875	0.5	1.75	2.5
B	50	25	3.75	1	3.5	5
C	100	50	7.5	2	7	10
D	200	100	15	4	14	20
E	400	200	30	8	28	40
F	800	400	60	16	56	80
G	1600	800	120	32	112	160
Combination ratio with (-)-*R,S*-dehydroemetine	--	--	6.667:1	1:25	140:1	100:1

4.4.4 **CalcuSyn-based analysis of the (-)-*R,S*-dehydroemetine - artemether combination**

The CalcuSyn based analysis of the drug interactivity between (-)-*R,S*-dehydroemetine and artemether using a constant-ratio combination of 6.667:1 dose was done (Figure 4.4.2). Specifically, CI = 1.615, 1.684 and 1.766 at the IC_{50}, IC_{75} and IC_{90} levels, respectively were obtained inferring antagonism at all measurement points. Good correlation coefficients of the median-effect plot were reported for (-)-*R,S*-dehydroemetine (r = 0.93), artemether (r = 0.90), and the combination (r = 0.91), inferring good conformity to the mass-action law (Table 4.4.4).

Table 4.4.4 CalcuSyn based analysis of drug interaction between (-)-*R,S*-dehydroemetine and artemether

Drug	CI Values at			nM		
	IC_{50}	IC_{75}	IC_{90}	Dm	M	R
(-)-*R,S*-dehydroemetine	N/A	N/A	N/A	89.56	1.49	0.93
Artemether	N/A	N/A	N/A	14.26	1.88	0.90
Combination (6.667:1)	1.62	1.68	1.77	74.49	1.57	0.91

Dm depicts the median effect dose at the ED_{50} level of inhibition. The m value refers to the kinetic order and shape of the curve m = 1, > 1, and < 1 indicates hyperbolic, sigmoidal, and negative sigmoidal shape, respectively. The r value represents the linear correlation coefficient for the median effect plot and indicates conformity to the mass action law.

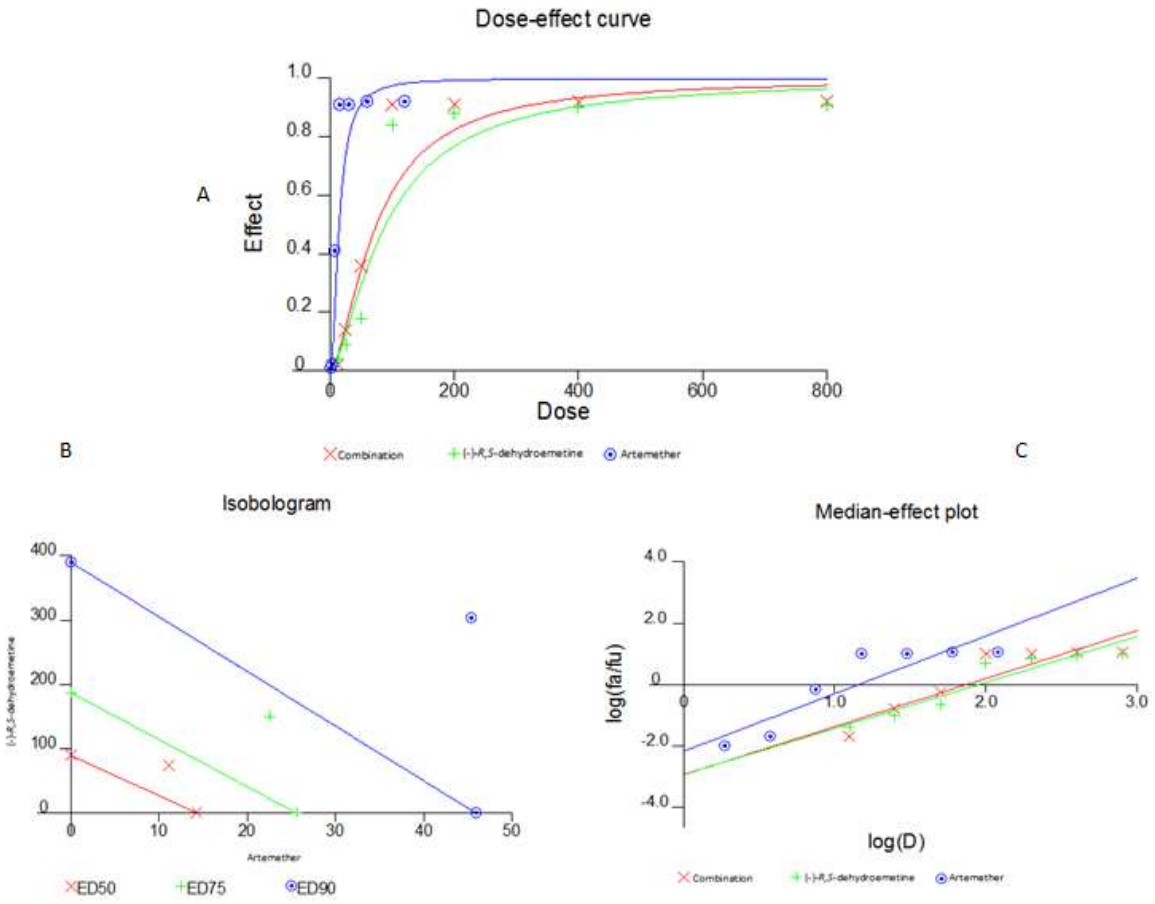

Figure 4.4.2: CalcuSyn drug interactivity analysis for (-)-*R,S*-dehydroemetine and artemether combination.

CalcuSyn based dose-effect curve (A), CalcuSyn based isobologram and CalcuSyn based median effect plot (C) for drug interactivity between (-)-*R,S*-dehydroemetine and artemether. (-)-*R,S*-dehydroemetine and artemether (6.667:1) combination was found to be antagonistic at IC_{50} (CI = 1.62), IC_{75} (CI = 1.68) and IC_{90} (CI = 1.77).

4.4.5 **CalcuSyn-based analysis of the (-)-*R,S*-dehydroemetine - atovaquone combination:**

The CalcuSyn based analysis of the drug interactivity between (-)-*R,S*-dehydroemetine and atovaquone using a constant-ratio combination of 25:1 dose was done (Figure 4.4.3). Specifically, CI = 0.88, 0.88 and 0.89 at the IC_{50}, IC_{75} and IC_{90} levels, respectively were obtained inferring mild synergism at all measurement points. Good correlation coefficients of the median-effect plot were reported for atovaquone (r = 0.94), (-)-*R,S*-dehydroemetine (r = 0.95), and the combination (r = 0.97), inferring good conformity to the mass-action law (Table 4.4.5).

Table 4.4.5 CalcuSyn based analysis of drug interaction between atovaquone and (-)-R,S-dehydroemetine

Drug	CI Values at			nM		
	IC_{50}	IC_{75}	IC_{90}	Dm	M	R
Atovaquone	N/A	N/A	N/A	8.56	1.52	0.94
(-)-R,S-dehydroemetine	N/A	N/A	N/A	85.98	2.41	0.95
Combination (1:25)	0.88	0.88	0.89	2.16	2.09	0.97

Dm depicts the median effect dose at the ED_{50} level of inhibition. The m value refers to the kinetic order and shape of the curve m = 1, > 1, and < 1 indicates hyperbolic, sigmoidal, and negative sigmoidal shape, respectively. The r value represents the linear correlation coefficient for the median effect plot and indicates conformity to the mass action law.

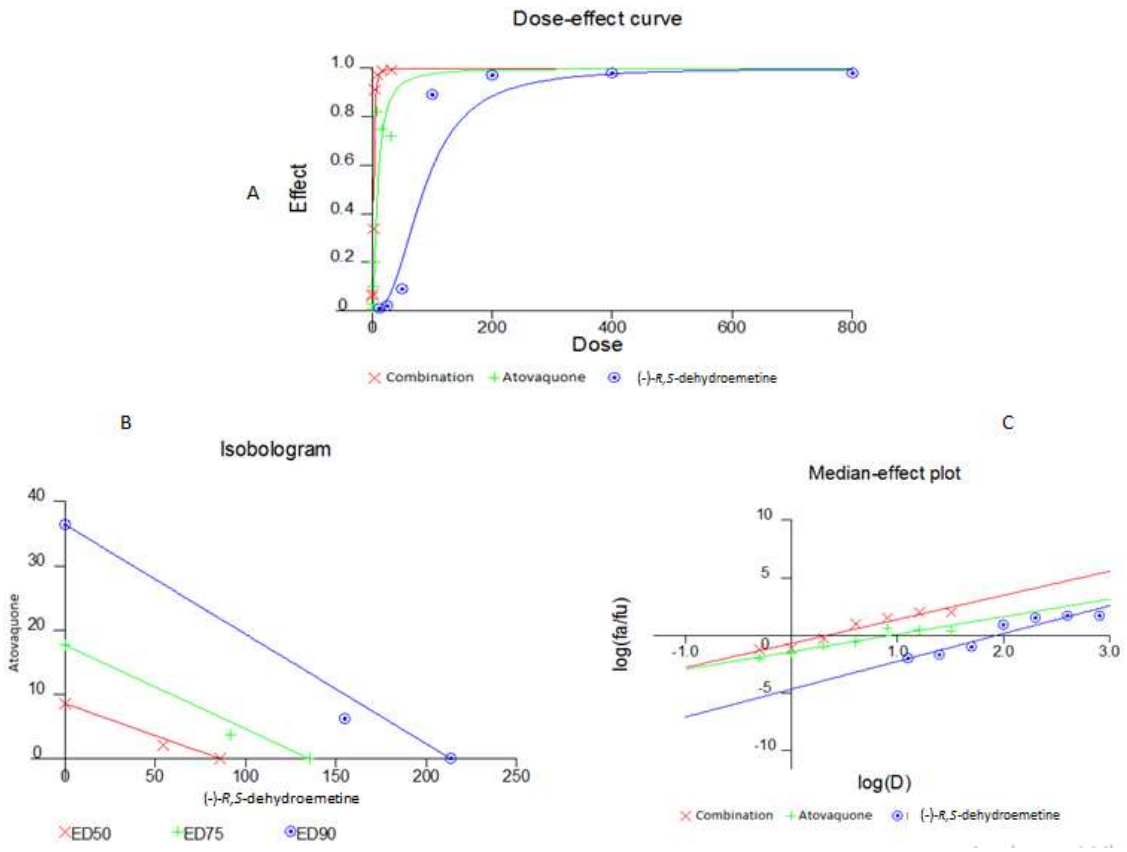

Figure 4.4.3: CalcuSyn drug interactivity analysis for atovaquone and (-)-*R,S*-dehydroemetine combination.

CalcuSyn based dose-effect curve (A), CalcuSyn based isobologram and CalcuSyn based median effect plot (C) for drug interactivity between (-)-*R,S*-dehydroemetine and atovaquone. Atovaquone and (-)-*R,S*-dehydroemetine (1:25) combination was found to be synergistic at IC_{50} (CI = 0.88), IC_{75} (CI = 0.88) and IC_{90} (CI = 0.89).

4.4.6 **CalcuSyn-based analysis of the (-)-*R,S*-dehydroemetine - doxycycline combination:**

The CalcuSyn based analysis of the drug interactivity between (-)-*R,S*-dehydroemetine and doxycycline using a constant-ratio combination of 1:100 dose was done (Figure 4.4.4) Specifically, CI = 1.55, 1.47 and 1.52 at the IC_{50}, IC_{75} and IC_{90} levels, respectively were obtained inferring antagonism at all measurement points. Good correlation coefficients of the median-effect plot were reported for doxycycline (r = 0.97), (-)-*R,S*-dehydroemetine (r = 0.84), and the combination (r = 0.81), inferring good conformity to the mass-action law (Table 4.4.6).

Table 4.4.6 CalcuSyn based analysis of drug interaction between doxycycline and (-)-*R,S*-dehydroemetine

Drug	CI Values at			µM		
	IC_{50}	IC_{75}	IC_{90}	Dm	M	R
Doxycycline	N/A	N/A	N/A	39.46	1.50	0.97
(-)-R,S-dehydroemetine	N/A	N/A	N/A	0.076	0.78	0.84
Combination (100:1)	1.55	1.47	1.52	9.84	0.91	0.81

Dm depicts the median effect dose at the ED_{50} level of inhibition. The m value refers to the kinetic order and shape of the curve m = 1, > 1, and < 1 indicates hyperbolic, sigmoidal, and negative sigmoidal shape, respectively. The r value represents the linear correlation coefficient for the median effect plot and indicates conformity to the mass action law.

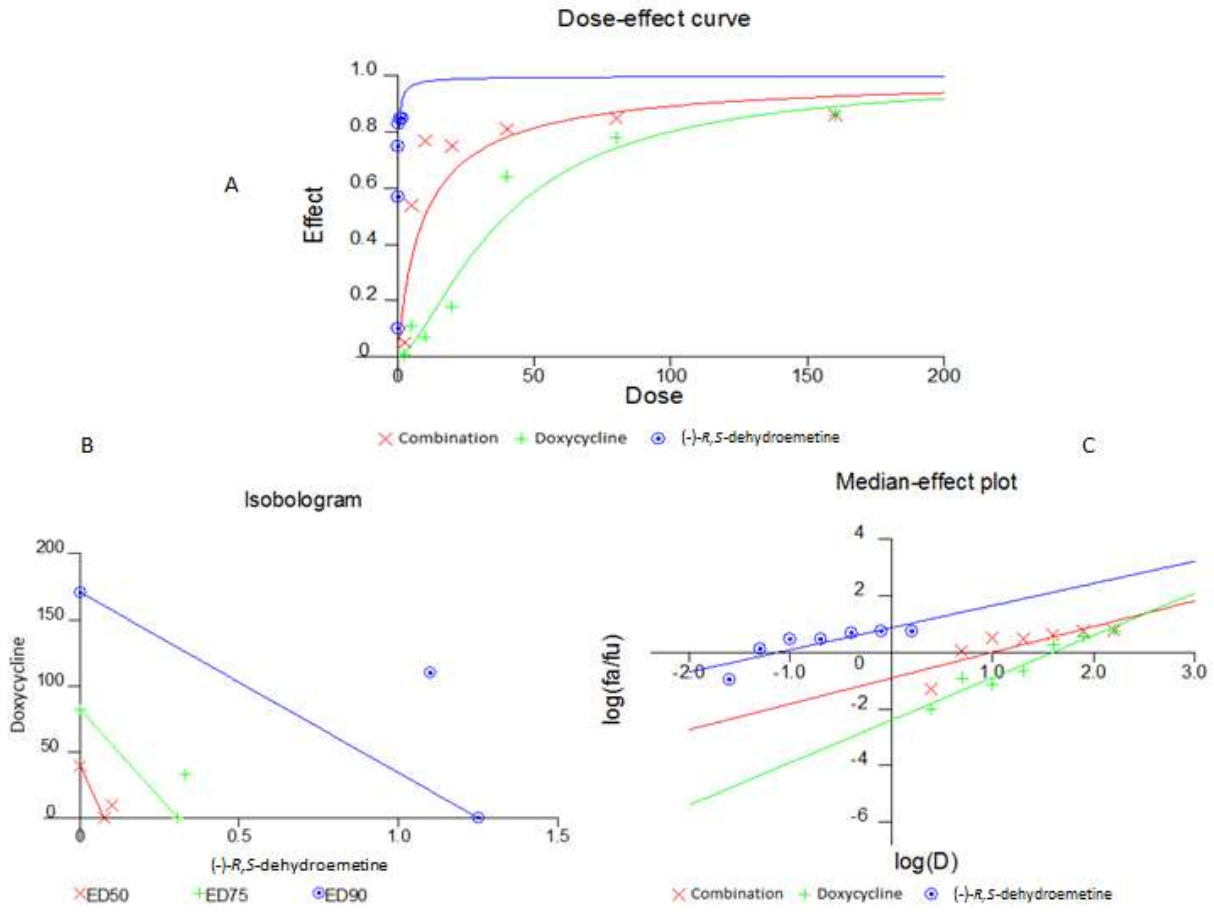

Figure 4.4.4: CalcuSyn drug interactivity analysis for doxycycline and (-)-*R,S*-dehydroemetine combination.

CalcuSyn based dose-effect curve (A), CalcuSyn based isobologram and CalcuSyn based median effect plot (C) for drug interactivity between (-)-*R,S*-dehydroemetine and doxycycline. Doxycycline and (-)-*R,S*-dehydroemetine (100:1) combination was found to be antagonistic at IC_{50} (CI = 1.55), IC_{75} (CI = 1.47) and IC_{90} (CI = 1.52).

4.4.7 CalcuSyn-based analysis of the (-)-*R,S*-dehydroemetine - proguanil combination:

The CalcuSyn based analysis of the drug interactivity between (-)-*R,S*-dehydroemetine and proguanil using a constant-ratio combination of 140:1 dose was done (Figure 4.4.5). Specifically, CI = 0.67, 1.04 and 1.62 at the IC_{50}, IC_{75} and IC_{90} levels, respectively, were obtained inferring synergism at IC_{50}, nearly additive at IC_{75} and antagonism at IC_{90}. Good correlation coefficients of the median-effect plot were reported for proguanil (r = 0.91), (-)-*R,S*-dehydroemetine (r = 0.86), and the combination (r = 0.96), inferring good conformity to the mass-action law (Table 4.4.7).

Table 4.4.7 CalcuSyn based analysis of drug interaction between proguanil and (-)-*R,S*-dehydroemetine

Drug	CI Values at			µM		
	IC_{50}	IC_{75}	IC_{90}	Dm	M	R
Proguanil	N/A	N/A	N/A	20.93	1.62	0.91
(-)-*R,S*-dehydroemetine	N/A	N/A	N/A	232.46	0.88	0.86
Combination ratio (140:1)	0.67	1.04	1.62	14.17	0.98	0.96

Dm depicts the median effect dose at the ED_{50} level of inhibition. The m value refers to the kinetic order and shape of the curve m = 1, > 1, and < 1 indicates hyperbolic, sigmoidal, and negative sigmoidal shape, respectively. The r value represents the linear correlation coefficient for the median effect plot and indicates conformity to the mass action law.

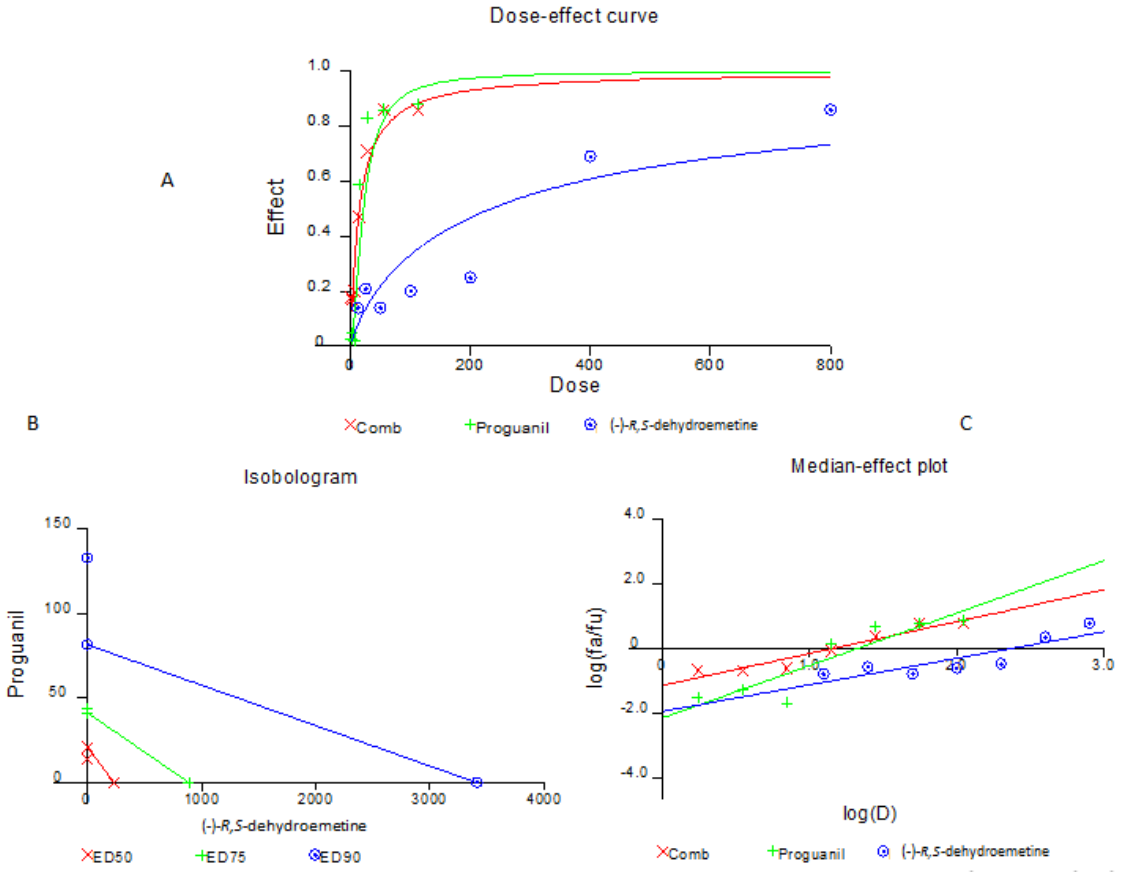

Figure 4.4.5: CalcuSyn drug interactivity analysis for (-)-*R,S*-dehydroemetine-proguanil combination.
CalcuSyn based dose-effect curve (A), CalcuSyn based isobologram and CalcuSyn based median effect plot (C) for drug interactivity between (-)-*R,S*-dehydroemetine and proguanil. (-)-*R,S*-Dehydroemetine and proguanil (1:140) combination was found to be synergistic at IC_{50} (CI = 0.67), additive at IC_{75} (CI = 1.04) and antagonistic at IC_{90} (CI = 1.62).

After 72 hours of incubation, the (-)-*R,S*-dehydroemetine and atovaquone interaction was classified as synergistic (25:1 ratio, CI = 0.88-0.89) at all inhibitory levels analysed. The interaction between (-)-*R,S*-dehydroemetine and artemether (1:6.667 ratio, CI = 1.6-1.7), and between (-)-*R,S*-dehydroemetine and doxycycline (1:100 ratio, CI = 1.5), at IC_{50}, IC_{75} and IC_{90} levels of inhibition were classified as antagonism. For the (-)-*R,S*-dehydroemetine and proguanil (1:140) combination the IC_{50} level of inhibition was classified as synergism (CI = 0.67), the IC_{75} as nearly additive (CI = 1.04) and IC_{90} as antagonism (CI = 1.62).

4.5 Results for virtual screening of FDA approved drug library to identify compounds for drug-interaction analysis with (-)-*R,S*-dehydroemetine:

Most docking software used in the study were unable to correctly predict the activity of the ligand molecules on 80S ribosome structure 3J7A. Due to lack of reliability of the cryo-EM structure, a virtual screen of FDA approved 1376 drugs was not performed against 3J7A 80S ribosome.

Experiments conducted in this study to detect combinatorial partnership depicted synergistic activity between atovaquone and (-)-*R,S*-dehydroemetine. Atovaquone is known to bind on cytochrome bc1 causing its inhibition which leads to interruption of pyrimidine biosynthesis (Srivastava et al., 1999). A virtual screen of FDA approved 1376 drugs was performed against cytochrome bc1 (4PD4). FDA approved library of drugs was obtained from zinc database. This library of FDA approved drugs was docked on cytochrome bc1 (4PD4). The receptor PDB file (4PD4) was obtained from protein databank.

4.5.1 Virtual screening on cytochrome bc1:

Virtual screening of FDA approved library of drugs was performed on cytochrome bc1 (4PD4) using autodock vina. 1376 drugs were docked on the atovaquone binding site of cytochrome bc1 using autodock vina (Figure 4.5.2. – Figure 4.5.4)

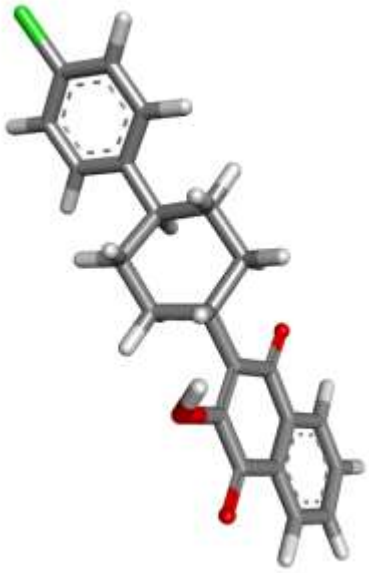

Figure 4.5.1: Atovaquone structure.

3D structure of atovaquone downloaded from Pubchem database visualised through Discovery Studio.

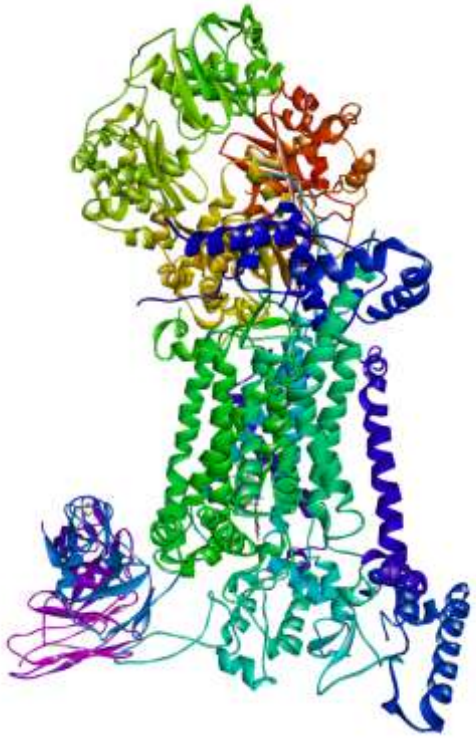

Figure 4.5.2: Pdb structure of cytochrome bc1.

X-ray crystallographic structure of cytochrome bc1 downloaded from protein data bank (4PD4) visualised through Discovery Studio.

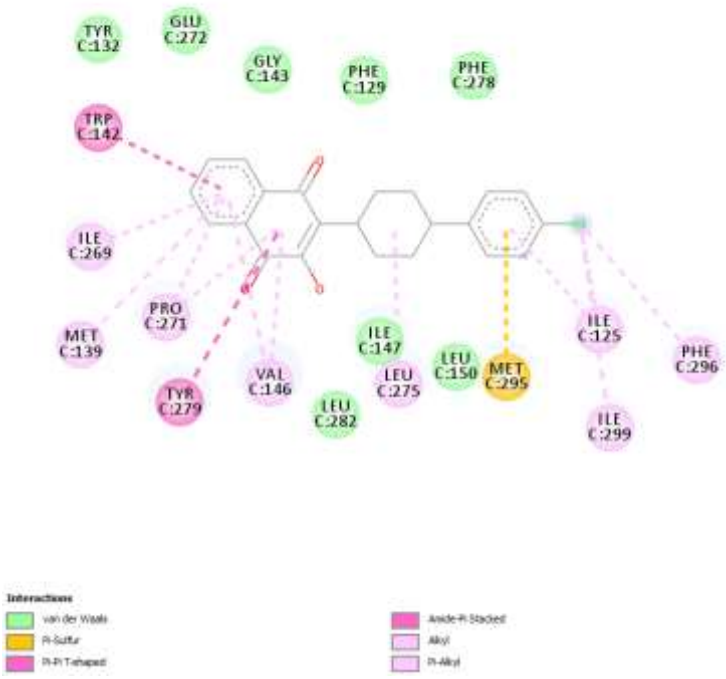

Figure 4.5.3: Atovaquone binding site residues.

Amino acid residues involved in the atovaquone binding site on cytochrome bc1 visualised through Discovery Studio

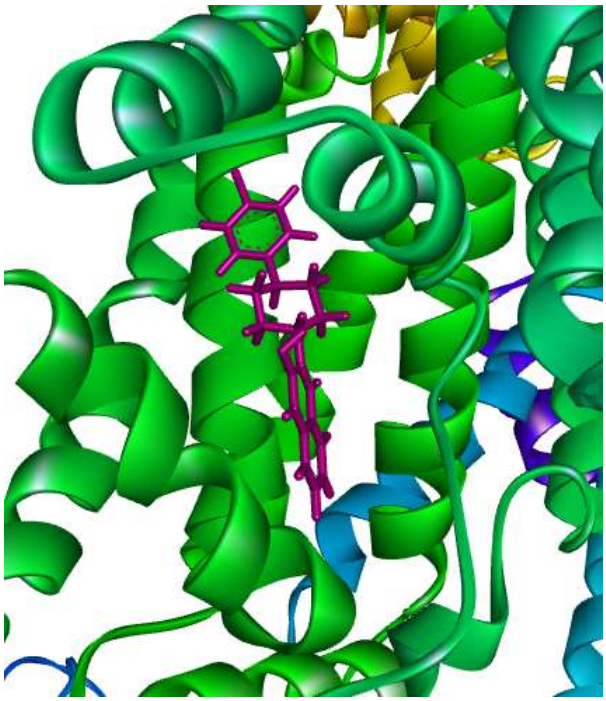

Figure 4.5.4: Atovaquone binding site.

Focussed view of atovaquone in the binding cavity on cytochrome bc1 visualised through Discovery Studio.

Receptor based Virtual Screening of FDA approved drugs library on cytochrome bc1 helped reduce the number of potential candidate compounds from 1376 to 80 by eliminating the compound which scored a binding affinity lower than atovaquone on cytochrome bc1. This was further reduced to 45 by filtering out anti-tumour, anti-viral and anti-psychotic drugs. Top 25 drugs are shown in Table 4.5.1. Five of the 25 drugs identified are already reported on zinc database (database of chemical molecules) to display activity against *P. falciparum.* These drugs could serve as potential leads for synergistic partners for emetine and (-)-*R,S*-dehydroemetine.

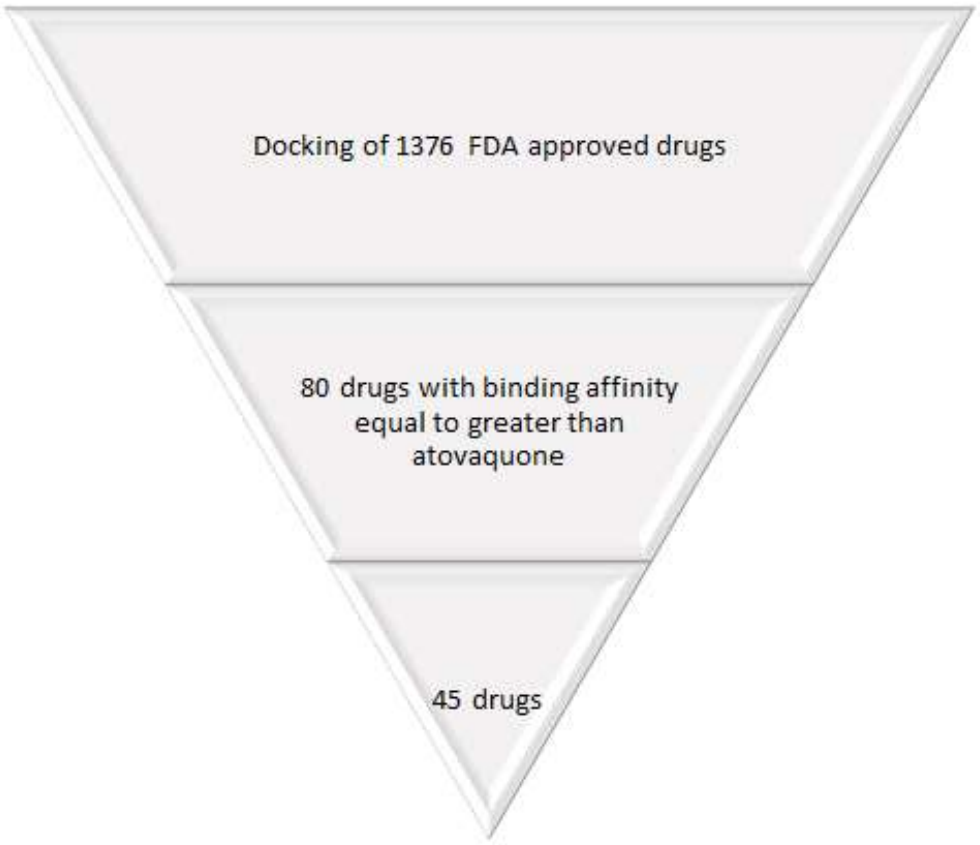

Figure 4.5.5: Filtering of FDA approved library of drugs.

Receptor based Virtual Screening of FDA approved drugs on cytochrome bc1 (4PD4) helped to narrow down the library from 1376 to 45 drugs as potential synergistic partners for emetine and (-)-*R,S*-dehydroemetine.

Table 4.5.1 FDA approved drugs identified through virtual screening.

Top 25 drugs screened on Cytochrome bc1

Generic	Activity against *Plasmodium falciparum*	Target/Current indications
Telmisartan		Angiotensin II Type 1 Receptor
Adapalene		Keratosis pilaris, Retinoic Acid Receptor Alpha
Dihydroergotamine mesylate	Yes	Migraines
Lomitapide		Lipid-lowering agent, Microsomal Triglyceride Transfer Protein Large Subunit
Lumacaftor		Experimental drug for the treatment of cystic fibrosis
Fexofenadine hydrochloride	Yes	Histamine H1 Receptor
Montelukast		Cysteinyl Leukotriene Receptor 1
Conivaptan Hydrochloride		Diuretic, Vasopressin V1a Receptor
Dutasteride		Steroid 5-alpha-reductase 1
Eltrombopag		Thrombopoietin Receptor
Rolapitant		Anti-emetic
Tolvaptan		Vasopressin V1a Receptor
Abiraterone		Cytochrome P450, steroidal antiandrogen
Sulindac		Non-steroidal anti-inflammatory drug
Vilazodone		Serotonin 1a (5-HT1a) Receptor
Ketoconazole	Yes	Cytochrome P450
Indacaterol		Beta-1 Adrenergic Receptor
CYPROHEPTADINE HYDROCHLORIDE	Yes	Serotonin 2a (5-HT2a) Receptor
Darifenacin hydrobromide		Muscarinic Acetylcholine Receptor M1
Ergotamine Tartrate		Serotonin 1d (5-HT1d) Receptor
Glimepiride		Sulfonylurea antidiabetic
Bromocriptine	Yes	Serotonin 1a (5-HT1a) Receptor
Trospium chloride		Muscarinic antagonist, overactive bladder
Dolasetron		Anti-emetic
Cinacalcet		Calcimimetic

List of top 25 drugs based on the virtual screening of FDA library of 1376 drugs on cytochrome bc1 (4PD4). Activity against *P. falciparum* for 5 of the 25 drugs identified in the screen has been reported on Zinc database of chemical molecules.

4.6 Conclusion

Accurate determination of parasite killing rate in response to treatment is crucial in development of drugs against *Plasmodium*, as chemotherapy still remains the most essential element in control of malaria. Speed of action of compounds on viability of parasites is difficult to measure through traditional techniques (Burrows et al., 2011). Emergence of parasite resistance against artemisinin-based combination therapy could jeopardise the recent

advances made against the disease. It is important to identify new drugs with rapid parasite killing kinetics early in the drug development process. (-)-*R,S*-Dehydroemetine was found to be potent against the multi-drug resistant K1 strain of *P. falciparum* with an IC_{50} of 69.58 $\pm$ 2.62 nM. It displayed gametocidal activity against male and females gametes, and on 3D7A, Dd2 and W2 strains showed no strain specific cross-resistance. (-)-*S,S*-Dehydroisoemetine, on the other hand displayed an IC_{50} value of 1.85 $\pm$ 0.2 µM against the multi-drug resistant K1 strain of *P. falciparum.* It did not inhibit the male and female gametes. As it could not reach 50% inhibitory values against Dd2 and W2 strains, it was found to display cross-resistance. Stage specificity experiment showed both diastereomers display more activity against the trophozoite stage of the parasite. Cell cytotoxicity experiments showed a low selectivity index against HepG2 liver cancer cell lines (SI= ~3 for (-)-*R,S*-dehydroemetine and SI= ~1 for (-)-*S,S*-dehydroisoemetine). Emetine shows good synergy with atovaquone (Matthews *et al*, 2013). Based on the same principle, drug interaction experiments were conducted between the more potent diastereomer, (-)-*R,S*-dehydroemetine and four known antimalarials atovaquone, proguanil, artemether and doxycycline. Artemether (CI= 1.6) and doxycycline (CI= 1.55) were found to be antagonistic while proguanil displayed mild synergy at IC_{50} (CI= 0.67) and nearly additive (CI= 1.04) to antagonistic (CI= 1.64) at IC_{75} and IC_{90}, respectively. Atovaquone was found to display mild synergy (CI = 0.88) with (-)-*R,S*-dehydroemetine. Following the experimental findings, a virtual screen of FDA approved library of drugs was conducted on atovaquone binding site and 45 drugs were identified which could potentially display synergy with emetine and (-)-*R,S*-dehydroemetine.

Chapter 5 Cellular basis for emetine and dehydroemetine cardiotoxicity: role of ATP, mitochondria and hERG K^+ channels

5.1 Introduction:

Blood flow to a target site and the drug's diffusion characteristics determine adequate delivery of the drug to the site. The pharmacological effect of a drug is dictated by its biochemical interactions in the body (Magee et al., 2007). Drugs could elicit their effect by binding to a receptor, such as atovaquone, or by changing the physical and chemical properties of the body like laxatives or antacids. It is important to know the mechanism of action of a drug. Microscopy, biochemical assays or computational methods could be used to identify a drug's mechanism of action (Cushnie et al., 2016). Knowing how a drug produces its effect could help guide dosing, anticipate clinical safety, determine target susceptibility, develop a new drug, formulate combination therapy or reposition it for use in other diseases (Schenone et al., 2013) (Chang et al., 2017). There are many drugs with known mechanism of action, however there many others which are widely used but the mechanism of action is unknown.

Cardiovascular side-effects were observed following treatment of amoebiasis with emetine which included ECG changes such as T-wave inversion, prolongation of QT interval and to some degree, increased width of QRS complex and PR interval. Hypotension, tachycardia and precordial pain were also observed (Yang and Dubick, 1980). Stoppage of treatment resulted in complete recovery of cardiovascular functions. Cardiac microscopic examination revealed separation of muscle fibres and destruction of myocardial fibres but absence of inflammatory cells led to the interpretation that myocarditis is toxic rather than inflammatory in origin. In a study conducted on thirty two patients treated with subcutaneous injections of emetine dihydrochloride in a dose range of 1 – 2 mg/kg/day, pain was noted at the injection site along with ECG abnormalities, myalgia, muscle weakness and increased levels of serum creatinine phosphatase (Mastrangelo et al., 1973).

A synthetic analogue of emetine, dehydroemetine was introduced in 1959 which is less emetic, can be given orally as resinate and was found to be comparatively safer than emetine when given parenterally in similar doses, with similar electrocardiographic changes but less

marked and of shorter duration (Dempsey and Salem, 1966). In a study conducted on 58 African adults with amoebic liver abscess (Powell et al., 1965), it was found that treatment with 80 to 120 mg daily of dehydroemetine plus chloroquine for 10 days followed by similar course for 6 days after 14 days interval was as effective as 65 mg daily of emetine plus chloroquine in a similar regimen.

Experimental results have also shown that changes observed in heart conduction, contractility, automaticity and ECG abnormalities by emetine and dehydroemetine could be due to their effect on membrane permeability to Na^+, K^+ and Ca^{2+} ions (Yang and Dubick, 1980). In another study, reversal of effects were observed by addition of ATP and NADH indicating nicotinamide adenine dinucleotide mediated (NAD) enzymatic oxidation of substrates to be potentially affected (Watkins and Guess, 1968).

Cell membranes function as a diffusion barrier to ion movements and are made of lipid bilayers with embedded proteins. A concentration gradient is established across the membrane by active pumping of ions by transmembrane ion transporter proteins. Movement of ions down the concentration gradient across the membrane through ion channels leads to a voltage difference between the two sides of the membrane. Sodium (Na^+), potassium (K^+), calcium (Ca^{++}) and chloride (Cl^-) are the important ions regulating the action potential (Fry and Jabr, 2010). In this study, the possibility of inhibition of glycolysis and mitochondria (sources of ATP), along with the effect of emetine and dehydroemetine on K^+ and Ca^{++} ion channels were analysed.

5.1.1 **Glycolysis:**

Glycolysis is a 10 step oxygen-independent metabolic pathway, with each step characterised by a different enzyme. It occurs in the cytosol and produces a net gain of two ATP molecules by anaerobic conversion of glucose to pyruvate while generating intermediate metabolites in the process which are used in other metabolic pathways (Li et al., 2015). The pathway has a preparatory or investment phase where there is consumption of ATP and the second phase is the ‘pay off’ phase where there is production of ATP. There are 3 rate-limiting steps in glycolysis. The first step is a rate-limiting step where glucose-6-phosphate (G6P) is generated by phosphorylation of glucose by hexokinase. It helps to transport glucose inside the cells by

converting it to G6P which cannot escape out as the cell membrane is impervious to it. The step catalyzed by phosphofructokinase-1 (PFK-1) for hydrolysis of ATP is also a rate-limiting step and is irreversible (Boscá and Corredor, 1984). Pyruvate kinase is the third regulatory enzyme which catalyses the final step which results in the formation of ATP and pyruvate. NADH is oxidised back to NAD^+ either aerobically or anaerobically. Lactic acid fermentation or ethanol fermentation converts pyruvate to lactate or ethanol respectively and NADH to NAD^+ in anoxic or hypoxic conditions (Berg et al., 2002).

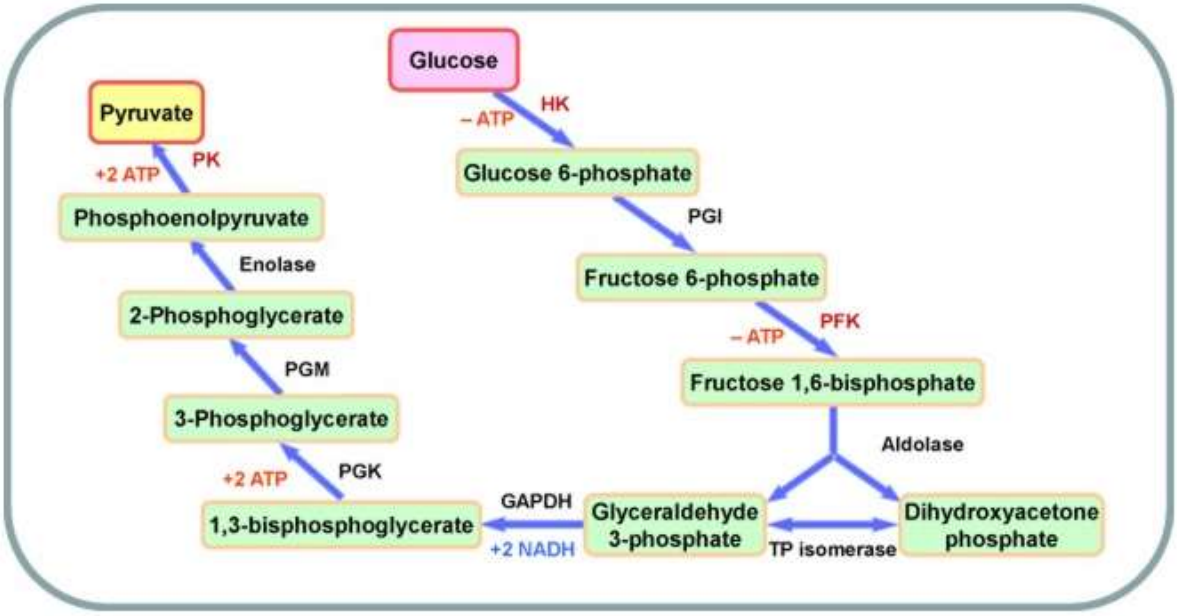

Figure 5.1.1 Schematic representation of the glycolysis (Li et al., 2015).

The enzymes (hexokinase (HK), phosphofructokinase (PFK) and pyruvate kinase (PK)) catalysing the rate-limiting steps are depicted in red. Glycolysis results in the net gain of 2 ATP molecules.

Emetine has been reported to inhibit glycolysis as addition of fructose-1,6-bisphosphate, a glycolysis intermediate, was found to reduce the adverse effects of emetine on isolated, perfused rat hearts (Pan and Combs, 2003). Studies have demonstrated high energy needs of the cells, such as muscle contraction, are met by oxidative metabolism whereas cellular membrane functions such as transmembrane electrical activity and ionic pumps are maintained through glycolysis derived ATP (Parker and Hoffman, 1967) (Paul, 1983) (MacLeod and Daniel, 1965) (Hasin and Barry, 1984). Disturbances in intracellular ionic concentrations and osmotic balance of the cell are observed when glycolysis is inhibited (Higgins et al., 1981) (Gebhard et al., 1977) (Bricknell et al., 1981). Rapidly multiplying

parasite cells could possibly have a higher dependency on glycolysis as observed in cancer cells exhibiting the 'Warburg effect', a phenomenon where glycolysis is up-regulated (Liberti and Locasale, 2016).

5.1.2 **hERG potassium channel:**

The human *Ether- à -go-go*-Related Gene (hERG) encodes the pore-forming alpha subunit of potassium ion channel of the rapidly activating delayed rectifier potassium (K^+) channel (I_{Kr}). The repolarising current in the cardiac action potential is mediated by the hERG channel (Lamothe et al., 2016). The cardiac 'rapid' delayed rectifier current is responsible for the movement of potassium (K^+) ions out of cardiac cells and bringing it back to resting membrane potential during repolarisation. Warmke and Ganetzky from University of Wisconsin-Madison were the first to describe the hERG gene which is a homolog of *Drosophila* fly's *Ether- à -go-go* gene. Flies with mutation in *Ether- à -go-go* gene would begin to shake their legs when anaesthetised with ether, resembling dancing at a popular nightclub of the time 'Whisky A Go Go' in California, leading to the gene being named *Ether- à -go-go* (Warmke and Ganetzky, 1994). The hERG potassium channel is made of 4 alpha subunits aligned to form the pore of the channel traversing through the plasma membrane. Inhibition of hERG channel by genetic mutations or by drugs could lead to shortening or prolongation of QT interval predisposing individuals to fatal ventricular arrhythmias such as torsades de pointes (Hedley et al., 2009) (Shah and Li, 2018). Decrease in serum potassium levels affects the hERG function. Many drugs which lengthen the QT interval, interact with hERG potassium channel (Milnes et al., 2003). Prolongation of QT interval is observed in unstable angina, ischemic cardiac disease and myocardial infarction thus making the extent of QT interval prolongation a strong predictor of sudden cardiac death (Shawl et al., 1990). The United States Food and Drug administration (FDA) recommends preclinical hERG studies during drug development to test the cardiac safety profile (Fermini et al., 2016).

5.1.3 **Role of mitochondria:**

The engulfment of an α-proteobacterium by a precursor of the modern eukaryotic cell resulted in the formation of mitochondria (Friedman and Nunnari, 2014). Mitochondria also

known as the powerhouse of the cell is a double-membrane bound organelle in most eukaryotic cells (Perier and Vila, 2012). Carl Benda in 1898 coined the term mitochondria (Mazzarello, 1999). In 1946, Albert Claude was able to isolate mitochondria through tissue fractionation and concluded the enzymes necessary for respiratory chain were from mitochondria. In 1948, Eugene Kennedy and Albert Lehninger concluded oxidative phosphorylation in eukaryotes occurred in the mitochondria (Ernster and Schatz, 1981). It is absent in certain cells such as mature mammalian red blood cells. Mitochondria supplies ATP to meet most of the energy needs of the cell and is involved in signalling, cellular differentiation and cell death (McBride et al., 2006). The ATP production occurs aerobically and requires the presence of oxygen. It produces more ATP than glycolysis. Mitochondria have its own genome which shows similarity to bacterial genome giving rise to the hypothesis of an endosymbiotic origin about 1.7 to 2 billion years ago (Gray, 2012). It replicates through binary division. Unlike the nuclear genes, the mitochondrial genes are inherited only from the egg cell. Mitochondria also have ribosomes (Martin et al., 2015). Mitochondria have five distinct parts which are an outer and inner phospholipid membrane with embedded proteins, inter-membrane space, cristae and the matrix. Mitochondria-associated ER-membrane (MAM) formed with association with endoplasmic reticulum plays an important role in transfer of lipids as well as calcium signalling (Hayashi et al., 2009). Mitochondria play an important role in regulation of cell proliferation through ATP production. Cell cycle is arrested when oxidative phosphorylation is inhibited (Porporato et al., 2018). Proteins from the inter-membrane space leak out in the cytosol up on disruption of the outer membrane which could result in cell death. The inner mitochondrial membrane contains proteins which perform the redox reactions in oxidative phosphorylation. The enzymes of the electron transport chain leads to a membrane potential across the inner membrane (Jastroch et al., 2010). Matrix of the mitochondria has enzymes for citric acid cycle and, oxidation of pyruvate and fatty acids. Acetyl CoA is reduced to carbon dioxide and 3 molecules of NADH, one molecule of $FADH_2$ (reduced cofactors for electron transport chain) and GTP (readily converted to ATP) are produced during the citric acid cycle. Matrix also contains the mitochondrial ribosomes, mitochondrial DNA, 22 tRNA and 2 rRNA (Anderson et al., 1981). Mitochondria play a role in Ca^{++} signalling pathway as well through MAM. Calcium can be stored in mitochondria transiently making mitochondria a cytosolic buffer for Ca^{++} (Santulli et al., 2015). Low affinity calcium channels are present on the outer membrane of the mitochondria but an efficient transmission of Ca^{++} occurs between the ER

and mitochondria MAM contact points. Transient depolarisation in mitochondrial membrane is caused by mild influx of calcium from cytosol into the matrix. ATP production is stimulated by the uptake of calcium by MAM and this provides energy to SERCA to move Ca^{++} in the ER. The MAM Ca^{++} uptake is operated in a certain window threshold which if crossed collapses the mitochondrial membrane potential essential for metabolism and stimulates apoptosis through intrinsic pathway (Rizzuto et al., 2009). Decrease in the ER Ca^{++} filling decreases the efflux of Ca^{++} in mitochondria and prevents the mitochondrial membrane potential collapse (Rizzuto et al., 2009).

Mitochondrial Ca uniporter (MCU) is a calcium channel situated on the inner mitochondrial membrane through which Ca^{++} enters the mitochondria (De Stefani et al., 2011). Influx of Calcium in the mitochondria activates many mitochondrial enzymes to increase the supply of ATP for increased demand during contraction. When compared to the Ca^{++} released from SR, only a small amount of calcium enters the mitochondria suggesting mitochondria does not play a major role in removing calcium from the cytoplasm (Lu et al., 2013) (Negretti et al., 1993).

In this chapter, to determine probable causes for the observed cardiotoxicity and a possible multi-modal mechanism of action, the effect of emetine and (-)-*R,S*-dehydroemetine was evaluated on ATP proliferation, mitochondrial membrane potential disruption and hERG K^+ channel.

5.2 Methods:

5.2.1 ATP bioluminescence assay (Luciferase assay) for detection of changes in ATP concentration:

ATP, which is generated by cellular respiration, is the primary source of energy in all organisms. Targeted luciferase probes could be used to measure ATP concentration *via* luminescence techniques. Light is emitted (emission ~560 nm at pH 7.8) when the substrate luciferin is oxidised to oxyluciferin by the protein luciferase (Morciano et al., 2017). ATP is required as a source of energy for this reaction. Emitted light is proportional to the concentration of ATP which can be used to assess the cell viability. ViaLight™ plus kit

(Lonza) was used to perform the experiments. Assay kit contained cell lysis reagent to extract ATP from the cells, ATP monitoring reagent plus (AMR plus) (reconstituted by adding assay buffer to the vial containing lyophilised ATP monitoring reagent pellet). Following reconstitution, unused AMR plus was stored at -20ºC. The experiment was performed at room temperature.

Synchronised culture of *P. falciparum* K1 strain at trophozoite stage incubated at 2.5% haematocrit was used for the experiment. Positive control was devoid of the test compounds and contained only complete media. Experiment was set on a 96 well plate with 2-fold serial dilutions of emetine and (-)-*R,S*-dehydroemetine from 0.5 µM to 2 µM with 100 µL in each well. The plate was incubated for two hours at 37ºC. Post-incubation, the culture plate was allowed to cool to room temperature and 50 µL of cell lysis reagent was added to control and test wells. After 10 minutes of incubation at room temperature, 100 µL of AMR plus was added to each well and further incubated for 5 minutes. The experiment was read using a microplate luminometer with luminescence set at 560 nm. Data was analysed using Microsoft excel.

5.2.2 **Staining with rhodamine123 and draq5 for fluorescence microscopy:**

Rhodamine123 and draq5 were used to observe the effect of emetine and its two synthetic analogues on mitochondrial membrane potential. Rhodamine123 is a mitochondrial specific dye which emits in FITC channel on flow-cytometry whereas draq5 stains the DNA and emits in APC-Cy7-A channel. The two dyes were chosen to perform the experiment as there is very minimal overlap in their emission signals. Synchronised cultures of *P. falciparum* K1 strain at trophozoite stage was incubated with 1 ml of 200 nM Rhodamine123 for 1 hour, followed by a further incubation with 100 µl of 10 µM Draq5 for 20 mins. Smear was prepared after the incubation and slides were immediately viewed under fluorescence microscope at 100x magnification with oil emersion to visualise localisation of the dyes inside the parasite.

5.2.3 **Staining with rhodamine123 and draq5 for flow-cytometry to detect mitochondrial membrane potential disruption:**

To test the effect of emetine and its analogues on mitochondria, synchronised cultures of *P. falciparum* K1 strain at trophozoite stage were incubated at 2.5% haematocrit (in a 96 well plate format, 200 µl final well volume) for 2 hours with IC_{50} concentrations of atovaquone, emetine hydrochloride and *(-)-R,S*-dehydroemetine. Atovaquone, a known mitochondrial inhibitor was used as a control. Compounds were then washed away by centrifuging the cultures and a pellet was prepared for each drug concentration. Pellets were then incubated with 1 ml of 200 nM rhodamine123 for 1 hour, followed by a further incubation with 100 µl of 5 µM of draq5 for 20 mins. After a wash with PBS, the experiment was read using a flow-cytometer on the FITC channel. Loss of mitochondrial membrane potential was indicated by a decrease in fluorescent intensity.

5.2.4 **hERG Channel Inhibition (IC_{50} Determination) assay:**

hERG channel inhibition assay was performed by Cyprotex, UK in the presence of the author. Figure 5.2.1 shows a schematic representation of the hERG channel. Chinese Hamster Ovary cells expressing the hERG potassium channel were dispensed into 384-well planar arrays and hERG tail-currents was measured by whole-cell voltage-clamping. Emetine, (-)-*R,S*-dehydroemetine and (-)-*S,S*-dehydroisoemetine in a range of concentrations were then added to the cells and a second recording of the hERG current was made. The percentage change in hERG current was measured and used to calculate an IC_{50} value.

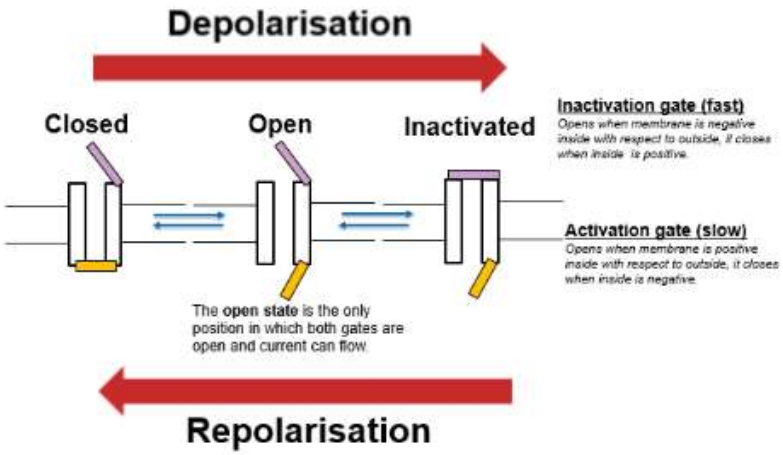

Figure 5.2.1 Schematic representation of the hERG channel.

The hERG channel mediates the repolarising current in the cardiac action potential. The cardiac 'rapid' delayed rectifier current is responsible for the movement of potassium (K^+) ions out of cardiac cells during repolarisation. Adapted from Cyprotex, UK

The assay was performed to test emetine, *(-)-R,S*-dehydroemetine and *(-)-S,S*-dehydroisoemetine's potential to inhibit the hERG channel. 100 µL in 20 mM concentration of emetine, *(-)-R,S*-dehydroemetine and *(-)-S,S*-dehydroisoemetine in DMSO was provided to Cyprotex. The experiments were performed on an IonWorks™ automated patch clamp instrument (Molecular Devices LLC), which simultaneously performs electrophysiology measurements for 48 single cells in a specialised 384-well plate (PatchPlate™). All buffers, cell suspensions and drug compound solutions were at room temperature.

Chinese hamster ovary (CHO) cells stably transfected with hERG (cell-line obtained from Cytomyx, UK) were used for the experiment. A single-cell suspension was prepared in extracellular solution (Dulbecco's phosphate buffered saline with calcium and magnesium pH 7.2) and aliquots were added automatically to each well of a PatchPlate™. Vacuum was applied beneath the plate to form an electrical seal after positioning over a small hole at the bottom of each well. The vacuum was applied through a single compartment common to all wells which were filled with intracellular solution (buffered to pH 7.2 with HEPES). The resistance of each seal was measured via a common ground-electrode in the intracellular compartment and individual electrodes were placed into each of the upper wells.

Amphotericin B was used as a perforating agent and circulated underneath the PatchPlate™ to gain electrical access to the cell. The pre-compound hERG current was then measured.

An electrode was positioned in the extracellular compartment and a holding potential of -80 mV was applied for 15 sec. The hERG channels were activated by applying a depolarising step to +40 mV for 5 sec and then clamped at -50 mV for 4 sec to elicit the hERG tail current, before returning to -80 mV for 0.3 sec.

5.3 Results:

5.3.1 ATP proliferation assay (luciferase assay) for detection of changes in ATP concentration:

Experiments were performed using the ATP proliferation assay (n=3, standard error represented by error bars on Figure 5.3.1) with each concentration of emetine and (-)-*R,S*-dehydroemetine (0.5, 1 and 2 µM for both compounds) tested in triplicates. Emetine and (-)-*R,S*-dehydroemetine showed slight decrease in ATP concentration. Less than 10% decrease was observed at 0.5 µM and approximately 15% decrease was observed with higher concentrations of 1 µM and 2 µM for both emetine and (-)-*R,S*-dehydroemetine.

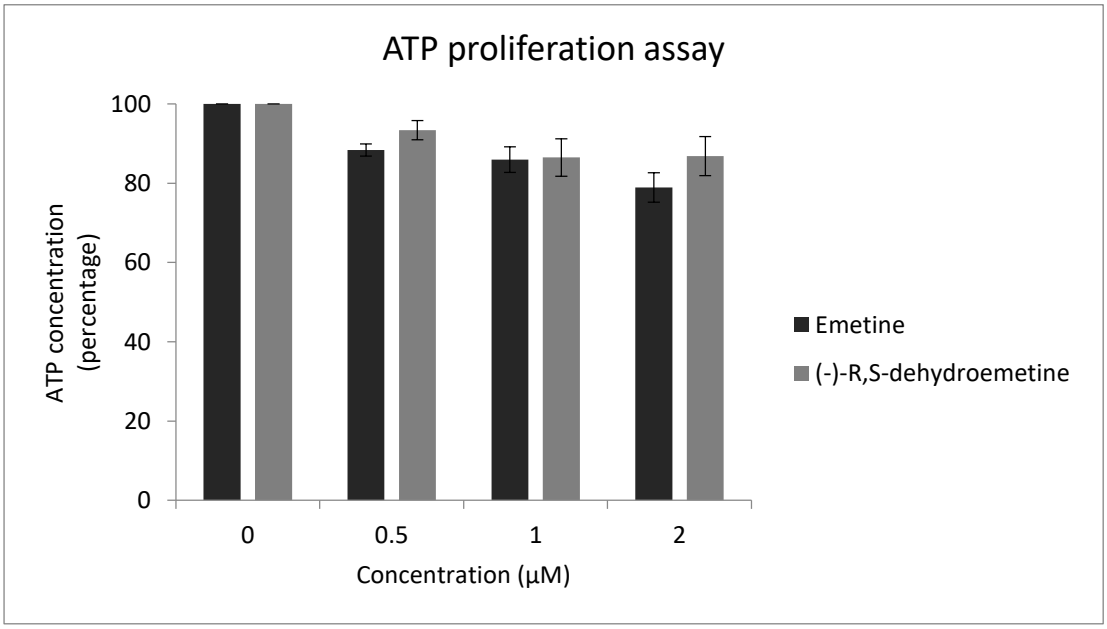

Figure 5.3.1 ATP proliferation assay for detection of changes in ATP concentration

Emetine and *(-)-R,S*-dehydroemetine tested at 0.5 µM, 1 µM and 2 µM concentration. Following 1-hour incubation, ~15% decrease in ATP concentration was observed with emetine and (-)-*R,S*-dehydroemetine. Error bars denote the standard error observed in experiments performed thrice in triplicates.

5.3.2 **Staining with rhodamine123 and draq5 for fluorescence microscopy and flowcytometry for measurement of mitochondrial membrane potential:**

Changes in mitochondrial membrane potential was measured using rhodamine123, a cationic fluorescent dye (Tanabe, 1990). Fluorescence microscopy was used to visualise localisation of rhodamine123 within the cytoplasm of the parasites (Figure 5.3.2). Draq5 is a far-red fluorescent DNA dye which is cell permeable and was used to identify the parasites. SYBR green was not preferred for this experiment as it emits in the same channel as rhodamine123 and would result in the overlap of emission signals.

Changes in mitochondrial membrane potential can be observed using rhodamine123 (excitation wavelength: 511 nm and emission wavelength: 534 nm), a membrane permeable fluorescent dye which accumulates by electrostatic attraction in the mitochondria because of its negative transmembrane potential. A change in the dye's concentration in the mitochondria is caused by a depolarisation event and can be visualised as a shift in fluorescent intensity of rhodamine123 (Gaur et al., 2016). Draq5, (excitation wavelength: 647 nm and emission wavelength: >665 nm) a DNA dye was used to distinguish the parasites on flow-cytometry in APC-Cy7-A channel. Atovaquone, a known mitochondrial inhibitor was used as a control. A decrease in fluorescent intensity measured in FITC-A channel indicates a loss of mitochondrial membrane potential. A shift in fluorescent intensity was observed after treatment with all three compounds. The compounds were tested at IC_{50} and 10 x IC_{50} values. Emetine and *(-)-R,S*-dehydroemetine showed a shift in fluorescent intensity of rhodamine123 in a direction similar to atovaquone indicating a possible mitochondrial effect. Atovaquone produced a ~40 to 43% change in mean fluorescent intensity, emetine produced a change of approximately 30 to 35% in a direction similar to atovaquone and (-)-*R,S*-dehydroemetine produced a change of approximately 25 to 30% in a direction similar to atovaquone (Figure 5.3.3).

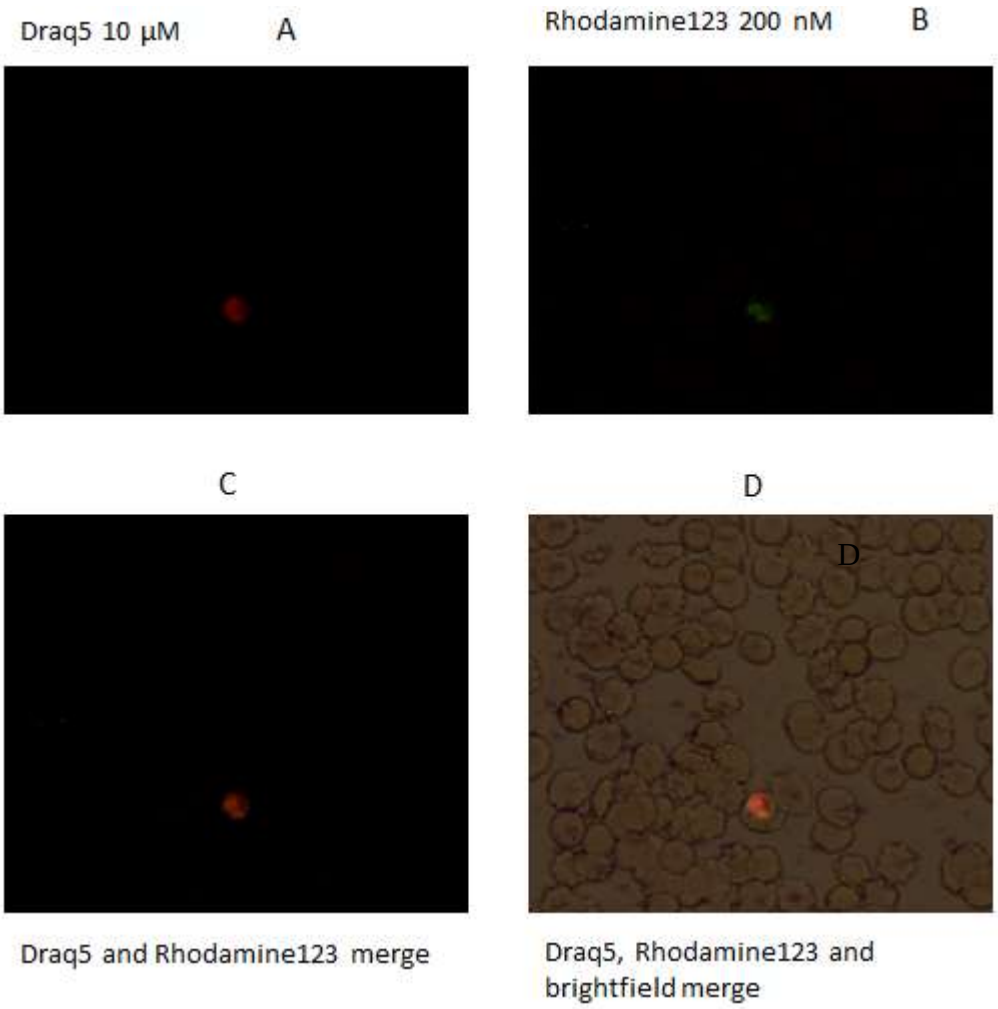

Figure 5.3.2 Staining with rhodamine123 and draq5 for fluorescence microscopy and the merge with brightfield.

P. falciparum K1 strain trophozoites stained with (A) Draq5 10 µM, (B) Rhodamine123 200 nM, (C) Draq5 and Rhodamine merge and (D) Draq5, rhodamine123 and brightfield merge. Visualised under fluorescence microscope at 100x magnification.

Rhodamine and Draq5	Parasitemia	FITC-A mean	FITC-A mean (range gate)	Change in fluorescense intensity
Blood no dye	0.00%	N/A	0	N/A
Uninfected blood	0.16%	280	0	-94.21%
Infected blood w/o drugs	1.70%	4839	6026	0
Atovaquone (IC50)	1.69%	2809	3705	-41.95%
Atovaquone (IC50 x 10)	1.66%	2750	3821	-43.17%
Emetine (IC50)	1.73%	3333	4491	-31.12%
Emetine (IC50 x 10)	1.72%	3139	4301	-35.13%
(-)-*R,S*-dehydroemetine (IC50)	1.78%	3544	4894	-26.76%
(-)-*R,S*-dehydroemetine (IC50 x 10)	1.67%	3243	4390	-32.98%

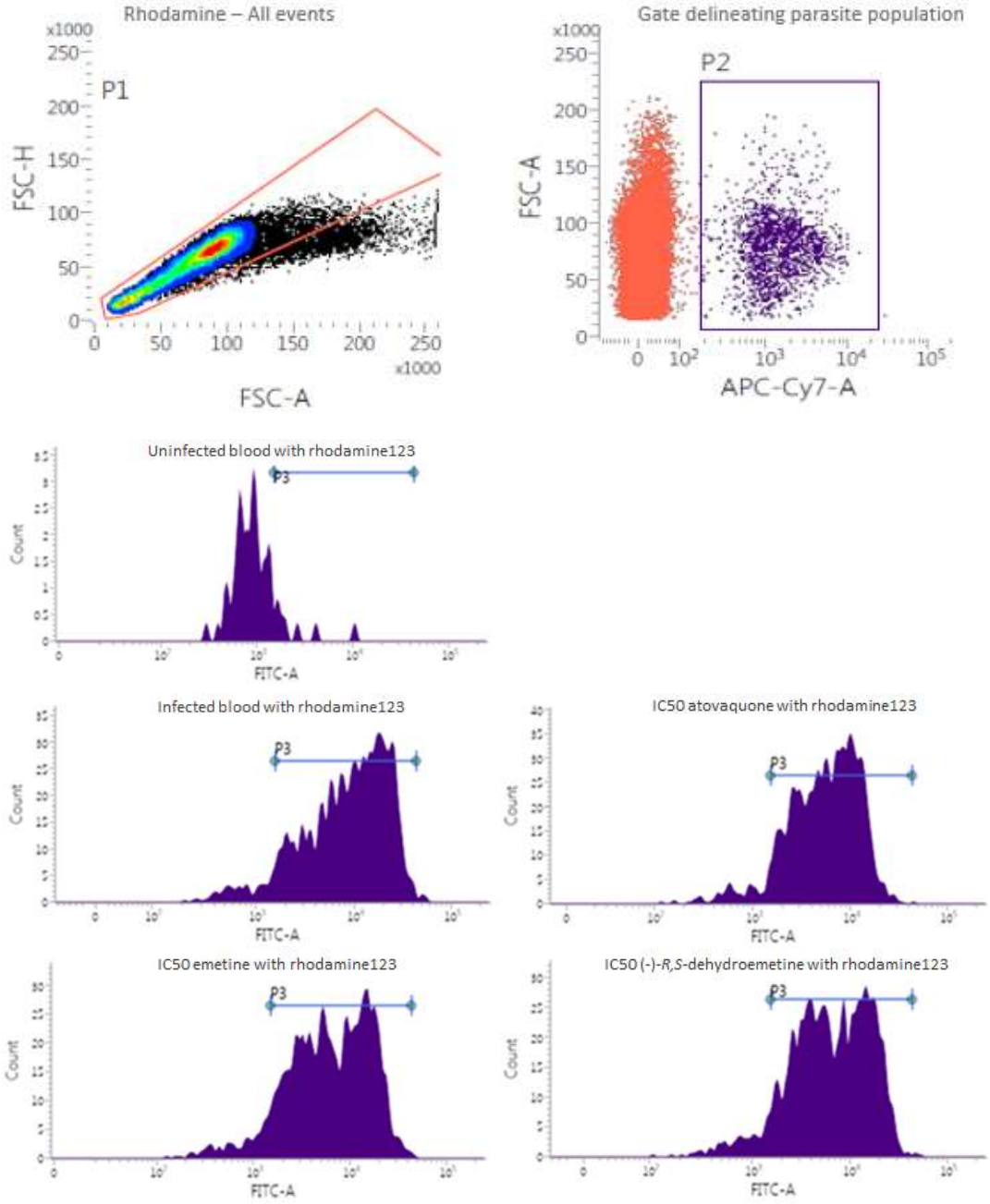

Figure 5.3.3 Disruption of mitochondrial membrane potential

Changes in mitochondrial membrane potential observed on treatment with IC_{50} of atovaquone, emetine and (-)-*R,S*-dehydroemetine. (A) Changes in fluorescent intensity on application of drugs, (B) Gating for the experiment, (C) Graphical representation of change in fluorescent intensity.

5.3.3 **hERG Channel Inhibition (IC_{50} Determination) assay:**

Compound dilutions were prepared by diluting a DMSO solution (default 10 mM) of the test compound using a factor 5 dilution scheme into DMSO, followed by dilution into extracellular buffer such that the final concentrations tested were typically 0.008, 0.04, 0.2, 1, 5, 25 µM (final DMSO concentration 0.25 %). The IonWorks™ instrument was used to automatically add (-)-*R,S*-dehydroemetine and (-)-*S,S*-dehydroisoemetine dilutions to the upper wells of the PatchPlate™. The compounds were left in contact with the cells for 300 sec before recording currents using the same voltage-step protocol as in the pre-compound scan. Quinidine, an established hERG inhibitor, was included as a positive control, and vehicle control (0.25 % DMSO) as negative control. Each concentration was tested in 4 replicate wells on the PatchPlate™ (maximum of 24 data points). It was ensured only acceptable cells which maintain a seal resistance of greater than 50 MOhm and a pre-compound current of at least 0.1 nA, were used to assess hERG inhibition by applying filters to ensure cell stability between pre- and post-compound measurements.

Data Analysis:

For each replicate the hERG response was calculated using the following equation:

$$\%\ \text{hERG response} = \frac{\text{Post} - \text{compound current (nA)}}{\text{Pre} - \text{compound current (nA)}}\ \text{x}\ 100$$

The % hERG response was plotted against concentration for the test compound and, where concentration-dependent inhibition was observed, and an IC_{50} value was calculated (Table 5.3.1). (-)-*R,S*-Dehydroemetine was found to have an IC_{50} value of 19.3 µM for hERG channel whereas (-)-*S,S*-dehydroisoemetine was found to have an IC_{50} value of 2.99 µM. The IC_{50} of quinidine which was used as a positive control is 1.99 µM. Thus, it was found that with a selectivity index (SI) of over 285, (-)-*R,S*-dehydroemetine is not a hERG channel inhibitor, but (-)-*S,S*-dehydroisoemetine is a potent inhibitor (selectivity index = 2).

Table 5.3.1 hERG channel inhibition assay results for (-)-*R,S*-dehydroemetine and (-)-*S,S*-dehydroisoemetine

Cyprotex	hERG channel inhibition (IC_{50} determination)							
Compounds	% Mean inhibition							
	0 µM	0.016 µM	0.08 µM	0.4 µM	2 µM	10 µM	50 µM	IC_{50} (µM)
(-)-R,S-dehydroemetine	0	7.79	6.34	12.7	7.21	39.4	61.4	19.3
(-)-S,S-dehydroisoemetine	0	8.13	4.61	9.33	36	70.7	96.9	2.99

Effect of *(-)-R,S*-dehydroemetine and *(-)-S,S*-dehydroisoemetine determined using hERG channel inhibition assay. Each value is a mean ± SEM of triplicate values.

5.4 Conclusion:

Emetine and dehydroemetine have been known to produce cardiotoxic side-effects during anti-amoebic therapy. In a bid to resolve the cellular basis of cardiotoxicity and to identify other mechanisms of action besides the inhibition of protein translation, emetine and (-)-*R,S*-dehydroemetine were tested for their effect on ATP proliferation and mitochondrial membrane potential disruption. Emetine has previously been identified as a non-inhibitor of hERG K^+ channel in previous work conducted at the University of Salford. In this study, (-)-*R,S*-dehydroemetine and (-)-*S,S*-dehydroisoemetine were evaluated for their effect on hERG K^+ channel. It was observed that both emetine and (-)-*R,S*-dehydroemetine produce an approximate 10 to 15% reduction in ATP concentration in RBCs infected with multi-drug resistant K1 strain of *P. falciparum* following one hour exposure at 10 to 40 times IC_{50} values in 2 fold serial dilutions. Both emetine and (-)-*R,S*-dehydroemetine also produced a change in rhodamine123 fluorescent intensity in RBCs infected with multi-drug resistant K1 strain of *P. falciparum* following a 2 hour exposure with IC_{50} and 10 x IC_{50} values in a manner similar to atovaquone (a known mitochondrial inhibitor). This is suggestive of a disruption in mitochondrial membrane potential. (-)-*R,S*-Dehydroemetine and (-)-*S,S*-dehydroisoemetine were tested to determine their activity on hERG K^+ channel. (-)-*R,S*-Dehydroemetine was found to be a non-inhibitor (SI < 285) whereas its isomer (-)-*S,S*-dehydroisoemetine was found to inhibit hERG K^+ channel (SI = ~2). The two diastereomers not only differ in their activity against the multi-drug resistant K1 strain of *P. falciparum* but also display

differential potencies against hERG K^+ channel. This suggests the (R) configuration at C-1´ is important for emetine and dehydroemetine's biological activity.

Chapter 6 Cellular basis of emetine and dehydroemetine cardiotoxicity: a role for dysregulated Ca handling and contractility

6.1 Introduction

Heart contraction is dependent on cell contraction which is dependent on a cyclical rise and fall of intracellular calcium on each heartbeat. Levels of intracellular calcium are much lower than that in extracellular space. Intracellular calcium levels in cardiomyocytes increase from ~100 nM to ~1 µM during systole on each heart beat (Marks, 2003). Most of the calcium required for contraction is released from the sarcoplasmic reticulum (SR); an intracellular calcium store. SR Ca is released during a process known as cardiac cellular excitation-contraction coupling (ECC).

ECC is initiated when a cardiac cellular action potential depolarises the sarcolemma which activates the voltage-gated L-type Ca channels. The L-type Ca channels are located on the surface membrane and transverse tubules. Activation allows a small influx of calcium which results in the opening of Ca release channels (ryanodine receptors (RyR)) on the sarcoplasmic reticulum (SR) membrane. This causes release of a large amount of Ca^{++} from the SR in a process called calcium-induced calcium release (CICR) (Eisner et al., 2017). Intracellular Ca levels are then sufficient to allow the binding of Ca^{++} to troponin and so produce myofilament sliding. Cell shortening occurs and the pressure generated leads to systole with ventricles ejecting the blood (Allen and Kurihara, 1980).

For diastole, the cell must relax requiring removal of systolic Ca and so restoration of diastolic Ca levels. This occurs by (1) closure of RyRs post-systole and so cessation of Ca release and (2) the active removal of Ca from the cytosol. The latter is primarily achieved by two proteins (A) the SR Ca-ATPase (SERCA), which pumps Ca back into the ST and (B) the sodium-calcium exchanger (NCX) which takes Ca outside the cell. NCX exchanges 3 Na^{+} ions for one Ca^{++} ion (Greensmith et al., 2014) so is electrogenic. During each Ca^{++} transient only 50% of SR Ca^{++} is released (Picht et al., 2011) and it remains localised without affecting other release sites (Cheng et al., 1993). Surface membrane depolarisation results in activation of more L-type Ca channels leading to a more uniform Ca^{++} release (Cannell et al., 1995).

The specialised signalling nexus which initiates the contraction is called 'cardiac dyad' which is formed by L-type Ca^{++} channel clusters on the sarcolemma in close apposition with RyR clusters on SR membrane (Eisner et al., 2017). Large RyR clusters increases the chances of Ca^{++} spark whereas large uniformly distributed clusters of RyR leads to a more synchronous rise of Ca^{++} during depolarisation. In the steady state, the influx of Ca^{++} is equal to the efflux of Ca^{++} (Negretti et al., 1995). Any imbalances in the Ca^{++} flux are corrected by cells via autoregulation. For example, the potentiation of RyR by sub-millimolar concentrations of caffeine results in increased amplitude of systolic Ca^{++} transient as Ca^{++} efflux is increased (O'Neill and Eisner, 1990). This causes the SR to lose Ca^{++} decreasing the SR Ca^{++} content which offsets the RyR potentiation and brings the amplitude of Ca^{++} transient back to steady state level i.e. the Ca^{++} efflux is equal to Ca^{++} influx.

The amplitude of the $[Ca^{2+}]_i$ transient is proportional to the cube of SR Ca^{++} content (Greensmith et al., 2010). Due to this relationship, any change to SR Ca^{++} has a profound effect on systolic Ca^{++}. As such, in the steady state (i.e. for a given inotropic tone) SR Ca^{++} must be tightly regulated. SR Ca^{++} content is usually 1 to 1.5 mmol/L at the end of diastole and it decreases in systole by 50% to 75% (Shannon et al., 2003). SR Ca^{++} content is determined by cytosolic Ca^{++} concentration, the release of Ca^{++} through RyR and uptake of Ca^{++} in SR via SERCA. SR Ca^{++} content is decreased by increasing NCX activity and increased by decreasing RyR opening or increasing SERCA activity. Ca-sensitive indicators could be used to measure Ca^{++} content in SR (Eisner et al., 2017). However, these indicators could get saturated at high Ca^{++} levels. Application of 10 mmol/L of caffeine empties the SR by releasing all Ca^{++} from SR and measurement of the amplitude of the resulting Ca^{++} transient provides a simple way of measuring SR Ca^{++} content.

6.2 General methodology

6.2.1 Primary myocyte isolation and preparation:

Freshly isolated primary myocytes were sourced from the University of Manchester on each day of experimentation. Myocyte storage, loading and experiment set-up was performed by Natasha Hadcraft (University of Salford) in the author's presence and analysis of the data was done by the author.

6.2.2 **Animals, tissue preparation and ethics:**

Young control sheep at approximately 18 months old and in good health were used to isolate ventricular myocytes and tissue at the University of Manchester. All procedures accord with the Animals (Scientific Procedures) Act, UK, 1986 and Directive 2010/63/EU of the European Parliament (Home Office, 1986). Heparin was administered to limit the loss of tissue due to ischemia by minimising clot formation. Cardiothoracic incision was made and excess blood was removed to prevent tissue deterioration by briefly storing the heart in Ca^{2+} free isolation.

6.2.3 **Isolation of sheep left ventricular myocytes**

Left ventricle was cannulated via the coronary artery onto Langendorff apparatus and perfused with Ca^{2+} free isolation solution for 10 minutes. Tissue digestion was done by adding collagenase type II (Worthington) and protease (Sigma) to the perfusate to allow the dissociation of myocytes. Due to the narrow temperature window for digestive enzymes, solutions used were preheated to 37°C. Following digestion and perfusion with low Ca^{2+} taurine containing solution, left ventricle was dissected and the pericardium and endocardium were removed. Remaining tissue was minced and agitated in fresh taurine solution, then filtered through a net mesh (200 µm pores). The pH of the perfusion solutions was maintained to 7.34 at room temperature (~22°C). All components were sourced from Sigma-Aldrich or Fisher.

6.2.4 **Myocyte storage and loading**

Freshly isolated cells were viewed at 40 x magnification with emersion oil. Good quality, viable cells identified by distinctive rod shape and striated structure were used. Dead or non-viable cells were often identified by their round shape due to hyper-contracture (Kivisto et al., 1995). Cells were stored at room temperature (~22°C) before the experiments and loaded in an intermediate solution. The desired Ca^{2+} was maintained at 1.8 mM, and cells were stored in a (1:1) taurine:tyrodes solution (approximately 0.95 mM Ca^{2+}). An aliquot of cells suspended in a storage solution (3-4 ml) were loaded with 2 µg/µl Fura-2-AM (Thermofisher) in pluronic F-127 (20 % solution in DMSO), for 10 minutes.

6.2.5 **Standard experimental solution**

Tyrodes solution was used for all experiments. Control solution, and emetine (50 nM) and *(-)-R,S*-dehydroemetine (80 nM) were also dissolved in tyrodes solution (components: NaCl, HEPES, glucose, BSA, KCl, MgCl, $CaCl_2$ and Probenecid). All components were sourced from Sigma-Aldrich, Fisher or Fluka.

Cells were allowed to settle in a cell bath for ~10 minutes after the loading procedure and viewed again using an epi-fluorescent inverted microscope under x 40 magnification with emersion oil. The cells for the experiment were selected.

With aid of the eyepiece, the viable cell was positioned into the centre of the window, and the imaging was provided by an Ion Optix MyoCam-S CCD camera. Isolation of single cells from nearby cells and debris was done by using blinds to separate them. In order for experiments to be physiologically relevant, temperature of solutions were kept at 37°C.

6.2.6 **Measurement of intracellular calcium and contractility:**

Epi-fluorescence photometry was used to detect changes in intracellular Ca^{2+} in real time. Fura-2-AM was used to measure the intracellular calcium. Contractility was measured *via* video detection using an Ion Optix MyoCam-S high speed digital camera with a charge-coupled device (CCD). Quantification of relaxation was done by measuring the time taken for the cell to relax at 50% of maximal shortening. Length of myocyte was plotted against $[Ca^{2+}]_i$ from the point of cell re-lengthening during systole, the range where myocyte length and $[Ca^{2+}]_i$ are in equilibrium (Greensmith et al., 2010).

6.2.7 **Quantification of Ca^{2+} fluxes, the activity of the $[Ca^{2+}]_i$ removal mechanisms and SR Ca^{2+} content:**

All fluxes were normalised to cell volume. Rapid emptying of the SR was used to measure the SR Ca^{2+} content during application of 10 mM caffeine (Sigma–Aldrich, UK). The descending phase of the systolic $[Ca^{2+}]_i$ transient was fitted to a single exponential decay. The rate constant of decay (k_{sys}) depends on the combined activity of SERCA and NCX whereas

that of the caffeine response (k_{caff}) predominantly depends on NCX. Subtracting these rate constants gives k_{SERCA} and so a calculated indication of SERCA activity. In the paced experiments, the above parameters, and the SR Ca^{2+} content, global $[Ca^{2+}]_i$ and contractility were measured simultaneously in each cell (Greensmith et al., 2010) (Greensmith et al., 2014).

6.2.8 **Field stimulation of ventricular myocytes**

Two electrodes were used to a current of electricity across the cell bath for field stimulation. The voltage and direction of current was controlled by a Constant Voltage Isolated Stimulator (model DS2A, Digitimer ltd). The amplitude was increased until cells began to respond, the resulting pacing of myocytes usually occurred with field stimulation between 40 – 70 V. A Train/delay generator (model DG2A, Digitimer ltd) was controlled the frequency at which cells were paced. In the majority of experiments the pacing frequency was 0.5 Hz. (Greensmith et al., 2010) (Greensmith et al., 2014).

6.2.9 **Data analysis and statistics:**

Data were analysed with custom-written Excel routines (Greensmith, 2014). Statistical significance was determined using either an unpaired *t*-test (to compare two groups) or repeated-measures ANOVA (to compare multiple, sequentially recorded groups).

6.3 Results:

All figures illustrate the experiment performed on sheep ventricular myocyte (representative of data from 16 cells from 6 animals for *(-)-R,S*-dehydroemetine and data from 13 cells from 4 animals for emetine). Field stimulation was used to stimulate the myocytes with a pacing frequency of 0.5 Hz. Specimen figures demonstrate a typical example and histograms depict the means.

6.3.1 **The effects of *(-)-R,S*-dehydroemetine on contractility:**

The specimen record of Figure 6.3.1 shows an example of the effect of *(-)-R,S*-dehydroemetine on contractility. Figure 6.3.1 A shows the myocytes stimulated by *(-)-R,S*-dehydroemetine at IC_{50}. On average, the new steady state sarcomere length, a measurement for myocyte contractility, after application of *(-)-R,S*-dehydroemetine showed a statistically significant decrease in the degree of shortening ($p<0.005$, mean: 0.722, SEM: 0.059) below the pre *(-)-R,S*-dehydroemetine steady state levels. On removal of *(-)-R,S*-dehydroemetine, the sarcomere length to recovered to the pre *(-)-R,S*-dehydroemetine levels. There was no significant difference between the pre and post *(-)-R,S*-dehydroemetine levels. Figure 6.3.1 B shows the amplified records of the sarcomere length in pre *(-)-R,S*-dehydroemetine, *(-)-R,S*-dehydroemetine and post *(-)-R,S*-dehydroemetine steady state levels. Figure 6.3.1 C outlines the mean data showing the reproducibility of the decrease in steady state sarcomere length on the application of *(-)-R,S*-dehydroemetine which is followed by a recovery to control steady state levels after removing *(-)-R,S*-dehydroemetine. Figure 6.3.1 D shows no significant effect on diastolic sacrcomere length up on application of *(-)-R,S*-dehydroemetine. Figure 6.3.1 E relaxation was also impaired as the time taken by the myocyte to relax to 50% of maximal shortening showed a significant increase ($p<0.005$, mean: 1.352, SEM: 0.136) on application of (-)-*R,S*-dehydroemetine which was followed by a recovery to control steady state levels on removal of (-)-*R,S*-dehydroemetine.

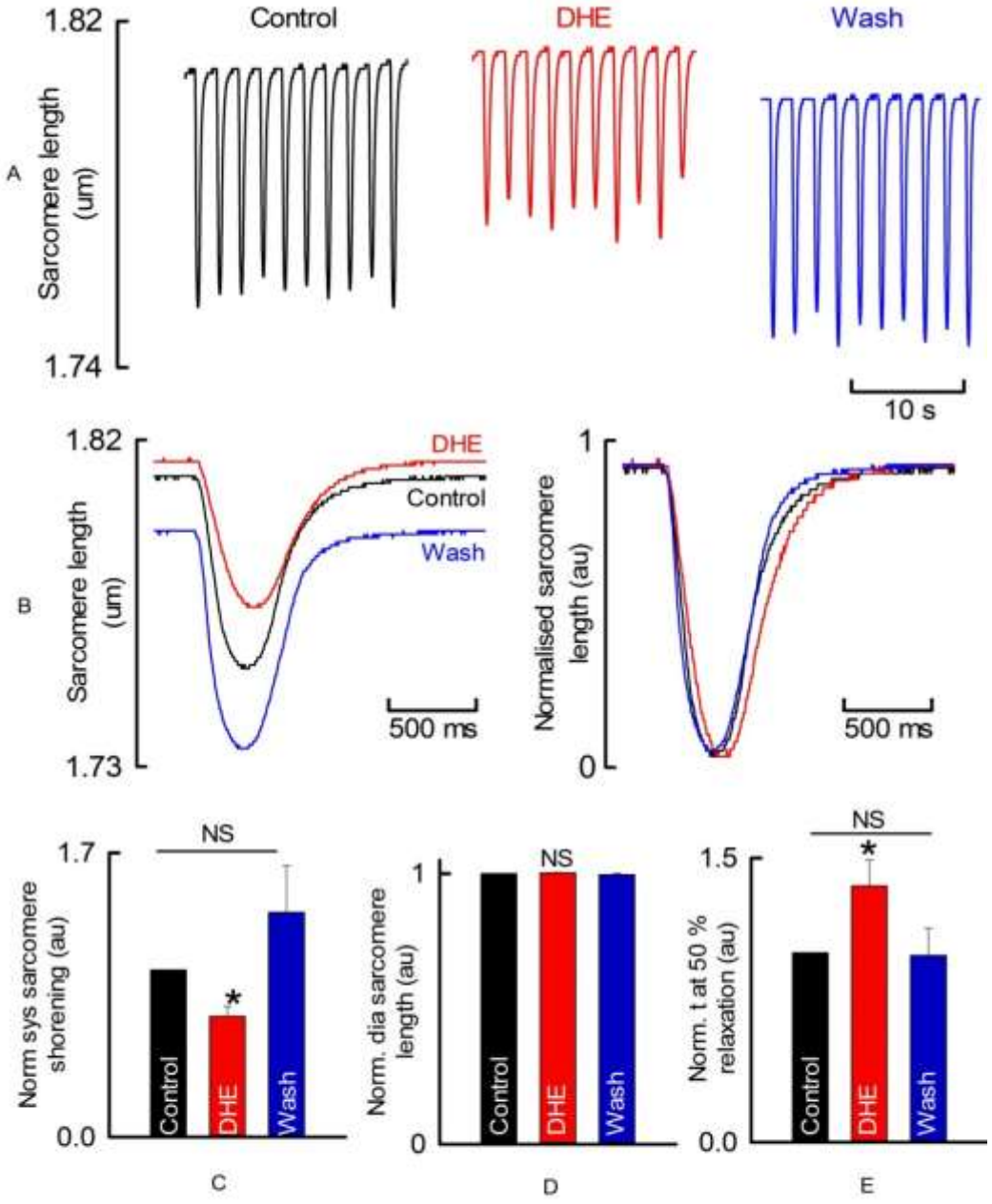

Figure 6.3.1 The effects of *(-)-R,S*-dehydroemetine on contractility

The effects of *(-)-R,S*-dehydroemetine (DHE) on sarcomere length$_i$ in sheep ventricular myocytes stimulated with current pulses. (*A*) Time course of changes in sarcomere length, *(-)-R,S*-dehydroemetine (80 nM) was applied for the period shown. (*B*) Specimen records of sarcomere length taken at the points indicated on *A*. (*C*) Average data for systolic sarcomere length and (D) Average data for diastolic sarcomere length (E) Average data for quantification of relaxation at 50% of maximal shortening (from left to right); steady state in control, steady state in *(-)-R,S*-dehydroemetine, steady-state wash. *n* = 16 cells from 6 animals. Asterisk represents a statistically significant difference. NS represents a statistically non-significant difference.

6.3.2 **The effects of emetine on contractility:**

The specimen record of Figure 6.3.2 shows an example of the effect of emetine on contractility. Figure 6.3.2 A shows the myocytes stimulated by emetine at IC_{50}. On average, the new steady state sarcomere length, a measurement for myocyte contractility, showed no statistically significant changes compared to the pre emetine steady state levels. On removal of emetine, the sarcomere length showed no significant difference compared to the pre emetine levels. Figure 6.3.2 B shows the amplified records of the sarcomere length in pre emetine, emetine and post-emetine steady state levels. Figure 6.3.2 C outlines the mean data showing the reproducibility lack of any change in steady state sarcomere length on the application of emetine. Figure 6.3.2 D shows no significant effect on diastolic sarcomere length up on application and removal of emetine. In Figure 6.3.2 E quantification of relaxation at 50% of maximal shortening showed no significant changes on application of emetine.

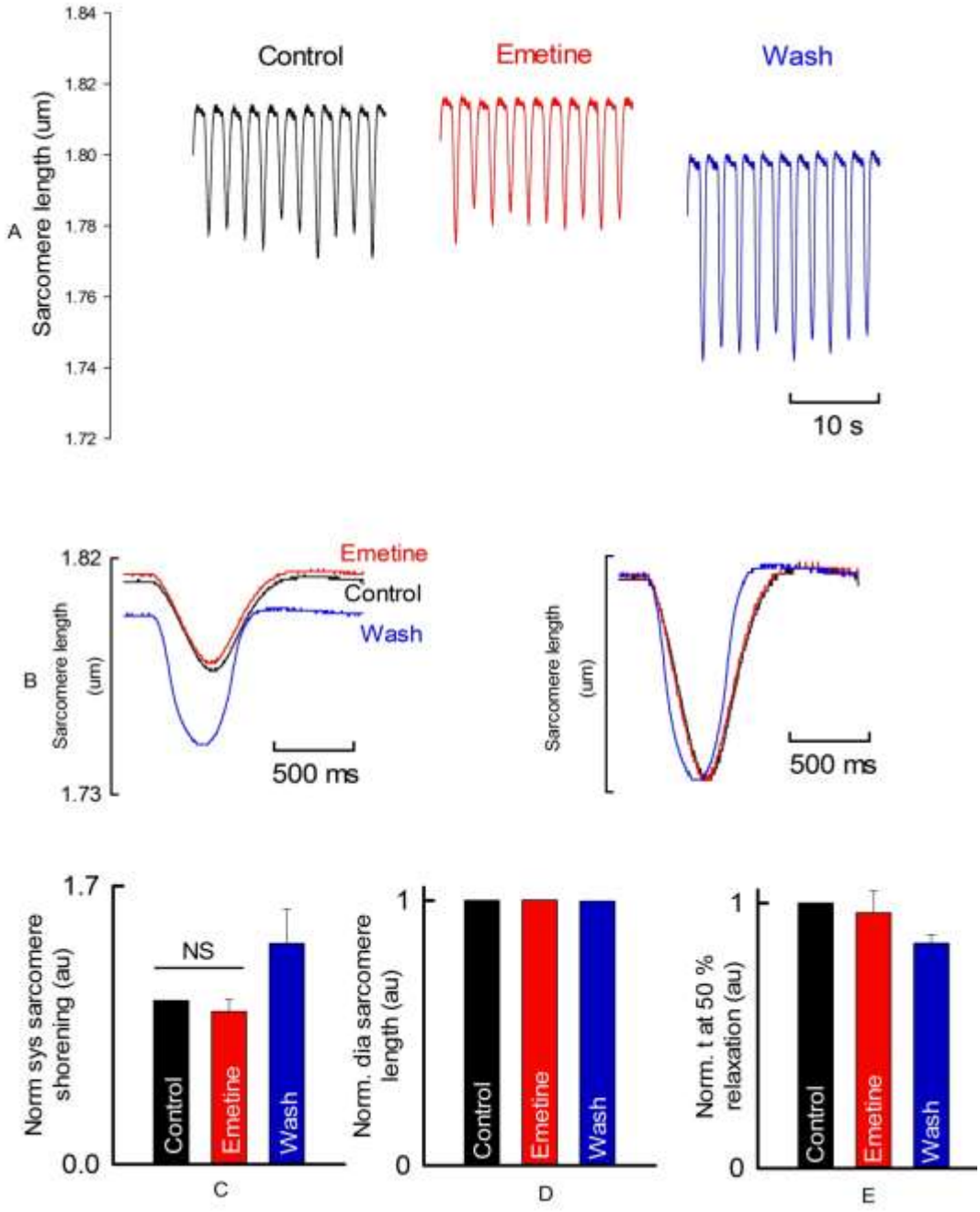

Figure 6.3.2 The effects of emetine on contractility

The effects of emetine on sarcomere length in sheep ventricular myocytes stimulated with current pulses. (*A*) Time course of changes in sarcomere length, emetine (50 nM) was applied for the period shown. (*B*) Specimen records of sarcomere length taken at the points indicated on *A*. (*C*) Average data for systolic sarcomere length and (D) Average data for diastolic sarcomere length. (E) Average data for quantification of relaxation at 50% of maximal shortening (from left to right); steady state in control, steady state in emetine, steady-state wash. $n = 13$ cells from 4 animals. Asterisk represents a statistically significant difference. NS represents a statistically non-significant difference.

6.3.3 **The effects of *(-)-R,S*-dehydroemetine on systolic calcium:**

The specimen record of Figure 6.3.3 shows an example of the effect of *(-)-R,S*-dehydroemetine on systolic calcium. Figure 6.3.3 A shows the myocytes exposed to *(-)-R,S*-dehydroemetine at IC_{50}. On average, the new steady state systolic $[Ca^{2+}]_i$ amplitude showed a statistically significant decrease ($p<0.005$, mean: 0.859, SEM: 0.027) below the pre *(-)-R,S*-dehydroemetine steady state levels. On removal of *(-)-R,S*-dehydroemetine, the amplitude of the Ca transient failed to recover to the pre *(-)-R,S*-dehydroemetine levels. Figure 6.3.3 B shows the amplified records of the Ca transient in pre *(-)-R,S*-dehydroemetine, *(-)-R,S*-dehydroemetine and post *(-)-R,S*-dehydroemetine steady state levels. Figure 6.3.3 C outlines the mean data showing the reproducibility of the decrease in steady state amplitude of the Ca transient on the application of *(-)-R,S*-dehydroemetine which is not followed by a recovery to control steady state levels after removing *(-)-R,S*-dehydroemetine. Figure 6.3.3 D shows no significant effect on diastolic calcium levels up on application of *(-)-R,S*-dehydroemetine.

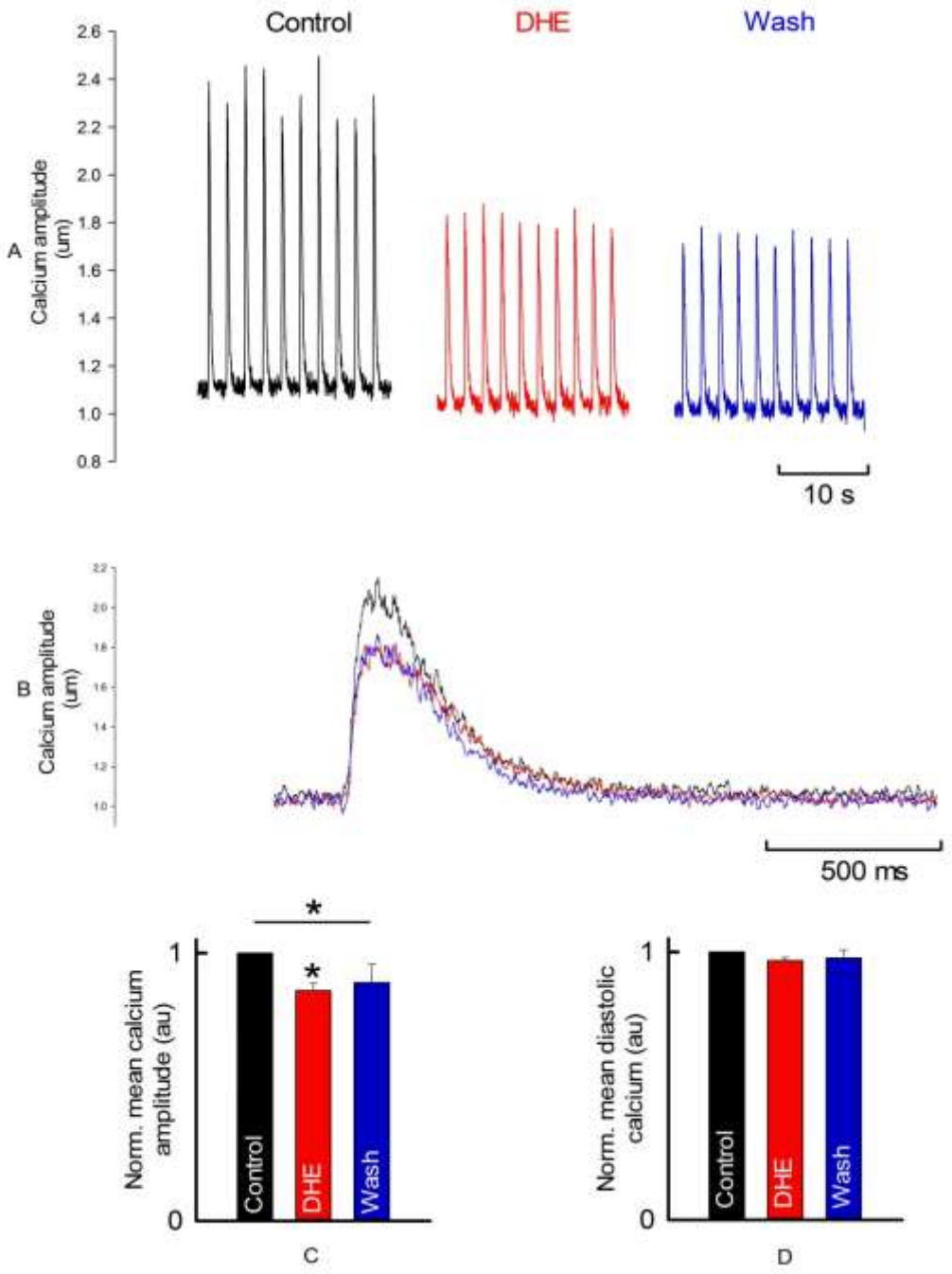

Figure 6.3.3 The effects of *(-)-R,S*-dehydroemetine on $[Ca^{2+}]_i$

The effects of *(-)-R,S*-dehydroemetine on systolic $[Ca^{2+}]_i$ in sheep ventricular myocytes stimulated with current pulses. (*A*) Time course of changes in cytoplasmic Ca measured with fura-2, *(-)-R,S*-dehydroemetine (80 nM) was applied for the period shown. (*B*) Specimen records of Ca taken at the points indicated on *A*. (*C*) Average data for systolic Ca transient amplitude and (D) Average data for diastolic Ca (from left to right); steady state in control, steady state in *(-)-R,S*-dehydroemetine, steady-state wash. n = 16 cells from 6 animals. Asterisk represents a statistically significant difference. NS represents a statistically non-significant difference.

6.3.4 **The effects of emetine on systolic calcium:**

The specimen record of Figure 6.3.4 shows an example of the effect of emetine on systolic calcium. Figure 6.3.4 A shows the myocytes stimulated by emetine at IC_{50}. On average, the new steady state systolic $[Ca^{2+}]_i$ amplitude did not show any statistically significant difference from the pre emetine steady state levels. Removal of emetine also did not produce any change in the steady state levels of Ca transient compared to emetine and pre emetine levels. Figure 6.3.4 B shows the amplified records of the Ca transient in pre emetine, emetine and post-emetine steady state levels. Figure 6.3.4 C outlines the mean data showing the reproducibility of no change in steady state amplitude of the Ca transient on the application and then removal of emetine. Figure 6.3.4 D shows no significant effect on diastolic calcium levels up on application of emetine.

Only *(-)-R,S*-dehydroemetine showed significant changes in global calcium levels and hence next further experiments were conducted only on *(-)-R,S*-dehydroemetine to measure SR Ca^{2+} content.

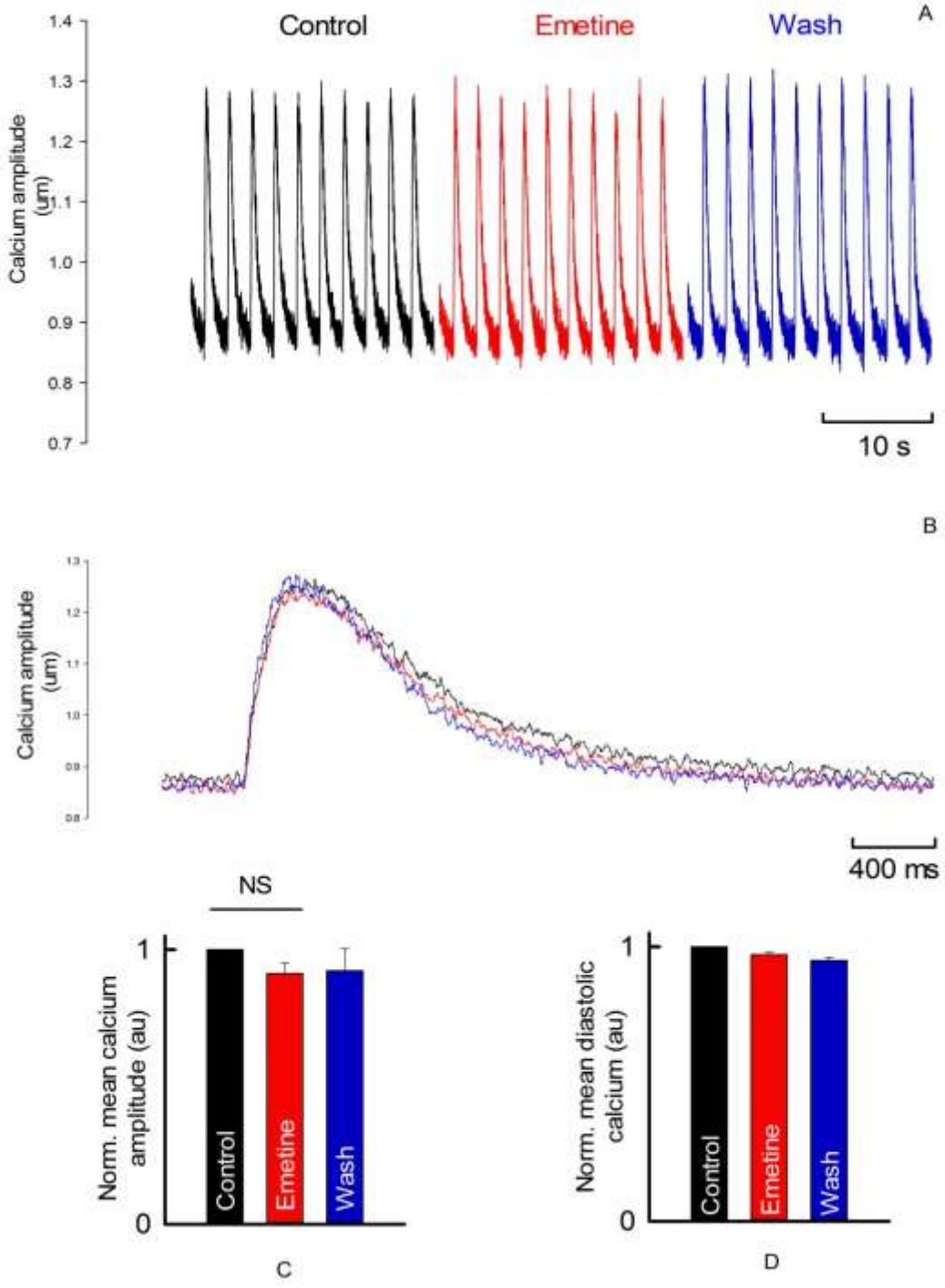

Figure 6.3.4 The effects of emetine on $[Ca^{2+}]_i$

The effects of emetine on systolic $[Ca^{2+}]_i$ in sheep ventricular myocytes stimulated with current pulses. (*A*) Time course of changes in cytoplasmic Ca measured with fura-2, emetine (50 nM) was applied for the period shown. (*B*) Specimen records of Ca taken at the points indicated on *A*. (*C*) Average data for systolic Ca transient amplitude and (D) Average data for diastolic Ca (from left to right); steady state in control, steady state in emetine, steady-state wash. *n* = 13 cells from 4 animals. Asterisk represents a statistically significant difference. NS represents a statistically non-significant difference.

6.3.5 **The effects of *(-)-R,S*-dehydroemetine on SR Ca^{2+} content:**

The specimen record of Figure 6.3.5 shows an example of the effect of *(-)-R,S*-dehydroemetine on SR Ca^{2+} content. Figure 6.3.5 A shows the SR Ca^{2+} content measurements estimated by the amplitude of the Ca transient following application of 10 mM caffeine. On average, an application of *(-)-R,S*-dehydroemetine at IC_{50} resulted in a significant decrease in the amplitude of the caffeine evoked Ca transient. On removal of *(-)-R,S*-dehydroemetine, the amplitude of the caffeine evoked Ca transient failed to recover to the pre *(-)-R,S*-dehydroemetine levels. Figure 6.3.5 B outlines the mean data showing the reproducibility of the decrease in caffeine evoked Ca transient amplitude on the application of *(-)-R,S*-dehydroemetine which is not followed by a recovery to control levels of caffeine evoked Ca transient amplitude up on removal of *(-)-R,S*-dehydroemetine.

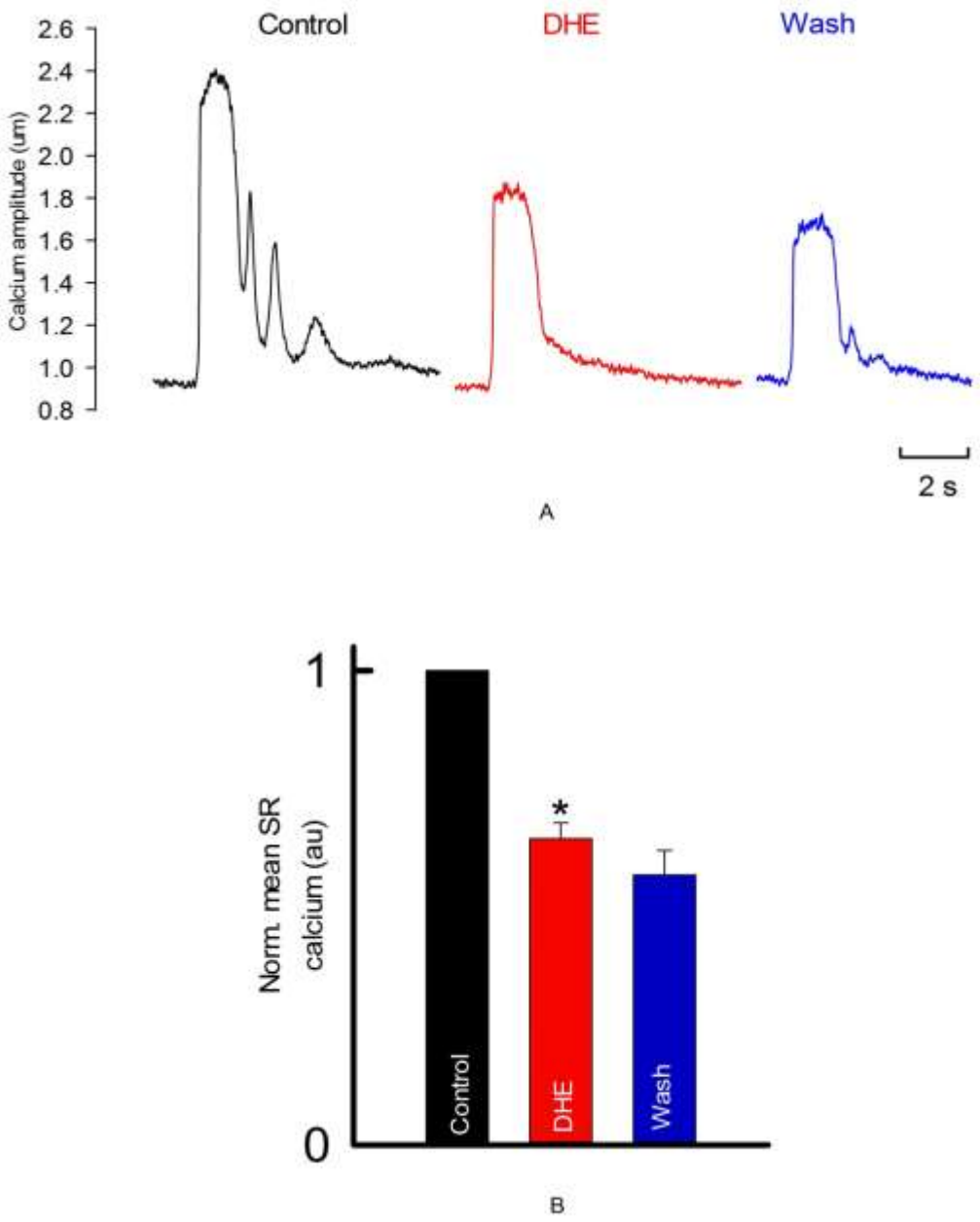

Figure 6.3.5 The effects of *(-)-R,S*-dehydroemetine on caffeine-evoked Ca transient amplitude

The effects of caffeine (10 mM) on systolic $[Ca^{2+}]_i$ in sheep ventricular myocytes stimulated with current pulses. (*A*) Changes in caffeine-evoked Ca transient amplitude measured with fura-2 observed on application of *(-)-R,S*-dehydroemetine (80 nM). (*B*) Average data for caffeine-evoked Ca transient amplitude (from left to right); caffeine-evoked Ca transient amplitude in control, caffeine-evoked Ca transient amplitude in *(-)-R,S*-dehydroemetine, caffeine-evoked Ca transient amplitude wash. *n* = 8 cells from 2 animals. Asterisk represents a statistically significant difference. NS represents a statistically non-significant difference.

6.3.6 **The effects of *(-)-R,S*-dehydroemetine on the activity of the $[Ca^{2+}]_i$ removal mechanisms:**

The cause of decrease in SR Ca^{2+} was investigated by quantifying the rate of $[Ca^{2+}]_i$ removal as shown in Figure 6.3.6. Figure 6.3.6 A shows normalised systolic $[Ca^{2+}]_i$ transients. Reduction in the rate of systolic $[Ca^{2+}]_i$ removal is indicated by slowing of descending phase. Figure 6.3.6 B shows a significant decrease ($p<0.005$, mean: 0.830, SEM: 0.035) in the rate constant of systolic calcium removal (k_{sys}) on application of *(-)-R,S*-dehydroemetine at IC_{50} which returned to control levels up on removal of *(-)-R,S*-dehydroemetine. The rate constant of decay of the caffeine evoked $[Ca^{2+}]_i$ transient (k_{caff}) (Figure 6.3.6 C) did not show any significant changes, indicating no change in NCX activity. $k_{SERCA} = k_{sys} - k_{caff}$ could be used to calculate activity of SERCA and (Figure 6.3.6 D) it showed a significant decrease on application of *(-)-R,S*-dehydroemetine at IC_{50} ($p<0.005$, mean: 0.82, SEM: 0.042) ($n >3$).

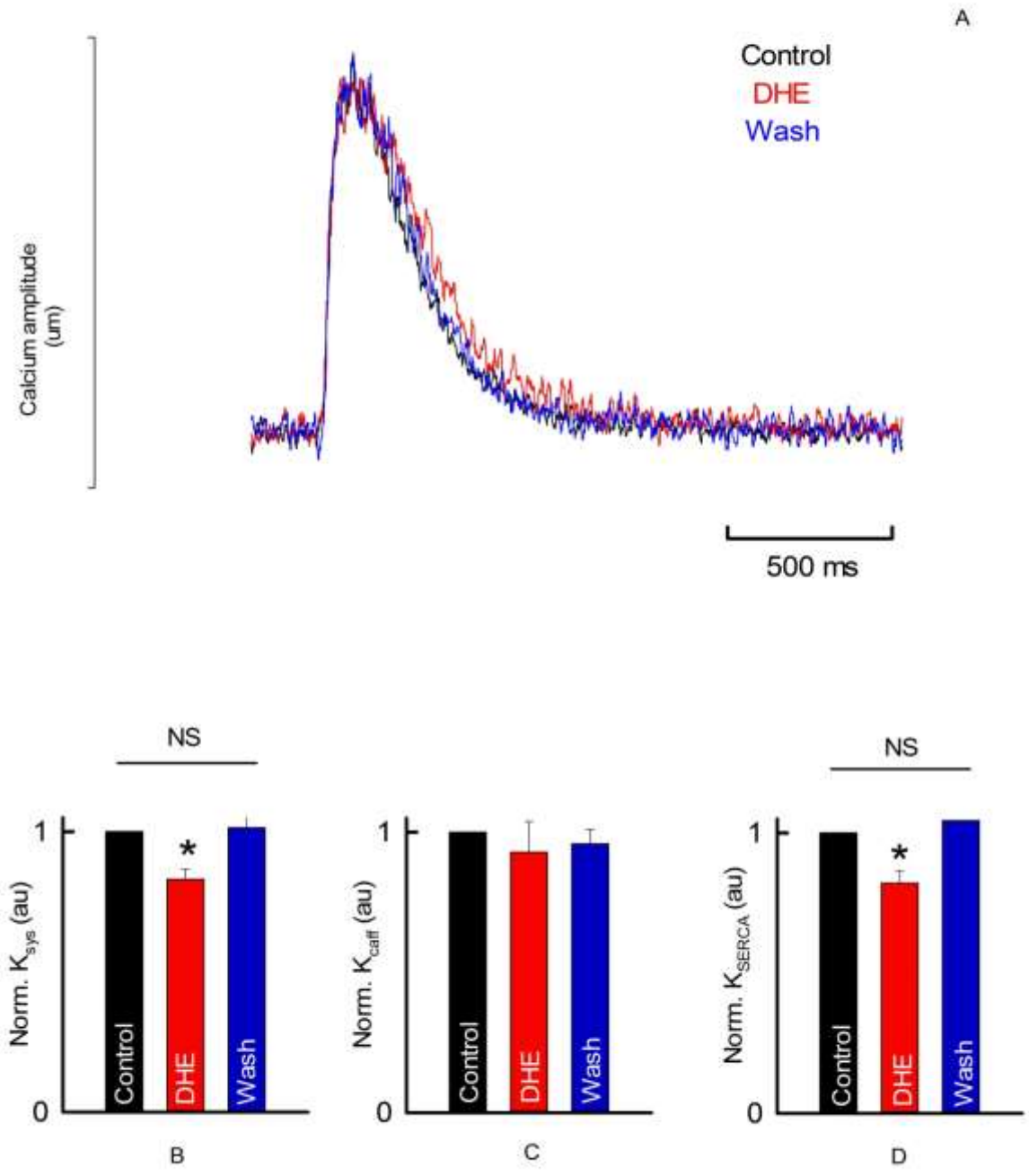

Figure 6.3.6 The effects of *(-)-R,S*-dehydroemetine on the activity of the $[Ca^{2+}]_i$ removal mechanisms

The effects of *(-)-R,S*-dehydroemetine (80 nM) on the activity of the $[Ca^{2+}]_i$ removal mechanisms. (A) Specimen normalised caffeine induced $[Ca^{2+}]_i$ transients. (B) Meank_{sys}. (C) Meank_{caff}. (D) Mean calculated k_{SERCA}. (n = 4–10 cells). Asterisk represents a statistically significant difference. NS represents a statistically non-significant difference.

6.3.7 **The effects of *(-)-R,S*-dehydroemetine and emetine on ryanodine receptor:**

The specimen records of Figure 6.3.7 shows an example of the effect of *(-)-R,S*-dehydroemetine and emetine on systolic Ca^{2+} and myocyte contractility. Figures 6.3.7 A and 6.3.7 B shows the myocytes stimulated by *(-)-R,S*-dehydroemetine and emetine respectively at IC_{50}. On average the systolic $[Ca^{2+}]_i$ amplitude showed a statistically significant increase ($p<0.05$, mean: 1.28, SEM: 0.06) above the control steady state levels immediately up on application of *(-)-R,S*-dehydroemetine and emetine, respectively, before declining to control steady state levels. Figures 6.3.7 C and 6.3.7 D show the corresponding sarcomere length record which depicts a corresponding increase in degree of shortening up on application of *(-)-R,S*-dehydroemetine and emetine respectively, which returns to control steady state levels. Figures 6.3.7 E and 6.3.7 F depicts the mean data showing the reproducibility of the increase in amplitude of the Ca transient on application of *(-)-R,S*-dehydroemetine and emetine respectively, followed by a recovery to control levels in the steady state. Figure 6.3.7 G shows the comparison between the increase in amplitude of the Ca transient on application of *(-)-R,S*-dehydroemetine and emetine.

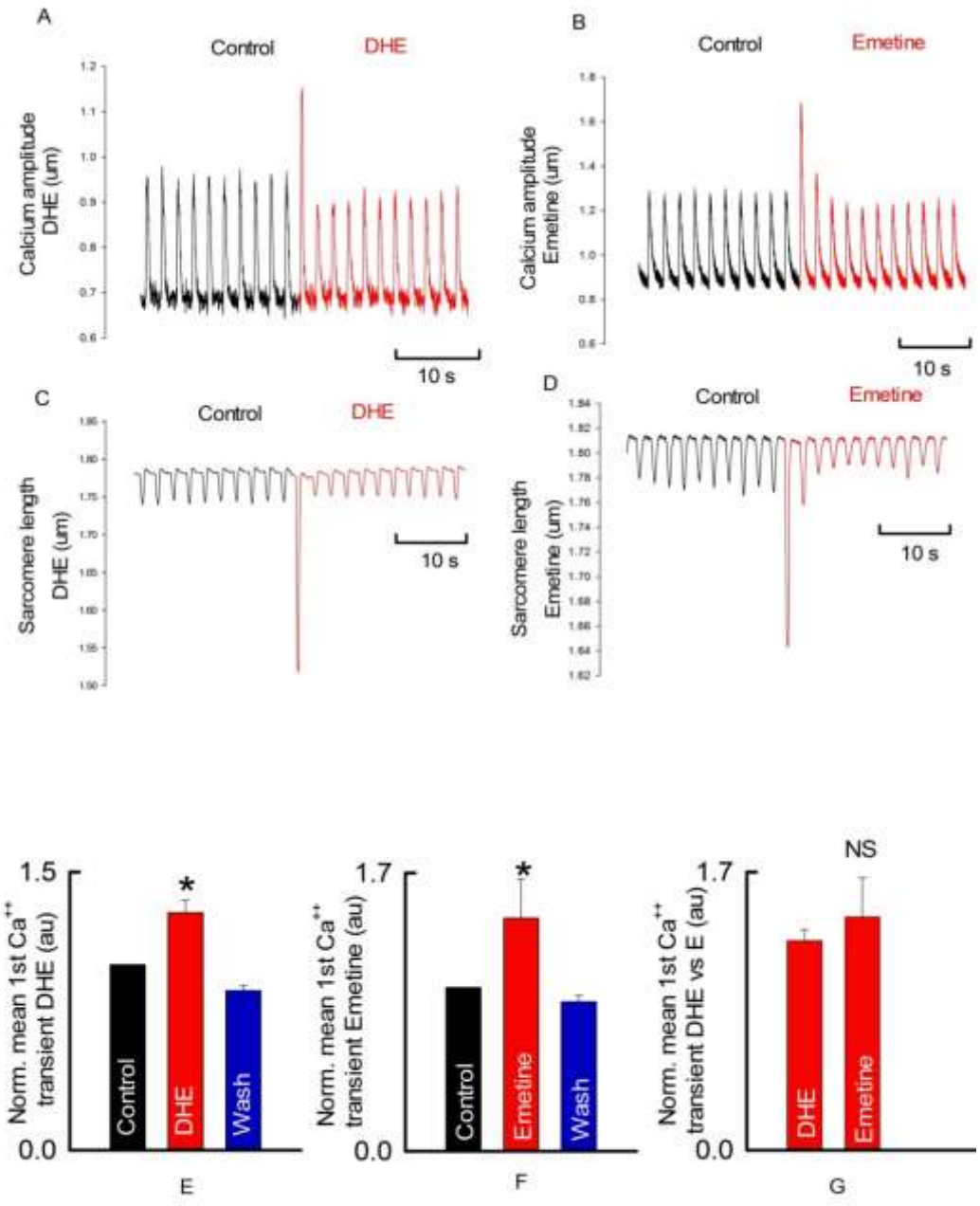

Figure 6.3.7 The effects of *(-)-R,S*-dehydroemetine and emetine on ryanodine receptor potentiation

The effects of *(-)-R,S*-dehydroemetine and emetine on systolic $[Ca^{2+}]_i$ in sheep ventricular myocytes stimulated with current pulses. (*A and B*) Time course of changes in cytoplasmic Ca measured with fura-2, *(-)-R,S*-dehydroemetine and emetine at IC_{50} were applied for the period shown. (*C and D*) Time course of changes in sarcomere length, *(-)-R,S*-dehydroemetine (80 nM) and emetine (50 nM) were applied for the period shown. (*E and F*) Average data for first Ca transient amplitude on application of *(-)-R,S*-dehydroemetine and emetine and (G) Comparison between average data for first Ca transient amplitude on application of *(-)-R,S*-dehydroemetine and emetine. ($p<0.05$, n=13-16). Asterisk represents a statistically significant difference. NS represents a statistically non-significant difference.

6.4 Discussion:

Studies conducted on emetine and dehydroemetine in amoebiasis have found dehydroemetine to be less toxic than emetine (Scragg and Powell, 1968). It was postulated that this effect however could be due to faster excretion of dehydroemetine from the body. In this study, experiments were conducted on sheep ventricular myocytes to determine the role of calcium imbalance in the cellular basis of cardiotoxicity observed in emetine and dehydroemetine. This study has attempted to comprehensively cover most major calcium handling mechanisms. The study found *(-)-R,S*-dehydroemetine decreased SERCA resulting in decreased SR Ca^{2+} content and decreased systolic calcium leading to decreased contractility. No effect was observed on diastolic calcium levels. Emetine on the other hand showed no significant effect on global $[Ca^{2+}]$ levels. It was also observed that both compounds, *(-)-R,S*-dehydroemetine and emetine, potentiated RyR.

6.4.1 The effects of *(-)-R,S*-dehydroemetine on global $[Ca^{2+}]_i$ and contractility

In paced ventricular myocytes, (-)-*R,S*-dehydroemetine decreased the $[Ca^{2+}]_i$ transient amplitude (Figure 6.3.3.1). A reduced degree of systolic shortening accompanied the reduction in $[Ca^{2+}]_i$ transient amplitude (Figure 6.3.1.1). Diastolic $[Ca^{2+}]_i$ did not show any changes. A decrease in the rate of systolic $[Ca^{2+}]_i$ decay and myocyte relaxation was also observed. This decrease in contractility could be accounted for by the decrease in systolic $[Ca^{2+}]_i$. The lack of changes to diastolic $[Ca^{2+}]_i$ explains the lack of change in resting sarcomere length. The data is suggestive of a negative inotropic effect by (-)-*R,S*-dehydroemetine as in the steady state during drug treatment, $[Ca^{2+}]_i$ transient amplitude and sarcomere length stay lower than the control levels.

6.4.2 The effects of emetine on global $[Ca^{2+}]_i$ and contractility

In paced ventricular myocytes, emetine did not show any significant effect on the $[Ca^{2+}]_i$ transient amplitude (Figure 6.3.4.1). No change was observed on the degree of systolic shortening accompanying the $[Ca^{2+}]_i$ transient amplitude (Figure 6.3.2.1). There were no changes observed in diastolic $[Ca^{2+}]_i$. In these experiments, emetine did not show any

significant effect on global $[Ca^{2+}]_i$ and contractility. This eliminated the need to study the effects of emetine on SR Ca^{2+} content.

6.4.3 **Does *(-)-R,S*-dehydroemetine affect SR Ca^{2+} content?**

Caffeine-evoked increase of $[Ca^{2+}]_i$ qualitatively measures the SR Ca^{2+} content. This study observed a significant decrease in SR Ca^{2+} content following exposure to *(-)-R,S*-dehydroemetine (Figure 6.3.5.1). The amplitude of the $[Ca^{2+}]_i$ transient is proportional to the cube of SR Ca^{2+} content (Greensmith et al., 2010). A small decrease in SR Ca^{2+} content would therefore cause an observable decrease in amplitude of the $[Ca^{2+}]_i$ transient. However, in these experiments, the SR Ca was not measured directly and the Ca buffering was not accounted for which might have been altered by *(-)-R,S*-dehydroemetine (Varro et al., 1993). However, the magnitude of change of the caffeine-evoked Ca trainset is far greater than could be produced by altered Ca buffering alone which gives confidence in the observed effect being real.

6.4.4 **Does *(-)-R,S*-dehydroemetine decrease SERCA activity?**

A significant decrease in the rate constant of systolic calcium removal (k_{sys}) on application of *(-)-R,S*-dehydroemetine at IC_{50} was observed which returned to control levels on removal of *(-)-R,S*-dehydroemetine (Figure 6.3.6.1). The rate constant of decay of the caffeine-evoked $[Ca^{2+}]_i$ transient (k_{caff}) did not show any significant changes, indicating no change in NCX activity. $k_{SERCA} = k_{sys} - k_{caff}$ could be used to calculate activity of SERCA. It showed a significant decrease on application of *(-)-R,S*-dehydroemetine at IC_{50}. Decreased SERCA activity seems to be the probable cause for observed decrease of SR Ca^{2+} content which ultimately leads to the decreased $[Ca^{2+}]_i$ transient amplitude.

6.4.5 **The effects of *(-)-R,S*-dehydroemetine and emetine on RyR**

From the data (Figure 6.3.7.1), it was observed both *(-)-R,S*-dehydroemetine and emetine produce a transient increase in the amplitude of the systolic Ca transient. RyR activity was not measured directly but RyR potentiation produces a characteristic effect on the Ca transient (temporary increase in Ca^{++} transient amplitude which recovers due to

autoregulation) (Greensmith et al., 2014) (Eisner et al., 2017) (Eisner et al., 2000). (-)-*R,S*-dehydroemetine produces a similar characteristic effect highly suggestive of RyR potentiation. It seems RyR potentiation by *(-)-R,S*-dehydroemetine and emetine leads to an initial increase in systolic calcium observed as an initial increase in Ca amplitude by increasing the release of calcium from the SR. Autoregulation brings Ca levels back down. The increased Ca efflux returns the Ca transient amplitude to control levels by decreasing SR Ca content (probably through decreased SERCA activity) in case of emetine, but lower than control levels in case of *(-)-R,S*-dehydroemetine.

6.4.6 **Implications of RyR is potentiation**

RyR potentiation will contribute to the decreased SR Ca^{++} content thus contributing to the negative inotropic effects of *(-)-R,S*-dehydroemetine.

RyR potentiation is proarrhythmogenic (Venetucci et al., 2012). It can lead to the formation of calcium waves and thus extra systole. This would make the heart susceptible to arrhythmias. RyR potentiation is observed in *(-)-R,S*-dehydroemetine and emetine indicating the compounds could be proarrhythmogenic. Arrythmia is indeed one of the toxic effects observed during use of emetine and dehydroemetine for amoebiasis.

6.4.7 **Arrhythmogenicity of *(-)-R,S*-dehydroemetine and emetine:**

The experimental data suggests (-)-*R,S*-dehydroemetine produces a decrease in SR Ca^{++} content whereas emetine does not produce any significant change on SR Ca^{++} content. Both compounds, (-)-*R,S*-dehydroemetine and emetine, cause a similar increase in RyR potentiation. RyR potentiation will decrease the threshold for generation of calcium waves which may lead to arrhythmia as the RyR will open spontaneously at lower levels of calcium. (-)-*R,S*-dehydroemetine however also causes a significant reduction in SR Ca^{++} content possibly through decreased SERCA activity. While this makes (-)-*R,S*-dehydroemetine negatively inotropic, decrease in SR Ca content does offer (-)-*R,S*-dehydroemetine some degree of protection against arrhythmia (Figure 6.4.1). Thus, making it potentially less arrythmogenic than emetine.

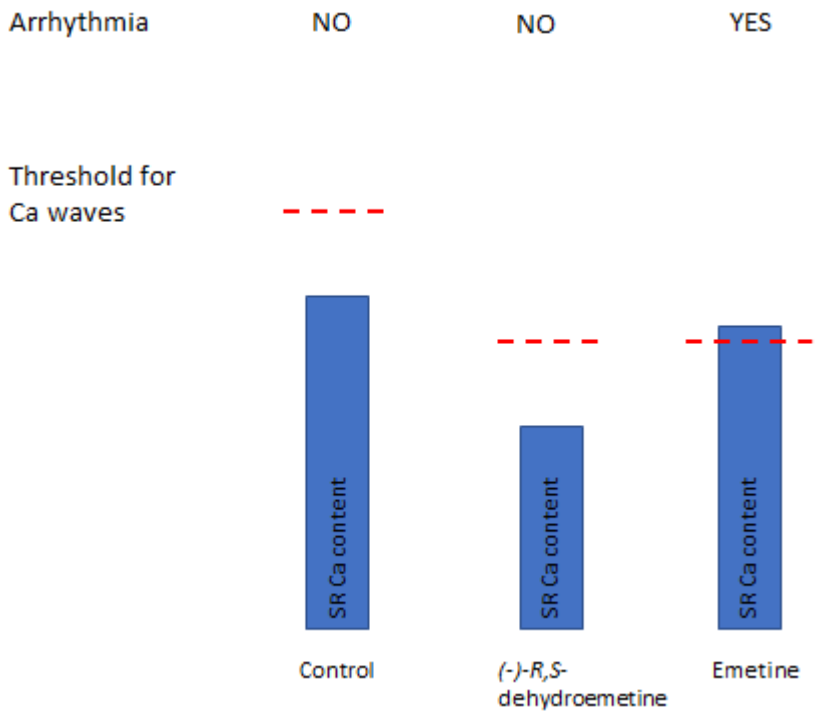

Figure 6.4.1 Potential for arrhythmia in *(-)-R,S*-dehydroemetine and emetine

Similar decrease in threshold for calcium waves is observed on application of *(-)-R,S*-dehydroemetine and emetine as observed by similar level of potentiation of RyR. SR Ca content is reduced by both *(-)-R,S*-dehydroemetine and emetine but significantly more so by *(-)-R,S*-dehydroemetine, which was also observed to be negatively inotropic.

Chapter 7 General Discussion and Conclusions:

Malaria is a disease mainly of tropical and sub-tropical regions of the world. The impact of the morbidity and mortality burdens of the disease on the endemic population has contributed adversely to the wider socio-economic developments of these countries. The mainstay of disease control has been largely reliant on the availability of affordable and effective chemotherapies. Drug discovery however has failed to keep abreast of resistance acquisition. Novel therapeutic antimalarial leads are urgently needed to prevent a potentially catastrophic gap in the drug market.

Recent reports of the emergence of resistance to the front-line drug artemisinin, has invigorated research efforts to define potential new drugs. The cost and long timelines of rational and target-based drug discovery can be bypassed by using drug repositioning or re-purposing. Emetine dihydrochloride hydrate has been identified as a potential candidate with antimalarial activity through drug repositioning screens conducted at the University of Salford (Matthews *et al*, 2013). Although widely used previously as an anti-amoebic drug, the usefulness of this compound is restricted by its dose-dependent side effects, namely, emesis and cardiotoxicity. Our previous work suggests an approximately 1000-fold difference in the drug's *in vitro* antimalarial and anti-amoebic potencies (47 $\pm$ 2.17 nM and 26.8 $\pm$ 1.27 µM, respectively) (Bansal et al., 2004) (Matthews et al., 2013), suggesting potentially different toxicity profiles for its repositioned used. The main objective of the work was to employ a chimeric approach to further optimise through rational design, a potent natural product drug discovered through repositioning. The research presented in this thesis focusses on its synthetic analogue dehydroemetine. The two diastereomers of dehydroemetine, (-)-*R,S*-dehydroemetine and (-)-*S,S*-dehydroisoemetine were synthesised and molecular modelling tools were used in this study in a bid to predict their activity on the multi-drug resistant strain K1 of *P. falciparum*. Further characterisation of its *in-vitro* antimalarial activity, mechanism of action and mechanism of toxicity strongly support progression of research to *in vivo* study models.

7.1 Lead optimisation of dehydroemetine:

The rational design of the dehydroemetine analogues was facilitated by the publication of the Wong et al., 2014 paper defining through cryo-EM studies, the target binding site for emetine on the 40S subunit of the 80S *P. falciparum* ribosome. However, due to poor temperature stability of the 3J7A cryo-EM structure (Wong *et al*, 2014), emetine possessed a high degree of freedom within the 3.2A distance of its predicted binding conformation. This was supported with our docking results of emetine on 3J7A, when none of the docking software were able to reproduce the binding pose as shown in 3J7A. Due to the large size of the ribosome, GOLD was unable to process the 3J7A structure. MOE, PyRx and Autodock vina were able to process the structure, but initially unable to replicate the predicted binding pose of emetine suggested in the Wong et al., 2014 publication. On closer inspection, emetine structure in 3J7A was found to have incorrect chirality, a likely reason for the inability of the software to reproduce the published binding pose. In addition, the presence of a magnesium ion in the vicinity of the binding pocket was another factor which complicated the docking. We present here data form new docking studies employing the emetine structure with correct chirality and removal of magnesium ion from the vicinity of the binding pocket. The results obtained through MOE software was able to replicate the U-shaped binding conformation and predicted a better fit for (-)-*R,S*-dehydroemetine in comparison with (-)-*S,S*-dehydroisoemetine. Binding site interactions observed through the docking of two diastereomers suggested potentially better activity for (-)-*R,S*-dehydroemetine compared to (-)-*S,S*-dehydroisoemetine.

(-)-*R,S*-dehydroemetine and (-)-*S,S*-dehydroisoemetine were synthesised by Chirobloc (Germany) and their activity was evaluated on multi-drug resistant K1 strain of *Plasmodium falciparum*. (-)-*R,S*-Dehydroemetine was found to show a similar potency as emetine against the K1 strain with an IC_{50} of 69.58 $\pm$ 2.62 nM. The isomer (-)-*S,S*-dehydroisoemetine was found to be less potent with an IC_{50} of 1.85 $\pm$ 0.2 µM. The IC_{50} speed assay showed that (-)-*R,S*-dehydroemetine and (-)-*S,S*-dehydroisoemetine analogues reached their IC_{50} in 48 hours despite exhibiting an early onset of action within 24 hours. Results from stage specificity assays depicted that the two isomers show activity against both ring and trophozoite stages, but they are more potent against the trophozoite stage of the parasite.

Emetine has been investigated as an antiviral (poliovirus, human cytomegalovirus, Zika virus and Ebola virus) and as a treatment for intractable lymphoma. 10 mg/kg of emetine administered intraperitoneally was found to be effective in NOD/SCID mice for the treatment of lymphoma, which is equivalent to 0.8 mg/kg in humans. 16.2 mg/kg has been established as the 50% lethal dose of emetine in mice. In clinical settings, 1 mg/kg is the recommended dose for emetine in humans. Pharmacokinetic study of low dose emetine (0.1 mg/kg to 1 mg/kg given orally) was found to be safe and highly efficacious in BALB/c mice with a half-life of 35 hours (Aoki et al., 2017) (Mukhopadhyay et al., 2016) (Yang et al., 2018). MTT assays were conducted on the recommended gold standard HepG2 liver cancer cell lines to evaluate cytotoxicity and safety profiles for (-)-*R,S*-dehydroemetine and (-)-*S,S*-dehydroisoemetine. 5000 cells per well were plated and incubated with serial dilutions of the two diastereomers of dehydroemetine for 48 hours. LD_{50} of (-)-*R,S*-dehydroemetine and (-)-*S,S*-dehydroisoemetine was found to be 196.4 $\pm$ 11 nM and 1.429 $\pm$ 0.18 µM, respectively. Selectivity index for (-)-*R,S*-dehydroemetine and (-)-*S,S*-dehydroisoemetine was found to be approximately 3 and 1, respectively. Selectivity index for emetine was found to be ~4. Low selectivity indices observed could be due to anti-cancer properties of emetine and dehydroemetine. HepG2 being a cancer cell line could explain the low LD_{50} observed. The data further adds to the ongoing debate whether as per recommendations, HepG2 is the best cell line for toxicity testing of antimalarial leads, given their propensity for anticancer activity.

Synergistic combinatorial drug regimens could be used to achieve dose reduction and improve dose-dependent toxicity profiles of drugs. In order to define synergistic/additive combinatorial partner drugs among currently used antimalarials, a range of drug interactivity studies were carried out. CalcuSyn analysis methodology previously validated in our laboratory for drug interactivity studies was used to identify synergistic partners (Matthews et al., 2017). CalcuSyn employs the Chou-Talalay method for *in vitro* drug interactivity analysis. Emetine was found to display good synergy with atovaquone (Matthews et al, 2013). Following this (-)-*R,S*-dehydroemetine was experimentally evaluated for *in-vitro* drug interactivity with four known antimalarials; artemether, atovaquone, proguanil and doxycycline. Artemether and doxycycline were found to be antagonistic (CI = 1.6 and 1.5, respectively) while proguanil displayed mild synergy at IC_{50} (CI = 0.67) and nearly additive to antagonistic activity at ED_{75} and ED_{90} (CI = 1.04 and 1.62, respectively). Mild synergy

was observed between atovaquone and (-)-*R,S*-dehydroemetine (CI = 0.88). In a bid to discover more compounds with activity similar to atovaquone, a virtual screen of an FDA approved library of drugs was conducted using the atovaquone binding site. Forty five drugs were found to show a positive hit for the atovaquone binding site on cytochrome bc1. These drugs should be tested for activity against *Plasmodium falciparum* and if positive, the drugs could potentially be synergistic with emetine and (-)-*R,S*-dehydroemetine.

7.2 Cellular basis for cardiotoxicity:

A study conducted (Turner, 1963) on 25 East African patients taking emetine for the treatment of amoebiasis detected ECG changes in all patients, with T-wave changes being the most frequent. This followed the recommendation that emetine should be given intramuscularly only to patients in a hospital setting and resting in bed. It was also reported (Grollman, 1966) that dehydroemetine and emetine were potent inhibitors of protein synthesis in HeLa cells. At a concentration of 5×10^{-8} M, emetine was able to effectively inhibit protein synthesis by 50% in HeLa cells. It was found that 1.4×10^{-4} M of emetine had no effect on the incorporation of amino acids into the mitochondrial fraction of HeLa cells (Perlman and Penman, 1970). The study observed that emetine was unable to inhibit mitochondrial protein synthesis at concentrations which resulted in complete inhibition of protein synthesis in cytoplasm.

The effects of emetine on cultured chicken embryo cardiac cells was also studied (Watkins and Guess, 1968). It was observed that 10^{-5} M or higher concentrations of emetine lead to the immediate cessation of contraction in atrial and ventricular cells, followed by detachment and lysis. Lower concentrations (10^{-8} to 10^{-6} M) of emetine progressively but rapidly decreased the rate of beating. Washing did not reverse the effects, but addition of NADH (10^{-5} M) increased the strength of beating and synchrony. The reversal lasted for 30 to 45 minutes. Intense and brief reversal of effects was observed by addition of ATP (10^{-6} M). The results showing brief reversal of effects by ATP and prolonged reversal by NADH, suggesting that at higher concentrations, emetine causes physical disruption of plasma membrane of the cells and at lower concentrations, it suppresses the process of formation of high energy phosphate compounds. It was thought that the site of inhibition was at the enzymatic oxidation of substrates mediated by nicotinamide adenine dinucleotide (NAD) (Watkins and Guess, 1968).

Under hypoxic conditions there is a greater flux through glycolysis. Glycolysis is activated by MYC and HIF-1α (Kim et al., 2007). Emetine has been found to inhibit glycolysis by suppressing HIF-1α along with enzymes hexokinase2 and PDK1 leading to apoptosis by accumulation of reactive oxygen species (Aoki et al., 2017). The experiments conducted in this current study found emetine decreased the ATP concentration by ~15% and also caused disruption in the mitochondrial membrane potential. (-)-*R,S*-Dehydroemetine also displayed a similar change in ATP concentration, and showed a disruption of mitochondrial membrane potential albeit to a slightly lesser degree compared to emetine.

Schwartz and Herrero, in 1965, observed the distribution and excretion of dehydroemetine and emetine in guinea pigs. The compounds were labelled at ^{14}C at 3^1 position. It was found that 91.5% of dehydroemetine compared to 67% of emetine was excreted 72 hours after stoppage of doses. Dehydroemetine was eliminated rapidly from heart rather than the liver and reverse was found to be true for emetine. This could be one of the reasons for reduced cardiotoxicity observed in treatment with dehydroemetine, as emetine binds more tightly to heart even though it is not specifically concentrated in cardiomyocytes (Schwartz and Herrero, 1965).

This study aimed to establish the mechanism of action for cardiotoxicity in a bid to propose analogues of emetine with reduced side-effects. Since emetine is presumed to affect the movements of Na+, K+ and Ca++ ions, dehydroemetine is also likely to affect the ion permeability. In a resting cardiac cell, the concentration of K+ is high intracellularly, which creates a chemical gradient for K+ to diffuse out of the cells. Subunit of rapid delayed rectifier potassium ion channel is involved in the cardiac repolarisation (Sanguinetti and Tristani-Firouzi, 2006). It is encoded by the hERG gene (Human ether-a-go-go related gene). Drugs inhibiting the hERG channel can prolong the QT intervals and cause the dangerous cardiac arrhythmia, *Torsades de pointes*. The experiment to test the potential of emetine, (-)-*R,S*-dehydroemetine and (-)-*S,S*-dehydroisoemetine to inhibit hERG K^+ channel was outsourced to Cyprotex, UK as the equipment to carry out the experiment was not available in the university. Emetine and (-)-*R,S*-dehydroemetine (SI > 285) were found to show no inhibition of hERG K^+ channel, whereas (-)-*S,S*-dehydroisoemetine was found to inhibit the hERG K^+ channel with a selectivity index of ~2.

With normal hERG results for emetine and (-)-*R,S*-dehydroemetine, the role of the drugs on the cardiac Ca^{++} channels was investigated. Tight regulation of calcium levels in the cells maintains various cellular functions and activities such as metabolism, cell cycle, secretion and neuronal signalling (Clapham, 2007) (Pandey et al., 2016). Interference with calcium levels could cause parasite death (Enomoto et al., 2012) as calcium and calcium channels play major roles in human cells as well as the *Plasmodium* parasite (Furuyama et al., 2014) (Bogdanova et al., 2013). Higher levels of calcium have been found in parasite-infected RBCs (between 289 nM and 352 nM) compared with non-infected RBCs (between 30 nM and 60 nM) (Desai et al., 1996) (Rohrbach et al., 2005) (Lourido and Moreno, 2015) (Gazarini et al., 2003) (Bogdanova et al., 2013). Merozoites shed surface proteins during RBC invasion along with antibodies attached by the host to their surface. This is presumably done to distract the host's immune response (Farrow et al., 2011) (Harvey et al., 2012). Invasion of RBCs *via* endocytosis results in development of a membrane which forms a vacuole (the PV) around the parasite. This allows an exchange of proteins and lipids between the PV membrane (PVM) and the host plasma membrane (Ward et al., 1993) (Eksi and Williamson, 2011), facilitating the entry of calcium required for parasite survival from the RBC cytosol to the PV.

In addition to its reported role in parasite survival, calcium regulation in the host is also linked to cardiotoxicity. The effect of emetine and its analogues on calcium handling was evaluated in this study in order to identify a potential basis for cardiotoxicity.

Arrythmias have been reported as adverse effects observed during emetine and dehydroemetine therapy in amoebiasis in the mid-20^{th} century. Cardiac myocyte ryanodine receptors enable potentiation lowers the threshold for generation of calcium waves which can ultimately lead to arrhythmia. Experiments conducted on sheep ventricular myocytes found both emetine and (-)-*R,S*-dehydroemetine caused similar potentiation of ryanodine receptor and could thus be considered arrhythmogenic as they could lower the threshold for generation of calcium waves. However, emetine displayed no significant changes in the SR calcium content whereas (-)-*R,S*-dehydroemetine showed a significant decrease in systolic calcium amplitude, systolic contractility, SERCA activity and thus a decrease in SR calcium content. (-)-*R,S*-dehydroemetine was also found to be negatively inotropic. Although at a cellular level, (-)-*R,S*-dehydroemetine appears to have more toxic effects, the decrease in SR calcium

content in the presence of ryanodine receptor potentiation makes (-)-*R,S*-dehydroemetine comparatively less arrhythmogenic than emetine. Decreased calcium wave threshold with a fuller SR calcium is potentially the reason for increased likelihood of arrhythmias observed in clinical settings during treatment with emetine as compared to dehydroemetine.

Emetine is a natural product derivative displaying potent nanomolar antimalarial efficacy. Despite its previous widespread use as an anti-amoebic drug, emetic and cardiotoxic side effects and stringent regulatory processes in the drug discovery pipeline, prevent consideration of the lead for repositioning as an antimalarial. However, emetine and dehydroemetine are approximately 1000-fold more potent against multi-drug resistant K1 strain of *P. falciparum* than against amoebiasis. Since toxicity is dose dependent, it is highly likely the adverse effects observed in antimalarial therapy with emetine and dehydroemetine would be significantly lower compared to the treatment in amoebiasis. Dehydroemetine, a synthetic analogue of emetine has been used in the past as a safer alternative and this study shows dehydroemetine is indeed less arrhythmogenic than emetine. The experimental validation of (-)-*R,S*-dehydroemetine shows it to be approximately as potent as emetine against the multi-drug resistant K1 strain of *Plasmodium falciparum*. Its transmission blocking capacity, lack of strain-specific cross-resistance, its ability to concentrate in hepatic tissues and synergistic interactions with atovaquone, makes (-)-*R,S*-dehydroemetine a valuable antimalarial candidate for complicated cerebral malaria. The recent availability of the target-binding site offers more opportunities for further modification of the lead with a view to achieving a safer toxicity profile. A role for such a drug in combating deaths due to cerebral malaria, where treatment would necessarily be carried out in a hospital setting with continuous cardiac monitoring, cannot be overlooked given the current state of early resistance to the front-line antimalarial drug. Dehydroemetine, although not available for purchase, still remains a WHO recommendation for the treatment of amoebiasis and giardiasis, in the event of treatment failure due to metranidozole (Appendix II). Antimalarial chemotherapy throughout the ages has been predominantly sustained by affordable, natural product drugs including derivatives of quinine and artemisinin. The work reported in this thesis, presents a strong argument for the further investigation of yet another potent, affordable, natural product lead; (-)-*R,S*-dehydroemetine.

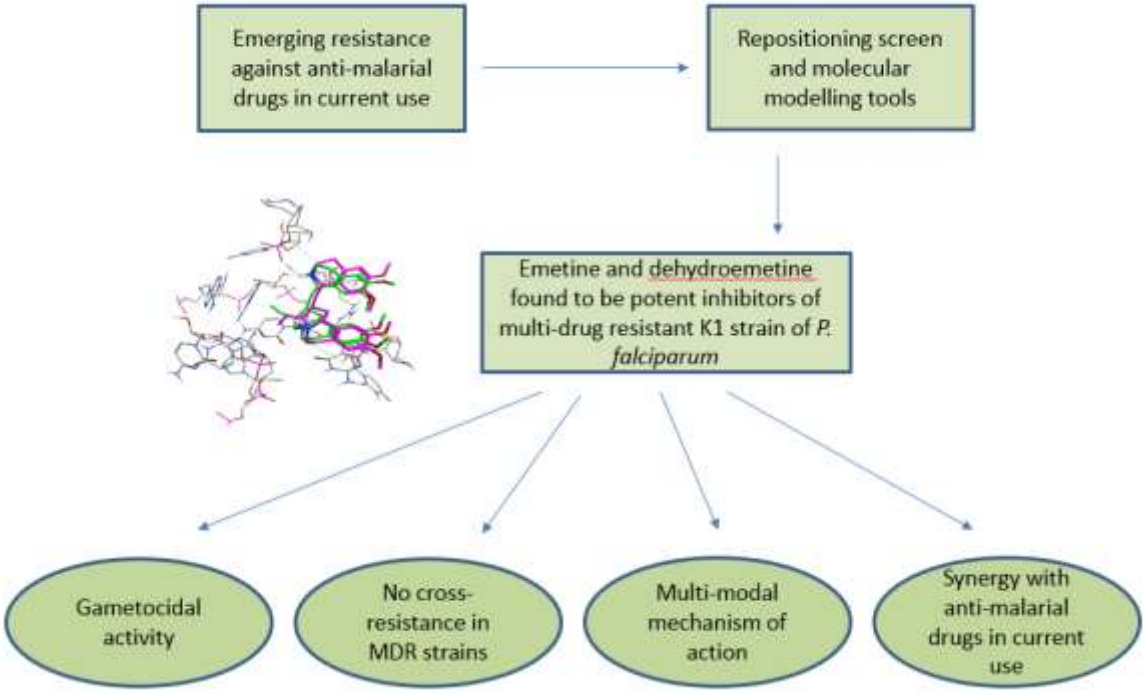

Figure 7.2.1 Activity-profile of emetine and dehydroemetine

Plant-derived anti-amoebic drug emetine dihydrochloride and its synthetic analogue dehydroemetine ((-)-*R,S*-dehydroemetine) are highly potent with nanomolar efficacy against multi-drug resistant K1 strain of *P. falciparum*.

7.3 Future work:

- To perform *in-vitro* cytotoxicity studies on non-cancer cell lines to determine the safety profile of emetine dihydrochloride and its synthetic analogue, dehydroemetine ((-)-*R,S*-dehydroemetine)
- To perform *in-vivo* cytotoxicity studies at low doses on animal models to determine the safety profile of emetine dihydrochloride and (-)-*R,S*-dehydroemetine
- To test the compounds identified through virtual screening for activity against *Plasmodium* parasites.
- To perform drug-interaction analysis on the compounds identified through virtual screening with emetine dihydrochloride and (-)-*R,S*-dehydroemetine to identify a synergistic partner drug for combination therapy.

- To perform further conclusive experiments to determine the effect of emetine dihydrochloride and (-)-*R,S*-dehydroemetine on ATP production through glycolysis.
- To perform further conclusive experiments to determine the effect of emetine dihydrochloride and (-)-*R,S*-dehydroemetine on mitochondria and mitochondrial membrane potential.
- To perform further conclusive experiments to determine the effect of emetine dihydrochloride and (-)-*R,S*-dehydroemetine on calcium waves and calcium sparks in cardiomyocytes.
- To perform experiments to determine which proteins are affected due to the inhibition of protein translation by emetine dihydrochloride and (-)-*R,S*-dehydroemetine.
- To perform experiments to determine any other target sites for emetine dihydrochloride and (-)-*R,S*-dehydroemetine.

Appendix I

Synthesis of dehydroemetine:

The synthesis began with Mannich reaction of ethyl 2-ethylacetoacetate **1** with dimethylamine and formaldehyde leading to Mannich base **2** isolated with 42% yield after distillation. The compound **2** was then transformed into quaternary ammonium salt after quaternization with slight excess of methyl iodide. The salts are known to readily eliminate trimethylammonium iodide thus generating corresponding active enones which further react with imines like **3** giving 4-piperidinone derivatives. The particular reaction between **2** and **3** was conducted in one-pot manner furnishing piperidinone **4** with best yield of 72%. It should be noted that minor amounts (10-20%) of the second diastereomer **5** were observed during the reaction control, workup, and purification processes (^{1}H-NMR, GC-MS). We did not especially try to completely separate diastereomer **5** because the second stereocenter vanished in the next steps. However, analytically pure sample could be obtained after recrystallization from ethanol. Knoevenagel condensation of ketone **4** with malononitrile under general basic conditions led to unsaturated dinitrile **6** with 69% yield. This was hydrolysed and decarboxylated in refluxing 20% hydrochloric acid, and exocyclic double C=C bond transformed into more favorable endocyclic one of the compound **7**. Usual esterification of carboxylic acid **7** to racemic methyl ester **8** in MeOH/HCl was followed by resolution of the racemate with (+)-dibenzoyl-D-tartaric acid. The salt was recrystallized twice from methanol to achieve rotation values known for optically pure compounds, and then set free to ester **9**, which was further hydrolyzed into dilute HCl to (*S*)-carboxylic acid **10**. Thermal amidation of the **10** with homoveratrylamine in refluxing xylenes furnished amide **11** with 55% yield. Bischler–Napieralski cyclization under general conditions (benzene, $POCl_3$) led to dihydroisoquinoline derivative **12**, also known as *2-dehydro-O-methyl psychotine, with 54% yield*. The cyclic imine **12** was reduced with sodium borohydride in methanol to a 1:1 mixture of target 2-dehydroemetine **13** and 2-dehydroisoemetine dihydrobromide **14**. Attempts were made to separate both diastereomers chromatographically as BOC-derivatives or as free bases on aluminium oxide, all unsuccessful. Finally fractional crystallization allowed separating the products **13** and **14** as dihydrobromide salts.

3-[(Dimethylamino)methyl]pentan-2-one **2** (Openshaw and Whittaker, 1963).

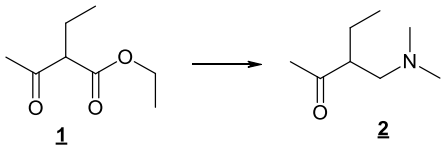

1 **2**

Commercially available ethyl 2-ethylacetoacetate **1** (200g, 1.3mol) was combined with ice-cold solution of potassium hydroxide (78g, 1.4mol) in water (1500ml). The mixture was stirred for 4.5 hours at r. t. before pH was adjusted to 7 with conc. HCl (2ml), and dimethylamine hydrochloride (104g, 1.3mole) and formaldehyde (98ml, 1.3mol, as 37% aqueous solution stabilized with 10-15% methanol) were added. After stirring for 10 minutes, conc. HCl (121ml, 1.4mol) was added dropwise during 1 hour. The reaction mixture was stirred for 16 hours at r.t. The solution was washed with diethyl ether (500ml), saturated with NaCl (500g) under stirring and cooled to 5°C. Diethylether (500 ml) was added, and cold concentrated solution of potassium hydroxide (106g, 1.9mol) in water (200ml) was added dropwise under vigorous stirring for 15 minutes while keeping the internal temperature <20°C in ice bath. Organic phase was gathered, aqueous solution extracted additionally with diethyl ether (3×500 ml). Combined organic solutions were dried over Na_2SO_4, filtered and carefully concentrated *in vacuo* (400mbar) to give the crude product (250g) as colorless oil. The latter was fractionally distilled to give the main pure fraction (151g, 42% yield) at 64°C/19mbar. Analytical data (^{1}H-NMR, GC-MS) confirmed identity and purity of the product.

(*3S*,11bS**)-3-ethyl-9,10-dimethoxy-1,3,4,6,7,11b-hexahydrobenzo[a]quinolizin-2-one **4** (Brossi et al., 1959).

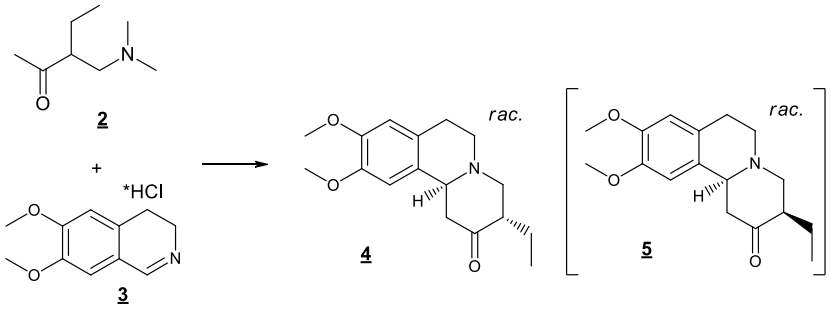

2 **3** **4** **5**

Mannich base **2** (110g, 0.77mol) was dissolved in absolute ethanol (220ml) cooled in ice bath and treated with methyl iodide (152.6g, 67ml, 1.1mol) keeping the internal temperature <20°C. After the exothermic reaction ceased, homogeneous solution turned into white suspension, which was allowed to stir for 24 hours, treated with toluene (200ml) and evaporated to dryness *in vacuo* to give crude iodomethylate (221g) as yellow solid (a sample was characterized with ^{1}H-NMR). The intermediate was suspended in absolute ethanol

(1400ml) and commercially available 6,7-dimethoxy-3,4-dihydroisoquinoline hydrochloride **3** (142g, 0.624mol) was added followed by anhydrous potassium acetate (61.2g, 0.624mol). The reaction was stirred at reflux for 3 hours until full conversion of **3** is achieved (>98%, GC-MS). The reaction was quenched with chloroform (1000ml), water (500ml), 1N NaOH (500ml). Organic phase was separated, aqueous solution extracted additionally with chloroform (500 ml). Combined organic solutions were dried over Na_2SO_4, filtered and concentrated *in vacuo* to give the crude product (390g) as orange solid. This was purified chromatographically (silica gel, ethyl acetate) to give the pure product **4** (159.85g, 72% yield) as pale-yellow solid. Analytical data (^{1}H-NMR, GC-MS) confirmed identity and purity of the product.

2-[(*3R*,11bS**)-3-Ethyl-9,10-dimethoxy-1,3,4,6,7,11b-hexahydrobenzo[a]quinolizin-2-ylidene]propanedinitrile **6** (Battersby et al., 1953).

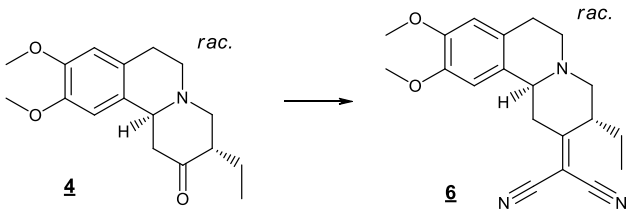

Ketone **4** (122.1g, 0.422mol), malononitrile (33.45g, 0.506mol), ammonium acetate (13.3g, 0.173mol) and acetic acid (26.6g, 25.3ml, 0.443mol) were dissolved in toluene (1120ml), and the yellow homogeneous solution was stirred under reflux for 2.5hours. After cooling to r.t., the reaction was treated with ethyl acetate (900ml) and saturated $NaHCO_3$ (1000ml). Organic phase was separated, aqueous phase additionally extracted with ethyl acetate (600ml). Combined organic solutions were dried with Na_2SO_4, filtered and concentrated *in vacuo* to give crude product **6** (121g). Recrystallization from ethyl acetate and chromatography of mother liquor on silica gel with ethyl acetate-hexane 1:1 gave combined yield of 109g (69%) of the title product **6**. Analytical data (^{1}H-NMR, GC-MS) confirmed identity and purity of the product.

rac-2-(3-Ethyl-9,10-dimethoxy-4,6,7,11b-tetrahydro-1H-benzo[a]quinolizin-2-yl)acetic acid **7** (Brossi et al., 1959).

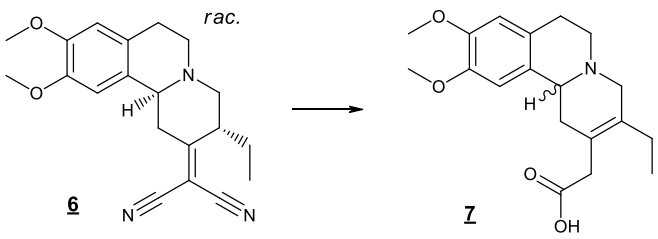

The Knoevenagel product **6** (40g, 119mmol) was dissolved in hydrochloric acid (720ml of 20% aq. solution) under reflux, and the clear brown solution was stirred under reflux for 5 hours before concentrated *in vacuo* to dryness. The yellow solid residue was dissolved in water (50ml), made alkaline with Na_2CO_3 (pH=8-9) and extracted with toluene (100ml). Aqueous phase was separated, saturated with NaCl, neutralized with acetic acid (pH=5.5-6) and extracted with chloroform (2x200ml). Organic phase was separated, concentrated *in vacuo* and coevaporated with acetone (2x200ml) to give the title product **7** (40.1g, 71% yield, 70% purity) as orange solid.

rac-Methyl 2-(3-ethyl-9,10-dimethoxy-4,6,7,11b-tetrahydro-1H-benzo[a]quinolizin-2-yl)acetate **8** (Brossi et al., 1959).

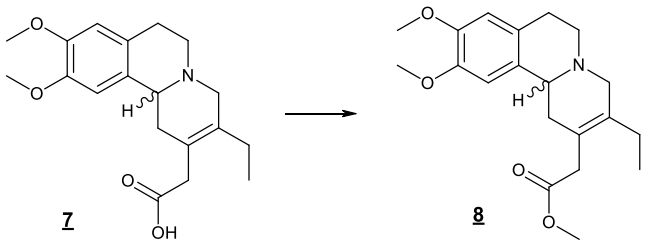

Cold (5°C) methanol (1000ml) was treated dropwise within 15 minutes with acetyl chloride (220g, 200ml, 2.8mol) under vigorous stirring. Acid **7** (97g, 0.293mol) was then dissolved in the mixture, and the clear brown solution was stirrerd at r.t. for 18 hours. The reaction was concentrated to dryness, and brown-yellow rest partitioned between CH_2Cl_2 (1000ml) and saturated $NaHCO_3$ (1000ml). Organic phase was separated, aqueous phase extracted with CH_2Cl_2 (2x250ml). Combined organic phases were dried with Na2SO4, filtered and evaporated *in vacuo* to give crude product (110g) as brown oil. Chromatographic purification (silica gel, ethyl acetate – methanol 9:1) furnished the title product (92.3g, 64% yield, 95% purity according to GC) as brown oil. Analytical data (^{1}H-NMR, GC-MS) confirmed identity of the product.

Methyl 2-[(*11bS*)-3-ethyl-9,10-dimethoxy-4,6,7,11b-tetrahydro-1H-benzo[a]quinolizin-2-yl]acetate **9** (Brossi et al., 1962).

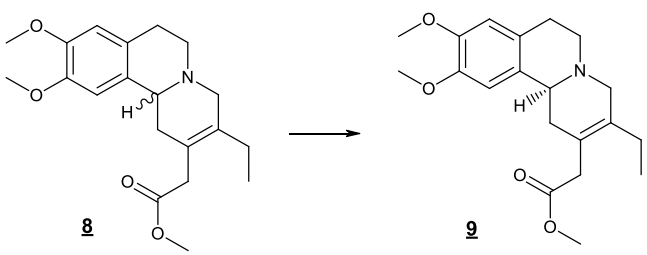

Ester **8** (32.3g, 93.5mmol) was dissolved in methanol (100ml) and treated with solution of (+)-dibenzoyl-D-tartaric acid monohydrate (35.2g, 93.5mmol). 10 Minutes later

crystallization appeared, and the mixture was stored for 16 hours at 5°C. Crude tartrate was filtered, washed with cold methanol (3x20ml) and dried to give 51.13g with optical rotation -46,0° (c=1, MeOH, 24°C). Additional recrystallization from methanol (200ml) improved the optical rotation to the constant value of -49.2° (c=1, MeOH, 24°C) which is identical with the value $[a]_D$ = +49° described for the opposite enantiomer. Free base was set free by stirring the salt with diethyl ether (400ml), saturated $NaHCO_3$ solution (500ml) and water (500ml). Organic phase was separated and aqueous layer additionally extracted with diethyl ether (2x200ml). Combined organic phases were dried (Na_2SO_4), filtered and evaporated to dryness to give the title compound **9** (21.2g, 25% yield) as pale yellow oil. Analytical data (^{1}H-NMR, GC-MS) confirmed identity and purity of the product.

2-[(*11bS*)-3-Ethyl-9,10-dimethoxy-4,6,7,11b-tetrahydro-1H-benzo[a]quinolizin-2-yl]acetic acid **10** (Brossi et al., 1962).

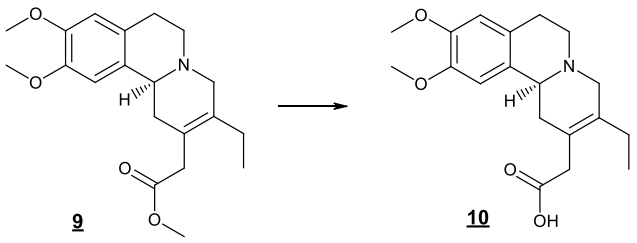

Ester **9** (21.2g, 61.4mmol) was refluxed with 3N HCl (340ml) under stirring for 1.5 hour. Reaction was concentrated to dryness and treated with diethyl ether (200ml) and saturated $NaHCO_3$ (250ml). Aqueous phase was separated, neutralized with acetic acid (pH=7), saturated with NaCl and chloroform (4x150ml). Organic solutions were dried with Na_2SO_4, filtered, evaporated to dryness and coevaporated once with ethyl acetate (150ml). The title product was isolated as yellow foam (21.3g, 94%, 90% purity). Analytical data (^{1}H-NMR, GC-MS) confirmed identity of the product.

2-[(*11bS*)-3-ethyl-9,10-dimethoxy-4,6,7,11b-tetrahydro-1H-benzo[a]quinolizin-2-yl]-N-[2-(3,4-dimethoxyphenyl)ethyl]acetamide **11** (Brossi et al., 1962).

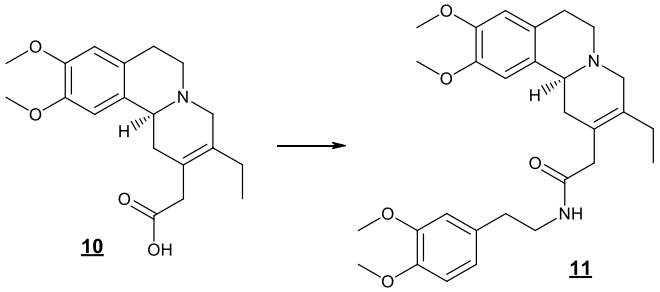

Carboxylic acid **10** (21.3g, 64mmol) and 3,4-dimethoxy-phenylethylamine (12.23g, 11.4ml, 67.5mmol) were dissolved in xylene (500ml, mixture of isomers) and refluxed under stirring

for 18hours with Dean-Stark trap. The reaction was concentrated to dryness to give crude product as brown oil. This was purified chromatographically (silica gel, ethyl acetate – methanol 9:1) to give the title product **11** (17.5g, 55% yield) as beige solid. Analytical data (^{1}H-NMR, LC-MS) confirmed identity and purity of the product. Optical rotation of the sample (-181°, c=1, MeOH, 21°C) corresponds to the values reported in literature ($[a]_D$ = -189°).

(*11bS*)-2-[(6,7-Dimethoxy-3,4-dihydroisoquinolin-1-yl)methyl]-3-ethyl-9,10-dimethoxy-4,6,7,11b-tetrahydro-1H-benzo[a]quinolizine **12** (Brossi et al., 1959).

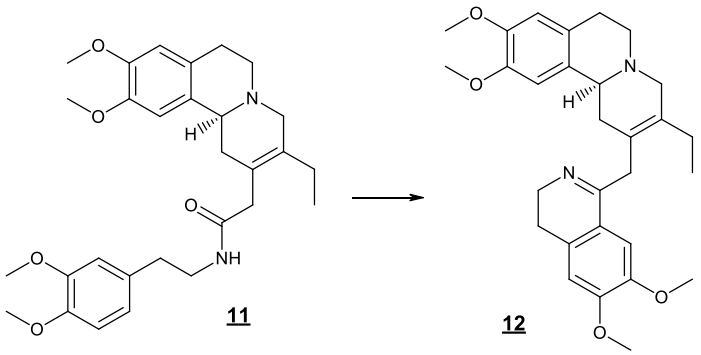

Amide **11** (2.2g, 4.4mmol) and phosphorus oxychloride (1.7g, 1ml, 11.1mmol) were dissolved in benzene (45ml) and stirred under reflux for 1 hour. After cooling to r.t., supernatant solution was decanted from dark oil. The latter was dissolved in warm methanol (30ml, 40°C) and treated with diethyl ether (60ml), which caused crystallization. The mixture was kept at 5°C for 18 hours. Hygroscopic beige dihydrochloride-monohydrate of the product **12** was filtered, washed with diethyl ether (2x20ml) and dried *in vacuo*. The salt was dissolved in cold water (50ml), made alkaline with conc. NH_4OH (pH=9) and extracted with diethyl ether (3x100ml). Combined organic phases were concentrated and dried *in vacuo* to give free base of the product **12** (1.28g, 54% yield, 90% purity) as yellow foam.

(*11bS*)-2-[[(*1R*)-6,7-Dimethoxy-1,2,3,4-tetrahydroisoquinolin-1-yl]methyl]-3-ethyl-9,10-dimethoxy-4,6,7,11b-tetrahydro-1H-benzo[a]quinolizine dihydrobromide (2-dehydroemetine dihydrobromide) **13** and (*11bS*)-2-[[(*1S*)-6,7-dimethoxy-1,2,3,4-tetrahydroisoquinolin-1-yl]methyl]-3-ethyl-9,10-dimethoxy-4,6,7,11b-tetrahydro-1H-benzo[a]quinolizine dihydrobromide (2-dehydroisoemetine dihydrobromide) **14** (Brossi et al., 1959).

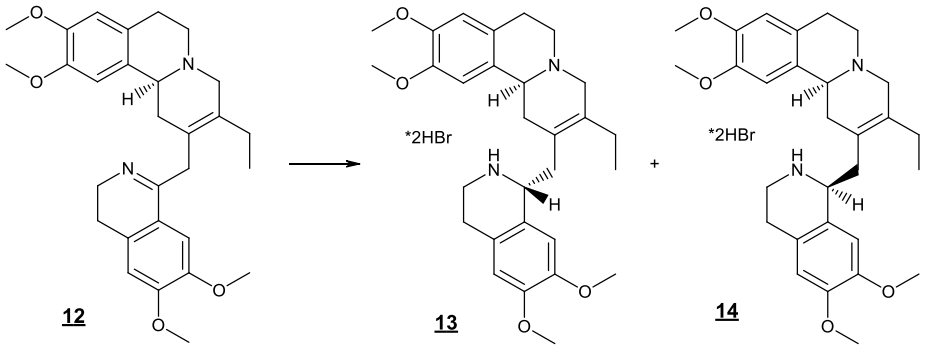

Cyclic imine **12** (8.5g, 17.8 mmol) was dissolved in methanol (300ml). The yellow solution was cooled to 5°C, and sodium borohydride (1.9g, 50mmol) was added in one portion. Conversion was complete in 1 hour, and the reaction was evaporated *in vacuo* and partitioned between diethyl ether (500ml) and water (150ml). Organic phase was separated, aqueous phase additionally extracted with diethyl ether (150ml). Combined organic phase were dried (Na_2SO_4) filtered and evaporated to give crude mixture of diastereomers (8.5g) in ratio 1:1 according to ^{1}H-NMR as yellow foam. The mixture was suspended in water (60ml), and conc. HBr (4.1ml, 35.7mmol) was added to give clear solution. Yellow crystalline solid deposited after standing at 5°C for 3 days. The solid was filtered, washed with methanol (25ml) and dried to give 3.93g of product **13** as single diastereomer (>95%*de*) according to ^{1}H-NMR. Mother liquor was concentrated and left to crystallize for 3 day to give additional amount of the product **13**. Both fractions were combined, stirred with methanol (25ml), filtered and dried to give 4.5g (40% overall yield, at >99% purity according to HPLC) of the dihydrobromide **13** as yellow crystalline solid. Optical rotation of the pure product was -106° (c=1, MeOH, 24°C) which corresponds to literature value $[a]_D$ = -97°.

2-Dehydroisoemetine dihydrobromide **14** could be isolated from mother liquor after second crystallization. Evaporation of the solution to dryness furnished the crude salt **14**, which was then redissolved twice from MeOH with diethyl ether to give 4.7g (41% overall yield) of amorphous solid with 94% purity according to HPLC. Optical rotation of the product was -92° (c=1, MeOH, 24°C) which corresponds to literature value $[a]_D$ = -107°.

- Synthesis of 2,3-dehydroemetine by Chiroblock GMBH, Germany.

ChiroBlock®

ChiroBlock® GmbH, Andreasenstraße 1a, 06766 Wolfen
Tel.: ++49 / 3494 / 63 83 23 Fax: ++49 / 3494 / 63 83 24

Internal Analysis for QC
MS

Sample Information

USF 2973 h2 III

Shimadzu CLASS-VP V6.12 SP5 Area % Report

Acquisition Date: 06.08.2015
Method Name: Z:\Labor\LC\LC-An\LC-An-HPL-01\Methoden\LC-MS\Methoden 210\Iso 20%A, 210nm, 0.2ml, M100
Data Name: Z:\Labor\LC\LC-An\LC-An-HPL-01\LC-MS-Läufe\10001-11000LC+LCMS\10163.lcd
Column: direct injection
Eluents: A) H2O B) acetonitrile
Flow rate: 0.2 ml/min
Detection: UV, 210 nm
Probe voltage: +1,5 kV (APCI-positive mode)

MS Chromatogram
USF 2973 h2 III Z:\Labor\LC\LC-An\LC-An-HPL-01\LC-MS-Läufe\10001-11000LC+LCMS\10163.lcd

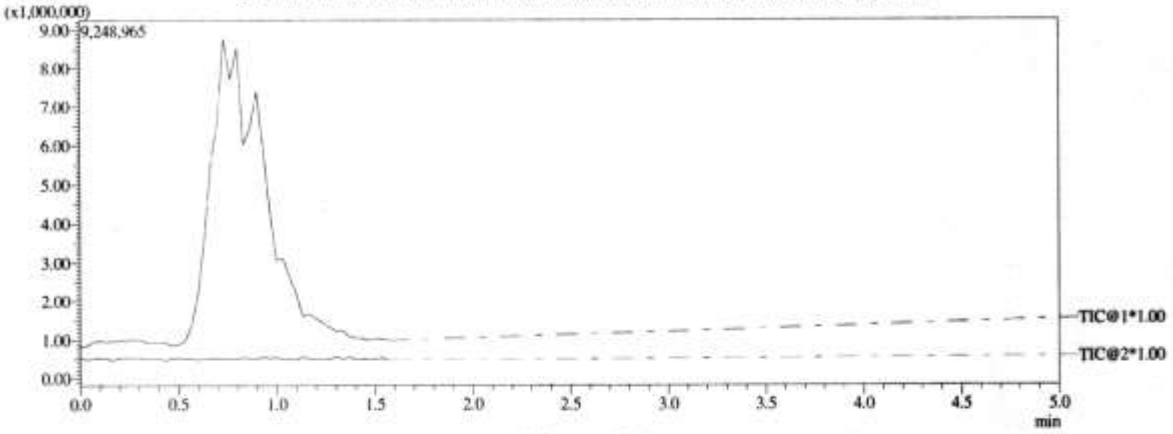

MS Spectrum Graph

#:1 Ret.Time:Averaged 0.567-1.033(Scan#:35-63)
BG Mode:Averaged 0.200-0.308(13-19)
Mass Peaks:1244 Base Peak::476.60(1998930) Polarity:Pos Segment 1 - Event1

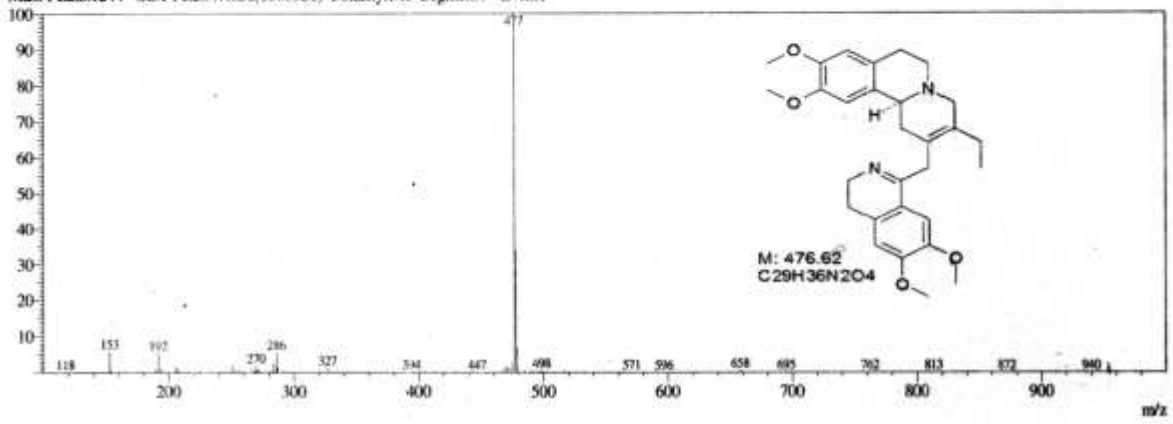

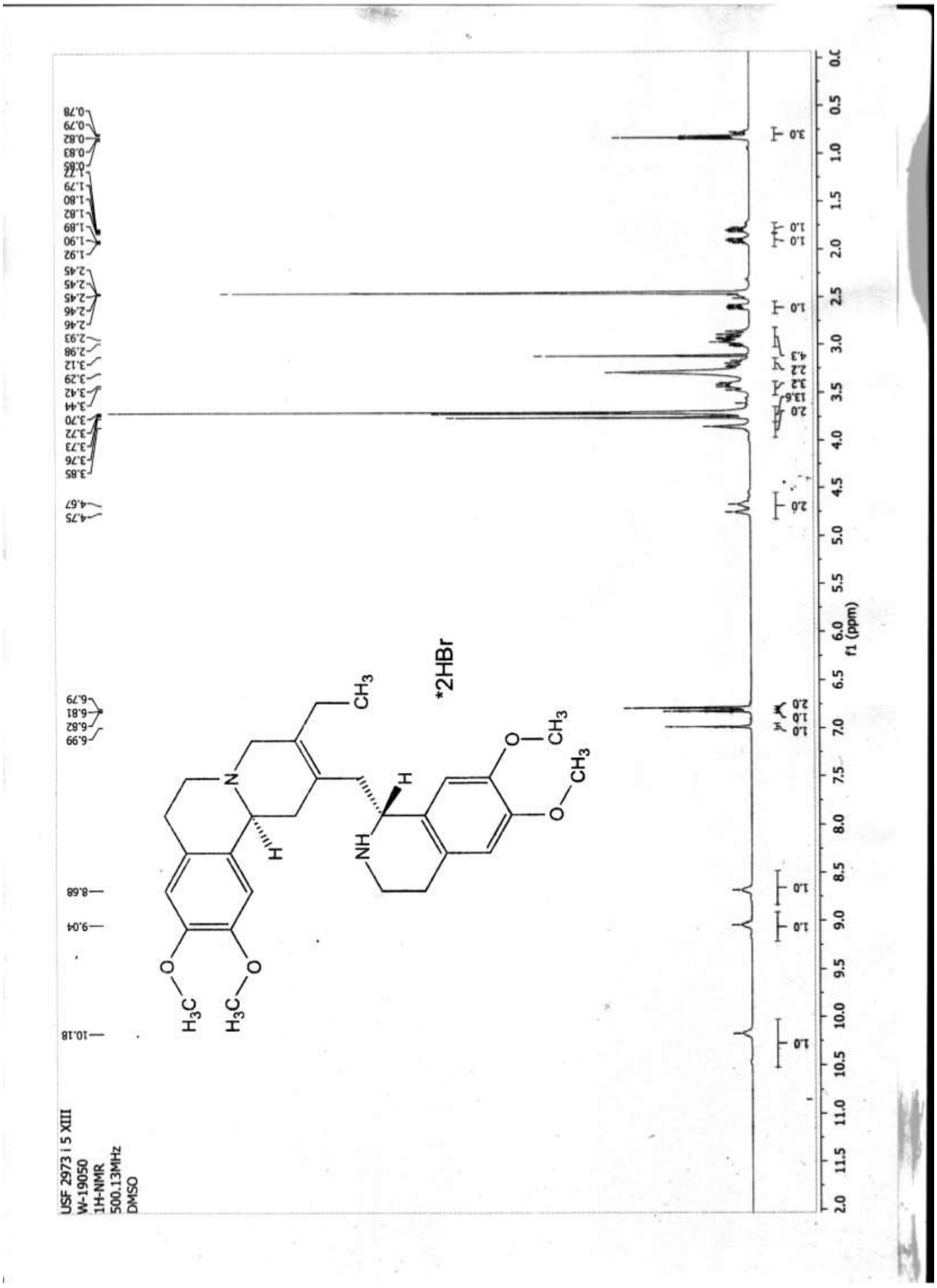
USF 2973 i 5 XIII
W-19050
1H-NMR
500.13MHz
DMSO
*2HBr
f1 (ppm)

ChiroBlock® GmbH, Andresenstraße 1a, 06766 Wolfen
Tel.: ++49 / 3494 / 63 83 23 Fax: ++49 / 3494 / 63 83 24

Internal Analysis for QC
MS

Sample Information

USF 2973 i5 XIII

Shimadzu CLASS-VP V6.12 SP5 Area % Report

Acquisition Date:	01.10.2015
Method Name:	Z:\Labor\LC\LC-An\LC-An-HPL-01\Methoden\LC-MS\Methoden 210\Iso 20%A, 210nm, 0.2ml, M100-
Data Name:	Z:\Labor\LC\LC-An\LC-An-HPL-01\LC-MS-Läufe\10001-11000LC+LCMS\10369.lcd
Column:	direct injection
Eluents:	A) H2O B) acetonitrile
Flow rate:	0.2 ml/min
Detection:	UV, 210 nm
Probe voltage:	+1,5 kV (APCI-positive mode)

MS Chromatogram
USF 2973 i5 XIII Z:\Labor\LC\LC-An\LC-An-HPL-01\LC-MS-Läufe\10001-11000LC+LCMS\10369.lcd

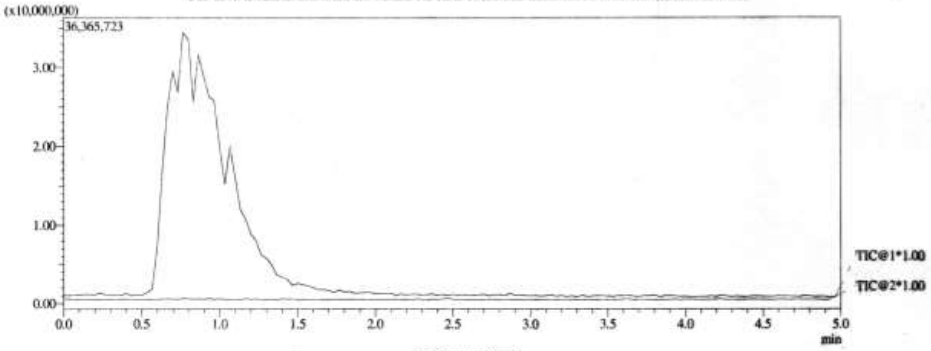

MS Spectrum Graph

#:1 Ret.Time:Averaged 0.567-1.267(Scan#:35-77)
BG Mode:Averaged 0.267-0.553(17-35)
Mass Peaks:1208 Base Peak:478.55(4750790) Polarity:Pos Segment1 - Event1

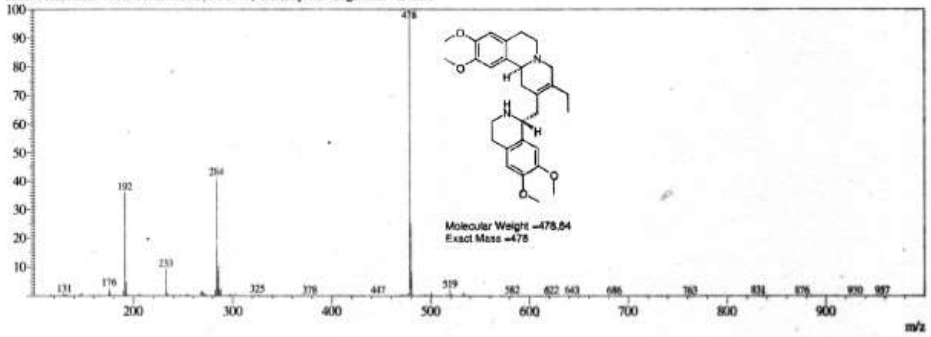

ChiroBlock® GmbH, Andreasstraße 1a, 06766 Wolfen
Tel.: ++49 / 3494 / 63 83 23 Fax: ++49 / 3494 / 63 83 24

Internal Analysis for QC
HPLC 210nm

Sample Information

USF 2973 i5 XIII

Shimadzu CLASS-VP V6.12 SP5 Area % Report
Acquisition Date: 01.10.2015
Method Name: Z:\Labor\LC\LC-An\LC-An-HPL-01\Methoden\LC\Methoden 210\Iso 20%A, 210nm, 1ml, 20min.lcm
Data Name: Z:\Labor\LC\LC-An\LC-An-HPL-01\LC-MS-Läufe\10001-11000LC+LCMS\10368.lcd
Column: YMC Pack Pro C18 150*4.6, 12 nm, S-3µm
Eluents: A) water B) acetonitrile
Flow rate: 1 ml/min
Detection: UV, 210 nm

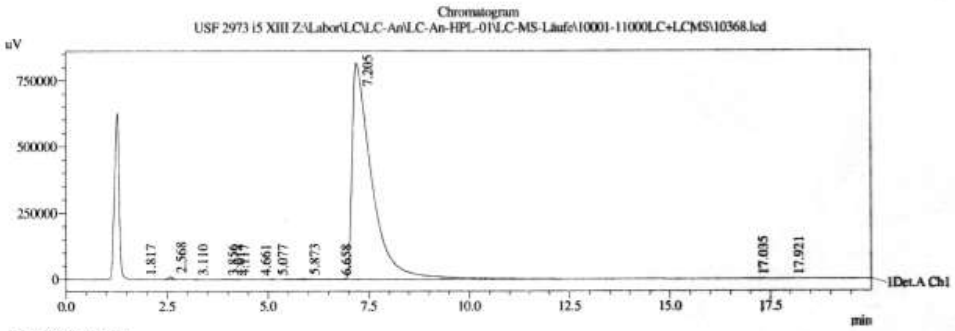

1 Det.A Ch1 / 210nm

PeakTable

Detector A Ch1 210nm

Peak#	Ret. Time	Area	Height	Area %	Height %
1	1.817	3355	477	0.012	0.057
2	2.568	76399	9886	0.274	1.185
3	3.110	4300	677	0.015	0.081
4	3.856	5099	587	0.018	0.070
5	4.014	1543	287	0.006	0.034
6	4.117	3847	289	0.014	0.035
7	4.661	1474	151	0.005	0.018
8	5.077	2671	258	0.010	0.031
9	5.873	51191	2339	0.183	0.280
10	6.658	13115	789	0.047	0.095
11	7.205	27710351	817472	99.259	97.991
12	17.035	24608	665	0.088	0.080
13	17.921	19281	351	0.069	0.042
Total		27917234	834229	100.000	100.000

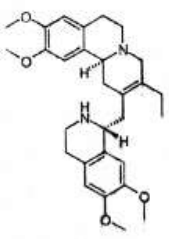

Molecular Weight =478,64
Exact Mass =478

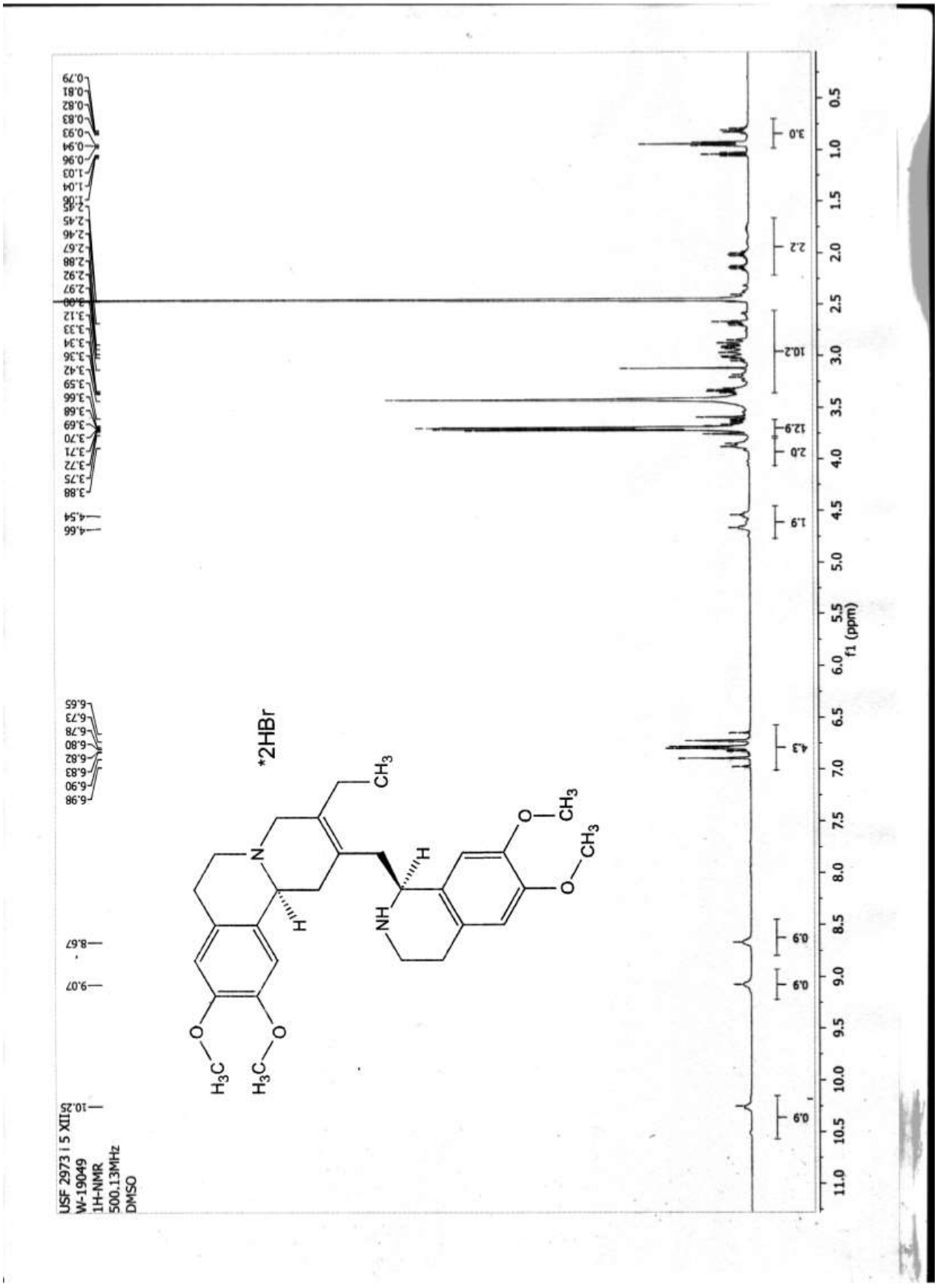
USF 2973 i 5 XIII
W-19049
1H-NMR
500.13MHz
DMSO
*2HBr
f1 (ppm)

ChiroBlock® GmbH, Andreasstraße 1a, 06766 Wolfen
Tel.: ++49 / 3494 / 63 83 23 Fax: ++49 / 3494 / 63 83 24

Internal Analysis for QC
MS

Sample Information

USF 2973 i5 XII

Shimadzu CLASS-VP V6.12 SP5 Area % Report
Acquisition Date: 01.10.2015
Method Name: Z:\Labor\LC\LC-An\LC-An-HPL-01\Methoden\LC-MS\Methoden 210\Iso 20%A, 210nm, 0.2ml, M100
Data Name: Z:\Labor\LC\LC-An\LC-An-HPL-01\LC-MS-Läufe\10001-11000LC+LCMS\10370.lcd
Column: direct injection
Eluents: A) H2O B) acetonitrile
Flow rate: 0.2 ml/min
Detection: UV, 210 nm
Probe voltage: +1,5 kV (APCI-positive mode)

MS Chromatogram
USF 2973 i5 XII Z:\Labor\LC\LC-An\LC-An-HPL-01\LC-MS-Läufe\10001-11000LC+LCMS\10370.lcd

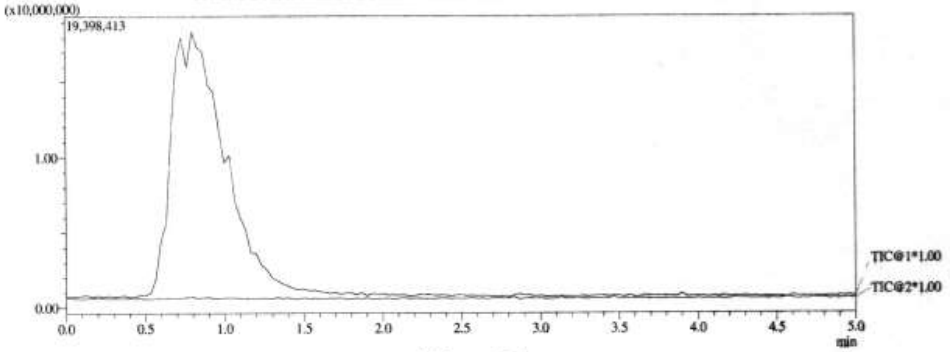

MS Spectrum Graph

#:1 Ret.Time:Averaged 0.533-1.233(Scan#:33-75)
BG Mode:Averaged 0.233-0.388(15-25)
Mass Peaks:1338 Base Peak:478.60(2581001) Polarity:Pos Segment 1 - Event1

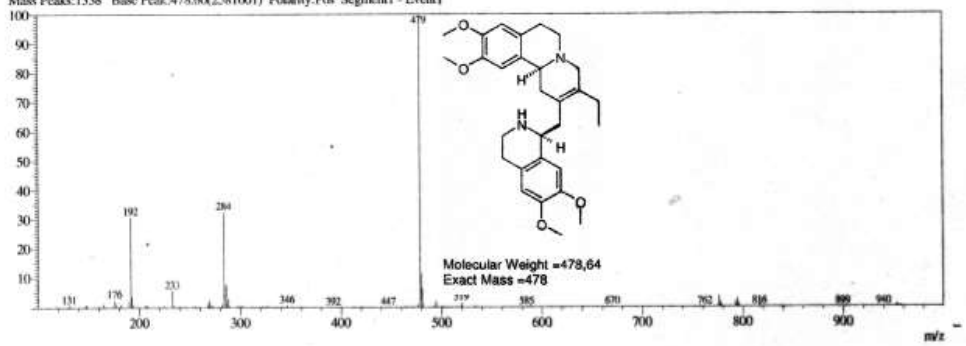

ChiroBlock® GmbH, Andreasstraße 1a, 06766 Wolfen
Tel.: ++49 / 3494 / 63 83 23 Fax: ++49 / 3494 / 63 83 24

Internal Analysis for QC
HPLC 210nm

Sample Information

USF 2973 i5 XII

Shimadzu CLASS-VP V6.12 SP5 Area % Report
Acquisition Date: 01.10.2015
Method Name: Z:\Labor\LC\LC-An\LC-An-HPL-01\Methoden\LC\Methoden 210\Iso 20%A, 210nm, 1ml, 20min.lcm
Data Name: Z:\Labor\LC\LC-An\LC-An-HPL-01\LC-MS-Läufe\10001-11000LC+LCMS\10367.lcd
Column: YMC Pack Pro C18 150*4.6, 12 nm, S-3µm
Eluents: A) water B) acetonitrile
Flow rate: 1 ml/min
Detection: UV, 210 nm

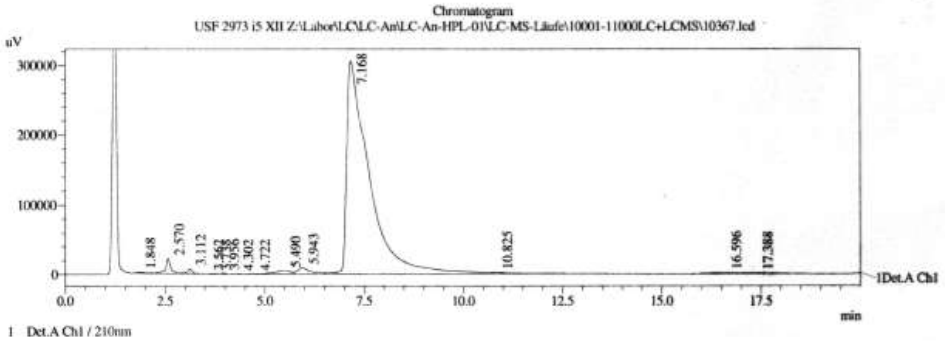

1 Det.A Ch1 / 210nm

PeakTable

Detector A Ch1 210nm

Peak#	Ret. Time	Area	Height	Area %	Height %
1	1.848	21574	1620	0.166	0.456
2	2.570	202383	22157	1.557	6.240
3	3.112	60221	7023	0.463	1.978
4	3.562	1745	204	0.013	0.058
5	3.738	1380	198	0.011	0.056
6	3.956	7995	1102	0.062	0.310
7	4.302	675	109	0.005	0.031
8	4.722	1760	179	0.014	0.050
9	5.490	127297	4505	0.980	1.269
10	5.943	201216	8835	1.548	2.488
11	7.168	12170775	305460	93.652	86.030
12	10.825	5818	373	0.045	0.105
13	16.596	96749	1803	0.744	0.508
14	17.388	96096	1494	0.739	0.421
Total		12995684	355062	100.000	100.000

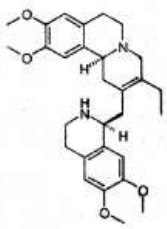

Molecular Weight =478,64
Exact Mass =478

Appendix II

WHO Model Prescribing Information: Drugs Used in Parasitic Diseases - Second Edition
(1995; 152 pages) [French] [Spanish]

Dehydroemetine

Group: antiprotozoal agent
Injection 60 mg of dehydroemetine dihydrochloride in 1-ml ampoule

General information

A derivative of emetine which is less toxic than the parent substance. It is claimed by some to be the most effective tissue amoebicide, but it is too irritant to be taken orally. Following intramuscular injection it is widely distributed in tissues, particularly in the liver and lungs. It is excreted in the urine.

Clinical information

Uses

Amoebic dysentery:

• as an alternative to parenteral metronidazole or other 5-nitroimidazole derivatives in severely ill patients unable to take drugs orally

• following an inadequate response to 5-nitroimidazoles.

Amoebic abscess:

• dehydroemetine is effective when used alone, but it is usually necessary to give a second course 6 weeks later in patients with extensive hepatic abscesses.

Dosage and administration

Adults: 1 mg/kg daily, to a maximum of 60 mg, for up to 4-6 days. This dosage should be reduced by up to 50% in elderly and severely ill patients.

Children: 1 mg/kg daily for no more than 5 days.

Injections should always be given intramuscularly. Intravenous injection is unacceptably dangerous and holds no advantage. At least 6 weeks should elapse before a second course is administered.

In amoebic dysentery, supplementary treatment with tetracycline reduces the risk of bacterial superinfection.

In hepatic abscess, supplementary treatment with chloroquine, which is selectively concentrated in the liver, may be given orally, either concurrently or immediately afterwards.

All patients should subsequently receive dilioxanide by mouth to eliminate surviving organisms in the colon.

Precautions

Dehydroemetine should only be considered as a last resort in patients with preexisting cardiac, renal or neuromuscular disease.

It should always be administered in a hospital setting.

Heart rate and blood pressure should be carefully monitored and treatment should be stopped immediately if tachycardia, severe hypotension or electrocardiographic changes develop.

Weakness and muscular pain frequently precede more serious toxic effects and serve as a warning to reduce dosage.

Use in pregnancy

Dehydroemetine is toxic to the fetus. However, amoebic dysentery may run a fulminating course in late pregnancy, and in this case treatment with dehydroemetine may be life-saving to the mother.

Adverse effects

Local reactions

The injections are painful. Abscess formation is common. A local eczematous rash may follow inadvertent subcutaneous injection. Generalized urticarial and purpuric rashes are rare.

Neuromuscular effects

Weakness and muscular pain are common, particularly in the limbs and neck. Dyspnoea may also occur as a result of generalized weakness. These symptoms are dose-related and often precede evidence of cardiotoxicity.

Cardiac effects

Hypotension, precordial pain, tachycardia and dysrhythmias are the most frequent signs of cardiac impairment. Electrocardiographic changes, particularly flattening and inversion of the T wave and prolongation of the Q-T interval, provide an early indication of toxicity.

Drug interactions

Cardiotoxic effects are potentiated by other drugs liable to cause dysrhythmias.

Storage

Ampoules should not be left exposed to light.

Appendix III

Example of a 72 hours dose response experiment read through plate-reader.

Raw Data

	Atovaquone				(-)-R,S-dehydroemetine				Combination			
Negative	1976	1976	1976	Negative	1976	1976	1976	Negative	1976	1976	1976	
Positive	19892	19892	19892	Positive	19892	19892	19892	Positive	19892	19892	19892	
0.25	20462	20525	20400	12.5	19906	19996	19346	0.25	19387	18250	18818	
0.5	19321	19087	19556	25	20255	20160	20036	0.5	18705	18981	17967	
1	18021	18011	18031	50	18216	18414	18019	1	13832	14737	12928	
2	16387	16367	16377	100	4460	3952	3640	2	3742	3584	3439	
4	5194	5598	4791	200	2578	2617	2605	4	2490	2597	2623	
8	6294	6496	6384	400	2243	2280	2353	8	2215	2271	2189	
16	7008	6308	7707	800	1998	2014	1985	16	1989	2027	1984	

Processed data after subtracting background

Dose				Dose				Dose				
0	17916	17916	17916	0	17916	17916	17916	0	17916	17916	17916	
0.25	18486	18549	18424	12.5	17930	18020	17370	0.25	17411	16274	16842	
0.5	17345	17111	17580	25	18279	18184	18060	0.5	16729	17005	15991	
1	16045	16035	16055	50	16240	16438	16043	1	11856	12761	10952	
2	14411	14391	14401	100	2484	1976	1664	2	1766	1608	1463	
4	3218	3622	2815	200	602	641	629	4	514	621	647	
8	4318	4520	4408	400	267	304	377	8	239	295	213	
16	5032	4332	5731	800	22	38	9	16	13	51	8	

100.00	100.00	100.00		100.00	100.00	100.00		100.00	100.00	100.00	
103.18	103.53	102.84		100.08	100.58	96.95		97.18	90.84	94.01	
96.81	95.51	98.12		102.03	101.50	100.80		93.37	94.92	89.26	
89.56	89.50	89.61		90.65	91.75	89.55		66.18	71.23	61.13	
80.44	80.32	80.38		13.86	11.03	9.29		9.86	8.98	8.17	
17.96	20.22	15.71		3.36	3.58	3.51		2.87	3.47	3.61	
24.10	25.23	24.60		1.49	1.70	2.10		1.33	1.65	1.19	
28.09	24.18	31.99		0.12	0.21	0.05		0.07	0.28	0.04	

Data normalised to percentages

Appendix IV

- Optimisation of rhodamine123 for mitochondrial membrane potential disruption experiment

Rhodamine123 200nM

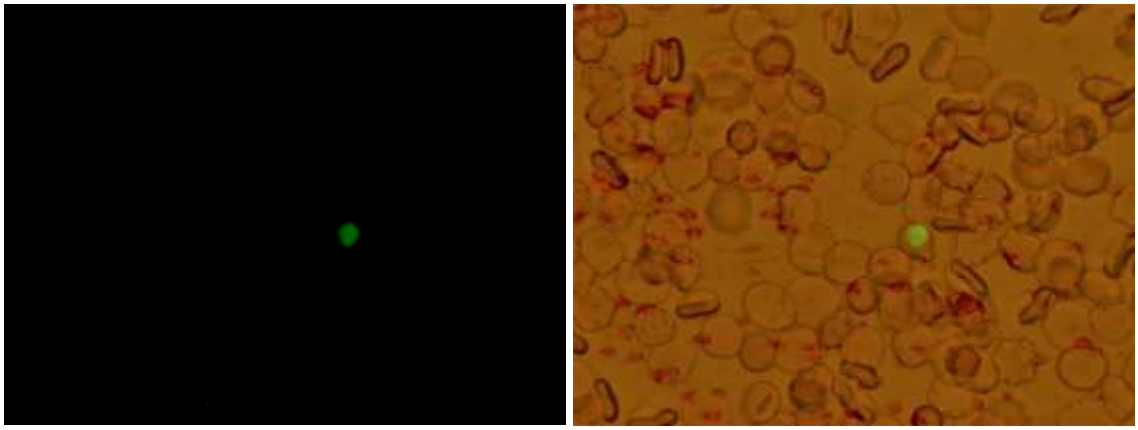

Rhodamine123 500nM

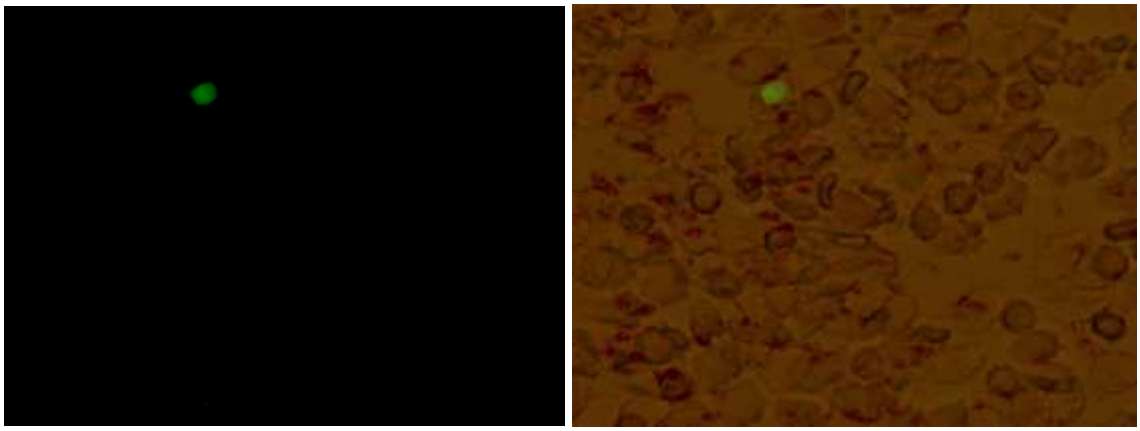

Rhodamine123 1µM

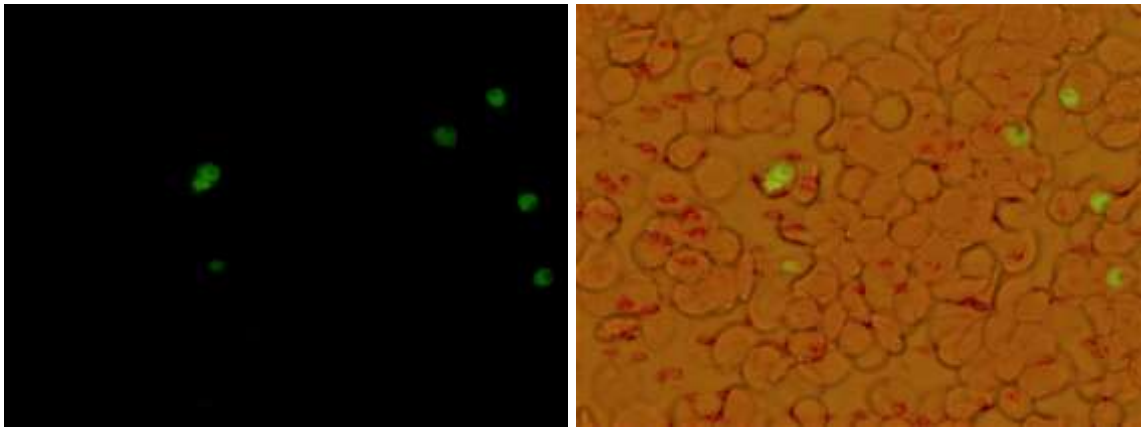

- Gating used for detecting changes in fluorescent intensity of rhodamine123 indicating disruption of mitochondrial membrane potential

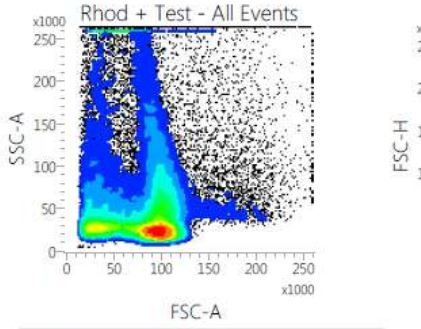

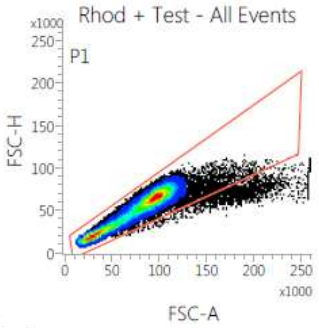

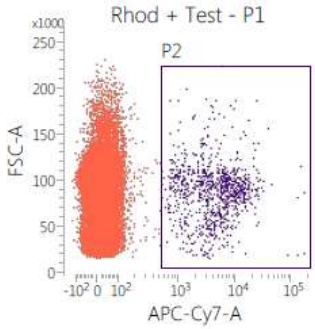

Rhod + Test RunPointerStatistics

Name	All Events	P1	P2
Events	50,000	48,173	883
% Total	100.00	96.35	1.77
FSC-A Mean	82,975	79,066	84,971
SSC-A Mean	76,551	74,421	96,945
FITC-A Mean	292	281	6,126
PE-A Mean	79	76	1,258
PerCP-Cy5.5-A Mean	176	170	1,517
PE-Cy7-A Mean	17	16	416
APC-A Mean	45	44	788
APC-Cy7-A Mean	177	171	8,074
Time Mean	1,011	1,011	1,016

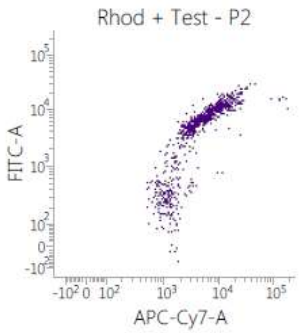

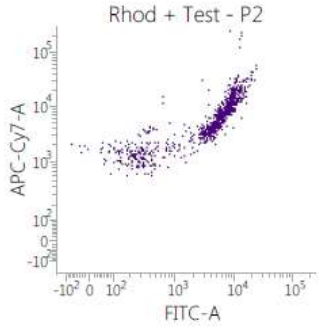

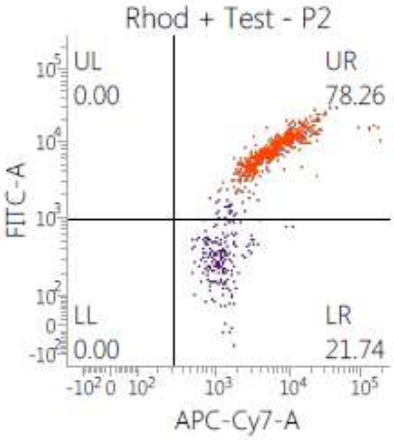

Rhod + Test RunPointerStatistics

Name	All Events	P1	P2	P3
Events	50,000	48,173	883	667
% Total	100.00	96.35	1.77	1.33
FSC-A Mean	82,975	79,066	84,971	84,522
SSC-A Mean	76,551	74,421	96,945	104,101
FITC-A Mean	292	281	6,126	7,858
PE-A Mean	79	76	1,258	1,598
PerCP-Cy5.5-A Mean	176	170	1,517	1,840
PE-Cy7-A Mean	17	16	416	525
APC-A Mean	45	44	788	958
APC-Cy7-A Mean	177	171	8,074	10,009
Time Mean	1,011	1,011	1,016	1,005

Appendix V

- Raw data showing increase in amplitude of 1st calcium transient after addition of (-)-*R,S*-dehydroemetine (circled in blue outline).

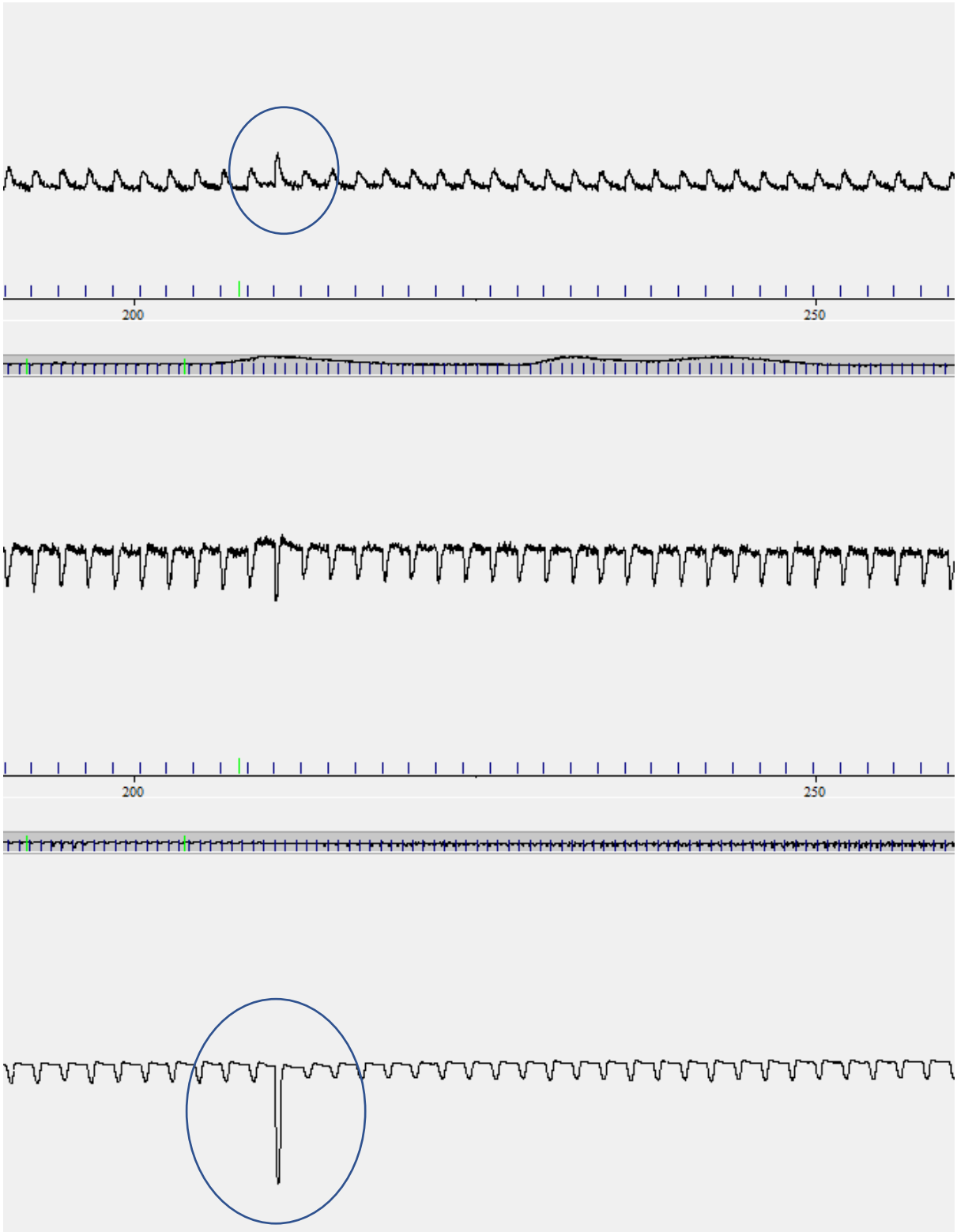

- Long time base raw data showing control caffeine, addition of emetine with increase in amplitude of 1st calcium transient, caffeine during treatment with emetine, wash steady state, and wash caffeine

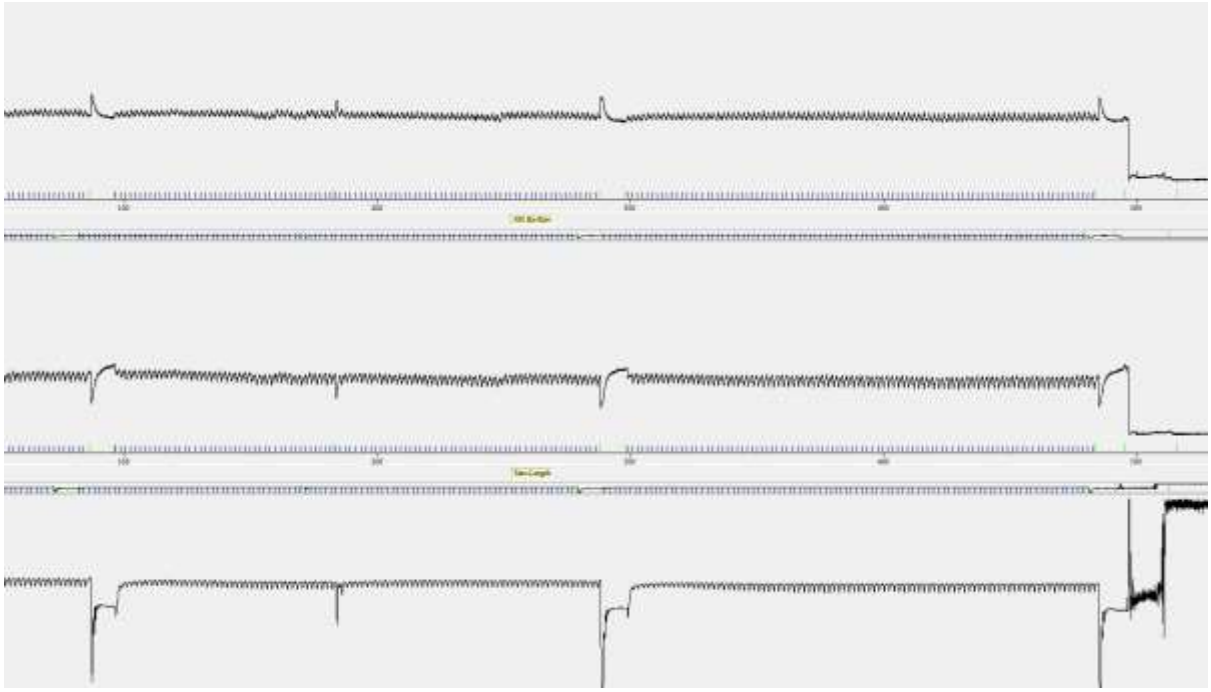

- Raw data showing control and wash caffeine and increase in amplitude of 1st calcium transient after addition of emetine (circled in blue outline).

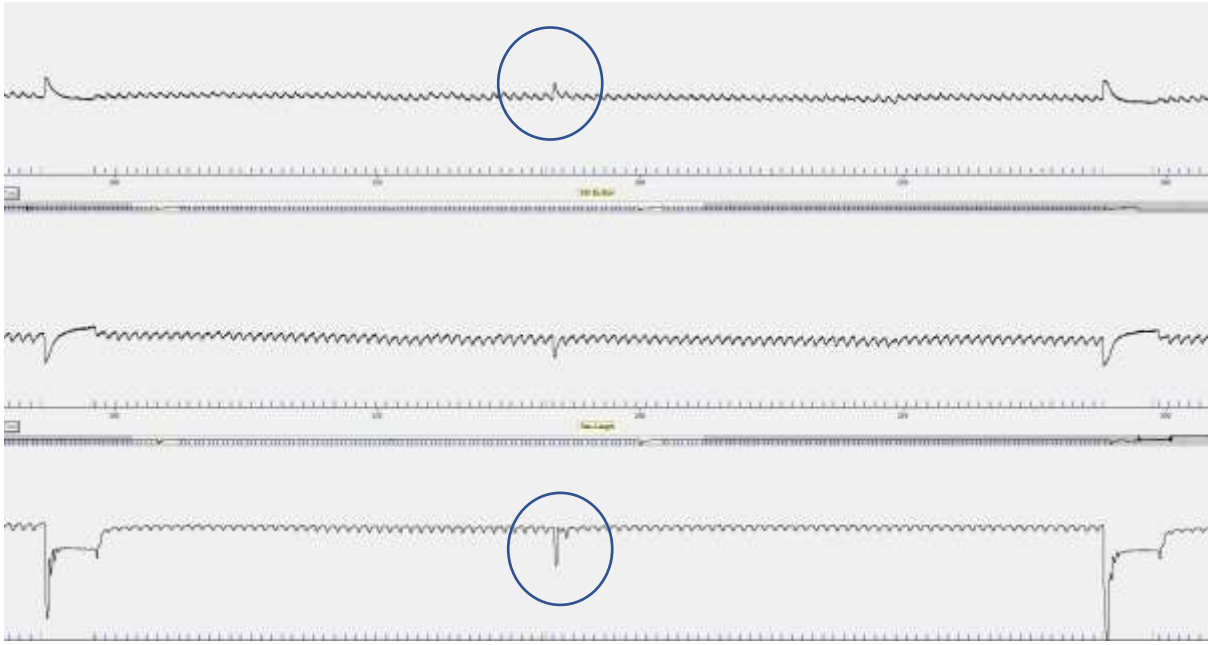

- Example of exported data from the raw data:

	SS Control	DHE			
Time from	210.517	236.238			
Time till	220.279	246.022			
SS Control					
Time 0	Ptnl(V).34	Ptnl(V).38	Time 2	sarc.Sarc Const	
0	1.474	1.449	0	1.817	
0.001	1.473	1.449	0.004	1.817	
0.002	1.473	1.449	0.008	1.817	
0.003	1.473	1.449	0.012	1.817	
0.004	1.473	1.449	0.016	1.817	
0.005	1.474	1.449	0.02	1.817	
0.006	1.473	1.447	0.02406	1.817	
0.007	1.473	1.447	0.028	1.817	
0.008	1.473	1.447	0.032	1.817	
0.009	1.473	1.447	0.036	1.817	
0.01	1.471	1.447	0.04	1.817	
0.011	1.471	1.447	0.044	1.817	
0.012	1.471	1.447	0.048	1.817	
0.013	1.471	1.447	0.052	1.818	
0.014	1.471	1.447	0.056	1.817	
0.015	1.471	1.446	0.06	1.818	
0.016	1.471	1.447	0.064	1.817	
0.017	1.471	1.447	0.068	1.818	
0.018	1.471	1.447	0.072	1.817	
0.019	1.471	1.447	0.076	1.817	
0.02	1.469	1.447	0.08	1.818	
0.021	1.472	1.447	0.084	1.818	
0.022	1.472	1.446	0.088	1.817	
0.023	1.472	1.447	0.092	1.818	
0.024	1.471	1.447	0.096	1.818	
0.025	1.472	1.444	0.1	1.818	
0.026	1.472	1.445	0.104	1.818	
0.027	1.472	1.445	0.108	1.818	
0.028	1.472	1.445	0.112	1.818	

- Example of data sheet used for calculating the effects of emetine and (-)-*R*,*S*-dehydroemetine on calcium regulatory mechanisms:

	Diastolic Ca				
Mean	1	0.99258	0.97149	0.95387	0.94975
SE	0	0.00446	0.00791	0.0167	0.01099
SD	0	0.01609	0.02739	0.02892	0.03477
n	13	13	12	3	10
Cell	SS Contro	1st Beat [SS Drug		1st Beat \ SS Wash	
10 5 18 C2 E	1	0.98945	0.99136		
10 5 18 C8 E	1	0.98418	0.96183	0.95915	0.94659
10 5 18 C6 E	1	1.03088	1.01353		0.89695
10 5 18 C7 E	1	0.98335	0.937		0.91806
14 11 17 C1 E	1	1.00017			
14 11 17 C3 E	1	0.99362	0.95912		
14 11 17 C5 E	1	0.9902	0.92343	0.92267	0.90445
15 5 18 C1 E	1	0.98322	0.96074		0.96347
15 5 18 C4 E	1	1.00804	1.00124		0.97841
15 5 18 C5 E	1	0.98445	0.99697		1.00127
15 5 18 C6 E	1	0.99037	0.98272		0.98272
15 5 18 C10 E	1	0.96255	0.94963		0.9415
16 11 17 C2 E	1	1	0.97979	0.97979	0.96407

	Peak Ca				
	1	1.11048	0.93002	0.9656	0.91133
	0	0.059	0.02563	0.02653	0.04291
	0	0.21272	0.08878	0.04595	0.13569
	13	13	12	3	10
	SS Contro	1st Beat [SS Drug		1st Beat \ SS Wash	
	1	1.01725	0.96859		
	1	0.99258	0.99247	1.01856	0.98512
	1	1.0279	0.70765		0.66631
	1	0.97592	0.90466		0.83839
	1	1.00195			
	1	1.00193	0.97285		
	1	0.99309	0.94801	0.93623	0.93377
	1	1.02	0.92142		1.00733
	1	1.29561	1.00647		1.03498
	1	1.71293	1.00202		1.0718
	1	1.31253	0.98168		1.00481
	1	1.00651	0.80748		0.74248
	1	1.0784	0.94696	0.94201	0.82825

	Ca Amp				
	1	1.42469	0.91287	0.97579	0.92317
	0	0.23899	0.0382	0.04588	0.08035
	0	0.86168	0.13234	0.07946	0.25409
	13	13	12	3	10
	SS Contro	1st Beat [SS Drug		1st Beat \ SS Wash	
	1	1.05633	0.93575		
	1	0.98791	1.0119	1.05623	1.00956
	1	1.02707	0.62306		0.60253
	1	0.96916	0.87526		0.76597
	1	0.99848			
	1	1.01261	0.9921		
	1	1.00107	1.01613	0.97379	1.01496
	1	1.05178	0.88744		1.04522
	1	2.18939	1.01275		1.21079
	1	3.94802	1.01751		1.2882
	1	2.05366	0.97929		1.05564
	1	1.04436	0.68512		0.57116
	1	1.17112	0.90815	0.89734	0.66765

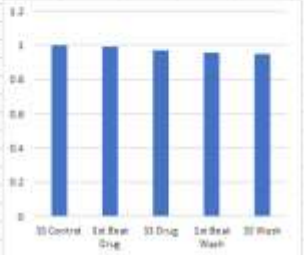

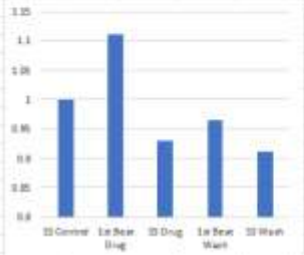

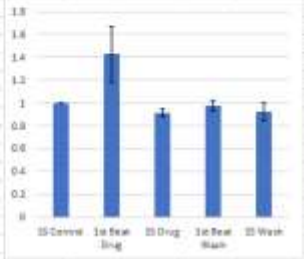

References:

1967. Dehydroemetine. *Drug and Therapeutics Bulletin,* 5**,** 25-26.

2015. *Ecology of Malaria* [Online]. USA. Available: http://www.cdc.gov/malaria/about/biology/ecology.html.

ACHAN, J., TALISUNA, A. O., ERHART, A., YEKA, A., TIBENDERANA, J. K., BALIRAINE, F. N., ROSENTHAL, P. J. & D'ALESSANDRO, U. 2011. Quinine, an old anti-malarial drug in a modern world: role in the treatment of malaria. *Malar J,* 10**,** 144.

ADAM, I., ALI, D. M. & ABDALLA, M. A. 2006. Artesunate plus sulfadoxine-pyrimethamine in the treatment of uncomplicated Plasmodium falciparum malaria during pregnancy in eastern Sudan. *Trans R Soc Trop Med Hyg,* 100**,** 632-5.

AGARWAL, D., GUPTA, R. D. & AWASTHI, S. K. 2017. Are Antimalarial Hybrid Molecules a Close Reality or a Distant Dream? *Antimicrob Agents Chemother,* 61.

AKINBOYE, E. S. & BAKARE, O. 2011. Biological activities of emetine. *The Open Natural Products Journal,* 4**,** 8-15.

AKINBOYE, E. S., BRENNEN, W. N., ROSEN, D. M., BAKARE, O. & DENMEADE, S. R. 2016. Iterative design of emetine‐based prodrug targeting fibroblast activation protein (FAP) and dipeptidyl peptidase IV DPPIV using a tandem enzymatic activation strategy. *The Prostate,* 76**,** 703-714.

AL-KHATEEB, G., AL-JEBOORI, T. & AL-JANABI, K. 1977. In vitro efficacy of some drugs on promastigotes of Leishmania donovani. *Chemotherapy,* 23**,** 267-275.

ALKER, A. P., LIM, P., SEM, R., SHAH, N. K., YI, P., BOUTH, D. M., TSUYUOKA, R., MAGUIRE, J. D., FANDEUR, T. & ARIEY, F. 2007. Pfmdr1 and in vivo resistance to artesunate-mefloquine in falciparum malaria on the Cambodian–Thai border. *The American journal of tropical medicine and hygiene,* 76**,** 641-647.

ALLEN, D. G. & KURIHARA, S. 1980. Calcium transients in mammalian ventricular muscle. *Eur Heart J,* Suppl A**,** 5-15.

ALONSO, H., BLIZNYUK, A. A. & GREADY, J. E. 2006. Combining docking and molecular dynamic simulations in drug design. *Medicinal research reviews,* 26**,** 531-568.

ALONSO, P., L. et al. (2011). A research agenda for malaria eradication: health systems and operational research. *PLoS medicine,* 8**,** e1000397.

ANDERSON, A. C. 2003. The process of structure-based drug design. *Chemistry & biology,* 10**,** 787-797.

ANDERSON, S., BANKIER, A. T., BARRELL, B. G., DE BRUIJN, M. H., COULSON, A. R., DROUIN, J., EPERON, I. C., NIERLICH, D. P., ROE, B. A., SANGER, F., SCHREIER, P. H., SMITH, A. J., STADEN, R. & YOUNG, I. G. 1981. Sequence and organization of the human mitochondrial genome. *Nature,* 290**,** 457-65.

ANDREWS, K. T., FISHER, G. & SKINNER-ADAMS, T. S. 2014. Drug repurposing and human parasitic protozoan diseases. *Int J Parasitol Drugs Drug Resist,* 4**,** 95-111.

ANGER, A. M., ARMACHE, J. P., BERNINGHAUSEN, O., HABECK, M., SUBKLEWE, M., WILSON, D. N. & BECKMANN, R. 2013. Structures of the human and Drosophila 80S ribosome. *Nature,* 497**,** 80-5.

ANYAEHIE, U. 2009. Medicinal properties of fractionated acetone/water neem (Azadirachta indica) leaf extract from Nigeria: a review. *Nigerian journal of physiological sciences,* 24.

AOKI, T., SHIMADA, K., SAKAMOTO, A., SUGIMOTO, K., MORISHITA, T., KOJIMA, Y., SHIMADA, S., KATO, S., IRIYAMA, C., KUNO, S., HARADA, Y., TOMITA, A., HAYAKAWA, F. & KIYOI, H. 2017. Emetine elicits apoptosis of intractable B-cell lymphoma cells with MYC rearrangement through inhibition of glycolytic metabolism. *Oncotarget,* 8**,** 13085-13098.

ARTAVANIS-TSAKONAS, K., TONGREN, J. E. & RILEY, E. M. 2003. The war between the malaria parasite and the immune system: immunity, immunoregulation and immunopathology. *Clinical and Experimental Immunology,* 133**,** 145-152.

ARTZY-RANDRUP, Y., ALONSO, D. & PASCUAL, M. 2010. Transmission intensity and drug resistance in malaria population dynamics: implications for climate change. *PLoS One,* 5**,** e13588.

ASHBURN, T. T. & THOR, K. B. 2004. Drug repositioning: identifying and developing new uses for existing drugs. *Nature reviews Drug discovery,* 3**,** 673-683.

ASHLEY, E. A., DHORDA, M., FAIRHURST, R. M., AMARATUNGA, C., LIM, P., SUON, S., SRENG, S., ANDERSON, J. M., MAO, S. & SAM, B. 2014. Spread of artemisinin resistance in Plasmodium falciparum malaria. *New England Journal of Medicine,* 371**,** 411-423.

BAEK, M. C., JUNG, B., KANG, H., LEE, H. S. & BAE, J. S. 2015. Novel insight into drug repositioning: Methylthiouracil as a case in point. *Pharmacological Research,* 99**,** 185-193.

BAGGISH, A. L. & HILL, D. R. 2002. Antiparasitic agent atovaquone. *Antimicrobial agents and chemotherapy,* 46**,** 1163-1173.

BAIRD, J. K. & HOFFMAN, S. L. 2004. Primaquine therapy for malaria. *Clinical infectious diseases,* 39**,** 1336-1345.

BANIECKI, M. L., WIRTH, D. F. & CLARDY, J. 2007. High-throughput Plasmodium falciparum growth assay for malaria drug discovery. *Antimicrob Agents Chemother,* 51**,** 716-23.

BANSAL, D., SEHGAL, R., CHAWLA, Y., MAHAJAN, R. C. & MALLA, N. 2004. In vitro activity of antiamoebic drugs against clinical isolates of Entamoeba histolytica and Entamoeba dispar. *Annals of Clinical Microbiology and Antimicrobials,* 3**,** 27.

BARRY, A. E. & ARNOTT, A. 2014. Strategies for designing and monitoring malaria vaccines targeting diverse antigens. *Front Immunol,* 5**,** 359.

BARTOLONI, A. & ZAMMARCHI, L. 2012. Clinical aspects of uncomplicated and severe malaria. *Mediterranean journal of hematology and infectious diseases,* 4.

BATTERSBY, A., OPENSHAW, H., BATTERSBY, A., OPENSHAW, H., WOOD, H., EVSTIGNEEVA, R., LIVSHITS, R., ZAKHARKIN, L., BAINOVA, M. & PREOBRAZHENSKII, N. 1953. 6 (1950). *J. Chem. Soc***,** 2463.

BELL, A. 2005. Antimalarial drug synergism and antagonism: mechanistic and clinical significance. *FEMS microbiology letters,* 253**,** 171-184.

BENET, L. Z., HOSEY, C. M., URSU, O., & OPREA, T. I. 2016. BDDCS, the Rule of 5 and drugability. *Advanced drug delivery reviews, 101,* 89–98. doi:10.1016/j.addr.2016.05.007

BERG, J., TYMOCZKO, J. & STRYER, L. 2002. Gluconeogenesis and glycolysis are reciprocally regulated. *Biochemistry*. 5th edition. New York: W H Freeman. Section 16.4

BERRY, M., FIELDING, B. & GAMIELDIEN, J. 2015. Practical considerations in virtual screening and molecular docking. *Emerging Trends in Computational Biology, Bioinformatics, and Systems Biology; Tran, QN, Hamid, AR, Eds***,** 487-502.

BERTANI, S., HOUEL, E., STIEN, D., CHEVOLOT, L., JULLIAN, V., GARAVITO, G., BOURDY, G. & DEHARO, E. 2006. Simalikalactone D is responsible for the

antimalarial properties of an Amazonian traditional remedy made with Quassia amara L.(Simaroubaceae). *Journal of ethnopharmacology,* 108**,** 155-157.

BHATTARAO, A., ALI, A., KACHUR, S., MARTENSSON, A., ABBAS, A., KHATIB, R., AL-MAFAZY, A. & RAMSAN, M. 2007. Rotllant g, Gerstenmaier JF, Molteni F, Abdulla S, Montgomery SM, Kaneko A, Bjorkman A: Impact of artemisinin-based combination therapy and insecticide-treated nets on malaria burden in Zanzibar. *PLoS Med,* 4**,** e309.

BIRKETT, A. J., MOORTHY, V. S., LOUCQ, C., CHITNIS, C. E. & KASLOW, D. C. 2013. Malaria vaccine R&D in the Decade of Vaccines: breakthroughs, challenges and opportunities. *Vaccine,* 31 Suppl 2**,** B233-43.

BLAAZER, A. R., ORRLING, K. M., SHANMUGHAM, A., JANSEN, C., MAES, L., EDINK, E., STERK, G. J., SIDERIUS, M., ENGLAND, P. & BAILEY, D. 2015. Fragment-based screening in tandem with phenotypic screening provides novel antiparasitic hits. *Journal of biomolecular screening,* 20**,** 131-140.

BLASCO, B., LEROY, D. & FIDOCK, D. A. 2017. Antimalarial drug resistance: linking Plasmodium falciparum parasite biology to the clinic. *Nature medicine,* 23**,** 917.

BOGDANOVA, A., MAKHRO, A., WANG, J., LIPP, P. & KAESTNER, L. 2013. Calcium in red blood cells-a perilous balance. *Int J Mol Sci,* 14**,** 9848-72.

BOGUSKI, M. S., MANDL, K. D. & SUKHATME, V. P. 2009. Drug discovery. Repurposing with a difference. *Science,* 324**,** 1394-5.

BOJANG, K., SCHNEIDER, G., FORCK, S., OBARO, S., JAFFAR, S., PINDER, M., ROWLEY, J. & GREENWOOD, B. 1998. A trial of Fansidar® plus chloroquine or Fansidar® alone for the treatment of uncomplicated malaria in Gambian children. *Transactions of the Royal Society of Tropical Medicine and Hygiene,* 92**,** 73-76.

BORAN, A. D. & IYENGAR, R. 2010. Systems approaches to polypharmacology and drug discovery. *Current opinion in drug discovery & development,* 13**,** 297.

BORISY, A. A., ELLIOTT, P. J., HURST, N. W., LEE, M. S., LEHÁR, J., PRICE, E. R., SERBEDZIJA, G., ZIMMERMANN, G. R., FOLEY, M. A. & STOCKWELL, B. R. 2003. Systematic discovery of multicomponent therapeutics. *Proceedings of the National Academy of Sciences,* 100**,** 7977-7982.

BOSCÁ, L. & CORREDOR, C. 1984. Is phosphofructokinase the rate-limiting step of glycolysis? *Trends in Biochemical Sciences,* 9**,** 372-373.

BRICKNELL, O., DARIES, P. & OPIE, L. 1981. A relationship between adenosine triphosphate, glycolysis and ischaemic contracture in the isolated rat heart. *Journal of molecular and cellular cardiology,* 13**,** 941-945.

BRODERSEN, D. E., CLEMONS, W. M., JR., CARTER, A. P., MORGAN-WARREN, R. J., WIMBERLY, B. T. & RAMAKRISHNAN, V. 2000. The structural basis for the action of the antibiotics tetracycline, pactamycin, and hygromycin B on the 30S ribosomal subunit. *Cell,* 103**,** 1143-54.

BROSSI, A., BAUMANN, M., BURKHARDT, F., RICHLE, R. & FREY, J. 1962. Syntheseversuche in der Emetinreihe. 9. Mitteilung. Die absolute Konfiguration von (−) - 2 - Dehydro - emetin. *Helvetica Chimica Acta,* 45**,** 2219-2226.

BROSSI, A., BAUMANN, M., CHOPARD - DIT - JEAN, L., WÜRSCH, J., SCHNEIDER, F. & SCHNIDER, O. 1959a. Syntheseversuche in der Emetin - Reihe. 4. Mitteilung. Racemisches 2 - Dehydro - emetin. *Helvetica Chimica Acta,* 42**,** 772-788.

BROSSI, A., BAUMANN, M. & SCHNIDER, O. 1959b. Syntheseversuche in der Emetin - Reihe. 5. Mitteilung. Eine neue Totalsynthese von Emetin. *Helvetica Chimica Acta,* 42**,** 1515-1522.

BROWN, G. D. 2010. The biosynthesis of artemisinin (Qinghaosu) and the phytochemistry of Artemisia annua L.(Qinghao). *Molecules,* 15**,** 7603-7698.

BRUCE-CHWATT, L. J. 1964. Changing Tides of Chemotherapy of Malaria. *Br Med J,* 1**,** 581-6.

BUCHER, D., GRANT, B. J. & MCCAMMON, J. A. 2011. Induced fit or conformational selection? The role of the semi-closed state in the maltose binding protein. *Biochemistry,* 50**,** 10530-10539.

BURROWS, J. N., LEROY, D., LOTHARIUS, J. & WATERSON, D. 2011. Challenges in antimalarial drug discovery. *Future medicinal chemistry,* 3**,** 1401-1412.

BUTLER, A. R., KHAN, S. & FERGUSON, E. 2010. A brief history of malaria chemotherapy. *J R Coll Physicians Edinb,* 40**,** 172-7.

BYAKIKA-KIBWIKA, P., LAMORDE, M., MAYANJA-KIZZA, H., KHOO, S., MERRY, C. & VAN GEERTRUYDEN, J. P. 2011. Artemether-Lumefantrine Combination Therapy for Treatment of Uncomplicated Malaria: The Potential for Complex Interactions with Antiretroviral Drugs in HIV-Infected Individuals. *Malar Res Treat,* 2011**,** 703730.

CANFIELD, C. J., PUDNEY, M. & GUTTERIDGE, W. E. 1995. Interactions of atovaquone with other antimalarial drugs against Plasmodium falciparum in vitro. *Exp Parasitol,* 80**,** 373-81.

CANNELL, M. B., CHENG, H. & LEDERER, W. J. 1995. The control of calcium release in heart muscle. *Science,* 268**,** 1045-9.

CAPANNA, E. 2006. Grassi versus Ross: who solved the riddle of malaria? *Int Microbiol,* 9**,** 69-74.

CAPDEVILLE, R., BUCHDUNGER, E., ZIMMERMANN, J. & MATTER, A. 2002. Glivec (STI571, imatinib), a rationally developed, targeted anticancer drug. *Nature reviews Drug discovery,* 1**,** 493.

CARTER, R. & MENDIS, K. N. 2002. Evolutionary and historical aspects of the burden of malaria. *Clinical microbiology reviews,* 15**,** 564-594.

CARVALHO, L., ROCHA, E., RASLAN, D., OLIVEIRA, A. D. & KRETTLI, A. 1988. In vitro activity of natural and synthetic naphthoquinones against erythrocytic stages of Plasmodium falciparum. *Brazilian journal of medical and biological research= Revista brasileira de pesquisas medicas e biologicas,* 21**,** 485-487.

CELLIER-HOLZEM, E., ESPARZA-SALAS, R., GARNIER, S. & SORCI, G. 2010. Effect of repeated exposure to Plasmodium relictum (lineage SGS1) on infection dynamics in domestic canaries. *Int J Parasitol,* 40**,** 1447-53.

CERQUEIRA, N., BRAS, N., FERNANDES, P. & RAMOS, M. 2009. MADAMM: a multistaged docking with an automated molecular modeling protocol. *Proteins: Structure, Function, and Bioinformatics,* 74**,** 192-206.

CHANG, C. C., SLAVIN, M. A. & CHEN, S. C. 2017. New developments and directions in the clinical application of the echinocandins. *Arch Toxicol,* 91**,** 1613-1621.

CHATTERJEE, A. K. & YEUNG, B. K. 2012. Back to the future: lessons learned in modern target-based and whole-cell lead optimization of antimalarials. *Curr Top Med Chem,* 12**,** 473-83.

CHENG, H., LEDERER, W. J. & CANNELL, M. B. 1993. Calcium sparks: elementary events underlying excitation-contraction coupling in heart muscle. *Science,* 262**,** 740-4.

CHERNIN, E. 1988. Sir Ronald Ross, malaria, and the rewards of research. *Med Hist,* 32**,** 119-41.

CHIN, W., CONTACOS, P. G., COATNEY, G. R. & KING, H. K. 1966. The evaluation of sulfonamides, alone or in combination with pyrimethamine, in the treatment of multi-

resistant falciparum malaria. *The American journal of tropical medicine and hygiene,* 15**,** 823-829.

CHINTANA, T., SUCHARIT, P., MAHAKITTIKUN, V., SIRIPANTH, C. & SUPHADTANAPHONGS, W. 1986. In vitro studies on the sensitivity of local Entamoeba histolytica to anti-amoebic drugs. *Southeast Asian J Trop Med Public Health,* 17**,** 591-4.

CHONG, C. R., CHEN, X., SHI, L., LIU, J. O. & SULLIVAN, D. J., JR. 2006. A clinical drug library screen identifies astemizole as an antimalarial agent. *Nat Chem Biol,* 2**,** 415-6.

CHOU, T.-C. 2006. Theoretical basis, experimental design, and computerized simulation of synergism and antagonism in drug combination studies. *Pharmacological reviews,* 58**,** 621-681.

CHOU, T.-C. 2010. Drug combination studies and their synergy quantification using the Chou-Talalay method. *Cancer research,* 70**,** 440-446.

CHURCHER et al. 2017. malERA: An updated research agenda for insecticide and drug resistance in malaria elimination and eradication. *PLoS medicine,* 14**,** e1002450.

CIEMNY, M., KURCINSKI, M., KAMEL, K., KOLINSKI, A., ALAM, N., SCHUELER-FURMAN, O. & KMIECIK, S. 2018. Protein–peptide docking: opportunities and challenges. *Drug discovery today*.

CLAPHAM, D. E. 2007. Calcium signaling. *Cell,* 131**,** 1047-1058.

CLAUSSEN, H., BUNING, C., RAREY, M. & LENGAUER, T. 2001. FlexE: efficient molecular docking considering protein structure variations1. *Journal of molecular biology,* 308**,** 377-395.

COOK, G. C. & WEBB, A. J. 2000. Perceptions of malaria transmission before Ross' discovery in 1897. *Postgraduate Medical Journal,* 76**,** 738-740.

CRAFT, J. C. 2008. Challenges facing drug development for malaria. *Curr Opin Microbiol,* 11**,** 428-33.

CROFT, A. M. 2007. A lesson learnt: the rise and fall of Lariam and Halfan. *Journal of the Royal Society of Medicine,* 100**,** 170-174.

CROFT, S. L., DUPARC, S., ARBE-BARNES, S. J., CRAFT, J. C., SHIN, C.-S., FLECKENSTEIN, L., BORGHINI-FUHRER, I. & RIM, H.-J. 2012. Review of pyronaridine anti-malarial properties and product characteristics. *Malaria journal,* 11**,** 270.

CUI, L., MHARAKURWA, S., NDIAYE, D., RATHOD, P. K. & ROSENTHAL, P. J. 2015. Antimalarial drug resistance: literature review and activities and findings of the ICEMR network. *The American journal of tropical medicine and hygiene,* 93**,** 57-68.

CUI, L., MHARAKURWA, S., NDIAYE, D., RATHOD, P. K. & ROSENTHAL, P. J. 2015. Antimalarial Drug Resistance: Literature Review and Activities and Findings of the ICEMR Network. *The American journal of tropical medicine and hygiene***,** 15-0007.

CUI, L. & SU, X. Z. 2009. Discovery, mechanisms of action and combination therapy of artemisinin. *Expert Rev Anti Infect Ther,* 7**,** 999-1013.

CUSHNIE, T. P., O'DRISCOLL, N. H. & LAMB, A. J. 2016. Morphological and ultrastructural changes in bacterial cells as an indicator of antibacterial mechanism of action. *Cell Mol Life Sci,* 73**,** 4471-4492.

DAHL, E. L. & ROSENTHAL, P. J. 2007. Multiple Antibiotics Exert Delayed Effects against the Plasmodium falciparum Apicoplast. *Antimicrobial Agents and Chemotherapy,* 51**,** 3485-3490.

DALLAKYAN, S. & OLSON, A. J. 2015. Small-molecule library screening by docking with PyRx. *Methods Mol Biol,* 1263**,** 243-50.

DASTMALCHI, S. 2016. *Methods and Algorithms for Molecular Docking-based Drug Design and Discovery*, IGI Global.

DATTA, D., SINGH, S. A. & CHHUTTANI, P. 1974. Treatment of amebic liver abscess with emetine hydrochloride, niridazole, and metronidazole. *The American journal of tropical medicine and hygiene,* 23**,** 586-589.

DE BEER, T. A., LOUW, A. I. & JOUBERT, F. 2006. Elucidation of sulfadoxine resistance with structural models of the bifunctional Plasmodium falciparum dihydropterin pyrophosphokinase–dihydropteroate synthase. *Bioorganic & medicinal chemistry,* 14**,** 4433-4443.

DE STEFANI, D., RAFFAELLO, A., TEARDO, E., SZABO, I. & RIZZUTO, R. 2011. A forty-kilodalton protein of the inner membrane is the mitochondrial calcium uniporter. *Nature,* 476**,** 336-40.

DEMPSEY, J. J. & SALEM, H. H. 1966. An enzymatic electrocardiographic study on toxicity of dehydroemetine. *Br Heart J,* 28**,** 505-11.

DESAI, S. A., MCCLESKEY, E. W., SCHLESINGER, P. H. & KROGSTAD, D. J. 1996. A novel pathway for Ca++ entry into Plasmodium falciparum-infected blood cells. *Am J Trop Med Hyg,* 54**,** 464-70.

DINOS, G., WILSON, D. N., TERAOKA, Y., SZAFLARSKI, W., FUCINI, P., KALPAXIS, D. & NIERHAUS, K. H. 2004. Dissecting the ribosomal inhibition mechanisms of edeine and pactamycin: the universally conserved residues G693 and C795 regulate P-site RNA binding. *Mol Cell,* 13**,** 113-24.

DJIMDÉ, A., DOUMBO, O. K., CORTESE, J. F., KAYENTAO, K., DOUMBO, S., DIOURTÉ, Y., COULIBALY, D., DICKO, A., SU, X.-Z. & NOMURA, T. 2001. A molecular marker for chloroquine-resistant falciparum malaria. *New England journal of medicine,* 344**,** 257-263.

DONDORP, A. M., SMITHUIS, F. M., WOODROW, C. & VON SEIDLEIN, L. 2017. How to contain artemisinin-and multidrug-resistant falciparum malaria. *Trends in parasitology,* 33**,** 353-363.

DONDORP, A. M., YEUNG, S., WHITE, L., NGUON, C., DAY, N. P., SOCHEAT, D. & VON SEIDLEIN, L. 2010. Artemisinin resistance: current status and scenarios for containment. *Nature Reviews Microbiology,* 8**,** 272.

DREWS, J. 2000. Drug discovery: a historical perspective. *Science,* 287**,** 1960-1964.

DU, X., LI, Y., XIA, Y.-L., AI, S.-M., LIANG, J., SANG, P., JI, X.-L. & LIU, S.-Q. 2016. Insights into protein–ligand interactions: mechanisms, models, and methods. *International journal of molecular sciences,* 17**,** 144.

DUFFY, P. E., SAHU, T., AKUE, A., MILMAN, N. & ANDERSON, C. 2012. Pre-erythrocytic malaria vaccines: identifying the targets. *Expert Rev Vaccines,* 11**,** 1261-80.

DUNKER, A. K., GARNER, E., GUILLIOT, S., ROMERO, P., ALBRECHT, K., HART, J., OBRADOVIC, Z., KISSINGER, C. & VILLAFRANCA, J. E. Protein disorder and the evolution of molecular recognition: theory, predictions and observations. Pac Symp Biocomput, 1998. 473-484.

EISNER, D. A., CALDWELL, J. L., KISTAMAS, K. & TRAFFORD, A. W. 2017. Calcium and Excitation-Contraction Coupling in the Heart. *Circ Res,* 121**,** 181-195.

EISNER, D. A., CHOI, H. S., DIAZ, M. E., O'NEILL, S. C. & TRAFFORD, A. W. 2000. Integrative analysis of calcium cycling in cardiac muscle. *Circ Res,* 87**,** 1087-94.

EKINS, S., MESTRES, J. & TESTA, B. 2007. In silico pharmacology for drug discovery: methods for virtual ligand screening and profiling. *British journal of pharmacology,* 152**,** 9-20.

EKSI, S. & WILLIAMSON, K. C. 2011. Protein targeting to the parasitophorous vacuole membrane of Plasmodium falciparum. *Eukaryot Cell,* 10**,** 744-52.

ELLIS-PEGLER, R. B., BEECHING, N. J., EALES, M., FRASER, A. G. & WELLS, A. U. 1988. Fansimef [Fansidar plus mefloquine] is effective treatment for imported malaria in New Zealand. *Aust N Z J Med,* 18**,** 733-4.

ENOMOTO, M., KAWAZU, S., KAWAI, S., FURUYAMA, W., IKEGAMI, T., WATANABE, J. & MIKOSHIBA, K. 2012. Blockage of spontaneous Ca2+ oscillation causes cell death in intraerythrocitic Plasmodium falciparum. *PLoS One,* 7**,** e39499.

ERNSTER, L. & SCHATZ, G. 1981. Mitochondria: a historical review. *J Cell Biol,* 91**,** 227s-255s.

FARROW, R. E., GREEN, J., KATSIMITSOULIA, Z., TAYLOR, W. R., HOLDER, A. A. & MOLLOY, J. E. 2011. The mechanism of erythrocyte invasion by the malarial parasite, Plasmodium falciparum. *Semin Cell Dev Biol,* 22**,** 953-60.

FATUMO, S., PLAIMAS, K., MALLM, J. P., SCHRAMM, G., ADEBIYI, E., OSWALD, M., EILS, R. & KONIG, R. 2009. Estimating novel potential drug targets of Plasmodium falciparum by analysing the metabolic network of knock-out strains in silico. *Infect Genet Evol,* 9**,** 351-8.

FAWAZ, G. & FIESER, L. F. 1950. Naphthoquinone antimalarials. XXIV. A new synthesis of lapinone. *Journal of the American Chemical Society,* 72**,** 996-1000.

FEALA, J. D., CORTES, J., DUXBURY, P. M., PIERMAROCCHI, C., MCCULLOCH, A. D. & PATERNOSTRO, G. 2010. Systems approaches and algorithms for discovery of combinatorial therapies. *Wiley Interdisciplinary Reviews: Systems Biology and Medicine,* 2**,** 181-193.

FEIG, M., ONUFRIEV, A., LEE, M. S., IM, W., CASE, D. A. & BROOKS III, C. L. 2004. Performance comparison of generalized born and Poisson methods in the calculation of electrostatic solvation energies for protein structures. *Journal of computational chemistry,* 25**,** 265-284.

FENG, L., LUO, X., ZHOU, Y., GUO, X. & LI, G. 2016. Fast elimination of malaria by infectious source eradication with artemisinin-based compound. *Sci China Life Sci,* 59**,** 78-80.

FERMINI, B., HANCOX, J. C., ABI-GERGES, N., BRIDGLAND-TAYLOR, M., CHAUDHARY, K. W., COLATSKY, T., CORRELL, K., CRUMB, W., DAMIANO, B. & ERDEMLI, G. 2016. A new perspective in the field of cardiac safety testing through the comprehensive in vitro proarrhythmia assay paradigm. *Journal of biomolecular screening,* 21**,** 1-11.

FERREIRA, L., DOS SANTOS, R., OLIVA, G. & ANDRICOPULO, A. 2015. Molecular docking and structure-based drug design strategies. *Molecules,* 20**,** 13384-13421.

FERRI, F. F. 2009. *Ferri's color atlas and text of clinical medicine,* Philadelphia, PA, Saunders/Elsevier.

FIDOCK, D. A., EASTMAN, R. T., WARD, S. A. & MESHNICK, S. R. 2008. Recent highlights in antimalarial drug resistance and chemotherapy research. *Trends Parasitol,* 24**,** 537-44.

FIDOCK, D. A., ROSENTHAL, P. J., CROFT, S. L., BRUN, R. & NWAKA, S. 2004. Antimalarial drug discovery: efficacy models for compound screening. *Nat Rev Drug Discov,* 3**,** 509-20.

FINK, H. A., MAC DONALD, R., RUTKS, I. R., NELSON, D. B. & WILT, T. J. 2002. Sildenafil for male erectile dysfunction: a systematic review and meta-analysis. *Arch Intern Med,* 162**,** 1349-60.

FLORENS, L., WASHBURN, M. P., RAINE, J. D., ANTHONY, R. M., GRAINGER, M., HAYNES, J. D., MOCH, J. K., MUSTER, N., SACCI, J. B., TABB, D. L., WITNEY, A. A., WOLTERS, D., WU, Y., GARDNER, M. J., HOLDER, A. A., SINDEN, R. E., YATES, J. R. & CARUCCI, D. J. 2002. A proteomic view of the Plasmodium falciparum life cycle. *Nature,* 419**,** 520-6.

FOLB, P. & TROUNCE, J. 1970. Drugs Used in Tropical Medicine. *A Guide to Drugs in Current Use.* Springer.

FONG, K. Y., SANDLIN, R. D. & WRIGHT, D. W. 2015. Identification of beta-hematin inhibitors in the MMV Malaria Box. *Int J Parasitol Drugs Drug Resist,* 5**,** 84-91.

FONG, K. Y. & WRIGHT, D. W. 2013. Hemozoin and antimalarial drug discovery. *Future medicinal chemistry,* 5**,** 1437-1450.

FOREMAN, K., JESSE, J. & GUPTA, G. 2013. 599 EMETINE DIHYDROCHLORIDE: A NOVEL THERAPY FOR BLADDER UROTHELIAL CARCINOMA. *The Journal of Urology,* 189**,** e245.

FORLI, S., HUEY, R., PIQUE, M. E., SANNER, M. F., GOODSELL, D. S. & OLSON, A. J. 2016. Computational protein–ligand docking and virtual drug screening with the AutoDock suite. *Nature protocols,* 11**,** 905.

FOUARGE, M., DEWULFT, M., COUVREUR, P., ROLAND, M. & VRANCKX, H. 1989. Development of dehydroemetine nanoparticles for the treatment of visceral leishmaniasis. *Journal of microencapsulation,* 6**,** 29-34.

FRANCO-PAREDES, C. & SANTOS-PRECIADO, J. I. 2006. Problem pathogens: prevention of malaria in travellers. *The Lancet infectious diseases,* 6**,** 139-149.

FREARSON, J. A., WYATT, P. G., GILBERT, I. H. & FAIRLAMB, A. H. 2007. Target assessment for antiparasitic drug discovery. *Trends Parasitol,* 23**,** 589-95.

FREVERT, U., SPÄTH, G. F. & YEE, H. 2008. Exoerythrocytic development of Plasmodium gallinaceum in the White Leghorn chicken. *Int J Parasitol,* 38**,** 655-72.

FRIEDMAN, J. R. & NUNNARI, J. 2014. Mitochondrial form and function. *Nature,* 505**,** 335-43.

FRIESNER, R. A., MURPHY, R. B., REPASKY, M. P., FRYE, L. L., GREENWOOD, J. R., HALGREN, T. A., SANSCHAGRIN, P. C. & MAINZ, D. T. 2006. Extra precision glide: Docking and scoring incorporating a model of hydrophobic enclosure for protein− ligand complexes. *Journal of medicinal chemistry,* 49**,** 6177-6196.

FRY, C. H. & JABR, R. I. 2010. The action potential and nervous conduction. *Surgery (Oxford),* 28**,** 49-54.

FURUYAMA, W., ENOMOTO, M., MOSSAAD, E., KAWAI, S., MIKOSHIBA, K. & KAWAZU, S. 2014. An interplay between 2 signaling pathways: melatonin-cAMP and IP3-Ca2+ signaling pathways control intraerythrocytic development of the malaria parasite Plasmodium falciparum. *Biochem Biophys Res Commun,* 446**,** 125-31.

GALLUP, J. L. & SACHS, J. D. 2001. The economic burden of malaria. *The American journal of tropical medicine and hygiene,* 64**,** 85-96.

GAMO, F. J., SANZ, L. M., VIDAL, J., DE COZAR, C., ALVAREZ, E., LAVANDERA, J. L., VANDERWALL, D. E., GREEN, D. V., KUMAR, V., HASAN, S., BROWN, J. R., PEISHOFF, C. E., CARDON, L. R. & GARCIA-BUSTOS, J. F. 2010. Thousands of chemical starting points for antimalarial lead identification. *Nature,* 465**,** 305-10.

GARDNER, M. J., HALL, N., FUNG, E., WHITE, O., BERRIMAN, M., HYMAN, R. W., CARLTON, J. M., PAIN, A., NELSON, K. E., BOWMAN, S., PAULSEN, I. T., JAMES, K., EISEN, J. A., RUTHERFORD, K., SALZBERG, S. L., CRAIG, A., KYES, S., CHAN, M. S., NENE, V., SHALLOM, S. J., SUH, B., PETERSON, J., ANGIUOLI, S., PERTEA, M., ALLEN, J., SELENGUT, J., HAFT, D., MATHER,

M. W., VAIDYA, A. B., MARTIN, D. M., FAIRLAMB, A. H., FRAUNHOLZ, M. J., ROOS, D. S., RALPH, S. A., MCFADDEN, G. I., CUMMINGS, L. M., SUBRAMANIAN, G. M., MUNGALL, C., VENTER, J. C., CARUCCI, D. J., HOFFMAN, S. L., NEWBOLD, C., DAVIS, R. W., FRASER, C. M. & BARRELL, B. 2002. Genome sequence of the human malaria parasite Plasmodium falciparum. *Nature,* 419**,** 498-511.

GAUR, R., PATHANIA, A. S., MALIK, F. A., BHAKUNI, R. S. & VERMA, R. K. 2016. Synthesis of a series of novel dihydroartemisinin monomers and dimers containing chalcone as a linker and their anticancer activity. *European journal of medicinal chemistry,* 122**,** 232-246.

GAZARINI, M. L., THOMAS, A. P., POZZAN, T. & GARCIA, C. R. 2003. Calcium signaling in a low calcium environment: how the intracellular malaria parasite solves the problem. *J Cell Biol,* 161**,** 103-10.

GEBHARD, M., DENKHAUS, H., SAKAI, K. & SPIECKERMANN, P. 1977. ENERGY-METABOLISM AND ENZYME-RELEASE. *Journal of Molecular Medicine,* 2**,** 271-283.

GELB, M. H. 2007. Drug discovery for malaria: a very challenging and timely endeavor. *Curr Opin Chem Biol,* 11**,** 440-5.

GELBAND, H., PANOSIAN, C. B. & ARROW, K. J. 2004. *Saving lives, buying time: economics of malaria drugs in an age of resistance,* National Academies Press.

GHANA, K. 2017. Malawi to take part in WHO malaria vaccine pilot programme. *Geneva: World Health Organization*.

GILBERT, I. H. 2013. Drug discovery for neglected diseases: molecular target-based and phenotypic approaches. *J Med Chem,* 56**,** 7719-26.

GINSBURG, G. S. & MCCARTHY, J. J. 2001. Personalized medicine: revolutionizing drug discovery and patient care. *TRENDS in Biotechnology,* 19**,** 491-496.

GLASER, R. 1983. Clinical aspects of herpes zoster. *Western Journal of Medicine,* 139**,** 718.

GOESSLING, W. & CHUNG, R. T. 2002. Amebic liver abscess. *Current treatment options in gastroenterology,* 5**,** 443-449.

GOLDMAN, B. B. & WIPKE, W. T. 2000. QSD quadratic shape descriptors. 2. Molecular docking using quadratic shape descriptors (QSDock). *Proteins: Structure, Function, and Bioinformatics,* 38**,** 79-94.

GRANT, J. A., GALLARDO, M. & PICKUP, B. T. 1996. A fast method of molecular shape comparison: A simple application of a Gaussian description of molecular shape. *Journal of computational chemistry,* 17**,** 1653-1666.

GRAY, J. J. 2006. High-resolution protein–protein docking. *Current opinion in structural biology,* 16**,** 183-193.

GRAY, M. W. 2012. Mitochondrial evolution. *Cold Spring Harb Perspect Biol,* 4**,** a011403.

GREENSMITH, D. J. 2014. Ca analysis: an Excel based program for the analysis of intracellular calcium transients including multiple, simultaneous regression analysis. *Comput Methods Programs Biomed,* 113**,** 241-50.

GREENSMITH, D. J., EISNER, D. A. & NIRMALAN, M. 2010. The effects of hydrogen peroxide on intracellular calcium handling and contractility in the rat ventricular myocyte. *Cell Calcium,* 48**,** 341-51.

GREENSMITH, D. J., GALLI, G. L., TRAFFORD, A. W. & EISNER, D. A. 2014. Direct measurements of SR free Ca reveal the mechanism underlying the transient effects of RyR potentiation under physiological conditions. *Cardiovasc Res,* 103**,** 554-63.

GREENWOOD, B. M., FIDOCK, D. A., KYLE, D. E., KAPPE, S. H., ALONSO, P. L., COLLINS, F. H. & DUFFY, P. E. 2008. Malaria: progress, perils, and prospects for eradication. *The Journal of clinical investigation,* 118**,** 1266-1276.

GREER, J., ERICKSON, J. W., BALDWIN, J. J. & VARNEY, M. D. 1994. Application of the three-dimensional structures of protein target molecules in structure-based drug design. *Journal of medicinal chemistry,* 37**,** 1035-1054.

GREGSON, A. & PLOWE, C. V. 2005. Mechanisms of resistance of malaria parasites to antifolates. *Pharmacological reviews,* 57**,** 117-145.

GRIBBLE, F. M., DAVIS, T. M., HIGHAM, C. E., CLARK, A. & ASHCROFT, F. M. 2000. The antimalarial agent mefloquine inhibits ATP‐sensitive K‐channels. *British journal of pharmacology,* 131**,** 756-760.

GRIMBERG, B. T. & MEHLOTRA, R. K. 2011. Expanding the Antimalarial Drug Arsenal-Now, But How? *Pharmaceuticals (Basel),* 4**,** 681-712.

GROLLMAN, A. P. 1966. Structural Basis for Inhibition of Protein Synthesis by Emetine and Cycloheximide Based on an Analogy between Ipecac Alkaloids and Glutarimide Antibiotics. *Proceedings of the National Academy of Sciences of the United States of America,* 56**,** 1867-&.

GROSSMAN, G. L., RAFFERTY, C. S., CLAYTON, J. R., STEVENS, T. K., MUKABAYIRE, O. & BENEDICT, M. Q. 2001. Germline transformation of the malaria vector, Anopheles gambiae, with the piggyBac transposable element. *Insect Mol Biol,* 10**,** 597-604.

GRÜNBERG, R., LECKNER, J. & NILGES, M. 2004. Complementarity of structure ensembles in protein-protein binding. *Structure,* 12**,** 2125-2136.

GUBERNATOR, K. & BÖHM, H. 1998. 2 Examples of Active Areas of Structure Based-Design. *Structure-based Ligand Design*.

GUERIN, P. J., OLLIARO, P., NOSTEN, F., DRUILHE, P., LAXMINARAYAN, R., BINKA, F., KILAMA, W. L., FORD, N. & WHITE, N. J. 2002. Malaria: current status of control, diagnosis, treatment, and a proposed agenda for research and development. *The Lancet infectious diseases,* 2**,** 564-573.

GUIGUEMDE, W. A., SHELAT, A. A., GARCIA-BUSTOS, J. F., DIAGANA, T. T., GAMO, F. J. & GUY, R. K. 2012. Global phenotypic screening for antimalarials. *Chem Biol,* 19**,** 116-29.

GÜNER, O. F. 2000. *Pharmacophore perception, development, and use in drug design*, Internat'l University Line.

GUPTA, R. S. & SIMINOVITCH, L. 1977. Mutants of CHO cells resistant to the protein synthesis inhibitors, cryptopleurine and tylocrebrine: genetic and biochemical evidence for common site of action of emetine, cryptopleurine, tylocrebrine, and tubulosine. *Biochemistry,* 16**,** 3209-3214.

HALPERIN, I., MA, B., WOLFSON, H. & NUSSINOV, R. 2002. Principles of docking: An overview of search algorithms and a guide to scoring functions. *Proteins: Structure, Function, and Bioinformatics,* 47**,** 409-443.

HAN, Y., PARK, S., KINYUA, A. W., ANDERA, L., KIM, K. W. & KIM, I. 2014. Emetine enhances the tumor necrosis factor-related apoptosis-inducing ligand-induced apoptosis of pancreatic cancer cells by downregulation of myeloid cell leukemia sequence-1 protein. *Oncology reports,* 31**,** 456-462.

HANBOONKUNUPAKARN, B. & WHITE, N. J. 2016. The threat of antimalarial drug resistance. *Tropical diseases, travel medicine and vaccines,* 2**,** 10.

HARASYM, T. O., LIBOIRON, B. D. & MAYER, L. D. 2010. Drug ratio-dependent antagonism: a new category of multidrug resistance and strategies for its circumvention. *Multi-Drug Resistance in Cancer***,** 291-323.

HARVEY, K. L., GILSON, P. R. & CRABB, B. S. 2012. A model for the progression of receptor-ligand interactions during erythrocyte invasion by Plasmodium falciparum. *Int J Parasitol,* 42**,** 567-73.

HASIN, Y. & BARRY, W. H. 1984. Myocardial metabolic inhibition and membrane potential, contraction, and potassium uptake. *American Journal of Physiology-Heart and Circulatory Physiology,* 247**,** H322-H329.

HAYASHI, T., RIZZUTO, R., HAJNOCZKY, G. & SU, T. P. 2009. MAM: more than just a housekeeper. *Trends Cell Biol,* 19**,** 81-8.

HEDLEY, P. L., JØRGENSEN, P., SCHLAMOWITZ, S., WANGARI, R., MOOLMAN‐SMOOK, J., BRINK, P. A., KANTERS, J. K., CORFIELD, V. A. & CHRISTIANSEN, M. 2009. The genetic basis of long QT and short QT syndromes: a mutation update. *Human mutation,* 30**,** 1486-1511.

HEINBERG, A. & KIRKMAN, L. 2015. The molecular basis of antifolate resistance in Plasmodium falciparum: looking beyond point mutations. *Annals of the New York Academy of Sciences,* 1342**,** 10-18.

HELLGREN, U., ERICSSON, O., ADENABDI, Y. & GUSTAFSSON, L. L. 2014. *Handbook of drugs for tropical parasitic infections,* CRC Press.

HEMPELMANN, E. 2007. Hemozoin biocrystallization in Plasmodium falciparum and the antimalarial activity of crystallization inhibitors. *Parasitology research,* 100**,** 671-676.

HENRY, M., ALIBERT, S., ORLANDI-PRADINES, E., BOGREAU, H., FUSAI, T., ROGIER, C., BARBE, J. & PRADINES, B. 2006. Chloroquine resistance reversal agents as promising antimalarial drugs. *Current drug targets,* 7**,** 935-948.

HEPPNER, D. G. 2013. The malaria vaccine–status quo 2013. *Travel medicine and infectious disease,* 11**,** 2-7.

HERNANDEZ-PEREZ, E. 1980. Dehydroemetine therapy for herpes zoster. A comparison with corticosteroids. *Cutis,* 25**,** 424-426.

HIGGINS, T. J., ALLSOPP, D., BAILEY, P. J. & D'SOUZA, E. D. 1981. The relationship between glycolysis, fatty acid metabolism and membrane integrity in neonatal myocytes. *Journal of molecular and cellular cardiology,* 13**,** 599-615.

HILL, A. V. 2011. Vaccines against malaria. *Philosophical Transactions of the Royal Society B: Biological Sciences,* 366**,** 2806-2814.

HILLISCH, A., PINEDA, L. F. & HILGENFELD, R. 2004. Utility of homology models in the drug discovery process. *Drug discovery today,* 9**,** 659-669.

HILMY SALEM, H. & ABD-RABBO, H. 1964. Dehydroemetine in acute amoebiasis. *Transactions of the Royal Society of Tropical Medicine and Hygiene,* 58**,** 539-544.

HOME OFFICE 1986. Animals (Scientific Procedures) Act. *14.* London: Her Majesty's Stationery Office.

HYDE, J. E. 2005. Exploring the folate pathway in Plasmodium falciparum. *Acta tropica,* 94**,** 191-206.

HYDE, J. E. 2007. Drug‐resistant malaria− an insight. *The FEBS journal,* 274**,** 4688-4698.

IOSET, J.-R. & KAUR, H. 2009. Simple field assays to check quality of current artemisinin-based antimalarial combination formulations. *PloS one,* 4**,** e7270.

IRWIN, J. J. & SHOICHET, B. K. 2005. ZINC− A free database of commercially available compounds for virtual screening. *Journal of chemical information and modeling,* 45**,** 177-182.

JACKSON, K. E., HABIB, S., FRUGIER, M., HOEN, R., KHAN, S., PHAM, J. S., RIBAS DE POUPLANA, L., ROYO, M., SANTOS, M. A., SHARMA, A. & RALPH, S. A. 2011. Protein translation in Plasmodium parasites. *Trends Parasitol,* 27**,** 467-76.

JAIN, S., CHAUDHARY, P. N. & GAWADE, V. B. 2012. Late stages in the biosynthesis of ipecac alkaloids-cephaeline, emetine and psychotrine in Alangium lamarckii Thw.(Alangiaceae). *Scientific World,* 10**,** 24-28.

JANA, S. & PALIWAL, J. 2007. Novel molecular targets for antimalarial chemotherapy. *Int J Antimicrob Agents,* 30**,** 4-10.

JASTROCH, M., DIVAKARUNI, A. S., MOOKERJEE, S., TREBERG, J. R. & BRAND, M. D. 2010. Mitochondrial proton and electron leaks. *Essays Biochem,* 47**,** 53-67.

JENSEN, M. & MEHLHORN, H. 2009. Seventy-five years of Resochin® in the fight against malaria. *Parasitology research,* 105**,** 609.

JIMENEZ, A., CARRASCO, L. & VAZQUEZ, D. 1977. Enzymic and nonenzymic translocation by yeast polysomes. Site of action of a number of inhibitors. *Biochemistry,* 16**,** 4727-4730.

JONES, D. C., HALLYBURTON, I., STOJANOVSKI, L., READ, K. D., FREARSON, J. A. & FAIRLAMB, A. H. 2010. Identification of a kappa-opioid agonist as a potent and selective lead for drug development against human African trypanosomiasis. *Biochem Pharmacol,* 80**,** 1478-86.

JONES, R. M., CHICHESTER, J. A., MANCEVA, S., GIBBS, S. K., MUSIYCHUK, K., SHAMLOUL, M., NORIKANE, J., STREATFIELD, S. J., VAN DE VEGTE-BOLMER, M., ROEFFEN, W., SAUERWEIN, R. W. & YUSIBOV, V. 2015. A novel plant-produced Pfs25 fusion subunit vaccine induces long-lasting transmission blocking antibody responses. *Hum Vaccin Immunother,* 11**,** 124-32.

JORGENSEN, W. L. 1991. Rusting of the lock and key model for protein-ligand binding. *Science,* 254**,** 954-956.

JORGENSEN, W. L. 2009. Efficient drug lead discovery and optimization. *Accounts of chemical research,* 42**,** 724-733.

JOSEPH‐MCCARTHY, D., THOMAS IV, B. E., BELMARSH, M., MOUSTAKAS, D. & ALVAREZ, J. C. 2003. Pharmacophore‐based molecular docking to account for ligand flexibility. *Proteins: Structure, Function, and Bioinformatics,* 51**,** 172-188.

KIM, J. W., GAO, P., LIU, Y. C., SEMENZA, G. L. & DANG, C. V. 2007. Hypoxia-inducible factor 1 and dysregulated c-Myc cooperatively induce vascular endothelial growth factor and metabolic switches hexokinase 2 and pyruvate dehydrogenase kinase 1. *Mol Cell Biol,* 27**,** 7381-93.

KITCHEN, D. B., DECORNEZ, H., FURR, J. R. & BAJORATH, J. 2004. Docking and scoring in virtual screening for drug discovery: methods and applications. *Nature reviews Drug discovery,* 3**,** 935.

KITCHEN, L. W., VAUGHN, D. W. & SKILLMAN, D. R. 2006. Role of US military research programs in the development of US Food and Drug Administration--approved antimalarial drugs. *Clin Infect Dis,* 43**,** 67-71.

KIVISTO, T., MAKIRANTA, M., OIKARINEN, E. L., KARHU, S., WECKSTROM, M. & SELLIN, L. C. 1995. 2,3-Butanedione monoxime (BDM) increases initial yields and improves long-term survival of isolated cardiac myocytes. *Jpn J Physiol,* 45**,** 203-10.

KLEIN, E. 2013. Antimalarial drug resistance: a review of the biology and strategies to delay emergence and spread. *International journal of antimicrobial agents,* 41**,** 311-317.

KLONIS, N., CRESPO-ORTIZ, M. P., BOTTOVA, I., ABU-BAKAR, N., KENNY, S., ROSENTHAL, P. J. & TILLEY, L. 2011. Artemisinin activity against Plasmodium falciparum requires hemoglobin uptake and digestion. *Proc Natl Acad Sci U S A,* 108**,** 11405-10.

KNIGHT, R. 1980. The chemotherapy of amoebiasis. *Journal of Antimicrobial Chemotherapy,* 6**,** 577-593.

KOELLA, J. C., SÖRENSEN, F. L. & ANDERSON, R. 1998. The malaria parasite, Plasmodium falciparum, increases the frequency of multiple feeding of its mosquito

vector, Anopheles gambiae. *Proceedings of the Royal Society of London B: Biological Sciences,* 265**,** 763-768.
KORAM, K. A., ABUAKU, B., DUAH, N. & QUASHIE, N. 2005. Comparative efficacy of antimalarial drugs including ACTs in the treatment of uncomplicated malaria among children under 5 years in Ghana. *Acta Trop,* 95**,** 194-203.
KOTZ, J. 2012. Phenotypic screening, take two. *Science-Business eXchange,* 5**,** 380-380.
KREMSNER, P. G. & KRISHNA, S. 2004. Antimalarial combinations. *The Lancet,* 364**,** 285-294.
KROGSGAARD-LARSEN, P., STRØMGAARD, K. & MADSEN, U. 2010. *Textbook of drug design and discovery,* Boca Raton, FL, CRC Press/Taylor & Francis.
KRUNGKRAI, J., IMPRASITTICHAI, W., OTJUNGREED, S., PONGSABUT, S. & KRUNGKRAI, S. R. 2010. Artemisinin resistance or tolerance in human malaria patients. *Asian Pacific Journal of Tropical Medicine,* 3**,** 748-753.
KRUNGKRAI, S. R. & KRUNGKRAI, J. 2016. Insights into the pyrimidine biosynthetic pathway of human malaria parasite Plasmodium falciparum as chemotherapeutic target. *Asian Pac J Trop Med,* 9**,** 525-34.
KUHLMANN, F. M. & FLECKENSTEIN, J. M. 2017. Antiparasitic Agents. *Infectious Diseases (Fourth Edition).* Elsevier.
KUNTZ, I. D., MENG, E. C. & SHOICHET, B. K. 1994. Structure-based molecular design. *Accounts of Chemical research,* 27**,** 117-123.
KURTOVIC, L., AGIUS, P. A., FENG, G., DREW, D. R., UBILLOS, I., SACARLAL, J., APONTE, J. J., FOWKES, F. J., DOBAÑO, C. & BEESON, J. G. 2019. Induction and decay of functional complement-fixing antibodies by the RTS, S malaria vaccine in children, and a negative impact of malaria exposure. *BMC medicine,* 17**,** 45.
KYLE, R. A. & SHAMPE, M. A. 1974. Discoverers of quinine. *JAMA,* 229**,** 462.
LALLOO, D. G., SHINGADIA, D., BELL, D. J., BEECHING, N. J., WHITTY, C. J. & CHIODINI, P. L. 2016. UK malaria treatment guidelines 2016. *Journal of Infection,* 72**,** 635-649.
LAMOTHE, S. M., GUO, J., LI, W., YANG, T. & ZHANG, S. 2016. The Human Ether-a-go-go-related Gene (hERG) Potassium Channel Represents an Unusual Target for Protease-mediated Damage. *J Biol Chem,* 291**,** 20387-401.
LE MANACH, C., SCHEURER, C., SAX, S., SCHLEIFERBÖCK, S., CABRERA, D. G., YOUNIS, Y., PAQUET, T., STREET, L., SMITH, P. & DING, X. C. 2013. Fast in vitro methods to determine the speed of action and the stage-specificity of anti-malarials in Plasmodium falciparum. *Malaria journal,* 12**,** 424.
LEE, M. 2008. Ipecacuanha: the South American vomiting root. *The journal of the Royal College of Physicians of Edinburgh,* 38**,** 355-360.
LENGAUER, T. & RAREY, M. 1996. Computational methods for biomolecular docking. *Current opinion in structural biology,* 6**,** 402-406.
LI, J. J. 2013. History of Drug Discovery. *Drug Discovery: Practices, Processes, and Perspectives***,** 1-42.
LI, R., CHEN, X., GONG, B., SELZER, P. M., LI, Z., DAVIDSON, E., KURZBAN, G., MILLER, R. E., NUZUM, E. O. & MCKERROW, J. H. 1996. Structure-based design of parasitic protease inhibitors. *Bioorganic & medicinal chemistry,* 4**,** 1421-1427.
LI, X. B., GU, J. D. & ZHOU, Q. H. 2015. Review of aerobic glycolysis and its key enzymes - new targets for lung cancer therapy. *Thorac Cancer,* 6**,** 17-24.
LIBERTI, M. V. & LOCASALE, J. W. 2016. The Warburg Effect: How Does it Benefit Cancer Cells? *Trends Biochem Sci,* 41**,** 211-218.
LIM, P., ALKER, A. P., KHIM, N., SHAH, N. K., INCARDONA, S., DOUNG, S., YI, P., BOUTH, D. M., BOUCHIER, C. & PUIJALON, O. M. 2009. Pfmdr1 copy number

and arteminisin derivatives combination therapy failure in falciparum malaria in Cambodia. *Malaria journal,* 8**,** 11.

LISGARTEN, J. N., COLL, M., PORTUGAL, J., WRIGHT, C. W. & AYMAMI, J. 2002. The antimalarial and cytotoxic drug cryptolepine intercalates into DNA at cytosine-cytosine sites. *Nature Structural and Molecular Biology,* 9**,** 57.

LIU, J. & WANG, R. 2015. Classification of current scoring functions. *Journal of chemical information and modeling,* 55**,** 475-482.

LOOAREESUWAN, S., CHULAY, J. D., CANFIELD, C. J. & HUTCHINSON, D. 1999. Malarone (atovaquone and proguanil hydrochloride): a review of its clinical development for treatment of malaria. Malarone Clinical Trials Study Group. *The American journal of tropical medicine and hygiene,* 60**,** 533-541.

LORENZ, V., KARANIS, G. & KARANIS, P. 2014. Malaria vaccine development and how external forces shape it: an overview. *International journal of environmental research and public health,* 11**,** 6791-6807.

LOTHARIUS, J., GAMO-BENITO, F. J., ANGULO-BARTUREN, I., CLARK, J., CONNELLY, M., FERRER-BAZAGA, S., PARKINSON, T., VISWANATH, P., BANDODKAR, B., RAUTELA, N., BHARATH, S., DUFFY, S., AVERY, V. M., MÖHRLE, J. J., GUY, R. K. & WELLS, T. 2014. Repositioning: the fast track to new anti-malarial medicines? *Malaria Journal,* 13**,** 143.

LOURIDO, S. & MORENO, S. N. 2015. The calcium signaling toolkit of the Apicomplexan parasites Toxoplasma gondii and Plasmodium spp. *Cell Calcium,* 57**,** 186-93.

LU, W., ROONGSAWANG, N. & MAHMUD, T. 2011. Biosynthetic studies and genetic engineering of pactamycin analogs with improved selectivity toward malarial parasites. *Chemistry & biology,* 18**,** 425-431.

LU, X., GINSBURG, K. S., KETTLEWELL, S., BOSSUYT, J., SMITH, G. L. & BERS, D. M. 2013. Measuring local gradients of intramitochondrial [Ca(2+)] in cardiac myocytes during sarcoplasmic reticulum Ca(2+) release. *Circ Res,* 112**,** 424-31.

LUCUMI, E., DARLING, C., JO, H., NAPPER, A. D., CHANDRAMOHANADAS, R., FISHER, N., SHONE, A. E., JING, H., WARD, S. A., BIAGINI, G. A., DEGRADO, W. F., DIAMOND, S. L. & GREENBAUM, D. C. 2010. Discovery of potent small-molecule inhibitors of multidrug-resistant Plasmodium falciparum using a novel miniaturized high-throughput luciferase-based assay. *Antimicrob Agents Chemother,* 54**,** 3597-604.

MAC-DANIEL, L., BUCKWALTER, M. R., BERTHET, M., VIRK, Y., YUI, K., ALBERT, M. L., GUEIRARD, P. & MENARD, R. 2014. Local Immune Response to Injection of Plasmodium Sporozoites into the Skin. *Journal of Immunology,* 193**,** 1246-1257.

MACLEAN, W. 1875. PROFESSOR MACLEAN, CB, ON THE TRUE COMPOSITION AND THERAPEUTIC VALUE OF WARBURG'S TINCTURE. *The Lancet,* 106**,** 716-718.

MACLEOD, D. P. & DANIEL, E. 1965. Influence of glucose on the transmembrane action potential of anoxic papillary muscle. *The Journal of general physiology,* 48**,** 887-899.

MADJAR, J., NIELSEN-SMITH, K., FRAHM, M. & ROUFA, D. 1982. Emetine resistance in Chinese hamster ovary cells is associated with an altered ribosomal protein S14 mRNA. *Proceedings of the National Academy of Sciences,* 79**,** 1003-1007.

MAGAŃA‐GARCÍA, M. & ARISTA‐VIVEROS, A. 1993. Cutaneous amebiasis in children. *Pediatric dermatology,* 10**,** 352-355.

MAGEE, D. J., ZACHAZEWSKI, J. E. & QUILLEN, W. S. 2007. *Scientific foundations and principles of practice in musculoskeletal rehabilitation,* Elsevier Health Sciences.

MAJOR, L. L. & SMITH, T. K. 2011. Screening the MayBridge Rule of 3 Fragment Library for Compounds That Interact with the Trypanosoma brucei myo-Inositol-3-Phosphate Synthase and/or Show Trypanocidal Activity. *Mol Biol Int,* 2011**,** 389364.

MARKS, A. R. 2003. Calcium and the heart: a question of life and death. *J Clin Invest,* 111**,** 597-600.

MARTIN, W. F., GARG, S. & ZIMORSKI, V. 2015. Endosymbiotic theories for eukaryote origin. *Philosophical Transactions of the Royal Society B: Biological Sciences,* 370**,** 20140330.

MARTINS, A. C., CAYOTOPA, A. D. E., KLEIN, W. W., SCHLOSSER, A. R., SILVA, A. F. D., SOUZA, M. N. D., ANDRADE, B. W. B., FILGUEIRA-JÚNIOR, J. A., PINTO, W. D. J. & DA SILVA-NUNES, M. 2015. Side effects of chloroquine and primaquine and symptom reduction in malaria endemic area (Mâncio Lima, Acre, Brazil). *Interdisciplinary perspectives on infectious diseases,* 2015.

MASTRANGELO, M. J., GRAGE, T. B., BELLET, R. E. & WEISS, A. J. 1973. A phase I study of emetine hydrochloride (NSC 33669) in solid tumors. *Cancer,* 31**,** 1170-5.

MATSUURA, M., NAKAZAWA, H., HASHIMOTO, T. & MITSUHASHI, S. 1980. Combined antibacterial activity of amoxicillin with clavulanic acid against ampicillin-resistant strains. *Antimicrobial agents and chemotherapy,* 17**,** 908-911.

MATTHEWS, H., DEAKIN, J., RAJAB, M., IDRIS-USMAN, M. & NIRMALAN, N. J. 2017. Investigating antimalarial drug interactions of emetine dihydrochloride hydrate using CalcuSyn-based interactivity calculations. *PloS one,* 12**,** e0173303.

MATTHEWS, H., USMAN-IDRIS, M., KHAN, F., READ, M. & NIRMALAN, N. 2013. Drug repositioning as a route to anti-malarial drug discovery: preliminary investigation of the in vitro anti-malarial efficacy of emetine dihydrochloride hydrate. *Malaria Journal,* 12.

MATTIA, C. & COLUZZI, F. 2015. A look inside the association codeine-paracetamol: clinical pharmacology supports analgesic efficacy. *Eur Rev Med Pharmacol Sci,* 19**,** 507-516.

MAZZARELLO, P. 1999. A unifying concept: the history of cell theory. *Nature cell biology,* 1**,** E13.

MBUGI, E. V., MUTAYOBA, B. M., MALISA, A. L., BALTHAZARY, S. T., NYAMBO, T. B. & MSHINDA, H. 2006. Drug resistance to sulphadoxine-pyrimethamine in Plasmodium falciparum malaria in Mlimba, Tanzania. *Malar J,* 5**,** 94.

MCBRIDE, H. M., NEUSPIEL, M. & WASIAK, S. 2006. Mitochondria: more than just a powerhouse. *Current biology,* 16**,** R551-R560.

MCFADDEN, G. I., REITH, M. E., MUNHOLLAND, J. & LANG-UNNASCH, N. 1996. Plastid in human parasites. *Nature,* 381**,** 482.

MEDINA-FRANCO, J. L., GIULIANOTTI, M. A., WELMAKER, G. S. & HOUGHTEN, R. A. 2013. Shifting from the single to the multitarget paradigm in drug discovery. *Drug Discov Today,* 18**,** 495-501.

MENG, X.-Y., ZHANG, H.-X., MEZEI, M. & CUI, M. 2011. Molecular docking: a powerful approach for structure-based drug discovery. *Current computer-aided drug design,* 7**,** 146-157.

MERCER, A. E., COPPLE, I. M., MAGGS, J. L., O'NEILL, P. M. & PARK, B. K. 2011. The role of heme and the mitochondrion in the chemical and molecular mechanisms of mammalian cell death induced by the artemisinin antimalarials. *J Biol Chem,* 286**,** 987-96.

MERZ JR, K. M., RINGE, D. & REYNOLDS, C. H. 2010. *Drug design: structure-and ligand-based approaches*, Cambridge University Press.

MESHNICK, S. R. 2002. Artemisinin: mechanisms of action, resistance and toxicity. *Int J Parasitol,* 32**,** 1655-60.
METCALF, R. L. 1973. A century of DDT. *J Agric Food Chem,* 21**,** 511-9.
MIGUEL-BLANCO, C., LELIÈVRE, J., DELVES, M. J., BARDERA, A. I., PRESA, J. L., LÓPEZ-BARRAGÁN, M. J., RUECKER, A., MARQUES, S., SINDEN, R. E. & HERREROS, E. 2015. Imaging-based high-throughput screening assay to identify new molecules with transmission-blocking potential against Plasmodium falciparum female gamete formation. *Antimicrobial agents and chemotherapy,* 59**,** 3298-3305.
MILLER, L. H. & SU, X. 2011. Artemisinin: discovery from the Chinese herbal garden. *Cell,* 146**,** 855-858.
MILNES, J. T., CROCIANI, O., ARCANGELI, A., HANCOX, J. C. & WITCHEL, H. J. 2003. Blockade of HERG potassium currents by fluvoxamine: incomplete attenuation by S6 mutations at F656 or Y652. *British journal of pharmacology,* 139**,** 887-898.
MITA, T. & JOMBART, T. 2015. Patterns and dynamics of genetic diversity in Plasmodium falciparum: What past human migrations tell us about malaria. *Parasitology International,* 64**,** 238-243.
Molecular Operating Environment (MOE), 2015.10; Chemical Computing Group Inc., 1010 1001 Sherbrooke St. West, Suite #910, Montreal, QC, Canada, H3A 2R7, 2016.
MOJAB, F. 2012. Antimalarial natural products: a review. *Avicenna journal of phytomedicine,* 2**,** 52.
MÖLLER, M., HERZER, K., WENGER, T., HERR, I. & WINK, M. 2007. The alkaloid emetine as a promising agent for the induction and enhancement of drug-induced apoptosis in leukemia cells. *Oncology reports,* 18**,** 737-744.
MOODY, A. 2002. Rapid diagnostic tests for malaria parasites. *Clinical microbiology reviews,* 15**,** 66-78.
MORCIANO, G., SARTI, A. C., MARCHI, S., MISSIROLI, S., FALZONI, S., RAFFAGHELLO, L., PISTOIA, V., GIORGI, C. & DI VIRGILIO, F. 2017. Use of luciferase probes to measure ATP in living cells and animals. 12**,** 1542-1562.
MORTIER, J., DHAKAL, P. & VOLKAMER, A. 2018. Truly Target-Focused Pharmacophore Modeling: A Novel Tool for Mapping Intermolecular Surfaces. *Molecules,* 23**,** 1959.
MOUSCADET, J.-F. & TCHERTANOV, L. 2009. Raltegravir: molecular basis of its mechanism of action. *European journal of medical research,* 14**,** 5.
MUKESH, B. & RAKESH, K. 2011. Molecular docking: a review. *Int J Res Ayurveda Pharm,* 2**,** 746-1751.
MUKHOPADHYAY, R., ROY, S., VENKATADRI, R., SU, Y. P., Ye, W., BARNAEVA, E., … ARAV-BOGER, R. 2016. Efficacy and Mechanism of Action of Low Dose Emetine against Human Cytomegalovirus. *PLoS pathogens, 12*(6), e1005717. doi:10.1371/journal.ppat.1005717
MURCKO, M. A. 1995. Computational methods to predict binding free energy in ligand-receptor complexes. *Journal of medicinal chemistry,* 38**,** 4953-4967.
MURRAY, C. J., ORTBLAD, K. F., GUINOVART, C., LIM, S. S., WOLOCK, T. M., ROBERTS, D. A., DANSEREAU, E. A., GRAETZ, N., BARBER, R. M. & BROWN, J. C. 2014. Global, regional, and national incidence and mortality for HIV, tuberculosis, and malaria during 1990–2013: a systematic analysis for the Global Burden of Disease Study 2013. *The Lancet,* 384**,** 1005-1070.
MUTABINGWA, T. K. 2005. Artemisinin-based combination therapies (ACTs): best hope for malaria treatment but inaccessible to the needy! *Acta Trop,* 95**,** 305-15.
MUTHYALA, R. 2011. Orphan/rare drug discovery through drug repositioning. *Drug Discovery Today: Therapeutic Strategies,* 8**,** 71-76.

N'GUESSAN, R., CORBEL, V., AKOGBETO, M. & ROWLAND, M. 2007. Reduced efficacy of insecticide-treated nets and indoor residual spraying for malaria control in pyrethroid resistance area, Benin. *Emerg Infect Dis,* 13**,** 199-206.

NA - BANGCHANG, K. & KARBWANG, J. 2009. Current status of malaria chemotherapy and the role of pharmacology in antimalarial drug research and development. *Fundamental & Clinical Pharmacology,* 23**,** 387-409.

NABARRO, D. 1999. Roll Back Malaria. *Parassitologia,* 41**,** 501-4.

NAJERA, J. A., GONZALEZ-SILVA, M. & ALONSO, P. L. 2011. Some Lessons for the Future from the Global Malaria Eradication Programme (1955-1969). *Plos Medicine,* 8.

NANDAKUMAR, D. N., NAGARAJ, V. A., VATHSALA, P. G., RANGARAJAN, P. & PADMANABAN, G. 2006. Curcumin-artemisinin combination therapy for malaria. *Antimicrobial agents and chemotherapy,* 50**,** 1859-1860.

NEALON, J., PHILOMINA, L. & MCGUFFIN, L. 2017. Predictive and Experimental Approaches for Elucidating Protein–Protein Interactions and Quaternary Structures. *International Journal of Molecular Sciences,* 18**,** 2623.

NEGRETTI, N., O'NEILL, S. C. & EISNER, D. A. 1993. The relative contributions of different intracellular and sarcolemmal systems to relaxation in rat ventricular myocytes. *Cardiovasc Res,* 27**,** 1826-30.

NEGRETTI, N., VARRO, A. & EISNER, D. A. 1995. Estimate of net calcium fluxes and sarcoplasmic reticulum calcium content during systole in rat ventricular myocytes. *J Physiol,* 486 (Pt 3)**,** 581-91.

NEWTON, P. N., CHAULET, J. F., BROCKMAN, A., CHIERAKUL, W., DONDORP, A., RUANGVEERAYUTH, R., LOOAREESUWAN, S., MOUNIER, C. & WHITE, N. J. 2005. Pharmacokinetics of oral doxycycline during combination treatment of severe falciparum malaria. *Antimicrob Agents Chemother,* 49**,** 1622-5.

NIGAM, P., GUPTA, A., KAPOOR, K., SHARAN, G., GOYAL, B. & JOSHI, L. 1985. Cholestasis in amoebic liver abscess. *Gut,* 26**,** 140-145.

NKYA, T. E., AKHOUAYRI, I., POUPARDIN, R., BATENGANA, B., MOSHA, F., MAGESA, S., KISINZA, W. & DAVID, J. P. 2014. Insecticide resistance mechanisms associated with different environments in the malaria vector Anopheles gambiae: a case study in Tanzania. *Malar J,* 13**,** 28.

NOEDL, H., SE, Y., SCHAECHER, K., SMITH, B. L., SOCHEAT, D. & FUKUDA, M. M. 2008. Evidence of artemisinin-resistant malaria in western Cambodia. *New England Journal of Medicine,* 359**,** 2619-2620.

NWAKA, S., RIOPEL, L., UBBEN, D. & CRAFT, J. C. 2004. Medicines for Malaria Venture new developments in antimalarials. *Travel Med Infect Dis,* 2**,** 161-70.

NZILA, A. 2006. The past, present and future of antifolates in the treatment of Plasmodium falciparum infection. *Journal of Antimicrobial Chemotherapy,* 57**,** 1043-1054.

O'NEILL, S. C. & EISNER, D. A. 1990. A mechanism for the effects of caffeine on Ca2+ release during diastole and systole in isolated rat ventricular myocytes. *J Physiol,* 430**,** 519-36.

OBONYO, C. O. & JUMA, E. A. 2012. Clindamycin plus quinine for treating uncomplicated falciparum malaria: a systematic review and meta-analysis. *Malaria Journal,* 11**,** 2.

ODOLINI, S., PAROLA, P., GKRANIA-KLOTSAS, E., CAUMES, E., SCHLAGENHAUF, P., LOPEZ-VELEZ, R., BURCHARD, G. D., SANTOS-O'CONNOR, F., WELD, L., VON SONNENBURG, F., FIELD, V., DE VRIES, P., JENSENIUS, M., LOUTAN, L. & CASTELLI, F. 2012. Travel-related imported infections in Europe, EuroTravNet 2009. *Clin Microbiol Infect,* 18**,** 468-74.

OLASEHINDE, G., OJURONGBE, D., AKINJOGUNLA, O., EGWARI, L. & ADEYEBA, A. O. 2015. Prevalence of malaria and predisposing factors to antimalarial drug resistance in southwestern Nigeria. *Research Journal of Parasitology,* 10**,** 92-101.

OLSEN, T. G. 1981. Chloroquine and psoriasis. *Annals of Internal Medicine,* 94**,** 546-547.

OPENSHAW, H. & WHITTAKER, N. 1963. 276. The synthesis of emetine and related compounds. Part IV. A new synthesis of 3-substituted 1, 2, 3, 4, 6, 7-hexahydro-9, 10-dimethoxy-2-oxo-11bH-benzo [a] quinolizines. *Journal of the Chemical Society (Resumed),* 1449-1460.

OSADA, H. 2009. *Protein targeting with small molecules: chemical biology techniques and applications*, John Wiley & Sons.

OSAKWE, O. & RIZVI, S. A. 2016. *Social aspects of drug discovery, development and commercialization*, Academic Press.

OTOGURO, K., IWATSUKI, M., ISHIYAMA, A., NAMATAME, M., NISHIHARA-TUKASHIMA, A., SHIBAHARA, S., KONDO, S., YAMADA, H. & OMURA, S. 2010. Promising lead compounds for novel antiprotozoals. *J Antibiot (Tokyo),* 63**,** 381-4.

OVERBOSCH, D., SCHILTHUIS, H., BIENZLE, U., BEHRENS, R. H., KAIN, K. C., CLARKE, P. D., TOOVEY, S., KNOBLOCH, J., NOTHDURFT, H. D. & SHAW, D. 2001. Atovaquone-proguanil versus mefloquine for malaria prophylaxis in nonimmune travelers: results from a randomized, double-blind study. *Clinical Infectious Diseases,* 33**,** 1015-1021.

PAN, S. J. & COMBS, A. B. 2003. Emetine inhibits glycolysis in isolated, perfused rat hearts. *Cardiovascular Toxicology,* 3**,** 311-318.

PANDEY, K., FERREIRA, P. E., ISHIKAWA, T., NAGAI, T., KANEKO, O. & YAHATA, K. 2016. Ca2+ monitoring in Plasmodium falciparum using the yellow cameleon-Nano biosensor. *Scientific Reports,* 6**,** 23454.

PARKER, J. C. & HOFFMAN, J. F. 1967. The role of membrane phosphoglycerate kinase in the control of glycolytic rate by active cation transport in human red blood cells. *The Journal of General Physiology,* 50**,** 893-916.

PAUL, R. J. 1983. Functional compartmentalization of oxidative and glycolytic metabolism in vascular smooth muscle. *American Journal of Physiology-Cell Physiology,* 244**,** C399-C409.

PERIER, C. & VILA, M. 2012. Mitochondrial biology and Parkinson's disease. *Cold Spring Harbor perspectives in medicine,* 2**,** a009332.

PERLMAN, S. & PENMAN, S. 1970. Mitochondrial protein synthesis: resistance to emetine and response to RNA synthesis inhibitors. *Biochem Biophys Res Commun,* 40**,** 941-8.

PERMIN, H., NORN, S., KRUSE, E. & KRUSE, P. R. 2016. On the history of Cinchona bark in the treatment of Malaria. *Dan Medicinhist Arbog,* 44**,** 9-30.

PEROLA, E., WALTERS, W. P. & CHARIFSON, P. S. 2004. A detailed comparison of current docking and scoring methods on systems of pharmaceutical relevance. *Proteins: Structure, Function, and Bioinformatics,* 56**,** 235-249.

PETERS, J. M., CHEN, N., GATTON, M., KORSINCZKY, M., FOWLER, E. V., MANZETTI, S., SAUL, A. & CHENG, Q. 2002. Mutations in cytochrome b resulting in atovaquone resistance are associated with loss of fitness in Plasmodium falciparum. *Antimicrobial agents and chemotherapy,* 46**,** 2435-2441.

PETERS, M., DIETRICH, M., BIENZLE, U., KERN, P. & MANNWEILER, E. 1979. Amoebic liver abscess: a retrospective clinical evaluation of twenty-seven cases. *Tropenmedizin und Parasitologie,* 30**,** 409-416.

PHILLIPS-HOWARD, P. A. & WOOD, D. 1996. The safety of antimalarial drugs in pregnancy. *Drug Saf,* 14**,** 131-45.

PHILLIPSON, J., O'NEILL, M., WRIGHT, C., BRAY, D. & WARHURST, D. 1987. Plants as sources of antimalarial and amoebicidal compounds. *Leeuwenberg, AJM (compilers). Medicinal and Poisonous Plants of the Tropics. Wagneningen, Centre for Agricultural Publishing and Documentation***,** 70-79.

PHYO, A. P., NKHOMA, S., STEPNIEWSKA, K., ASHLEY, E. A., NAIR, S., MCGREADY, R., LER MOO, C., AL-SAAI, S., DONDORP, A. M. & LWIN, K. M. 2012. Emergence of artemisinin-resistant malaria on the western border of Thailand: a longitudinal study. *The Lancet,* 379**,** 1960-1966.

PICHT, E., ZIMA, A. V., SHANNON, T. R., DUNCAN, A. M., BLATTER, L. A. & BERS, D. M. 2011. Dynamic calcium movement inside cardiac sarcoplasmic reticulum during release. *Circ Res,* 108**,** 847-56.

PINA, A. S., HUSSAIN, A. & ROQUE, A. C. 2009. An historical overview of drug discovery. *Methods Mol Biol,* 572**,** 3-12.

PINA, A. S., HUSSAIN, A. & ROQUE, A. C. A. 2010. An historical overview of drug discovery. *Ligand-Macromolecular Interactions in Drug Discovery.* Springer.

PLOUFFE, D., BRINKER, A., MCNAMARA, C., HENSON, K., KATO, N., KUHEN, K., NAGLE, A., ADRIAN, F., MATZEN, J. T., ANDERSON, P., NAM, T. G., GRAY, N. S., CHATTERJEE, A., JANES, J., YAN, S. F., TRAGER, R., CALDWELL, J. S., SCHULTZ, P. G., ZHOU, Y. & WINZELER, E. A. 2008. In silico activity profiling reveals the mechanism of action of antimalarials discovered in a high-throughput screen. *Proc Natl Acad Sci U S A,* 105**,** 9059-64.

PLOWE, C. V. 2009. The evolution of drug-resistant malaria. *Transactions of the Royal Society of Tropical Medicine and Hygiene,* 103**,** S11-S14.

PORPORATO, P. E., FILIGHEDDU, N., PEDRO, J. M. B., KROEMER, G. & GALLUZZI, L. 2018. Mitochondrial metabolism and cancer. *Cell Res,* 28**,** 265-280.

POWELL, S. J., WILMOT, A. J., MACLEOD, I. N. & ELSDON-DEW, R. 1965. A comparative trial of dehydroemetine, emetine hydrochloride and chloroquine in the treatment of amoebic liver abscess. *Ann Trop Med Parasitol,* 59**,** 496-9.

PREMJI, Z., UMEH, R. E., OWUSU-AGYEI, S., ESAMAI, F., EZEDINACHI, E. U., OGUCHE, S., BORRMANN, S., SOWUNMI, A., DUPARC, S. & KIRBY, P. L. 2009. Chlorproguanil− dapsone− artesunate versus artemether− lumefantrine: a randomized, double-blind phase III trial in African children and adolescents with uncomplicated Plasmodium falciparum malaria. *PLoS One,* 4**,** e6682.

RADLOFF, P. D., PHILIPS, J., NKEYI, M., KREMSNER, P. & HUTCHINSON, D. 1996. Atovaquone and proguanil for Plasmodium falciparum malaria. *The Lancet,* 347**,** 1511-1514.

RAJAMANI, R. & GOOD, A. C. 2007. Ranking poses in structure-based lead discovery and optimization: current trends in scoring function development. *Curr Opin Drug Discov Devel,* 10**,** 308-15.

RAMANA, K. V., SINGHAL, S. S. & REDDY, A. B. 2014. Therapeutic potential of natural pharmacological agents in the treatment of human diseases. *BioMed research international,* 2014.

RAMHARTER, M., NOEDL, H., WINKLER, H., GRANINGER, W., WERNSDORFER, W., KREMSNER, P. & WINKLER, S. 2003. In vitro activity and interaction of clindamycin combined with dihydroartemisinin against Plasmodium falciparum. *Antimicrobial agents and chemotherapy,* 47**,** 3494-3499.

RAMIREZ, J. L., GARVER, L. S. & DIMOPOULOS, G. 2009. Challenges and approaches for mosquito targeted malaria control. *Curr Mol Med,* 9**,** 116-30.

RATCLIFF, A., SISWANTORO, H., KENANGALEM, E., WUWUNG, M., BROCKMAN, A., EDSTEIN, M., LAIHAD, F., EBSWORTH, E., ANSTEY, N. & TJITRA, E.

2007. Therapeutic response of multidrug-resistant Plasmodium falciparum and P. vivax to chloroquine and sulfadoxine–pyrimethamine in southern Papua, Indonesia. *Transactions of the Royal Society of Tropical Medicine and Hygiene,* 101**,** 351-359.

RATHOD, P. K., MCERLEAN, T. & LEE, P.-C. 1997. Variations in frequencies of drug resistance in Plasmodium falciparum. *Proceedings of the National Academy of Sciences,* 94**,** 9389-9393.

READ, M. & HYDE, J. E. 1993. Simple in vitro cultivation of the malaria parasite Plasmodium falciparum (erythrocytic stages) suitable for large-scale preparations. *Methods Mol Biol,* 21**,** 43-55.

REAUME, A. G. 2011. Drug repurposing through nonhypothesis driven phenotypic screening. *Drug Discovery Today: Therapeutic Strategies,* 8**,** 85-88.

REES, D. C., CONGREVE, M., MURRAY, C. W. & CARR, R. 2004. Fragment-based lead discovery. *Nature Reviews Drug Discovery,* 3**,** 660.

REITER, P. 2000. From Shakespeare to Defoe: malaria in England in the Little Ice Age. *Emerg Infect Dis,* 6**,** 1-11.

REYNOLDS, C. & MAURER, B. J. 2005. Evaluating response to antineoplastic drug combinations in tissue culture models. *Chemosensitivity: Volume 1 In Vitro Assays***,** 173-183.

RICCI, F. 2012. Social implications of malaria and their relationships with poverty. *Mediterranean journal of hematology and infectious diseases,* 4.

RIDLEY, R. G. 2002. Medical need, scientific opportunity and the drive for antimalarial drugs. *Nature,* 415**,** 686.

RIZZUTO, R., MARCHI, S., BONORA, M., AGUIARI, P., BONONI, A., DE STEFANI, D., GIORGI, C., LEO, S., RIMESSI, A., SIVIERO, R., ZECCHINI, E. & PINTON, P. 2009. Ca(2+) transfer from the ER to mitochondria: when, how and why. *Biochim Biophys Acta,* 1787**,** 1342-51.

ROCHE, O., KIYAMA, R. & BROOKS, C. L. 2001. Ligand− protein database: Linking protein− ligand complex structures to binding data. *Journal of Medicinal Chemistry,* 44**,** 3592-3598.

RODRIGUEZ-MORALES, A. J., ORREGO-ACEVEDO, C. A., ZAMBRANO-MUNOZ, Y., GARCIA-FOLLECO, F. J., HERRERA-GIRALDO, A. C. & LOZADA-RIASCOS, C. O. 2015. Mapping malaria in municipalities of the Coffee Triangle region of Colombia using Geographic Information Systems (GIS). *Journal of Infection and Public Health,* 8**,** 603-611.

ROHRBACH, P., FRIEDRICH, O., HENTSCHEL, J., PLATTNER, H., FINK, R. H. & LANZER, M. 2005. Quantitative calcium measurements in subcellular compartments of Plasmodium falciparum-infected erythrocytes. *J Biol Chem,* 280**,** 27960-9.

ROTH, J. M., SAWA, P., MAKIO, N., OMWERI, G., OSOTI, V., OKACH, S., CHOY, F., SCHALLIG, H. & MENS, P. 2018. Pyronaridine-artesunate and artemether-lumefantrine for the treatment of uncomplicated Plasmodium falciparum malaria in Kenyan children: a randomized controlled non-inferiority trial. *Malar J,* 17**,** 199.

ROTTMANN, M., MCNAMARA, C., YEUNG, B. K., LEE, M. C., ZOU, B., RUSSELL, B., SEITZ, P., PLOUFFE, D. M., DHARIA, N. V., TAN, J., COHEN, S. B., SPENCER, K. R., GONZALEZ-PAEZ, G. E., LAKSHMINARAYANA, S. B., GOH, A., SUWANARUSK, R., JEGLA, T., SCHMITT, E. K., BECK, H. P., BRUN, R., NOSTEN, F., RENIA, L., DARTOIS, V., KELLER, T. H., FIDOCK, D. A., WINZELER, E. A. & DIAGANA, T. T. 2010. Spiroindolones, a potent compound class for the treatment of malaria. *Science,* 329**,** 1175-80.

ROY, A. 2018. Early probe and drug discovery in academia: a minireview. *High-throughput,* 7**,** 4.

RUBIDGE, C., SCRAGG, J. & POWELL, S. 1970. Treatment of Children with Acute Amoebic Dysentery: Comparative Trial of Metronidazole against a Combination of Dehydroemetine, Tetracycline, and Diloxanide Furoate. *Archives of disease in childhood,* 45**,** 196-197.

RUBIN, R. P. 2007. A brief history of great discoveries in pharmacology: in celebration of the centennial anniversary of the founding of the American Society of Pharmacology and Experimental Therapeutics. *Pharmacol Rev,* 59**,** 289-359.

SACHS, J. & MALANEY, P. 2002. The economic and social burden of malaria. *Nature,* 415**,** 680-5.

SADASIVAIAH, S., TOZAN, Y. & BREMAN, J. G. 2007. Dichlorodiphenyltrichloroethane (DDT) for indoor residual spraying in Africa: how can it be used for malaria control? *The American journal of tropical medicine and hygiene,* 77**,** 249-263.

SALAKO, L. A., ADIO, R. A., SOWUNMI, A. & WALKER, O. 1990. Parenteral sulphadoxine-pyrimethamine (Fansidar): an effective and safe but under-used method of anti-malarial treatment. *Trans R Soc Trop Med Hyg,* 84**,** 641-3.

SALEM, S. 1967. Clinical trial of oral dehydroemetine in intestinal amoebiasis. *Transactions of the Royal Society of Tropical Medicine and Hygiene,* 61**,** 774-775.

SAMS-DODD, F. 2005. Target-based drug discovery: is something wrong? *Drug discovery today,* 10**,** 139-147.

SANGUINETTI, M. C. & TRISTANI-FIROUZI, M. 2006. hERG potassium channels and cardiac arrhythmia. *Nature,* 440**,** 463-9.

SANTULLI, G., XIE, W., REIKEN, S. R. & MARKS, A. R. 2015. Mitochondrial calcium overload is a key determinant in heart failure. *Proceedings of the National Academy of Sciences,* 112**,** 11389-11394.

SANZ, L. M., CRESPO, B., DE-CÓZAR, C., DING, X. C., LLERGO, J. L., BURROWS, J. N., GARCÍA-BUSTOS, J. F. & GAMO, F.-J. 2012. P. falciparum in vitro killing rates allow to discriminate between different antimalarial mode-of-action. *PloS one,* 7**,** e30949.

SCHENONE, M., DANCIK, V., WAGNER, B. K. & CLEMONS, P. A. 2013. Target identification and mechanism of action in chemical biology and drug discovery. *Nat Chem Biol,* 9**,** 232-40.

SCHLAGENHAUF, P., BLUMENTALS, W. A., SUTER, P., REGEP, L., VITAL-DURAND, G., SCHAERER, M. T., BOUTROS, M. S., RHEIN, H.-G. & ADAMCOVA, M. 2012. Pregnancy and fetal outcomes after exposure to mefloquine in the pre-and periconception period and during pregnancy. *Clinical Infectious Diseases,* 54**,** e124-e131.

SCHLITZER, M. 2007. Malaria chemotherapeutics part I: History of antimalarial drug development, currently used therapeutics, and drugs in clinical development. *ChemMedChem,* 2**,** 944-86.

SCHWARTZ, D. & HERRERO, J. 1965. Comparative pharmacokinetic studies of dehydroemetine and emetine in guinea pigs using spectrofluorometric and radiometric methods. *The American journal of tropical medicine and hygiene,* 14**,** 78-83.

SCRAGG, J. & POWELL, S. 1968. Emetine hydrochloride and dehydroemetine combined with chloroquine in the treatment of children with amoebic liver abscess. *Archives of disease in childhood,* 43**,** 121.

SHAH, S. & LI, Q. 2018. Systems and Methods for In Silico Drug Discover. Google Patents.

SHANNON, T. R., GUO, T. & BERS, D. M. 2003. Ca2+ scraps: local depletions of free [Ca2+] in cardiac sarcoplasmic reticulum during contractions leave substantial Ca2+ reserve. *Circ Res,* 93**,** 40-5.

SHARMA, G. K., YOGI, A., GAUR, K. & DASHORA, A. 2015. A Review On Anti Malarial Drug.

SHAWL, F. A., VELASCO, C. E., GOLDBAUM, T. S. & FORMAN, M. B. 1990. Effect of coronary angioplasty on electrocardiographic changes in patients with unstable angina secondary to left anterior descending coronary artery disease. *Journal of the American College of Cardiology,* 16**,** 325-331.

SHIMP, R. L., JR., ROWE, C., REITER, K., CHEN, B., NGUYEN, V., AEBIG, J., RAUSCH, K. M., KUMAR, K., WU, Y., JIN, A. J., JONES, D. S. & NARUM, D. L. 2013. Development of a Pfs25-EPA malaria transmission blocking vaccine as a chemically conjugated nanoparticle. *Vaccine,* 31**,** 2954-62.

SHIPPEY, E., WAGLER, V. D. & COLLAMER, A. N. 2018. Hydroxychloroquine: An old drug with new relevance. *Cleveland Clinic journal of medicine,* 85**,** 459-467.

SHOICHET, B. K. 2004. Virtual screening of chemical libraries. *Nature,* 432**,** 862.

SHOICHET, B. K., KUNTZ, I. D. & BODIAN, D. L. 1992. Molecular docking using shape descriptors. *Journal of Computational Chemistry,* 13**,** 380-397.

SIENKIEWICZ, N., JAROSŁAWSKI, S., WYLLIE, S. & FAIRLAMB, A. H. 2008. Chemical and genetic validation of dihydrofolate reductase–thymidylate synthase as a drug target in African trypanosomes. *Molecular microbiology,* 69**,** 520-533.

SLATER, A. F. 1993. Chloroquine: mechanism of drug action and resistance in Plasmodium falciparum. *Pharmacol Ther,* 57**,** 203-35.

SOMERVILLE, S. 2015. FDA's Expedited Review Process: The Need for Speed. *Applied Clinical Trials,* 24**,** 17.

SONG, C. M., LIM, S. J. & TONG, J. C. 2009. Recent advances in computer-aided drug design. *Briefings in bioinformatics,* 10**,** 579-591.

SOULARD, V., BOSSON-VANGA, H., LORTHIOIS, A., ROUCHER, C., FRANETICH, J. F., ZANGHI, G., BORDESSOULLES, M., TEFIT, M., THELLIER, M., MOROSAN, S., LE NAOUR, G., CAPRON, F., SUEMIZU, H., SNOUNOU, G., MORENO-SABATER, A. & MAZIER, D. 2015. Plasmodium falciparum full life cycle and Plasmodium ovale liver stages in humanized mice. *Nat Commun,* 6**,** 7690.

SOUSA, S. F., FERNANDES, P. A. & RAMOS, M. J. 2006. Protein–ligand docking: current status and future challenges. *Proteins: Structure, Function, and Bioinformatics,* 65**,** 15-26.

SRIVASTAVA, I. K., MORRISEY, J. M., DARROUZET, E., DALDAL, F. & VAIDYA, A. B. 1999. Resistance mutations reveal the atovaquone-binding domain of cytochrome b in malaria parasites. *Mol Microbiol,* 33**,** 704-11.

STOCKS, M. 2013. The small molecule drug discovery process–from target selection to candidate selection. *Introduction to Biological and Small Molecule Drug Research and Development.* Elsevier.

SU, X. Z., & Miller, L. H. 2015. The discovery of artemisinin and the Nobel Prize in Physiology or Medicine. *Science China. Life sciences*, *58*(11), 1175–1179. doi:10.1007/s11427-015-4948-7

SUN, Q., YOGOSAWA, S., IIZUMI, Y., SAKAI, T. & SOWA, Y. 2015. The alkaloid emetine sensitizes ovarian carcinoma cells to cisplatin through downregulation of bcl-xL. *International Journal of Oncology,* 46**,** 389-394.

SUN, W., TANAKA, T. Q., MAGLE, C. T., HUANG, W., SOUTHALL, N., HUANG, R., DEHDASHTI, S. J., MCKEW, J. C., WILLIAMSON, K. C. & ZHENG, W. 2014. Chemical signatures and new drug targets for gametocytocidal drug development. *Scientific Reports,* 4**,** 3743.

SUROLIA, N. & PADMANABAN, G. 1991. Chloroquine inhibits heme-dependent protein synthesis in Plasmodium falciparum. *Proceedings of the National Academy of Sciences,* 88**,** 4786-4790.

SWINNEY, D. 2013. Phenotypic vs. target-based drug discovery for first-in-class medicines. *Clinical Pharmacology & Therapeutics,* 93**,** 299-301.

SZYMANSKI, P., MARKOWICZ, M. & MIKICIUK-OLASIK, E. 2012. Adaptation of high-throughput screening in drug discovery-toxicological screening tests. *Int J Mol Sci,* 13**,** 427-52.

TAKASHIMA, E., MORITA, M. & TSUBOI, T. 2016. Vaccine candidates for malaria: what's new? *Expert Rev Vaccines,* 15**,** 1-3.

TAKENAKA, T. 2001. Classical vs reverse pharmacology in drug discovery. *BJU international,* 88**,** 7-10.

TALELE, T. T., KHEDKAR, S. A. & RIGBY, A. C. 2010. Successful applications of computer aided drug discovery: moving drugs from concept to the clinic. *Current Topics in Medicinal Chemistry,* 10**,** 127-141.

TALISUNA, A. O., BLOLAND, P. & D'ALESSANDRO, U. 2004. History, dynamics, and public health importance of malaria parasite resistance. *Clin Microbiol Rev,* 17**,** 235-54.

TALLARIDA, R. J. 2011. Quantitative methods for assessing drug synergism. *Genes & cancer,* 2**,** 1003-1008.

TAN, K. R., MAGILL, A. J., PARISE, M. E. & ARGUIN, P. M. 2011. Doxycycline for malaria chemoprophylaxis and treatment: report from the CDC expert meeting on malaria chemoprophylaxis. *The American Journal of Tropical Medicine and Hygiene,* 84**,** 517-531.

TANABE, K. 1990. Glucose transport in malaria infected erythrocytes. *Parasitology Today,* 6**,** 225-229.

THOMPSON, A. J., LOCHNER, M. & LUMMIS, S. 2007. The antimalarial drugs quinine, chloroquine and mefloquine are antagonists at 5 ‐ HT3 receptors. *British Journal of Pharmacology,* 151**,** 666-677.

THOMPSON, J. H. 1913. The treatment of dysentery by injections of emetine hydrochloride. *Dublin Journal of Medical Science (1872-1920),* 136**,** 102-109.

TINTO, H., D'ALESSANDRO, U., SORGHO, H., VALEA, I., TAHITA, M. C., KABORE, W., KIEMDE, F., LOMPO, P., OUEDRAOGO, S., DERRA, K., OUEDRAOGO, F., OUEDRAOGO, J. B., BALLOU, W. R., COHEN, J., GUERRA, Y., HEERWEGH, D., JONGERT, E., LAPIERRE, D., LEACH, A., LIEVENS, M., OFORI-ANYINAM, O., OLIVIER, A., VEKEMANS, J., AGNANDJI, S. T., LELL, B., FERNANDES, J. F., ABOSSOLO, B. P., KABWENDE, A. L., ADEGNIKA, A. A., MORDMULLER, B., ISSIFOU, S., KREMSNER, P. G., LOEMBE, M. M., BACHE, E., ALABI, A., OWUSU-AGYEI, S., ASANTE, K. P., BOAHEN, O., DOSOO, D., ASANTE, I., YIDANA, Z., ANIM, J., ADENIJI, E., YAWSON, A. K., KAYAN, K., CHANDRAMOHAN, D., GREENWOOD, B., ANSONG, D., AGBENYEGA, T., ADJEI, S., BOATENG, H. O., RETTIG, T., SYLVERKEN, J., SAMBIAN, D., BADU-PREPAH, A., KOTEY, A., BUABENG, P., PAINTSIL, V., ENIMIL, A., HAMEL, M. J., KARIUKI, S., ONEKO, M., ODERO, C., OTIENO, K., AWINO, N., MUTURI-KIOI, V., OMOTO, J., SANG, T., ODHIAMBO, S., LASERSON, K. F., SLUTSKER, L., OTIENO, W., OTIENO, L., OTSYULA, N., GONDI, S., OCHOLA, J., OKOTH, G., MABUNDE, D. C., WANGWE, A., OTIENO, A., OYIEKO, J., COWDEN, J., OGUTU, B., NJUGUNA, P., MARSH, K., AKOO, P., KERUBO, C., MAINGI, C., BEJON, P., OLOTU, A., CHILENGI, R., TSOFA, B., LANG, T., GITAKA, J., AWUONDO, K., MARTINSON, F., HOFFMAN, I., MVALO, T.,

KAMTHUNZI, P., NKOMO, R., et al. 2015. Efficacy and safety of RTS,S/AS01 malaria vaccine with or without a booster dose in infants and children in Africa: final results of a phase 3, individually randomised, controlled trial. *Lancet,* 386**,** 31-45.

TOLLENAERE, J. 1996. The role of structure-based ligand design and molecular modelling in drug discovery. *Pharmacy World and Science,* 18**,** 56-62.

TRAGER, W. & JENSEN, J. B. 1976. Human malaria parasites in continuous culture. *Science,* 193**,** 673-5.

TRIPATHI, A. & BANKAITIS, V. A. 2017. Molecular Docking: From Lock and Key to Combination Lock. *Journal of molecular medicine and clinical applications,* 2.

TRIPATHI, A. & MISRA, K. 2017. Molecular Docking: A Structure-Based Drug Designing Approach.

TROTT, O. & OLSON, A. J. 2010. AutoDock Vina: improving the speed and accuracy of docking with a new scoring function, efficient optimization, and multithreading. *J Comput Chem,* 31**,** 455-61.

TU, Y. Y. 2011. The discovery of artemisinin (qinghaosu) and gifts from Chinese medicine. *Nature Medicine,* 17**,** 1217-1220.

TUN, K. M., IMWONG, M., LWIN, K. M., WIN, A. A., HLAING, T. M., HLAING, T., LIN, K., KYAW, M. P., PLEWES, K. & FAIZ, M. A. 2015. Spread of artemisinin-resistant Plasmodium falciparum in Myanmar: a cross-sectional survey of the K13 molecular marker. *The Lancet infectious diseases,* 15**,** 415-421.

TURNER, P. P. 1963. The effects of emetine on the myocardium. *British heart journal,* 25**,** 81.

UZOR, P. F. 2016. Recent developments on potential new applications of emetine as anti-cancer agent. *EXCLI journal,* 15**,** 323.

VALDERRAMOS, S. G., SCANFELD, D., UHLEMANN, A. C., FIDOCK, D. A. & KRISHNA, S. 2010. Investigations into the role of the Plasmodium falciparum SERCA (PfATP6) L263E mutation in artemisinin action and resistance. *Antimicrob Agents Chemother,* 54**,** 3842-52.

VALE, N., MOREIRA, R. & GOMES, P. 2009. Primaquine revisited six decades after its discovery. *Eur J Med Chem,* 44**,** 937-53.

VARRO, A., NEGRETTI, N., HESTER, S. B. & EISNER, D. A. 1993. An estimate of the calcium content of the sarcoplasmic reticulum in rat ventricular myocytes. *Pflugers Arch,* 423**,** 158-60.

VENETUCCI, L., DENEGRI, M., NAPOLITANO, C. & PRIORI, S. G. 2012. Inherited calcium channelopathies in the pathophysiology of arrhythmias. *Nat Rev Cardiol,* 9**,** 561-75.

VESTERGAARD, L. S. & RINGWALD, P. 2007. Responding to the challenge of antimalarial drug resistance by routine monitoring to update national malaria treatment policies. *The American journal of tropical medicine and hygiene,* 77**,** 153-159.

VON SEIDLEIN, L. & BEJON, P. 2013. Malaria vaccines: past, present and future. *Archives of disease in childhood,* 98**,** 981-985.

VYAS, V., UKAWALA, R., GHATE, M. & CHINTHA, C. 2012. Homology modeling a fast tool for drug discovery: current perspectives. *Indian journal of pharmaceutical sciences,* 74**,** 1.

WALKER, S. L., WATERS, M. F. & LOCKWOOD, D. N. 2007. The role of thalidomide in the management of erythema nodosum leprosum. *Lepr Rev,* 78**,** 197-215.

WALSH, J. J., COUGHLAN, D., HENEGHAN, N., GAYNOR, C. & BELL, A. 2007. A novel artemisinin-quinine hybrid with potent antimalarial activity. *Bioorg Med Chem Lett,* 17**,** 3599-602.

WALTERS, W. P., STAHL, M. T. & MURCKO, M. A. 1998. Virtual screening—an overview. *Drug discovery today,* 3**,** 160-178.
WANG, R., SMITH, J. D. & KAPPE, S. H. 2009. Advances and challenges in malaria vaccine development. *Expert Rev Mol Med,* 11**,** e39.
WARD, G. E., MILLER, L. H. & DVORAK, J. A. 1993. The origin of parasitophorous vacuole membrane lipids in malaria-infected erythrocytes. *J Cell Sci,* 106 (Pt 1)**,** 237-48.
WARHURST, D. 1985. New drugs and their potential use against drug-resistant malaria. *Ann Ist Super Sanita,* 21**,** 327-36.
WARING, M. J., ARROWSMITH, J., LEACH, A. R., LEESON, P. D., MANDRELL, S., OWEN, R. M., PAIRAUDEAU, G., PENNIE, W. D., PICKETT, S. D. & WANG, J. 2015. An analysis of the attrition of drug candidates from four major pharmaceutical companies. *Nature reviews Drug discovery,* 14**,** 475.
WARMKE, J. W. & GANETZKY, B. 1994. A family of potassium channel genes related to eag in Drosophila and mammals. *Proceedings of the National Academy of Sciences,* 91**,** 3438-3442.
WARREN, G. L., ANDREWS, C. W., CAPELLI, A.-M., CLARKE, B., LALONDE, J., LAMBERT, M. H., LINDVALL, M., NEVINS, N., SEMUS, S. F. & SENGER, S. 2006. A critical assessment of docking programs and scoring functions. *Journal of Medicinal Chemistry,* 49**,** 5912-5931.
WARREN, J. 2011. Drug discovery: lessons from evolution. *British journal of clinical pharmacology,* 71**,** 497-503.
WATERS, A. P., SYIN, C. & MCCUTCHAN, T. F. 1989. Developmental regulation of stage-specific ribosome populations in Plasmodium. *Nature,* 342**,** 438-440.
WATKINS, W. D. & GUESS, W. L. 1968. Toxicity of emetine to isolated embryonic chick-heart cells. *J Pharm Sci,* 57**,** 1968-74.
WEI, B. Q., WEAVER, L. H., FERRARI, A. M., MATTHEWS, B. W. & SHOICHET, B. K. 2004. Testing a flexible-receptor docking algorithm in a model binding site. *Journal of molecular biology,* 337**,** 1161-1182.
WELLS, T. N. 2010. Is the tide turning for new malaria medicines? *Science,* 329**,** 1153-1154.
WELLS, T. N. 2011. Natural products as starting points for future anti-malarial therapies: going back to our roots? *Malaria journal,* 10**,** S3.
WHITE, N. J. 1985. Clinical pharmacokinetics of antimalarial drugs. *Clinical pharmacokinetics,* 10**,** 187-215.
WHITE, N. J. 2004. Antimalarial drug resistance. *The Journal of clinical investigation,* 113**,** 1084-1092.
WHITE, R. E., RONALD, T., EDWARD, H., KERNS CHRISTOPHER, A. & LIPINSKI DHIREN, R. 2004. A comprehensive strategy for ADME screening in drug discovery. *Pharmaceutical profiling in drug discovery for lead selection***,** 431.
WORLD HEALTH ORGANISATION. 1995. WHO model prescribing information: drugs used in parasitic diseases.
WORLD HEALTH ORGANISATION. 2005. Fact Sheet on the World Malaria Report 2003.
WORLD HEALTH ORGANISATION. 2015. Fact Sheet on the World Malaria Report 2014.
WORLD HEALTH ORGANISATION. 2015. *Guidelines for the treatment of malaria*, World Health Organization.
WORLD HEALTH ORGANISATION. 2016. Fact Sheet on the World Malaria Report 2015.
WORLD HEALTH ORGANISATION. 2018. Fact Sheet on the World Malaria Report 2017.
WILLCOX, M., BODEKER, G., RASOANAIVO, P. & ADDAE-KYEREME, J. 2004. *Traditional medicinal plants and malaria*, CRC press.

WILLIAMS, H. A., BLOLAND, P. B., COUNCIL, N. R. & POPULATION, C. O. 2003. *Malaria control during mass population movements and natural disasters*, National Academies Press.

WILSON, G. L. & LILL, M. A. 2011. Integrating structure-based and ligand-based approaches for computational drug design. *Future Medicinal Chemistry,* 3**,** 735-750.

WINSTANLEY, P., WARD, S., SNOW, R. & BRECKENRIDGE, A. 2004. Therapy of falciparum malaria in sub-saharan Africa: from molecule to policy. *Clinical microbiology reviews,* 17**,** 612-637.

WINSTANLEY, P. A. 2000. Chemotherapy for falciparum malaria: the armoury, the problems and the prospects. *Parasitol Today,* 16**,** 146-53.

WOLBER, G. & LANGER, T. 2005. LigandScout: 3-D pharmacophores derived from protein-bound ligands and their use as virtual screening filters. *Journal of chemical information and modeling,* 45**,** 160-169.

WOLFE, M. S. & CORDERO, J. F. 1985. Safety of chloroquine in chemosuppression of malaria during pregnancy. *Br Med J (Clin Res Ed),* 290**,** 1466-1467.

WOLFENSBERGER, H. 1968. Amoebiasis: Clinical trials of dehydroemetine late-release tablets (Ro 1-9334/20) compared with parenteral dehydroemetine and niridazole. *Transactions of the Royal Society of Tropical Medicine and Hygiene,* 62**,** 831-837.

WONG, W., BAI, X. C., BROWN, A., FERNANDEZ, I. S., HANSSEN, E., CONDRON, M., TAN, Y. H., BAUM, J. & SCHERES, S. H. 2014. Cryo-EM structure of the Plasmodium falciparum 80S ribosome bound to the anti-protozoan drug emetine. *Elife,* 3.

WONGSRICHANALAI, C., PICKARD, A. L., WERNSDORFER, W. H. & MESHNICK, S. R. 2002. Epidemiology of drug-resistant malaria. *Lancet Infect Dis,* 2**,** 209-18.

WRIGHT, C., PHILLIPSON, J., AWE, S., KIRBY, G., WARHURST, D., QUETIN‐LECLERCQ, J. & ANGENOT, L. 1996. Antimalarial activity of cryptolepine and some other anhydronium bases. *Phytotherapy Research,* 10**,** 361-363.

YADAV, D., PALIWAL, S., YADAV, R., PAL, M. & PANDEY, A. 2012. Identification of novel HIV 1-protease inhibitors: application of ligand and structure based pharmacophore mapping and virtual screening. *PloS one,* 7**,** e48942.

YANG, C.-Y., WANG, R. & WANG, S. 2006. M-score: a knowledge-based potential scoring function accounting for protein atom mobility. *Journal of medicinal chemistry,* 49**,** 5903-5911.

YANG, S., Xu, M., LEE, E. M., GORSHKOV, K., SHIRYAEV, S. A., HE, S., ... ZHENG, W. 2018. Emetine inhibits Zika and Ebola virus infections through two molecular mechanisms: Inhibiting viral replication and decreasing viral entry. *Cell Discovery*, *4*(1), [31]. https://doi.org/10.1038/s41421-018-0034-1

YANG, W. C. & DUBICK, M. 1980. Mechanism of emetine cardiotoxicity. *Pharmacol Ther,* 10**,** 15-26.

YARNELL, E. 2014. Artemisia annua (sweet Annie), other Artemisia species, artemisinin, artemisinin derivatives, and malaria. *Journal of Restorative Medicine,* 3**,** 69-84.

YEH, P. J., HEGRENESS, M. J., AIDEN, A. P. & KISHONY, R. 2009. Drug interactions and the evolution of antibiotic resistance. *Nature Reviews Microbiology,* 7**,** 460-466.

YIN LOW, J., CHEN, K., WU, K. & MAH-LEENM, H. 2009. Antiviral activity of emetine dihydrochloride against dengue virus infection. *J Antivir Antiretrovir,* 1**,** 062000.

YIN, N., MA, W., PEI, J., OUYANG, Q., TANG, C. & LAI, L. 2014. Synergistic and antagonistic drug combinations depend on network topology. *PloS one,* 9**,** e93960.

YU, H. & ADEDOYIN, A. 2003. ADME–Tox in drug discovery: integration of experimental and computational technologies. *Drug discovery today,* 8**,** 852-861.

YUAN, Y., PEI, J. & LAI, L. 2013. Binding site detection and druggability prediction of protein targets for structure-based drug design. *Current Pharmaceutical Design,* 19**,** 2326-2333.

ZHANG, S. & GERHARD, G. S. 2009. Heme mediates cytotoxicity from artemisinin and serves as a general anti-proliferation target. *PLoS One,* 4**,** e7472.

ZIMMERMANN, G. R., LEHAR, J. & KEITH, C. T. 2007. Multi-target therapeutics: when the whole is greater than the sum of the parts. *Drug discovery today,* 12**,** 34-42.

ZOLLER, T., NAUCKE, T. J., MAY, J., HOFFMEISTER, B., FLICK, H., WILLIAMS, C. J., FRANK, C., BERGMANN, F., SUTTORP, N. & MOCKENHAUPT, F. P. 2009. Malaria transmission in non-endemic areas: case report, review of the literature and implications for public health management. *Malar Journal,* 8**,** 71.